MAGNETIC QUANTUM OSCILLATIONS IN ORGANIC METALS BASED ON THE MOLECULE BIS(ETHYLENEDITHIO)TETRATHIAFULVALENE

Jason M. Caulfield
Corpus Christi College, Oxford

A thesis submitted for the degree of Doctor of Philosophy
at the University of Oxford
Michaelmas Term 1994

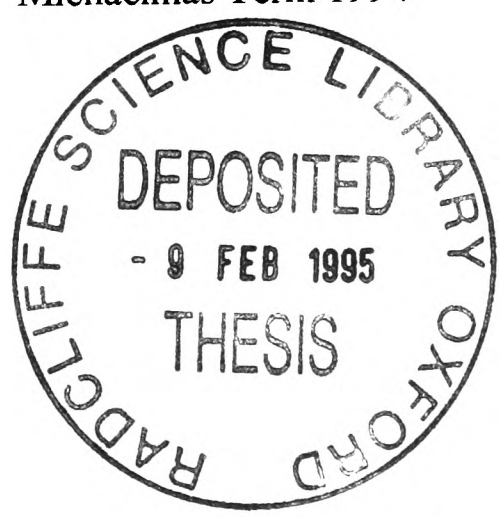

Magnetic Quantum Oscillations in Organic Metals Based on the Molecule bis(ethylenedithio)tetrathiafulvalene

Jason Michael Caulfield, Corpus Christi College, Oxford University,
Michaelmas Term 1994

Abstract of Thesis Submitted for the Degree of Doctor of Philosophy

ET charge transfer salts (where ET is *bis(ethylenedithio)-tetrathiafulvalene*) have relatively simple quasi two-dimensional Fermi surface topologies, making them ideal for the study of the relationship between bandstructure and properties such as superconductivity. Experimental studies of the Fermi surface areas and associated effective masses have been carried out using the Shubnikov-de Haas (SdH) and de Haas-van Alphen (dHvA) effects. By comparing the experimental results to theoretical bandstructure calculations the strength of many body interactions has been estimated.

High pressure magnetotransport experiments have been carried out on the superconductor $\kappa-ET_2Cu(NCS)_2$. The observation of SdH and magnetic breakdown oscillations has allowed the pressure dependences of the Fermi surface topology and effective masses to be deduced and compared with simultaneous measurements of the superconducting critical temperature. The data strongly suggest that the enhancement of the effective mass and the superconducting behaviour are directly connected. The results are compared with several current theories of superconductivity.

The dHvA effect has been used to probe the superconducting mixed state of $\kappa-ET_2Cu(NCS)_2$. A recent model of the superconducting mixed state is applied to the experimental data in an attempt to determine the value and symmetry of the superconducting energy gap.

SdH measurements up to 30 T have been used to study spin density-wave formation in $\alpha-ET_2KHg(SCN)_4$, and the reasons why a very slight increase of the unit cell volume (*i.e.* replacing the K in $\alpha-ET_2KHg(SCN)_4$ by NH_4) stabilises a superconducting state. Galvanomagnetic techniques have been used to measure the quasi one-dimensional Fermi surface orientation below the spin-density-wave transition, and to accurately determine the shape of the quasi two-dimensional Fermi surface above it.

The application of pressure has been used to gradually reduce the onset temperature of a metal-insulator transition and to eventually stabilise a superconducting state in $ET_3Cl_22H_2O$. The bandstructure of $ET_3Cl_22H_2O$ has been investigated using the SdH effect whilst hydrostatic pressure has been used to pass through the superconducting part of the phase diagram.

Acknowledgements

Firstly, I would like to thank R.A. Cowley and J.M. Baker for enabling me to participate in research of the highest standard at the Clarendon Laboratory.

John Singleton whose unremitting enthusiasm for Physics and constant support made him my mentor in every sense of the word. Thank you to Bill Hayes for always having time for me, and for those many golden words of wisdom about life in general.

Over the years I have made many trips to the broom cupboard to visit Steve Blundell and Francis Pratt who always had the patience to answer my endless questions. I must thank Mo Kurmoo for his constant support and for growing the best ET salts in the world, and to Dave Ko for 'theoretical' advice.

Wieslaw Lubczynski, a patient and experienced experimentalist, with whom I worked closely on the pressure measurements.

Some of the experiments reported in this thesis were performed at other European labs. I shared many long hours in the magnet lab at Nijmegen with Peter-Paul Hendriks, a most devoted and able lackey. The pulsating gang at Leuven, especially Fritz Herlach and Igne Deckers, initiated me in my first experimental work, also thanks to Neil Harrison and Johan Vanacken for useful discussions. Thank you to Mike Springford for use of the Bristol lab, to Steve Hayden for his guidance and Paul van der Wel for generally being a nice guy to work with.

To the Singleteenies Steve 'you finished yet' Hill, Phil 'Duckworth' Gee, Andy Plank, Geraldine Hendriks (née Houston) and Arzhang Aardvark, who are you going to throw the sponge at now ? Lucus du Croo de Jongh for building AMRO insert mk II. Special thanks to whatja doin Donkey Doporto for MRH and being himself, and to Paul Pattenden for showing me how to draw.

I am indebted to both mine and Helen's families for my computer and creature comforts, and especially to Helen for love, happiness and our future together.

To Mum, Dad and Helen.....

Contents

Chapter 1

An introduction to organic metals

1.1 Introduction

Semiconductor heterostructures are just one example of the many ways in which physicists construct artificial structures to produce 'tailor-made' bandstructure. Another approach is to use small organic molecules to build up solids with desirable (and eventually controllable) metallic, semiconducting or even superconducting properties [1]. Thirty years ago visualing such an approach, Little [2] calculated that it ought to be possible to make an organic polymer which would be superconducting above room temperature. The proposed system was based on an organic polymer chain with highly polarisable side branches. In this model the electrons moving along the chain interact strongly with the side branches. Calculations suggest that the formation of electron (Cooper) pairs by such an exciton-mediated interaction would lead to superconducting transition temperatures well in excess of room temperature. Spurred on by such a possibility, bandstructure "engineering" took a big step forward.

Needless to say, organic superconductors with such high transition temperatures have not yet been found. Research focused on highly conducting organic charge transfer salts, systems in which a number of molecules jointly donate an electron to another ion (the anion), thereby producing a stable lattice. A decade later Jérome and Bechgaard [3] discovered the first organic superconductors: charge transfer salts based on the molecule TMTSF (*tetramethyltetraselenafulvalene*) with a transition temperature below 1.5 K. This discovery stimulated a frenzy of activity in the physics and chemistry communities which led to the synthesis of a large number of superconducting organic compounds.

The next step was the synthesis of a family of charge transfer salts based upon the donor ion *bis(ethylenedithio)-tetrathiafulvalene* (BEDT-TTF or ET for short), from which superconducting salts were made. ET salts form a versatile system for the study of band formation; by varying the anion X in the salt $(ET)_n X$, the stoichiometry (and hence the band shape) and the band-filling may be adjusted. In this way a large number of ET salts have been synthesised showing a remarkable variety of phase transitions; some have been found to be superconducting with transition temperatures of up to 13 K. Although

the superconductive mechanisms seem to have nothing to do with those proposed by Little [2,4], the properties of superconducting ET salts have much in common with the exotic High T_c superconductors and Heavy Fermion systems [4-6].

The well separated molecular orbitals and the layered structural arrangement in ET charge transfer salts leads to relatively simple two-dimensional Fermi surface topologies, making the salts ideal for the study of the relationship between bandstructure and electronic properties such as superconductivity. Furthermore, as will be shown, excellent crystals have recently become available, so that phenomena such as the Shubnikov-de Haas effect may be readily observed, enabling the Fermi surface topology to be measured accurately (*e.g.* this work, chapter 3). In contrast to High T_c superconductors and Heavy Fermion systems, ET salts may be studied at reasonable laboratory magnetic fields and temperatures. They may, therefore, be the systems on which theoretical approaches to High T_c superconductors or Heavy Fermion systems are tested.

The principles behind organic charge transfer salts will be given in § 1.2, followed by a brief historical survey of synthetic organic conductors and superconductors in § 1.3. In § 1.4 ET charge transfer salts are introduced. An outline of the experimental work to be reported in this thesis will be given in § 1.5.

1.2 Organic charge transfer salts

Organic solids are generally regarded as good electrical insulators. However, the possibility of highly conducting organic solids was suggested at the beginning of this century [7]. Understanding how organic compounds conduct electricity at all is the first step in appreciating the varied properties of organic superconductors. The charge transfer salts, which are the subject of this thesis, are by far the largest and most diverse class of organic conductors or "organic metals". Unlike conventional molecular crystals, which are held together by weak van der Waals forces, charge transfer salts contain molecules with unpaired carriers in the π molecular orbitals. These orbitals usually

originate from rings containing sulphur or selenium and carbon; the overlap between neighbouring molecules allows electronic delocalization over all molecular sites in the crystal, and hence bandstructure formation (figure 1). The charge transfer comes from partial oxidation of donor molecules in the formation of a salt with an inorganic anion, thereby producing a stable crystal lattice. Charge transfer salts usually crystallise into of layers of organic molecules separated by sheets of the inorganic anions.

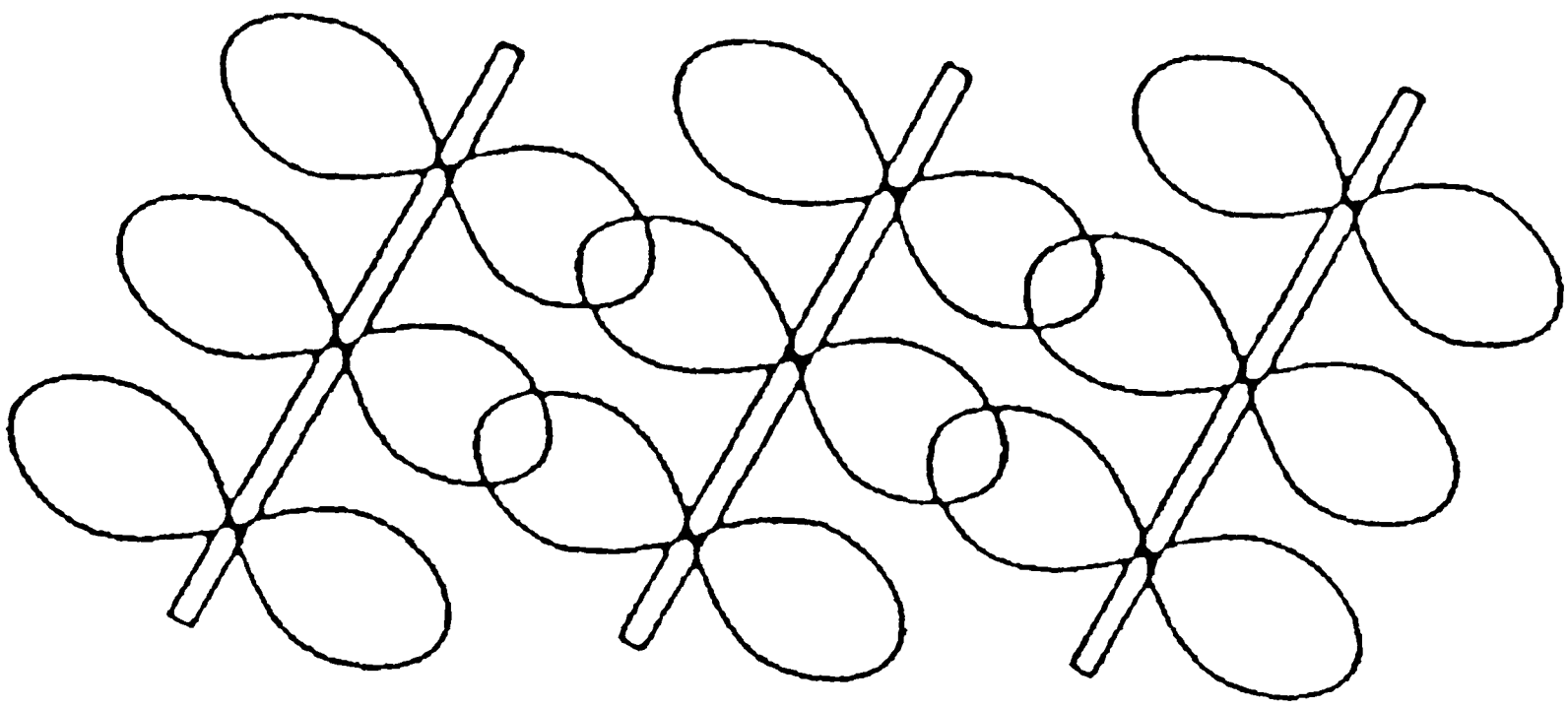

Figure 1 A schematic representation of molecular π orbital overlap between neighbouring molecules in a charge transfer salt

Superconducting charge transfer salts have attracted considerable interest because they exhibit many phenomena that do not appear in conventional superconducting or in nonsuperconducting materials. Organic superconductors show a remarkable variety of phase transitions, the nature of which depends on the constituents of the compound and on external parameters such as pressure, temperature and magnetic field. Most of the unusual properties arise because the organic crystals are highly anisotropic; the conductivity (molecular overlap) is principally along one or two of the crystal axes.

1.3 A brief History of organic metals

The first metallic charge transfer complex, TTF-TCNQ, was synthesised in the early 1970's at Dupont [3]. The combination of the electron acceptor TCNQ (*tetracyano-p-quinodimethane*) with the donor molecule TTF (*tetrathiafulvalene*) (figure 2a), arranged in a herring-bone structure (figure 2b), produced highly conducting crystals ($\rho \sim 1\ m\Omega cm$).

(a)

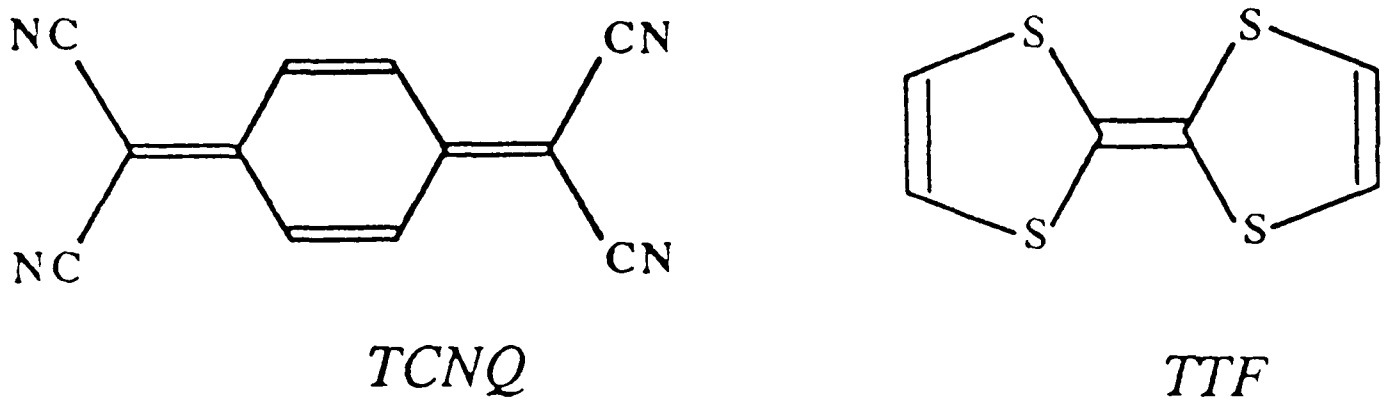

TCNQ *TTF*

(b)

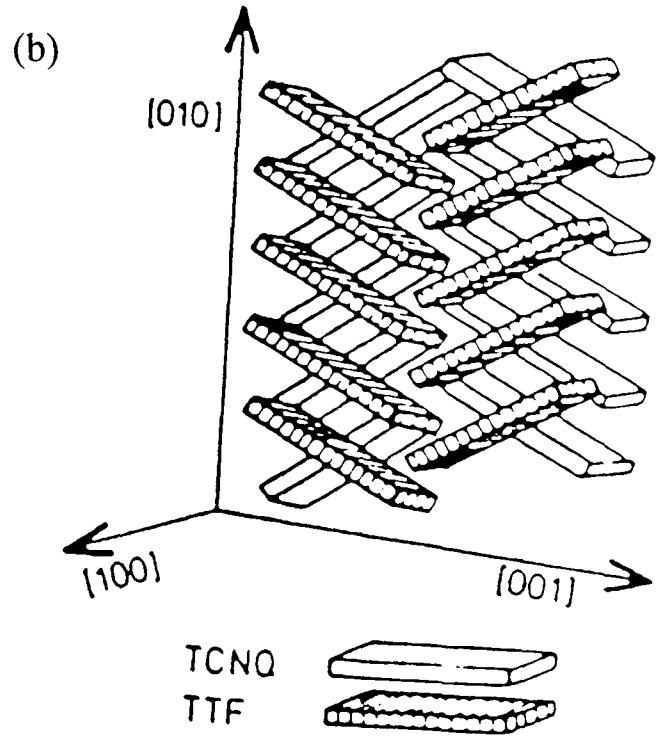

Figure 2 (a) The TTF and TCNQ molecules. (b) Schematic representation of the TTF-TCNQ structure, demonstrating the 'herring-bone' type packing.

On cooling below ~55 K TTF-TCNQ becomes semiconducting due a distortion of the lattice (a charge density wave), known as a Peierls distortion, associated with the one dimensional nature of the structure [8].

Encouraged by these findings researchers directed their efforts toward the development of new electron donor/acceptor molecules. Attempts were made to increase the dimensionality of new organic metals in order to induce lattice stability at low temperatures. In 1974, Bechgaard *et al* [9] synthesised the TMTSF molecule shown in figure 3a. TMTSF, a modification of the TTF molecule with the sulphurs substituted for selenium atoms, when combined with DMTCNQ (2,4-dimethyl-TCNQ) has increased side-by-side interactions and larger π-orbital overlap resulting in an even better metal, which remains conducting all the way down to liquid helium temperatures.

(a)

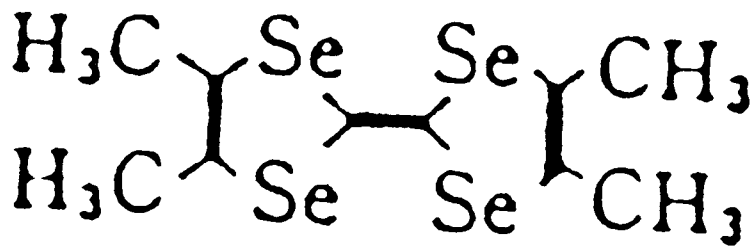

TMTSF

(b)

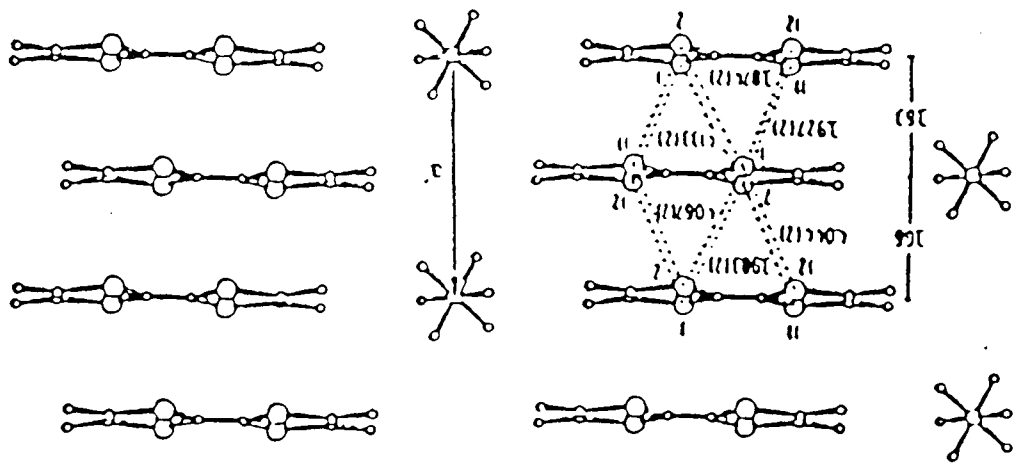

Figure 3 (a) The TMTSF molecule. (b) The crystal structure of $(TMTSF)_2X$ compounds.

The real breakthrough came in the use of inorganic monovalent anions in place of TCNQ. A family of salts of the type $(TMTSF)_2X$ were prepared, known as Bechgaard salts. Within a short time six superconducting Bechgaard salts had been synthesised (figure 3b), although externally applied pressure was required to increase the π-orbital overlap to prevent the onset of a spin density wave. Smaller anions were eventually synthesised in order to increase the degree of overlap between TMTSF molecules. In 1981, a superconductor with a transition temperature ~1 K at ambient pressure was created ($(TMTSF)_2ClO_4$) [10].

The discovery of superconductivity in these materials marked the onset of extensive research, devoted to the understanding of the physical properties of these quasi one-dimensional organic conductors. Furthermore the quantum Hall effect has also been measured in Bechgaard salts [11], bringing these materials into the mainstream of Condensed Matter Physics. The very peculiar properties of these charge-transfer salts are brought about by the fact that the overlap of the electron wave functions in the directions perpendicular to the chains of molecules is at least order of magnitude weaker than in the direction of good conductivity. This anisotropy leads to the characteristic open Fermi surface which consists of two warped sheets. It is well known that the metallic phase described by such a Fermi surface can become unstable due to Fermi surface nesting. At low temperatures TMTSF salts are prone to spin-density-wave formation, due to the almost perfect nesting characteristics of the Fermi surface, and this appears to compete with superconductivity. The spin-density wave state leads to antiferromagnetic order among the conduction electrons and a band gap at the Fermi surface, responsible for the metal insulator transition. The application of pressure leads to an enhancement of the two-dimensional character, and hence the likelihood of superconductivity, whereas application of magnetic fields instead make the material more one-dimensional, and hence liable to form a field induced spin density wave.

1.4 ET charge transfer salts

The ET molecule was the second molecule which produced superconducting charge transfer salts [1]. It was designed in an attempt to increase dimensionality in order to maintain the metallic properties to low temperatures. The electron delocalisation on the TMTSF rings was extended by adding another sulphur-carbon ring (making *bis(ethylenedithio)*-TTF), giving the molecule eight sulphur atoms (figure 4(a)). Figure 4(b) shows a typical ET charge transfer salt crystal structure (in this case κ-$ET_2Cu(NCS)_2$) and illustrates many of the typical features of ET salts. The ET molecules stack in two-dimensional planes separated by layers of the $Cu(NCS)_2$ anions.

(a)

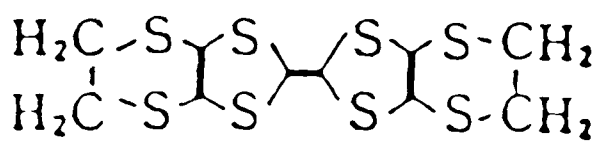

BEDT-TTF

(b)

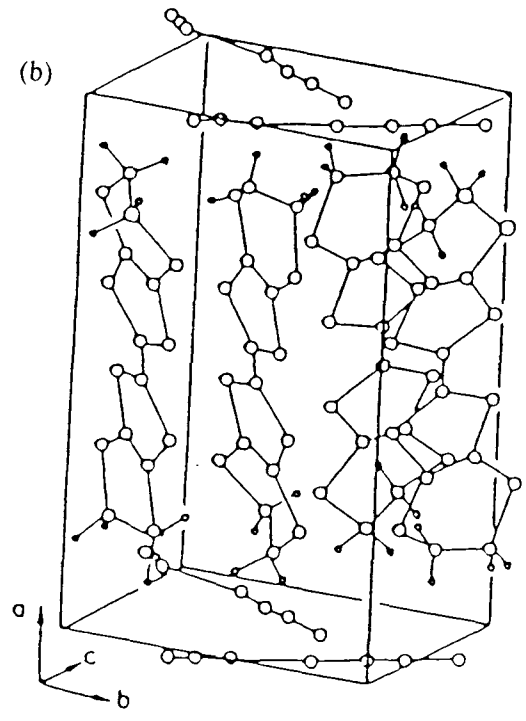

Figure 4 (a) The ET molecule, (b) the layered Crystal structure of κ-$ET_2Cu(NCS)_2$

Transfer of electrons occurs readily within the two-dimensional planes, but much less readily in the perpendicular direction through the anions. As a result the bandstructures and electrical properties of ET salts are rather two-dimensional. It should be emphasised that the molecular orbitals of the anions are usually well removed in energy from the Fermi level. They therefore play very little part in the electronic properties of ET charge transfer salts.

Altering the anion causes changes in the packing of the ET ions, enabling the molecular overlap and band filling to be adjusted with some dramatic results; *e.g.* the superconducting transition temperature may be raised by a factor ~3 in the β-phase ET salts by changing the anion [1]. Many different ET salt phases and stoichiometries have since been synthesised; some of the more common packing arrangements are shown in figure 5. By tuning the packing of the ET molecules using a suitable choice of anion, a transition to superconductivity of 13 K has been achieved in κ-$ET_2Cu[N(CN)_2]Cl$ [12].

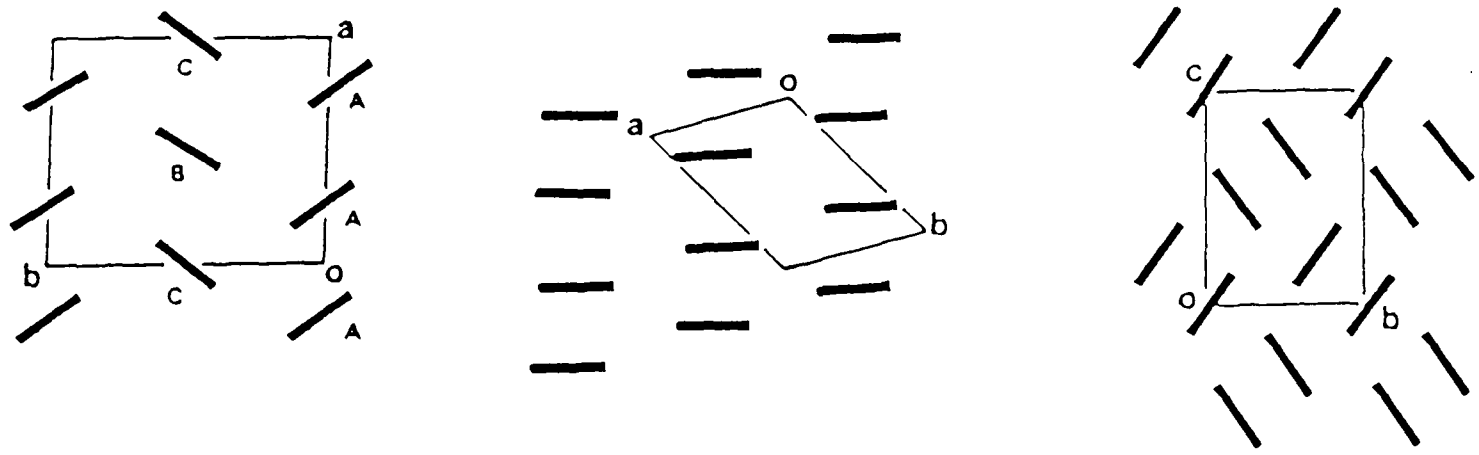

α-$(BEDT\text{-}TTF)_2I_3$ β-$(BEDT\text{-}TTF)_2I_3$ κ-$(BEDT\text{-}TTF)_2I_3$

Figure 5 Molecular packing schemes of the α, β and κ-phase ET salts using ET_2I_3 as an example.

The observation of Shubnikov-de Haas [13] and de Haas-van Alphen oscillations [14] in 1988, enabled the Fermi surface topology of organic charge-transfer salts to be measured accurately for the first time. It has become clear that the Fermi surface can be predicted with reasonable accuracy by the application of a tight binding method to the overlapping molecular π-orbitals, although the band width is over estimated by a factor of ~3; this is thought to be due to the effects of many-body interactions (see this thesis chapter 3).

1.5 Outline of this thesis

In this thesis I will describe the results obtained from an experimental study of four ET salts. I have used several experimental techniques throughout the past three years, although in this thesis I shall report only the most important experimental findings. The experiments have involved using magnetic fields up to 50 T, temperatures down to 20 mK and hydrostatic pressures up to 20,000 atmospheres.

The experimental techniques described in this thesis are by far the most important probes of the Fermi surface, and hence are very useful in the understanding of the groundstate properties of organic metals and superconductors. In chapter 3 the Shubnikov-de Haas effect has been used to gauge the Fermi surfaces and the associated carrier effective masses of the organic superconductor κ-$ET_2Cu(NCS)_2$. By comparing the experimental results to theoretical bandstructure calculations the strength of many body interactions has been estimated. In conjunction with these techniques, externally applied hydrostatic pressure has been used to alter the groundstate properties in a controlled way, whilst simultaneously using the Shubnikov-de Haas technique to accurately measure the corresponding changes in the electronic bandstructure. The data strongly suggest that the enhancement of the effective mass and the superconducting behaviour are directly connected. The results are fitted to several current theories of superconductivity. The experimental results may explain why chemists have found that

applying 'negative pressure' (*i.e.* using larger anions to increase the unit cell volume) in ET salts increases the superconducting transition temperature.

In chapter 4 the de Haas-van Alphen effect has been used to probe the superconducting mixed state of $\kappa-ET_2Cu(NCS)_2$. A very recent theoretical model of the superconducting mixed state is applied to the experimental data which may, with a little more work, be used to determine the value and symmetry of the superconducting energy gap.

In chapter 5 high field Shubnikov-de Haas measurements have been used to study spin density-wave formation in $\alpha-ET_2KHg(SCN)_4$, and the reasons why a very slight increase of the unit cell volume (*i.e.* replacing the K in $\alpha-ET_2KHg(SCN)_4$ by NH_4) stabilises a superconducting state. A rather new technique, 'angle dependent galvanomagnetic oscillations', has been used to measure the quasi one-dimensional Fermi surface orientations and to accurately determine the shape of the quasi two dimensional Fermi surface sections both above and below the spin-density-wave transition in order to help determine how the transition occurs.

In chapter 6 the application of pressure has been used to gradually reduce the onset temperature of a metal-insulator transition and to eventually stabilise a superconducting state in $ET_3Cl_22H_2O$. Using high magnetic fields and low temperatures the bandstructure of $ET_3Cl_22H_2O$ has been investigated using the Shubnikov-de Haas effect whilst using hydrostatic pressure simultaneously to pass through the superconducting part of the phase diagram.

Using these techniques the structure-property relationships of the charge transfer salts may begin to be understood, enabling chemists to design materials with desirable and eventually controllable properties.

References

[1] *Organic superconductors*, by T. Ishiguro and K. Yamaji (Springer-Verlag Berlin 1990).

[2] W.A. Little, *Phys. Rev.* **134** 1416 (1960).

[3] For an earley review of organic conductors see D. Jérome and H.J. Schultz, *Advances in Physics* **31** 299 (1982).

[4] *Organic superconductivity*, V.Z. Kresin and W.A. Little (eds) (Plenum Press, New York, 1990).

[5] F.L. Pratt, J. Singleton, M. Kurmoo, S.J.R.M. Spermon, W. Hayes and P. Day., *Springer Proceedings in Physics* **51** 200 (1990).

[6] N. Toyota, E.W. Fenton, T. Sasaki and M. Tachiki, *Solid State Commun.* **72** 859 (1990).

[7] H.N. McCoy and W.C. Moore, *J. Am. Chem. Soc.*, **33** 273 (1911).

[8] For an excellent review on Peierls distortions the reader is referred to [1].

[9] K. Bechgaard, D.O. Cowan and A.N. Bloch, *Chem. Commun.***74** 937 (1974).

[10] K. Bechgaard, K. Carneiro, M. Olsen, F.B. Rasmussen and C.S. Jacobsen, *Phys. Rev. Lett.* **46** 852 (1981)

D. Jérome, A. Mazaud, M. Ribault and K. Bechgaard, *J. Phys. (Paris) Lett.* **41** L95 (1981).

[11] J.R. Cooper, W. Kang, P. Auban, G. Montambaux, D. Jérome and K. Bechgaard, *Phys. Rev. Lett.* **63** 1984 (1989). S.T. Hannah, J.S. Brooks, W. Kang, L.Y. Chiang and P.M. Chaikin, *Phys. Rev. Lett.* **63** 1988 (1989)

[12] J.E. Schirber, D.L. Overmyer, K.D. Karlson, J.M. Williams, A.M. Kini, H. Hau Wang, H.A. Charlier, B.J. Love, D.M. Watkins, G.A. Yaconi, *Phys. Rev.* **B 44** 4666 (1991).

[13] K. Murata, N. Toyota, Y. Honda, T. Sasaki, M. Tokumoto, H. Bando, H. Anzai, Y. Muto and T. Ishiguro, *J. Phys. Soc. Japan* **57** 1540 (1988).

F.L. Pratt, A.J. Fisher, W. Hayes, J. Singleton, S.J.R.M. Spermon, M. Kurmoo and P. Day, *Phys. Rev. Lett.* **61** 2721 (1988).

[14] I.D. Parker, D.D. Pigram, R.H. Friend, M. Kurmoo and P. Day, *Synth. Metals* **27** 387 (1988).

Chapter 2

The theory of magnetic oscillations in metals.

2.1. Introduction

A knowledge of the Fermi surface of a metal is essential for calculating or explaining its basic properties. Experimental techniques which gauge the Fermi surface are making a great contribution to the understanding of organic metals and superconductors. Most studies have involved measurements of Shubnikov-de Haas oscillations in the magnetoresistance (*e.g.* this work chapters 3,5 and 6) or de Haas-van Alphen oscillations in the magnetisation. (*e.g.* this work chapter 4); recently galvanomagnetic studies have also been used to measure one-dimensional Fermi surfaces and to gauge the exact shape of two-dimensional sections (*e.g.* this work chapter 5).

This chapter is meant to give a compact derivation of the Lifshitz-Kosevich formula (the formula used in analysing Shubnikov-de Haas and de Haas-van Alphen data) and to explain the physical origin of the oscillations. In § 2.2 a simple semiclassical picture is presented of Bloch electrons moving through a crystal lattice subject to the Bohr-Sommerfeld quantisation rule as a description of electron dynamics in a magnetic field. § 2.3 gives a brief derivation of the Lifshitz-Kosevich formula, a quantitative expression for the amplitude, phase and periodicity of quantum oscillations under various experimental conditions. In § 2.4 magnetic quantum oscillations are discussed in the context of ET charge transfer salts.

2.2. Electron motion in a magnetic field

The semiclassical description of a Bloch electron in the presence of a magnetic field **B** is based on the Lorentz force equation

$$\hbar \dot{\boldsymbol{k}} = -e(\mathbf{v} \times \mathbf{B}) \tag{2.1}$$

where $\boldsymbol{k}(t)$ is the electron wavevector and $\hbar\boldsymbol{k}$ is the crystal momentum. The velocity **v** is related to the electron energy by

$$\mathbf{v} = \frac{1}{\hbar}\frac{\partial \varepsilon(\boldsymbol{k})}{\partial \boldsymbol{k}} \tag{2.2}$$

where $\varepsilon(\boldsymbol{k}(t))$ is the electron energy [1]. It follows from the above equations that both $\varepsilon(\boldsymbol{k}(t))$ and the component of the electron wavevector parallel to the applied magnetic field, $\boldsymbol{k}_{//}$, are constants of motion. Since no work is done on the electron, it will move along curves of constant energy perpendicular to the magnetic field. If we integrate equation (2.1) with respect to time we find

$$\hbar(\boldsymbol{k} - \boldsymbol{k}_0) = -e(\mathbf{r} - \mathbf{r}_0) \times \mathbf{B} \tag{2.3}$$

where **r** is the position vector of the electron in its classical trajectory. The projection **r'** of the orbit on to the plane perpendicular to **B** is a scaled version of the trajectory $\boldsymbol{k}$ in reciprocal space. The scaling factor is $\hbar / e\mathbf{B}$. Furthermore the real space orbit is rotated by 90° with respect to the $\boldsymbol{k}$-space orbit. In the free electron case the constant energy surfaces are spheres and the orbits are circular (figure 1). In general the $\boldsymbol{k}$-space orbits will not be circular and they often are not even closed. The angular frequency with which the orbit is traversed is the cyclotron frequency

$$\omega_c = \frac{e\mathbf{B}}{m^*} \tag{2.4}$$

which depends on the orbit effective mass

$$m^*(\varepsilon, \boldsymbol{k}_{\backslash\backslash}) = \frac{\hbar^2}{2\pi}\left(\frac{\partial A}{\partial \varepsilon}\right) \tag{2.5}$$

where A is the cross-sectional area of the Fermi surface at $\boldsymbol{k}_{//}$. For those trajectories in k-space which are closed, the projected r-space orbit will also be closed and according to the Bohr-Sommerfeld rule the periodic motion is expected to be quantised:

$$\oint \boldsymbol{p} \cdot d\boldsymbol{r}' = \oint (\hbar \boldsymbol{k} - e\mathbf{A}) \cdot d\boldsymbol{r}' = (\nu + \gamma) 2\pi\hbar \tag{2.6}$$

υ is an integer, γ is an undetermined phase factor and **A** is the vector potential of **B**. This quantum condition can be written in terms of the flux Φ of **B** through the real space orbit:

$$\Phi = \frac{2\pi\hbar}{e}(\upsilon + \gamma) \tag{2.7}$$

expressing the fact that only those orbits through which the flux (apart from the phase factor) is an integral multiple of the fundamental quantum $2\pi\hbar/e$ are allowed. The areas of the allowed orbits in real space are therefore given by $(\upsilon+\gamma)2\pi\hbar/eB$, corresponding to allowed areas A_υ in ***k***-space:

$$A_\nu(\varepsilon_\nu, k_{\backslash\backslash}) = \frac{2\pi e}{\hbar}(\nu+\gamma)B \tag{2.8}$$

Equation (2.8) is known as the Onsager relation, and shows that the effect of the magnetic field is to constrain the allowed states in *k*-space in the plane perpendicular to **B** to lie on a series of so called Landau levels with energies ε_ν. The energy levels of a free electron in a magnetic field are given by:

$$\varepsilon_\upsilon(k) = \frac{\hbar^2}{2m}k_{\backslash\backslash}^2 + (\upsilon+\gamma)\hbar\omega_c \tag{2.9}$$

the phase constant γ is exactly 1/2 for a parabolic band [3].

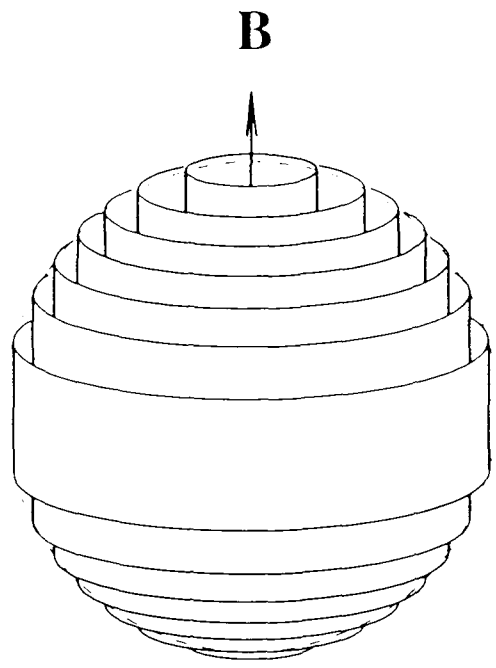

Figure 1 The semi-classical representation of the allowed states in *k*-space for a free electron metal in an applied magnetic field **B**. Only energy states less than the Fermi energy are shown.

In ET salts at typical laboratory fields the quantum numbers ν are large (10^2). In this limit, the correspondence principle, which relates quantum behaviour at high quantum numbers with classical motion, may be applied allowing electron motion to be treated semiclassically. The degeneracy of each Landau level is expected to be such that it can just accommodate all the $(V/4\pi^3)\Delta A\,\partial k_{\backslash\backslash}$ electrons which would be contained at zero magnetic field in an annular area $\Delta A = 2\pi eB/\hbar$ surrounding the orbit. On average, the number of electron states D on a length of tube lying between $\boldsymbol{k}_{\backslash\backslash}$ and $\boldsymbol{k}_{\backslash\backslash} + \delta\boldsymbol{k}_{\backslash\backslash}$ will be

$$D = \frac{eBV}{2\pi^2\hbar}\delta k_{\backslash\backslash} \tag{2.10}$$

where $V/4\pi^3$ is the number of states per unit volume of k-space in zero magnetic field. The area of the k-space orbit with quantum number ν grows with increasing magnetic field and at the same time the projected orbit area in real space decreases in order to conserve the magnetic flux. When the Landau level approaches an extremal cross-section of the Fermi surface A_{extr}, the free energy will increase to a maximum. If the magnetic field is increased a little further, the tube becomes depleted, causing a sudden lowering of the free energy. Now the Landau state with the quantum number $(\nu - 1)$ is the outermost non-empty tube and will again give rise to an increase in the free energy until a new maximum is reached. The maxima occur whenever $A_\upsilon = A_{extr}$, at regular spaced intervals of $1/\mathbf{B}$ given by

$$\frac{1}{B} = \frac{2\pi e}{\hbar}\frac{1}{A_{extr}} \tag{2.11}$$

This expression directly relates the periodicity of the oscillations in free energy to the cross-sectional area of the Fermi surface, *i.e.* it provides information about the Fermi surface topology.

2.3. Magnetic quantum oscillations

A quantitative treatment of magneto-oscillatory behaviour was first made by Lifshitz and Kosevich [2]. In order to derive the oscillatory magnetisation or magnetoresistance, one must begin with the thermodynamic potential $\Omega = F - N\mu$, where F is the free energy of the electron gas, μ is the chemical potential and N is the number of electrons. The vector magnetic moment is given by

$$\mathbf{M} = -\left(\frac{\partial \Omega}{\partial \mathbf{B}}\right)_{\mu} \tag{2.12}$$

Although **M** is derived from Ω by differentiation at constant μ, it does not imply that μ is constant as **B** changes. By summing the free energy of an electron gas over all available states and keeping in mind the degeneracy specified in equation (2.10), the thermodynamic potential can be written as

$$\Omega = -k_B T \int_{-\infty}^{\infty} dk_{\backslash\backslash} \left(\frac{eBV}{2\pi^2 \hbar}\right) \sum_{\upsilon} \ln\left(1 + e^{(\mu - \varepsilon_{\upsilon})/k_B T}\right) \tag{2.13}$$

The summation over energy states (Landau tubes) defined by the quantum number ν is rather tedious, so we shall quote the result from Shoenberg ([2], page 481), where the linear components have been analytically removed, leaving only the oscillatory terms, $\tilde{\Omega}$. Often the higher harmonics are significantly suppressed by phase smearing effects, such that the main feature resembles a sine wave. The oscillatory terms are given by:

$$\tilde{\Omega} \propto \frac{B^{5/2}}{m} \left|\frac{\partial^2 A}{\partial k_{\backslash\backslash}^2}\right|^{-1/2} \sum_{p=0}^{\infty} \frac{1}{p^{5/2}} \cos\left[2\pi p\left(\frac{B_F}{B} + \phi\right)\right] \tag{2.14}$$

where B_F is the frequency of an oscillation (which is often referred to as the fundamental field), with period $\Delta 1/B$

$$B_F \equiv \frac{1}{\Delta(1/B)} = \frac{\hbar}{2\pi e} A_{extr} \tag{2.15}$$

m is the cyclotron mass, p is the harmonic number and ϕ is a phase factor, which is usually close to 0.5 [2]. The term $\partial^2 A / \partial k_{\backslash\backslash}^2$ is the Fermi surface curvature factor *i.e.*

the change in extremal area A perpendicular to the applied magnetic field B with respect to $k_{\backslash\backslash}$. Equation (2.14) is responsible for the de Haas-van Alphen effect. The oscillatory part of the density of states also obeys a similar relationship

$$\tilde{D} \propto B^{1/2} m \left| \frac{\partial^2 A}{\partial k_{\backslash\backslash}^2} \right|^{-1/2} \sum_{p=0}^{\infty} \frac{1}{p^{1/2}} \cos\left[2\pi p \left(\frac{B_F}{B} + \phi \right) \right] \qquad (2.16)$$

As the magnetic field increases Landau tubes (figure 1) will pass through the Fermi surface. At a magnetic field where (2.11) is satisfied there will be a discontinuity in the density of states at the Fermi energy giving rise to oscillations in properties such as resistance (the Shubnikov-de Haas effect) [1].

The evaluations of $\tilde{\Omega}$ reviewed so far, have been made under the under the gross simplifications that the temperature T is zero, the metal contains no impurities or defects and that there is no interference between spin up and spin down Fermi surfaces. To take into account these effects Shoenberg introduced the concept of "phase smearing" [2] *i.e.* the frequency or phase of the oscillations, in the argument of the cosine of (2.15), are varied over a small range around the value corresponding to the idealised situation. Hence the resulting superposition of oscillations will reduce the amplitude of each of the periodic terms.

At finite but low temperatures the Fermi surface becomes slightly diffuse and the depletion of the states associated with the outermost tubes becomes less abrupt, leading to a thermal damping of the oscillations. The effect of a finite temperature an the amplitude of each harmonic p of $\tilde{\Omega}$ is an extra factor [2]

$$R_T = \frac{\chi}{\sinh \chi} \qquad (2.17)$$

where $\chi = 14.7 pmT / B$; as T$\rightarrow$0 $R_T \rightarrow 1$.

In real metals the scattering of electrons causes a finite lifetime of the states and the otherwise sharp quantum levels ε_υ become broadened according to the

Uncertainty Principle. This is equivalent to a spread in the chemical potential around the actual value μ.

$$R_D = e^{-\pi p/\omega_c \tau} = e^{-14.7 pmT_D/B} \tag{2.18}$$

The reduction factor, R_D, first introduced by Dingle [4] takes account of scattering effects. Because of the similarity of R_D with R_T (equation (2.17)) it is useful to define the *Dingle temperature* T_D, which parameterises the scattering time.

$$T_D = \frac{\hbar}{2\pi k_B \tau} \tag{2.19}$$

In a magnetic field, the Landau levels (themselves separated in energy by $\hbar\omega_c$) can be further split into a set of spin-up and spin-down levels (Zeeman levels), each separated by $g\mu_B B$. Each set of splittings leads to quantum oscillations of the same frequency [2] but with a phase difference equal to the field independent ratio $g\mu_B B/\hbar\omega_c$ and hence to a reduction factor (R_S) [2]. The value of g may differ from the free electron value because of the effects of spin-orbit coupling and exchange interactions on the spin moment.

$$R_S = \cos(\pi p S), \text{ where } S = \frac{1}{2} mg \tag{2.20}$$

After correcting (2.14) and (2.15) by including the reduction factors R_T, R_D and R_S the oscillatory magnetisation as obtained by Lifshitz and Kosevich, may be written as

$$\tilde{\mathbf{M}} \propto T\left(\frac{B}{\left|\partial^2 A/\partial k_{\parallel}^2\right|}\right)^{1/2} \sum_{p=0}^{\infty} \frac{1}{p^{3/2}} \frac{e^{14.7 pmT_D/B}}{\sinh(14.7 pm/B)} \cos(p\pi S) \sin\left[2\pi p\left(\frac{B_F}{B} + \phi\right)\right] \tag{2.21}$$

$$\textit{i.e.} \quad \tilde{\mathbf{M}} \propto \left(\frac{B}{\left|\partial^2 A/\partial k_{\parallel}^2\right|}\right)^{1/2} \sum_{p=0}^{\infty} \frac{1}{p^{3/2}} R_T R_D R_S \sin\left[2\pi p\left(\frac{B_F}{B} + \phi\right)\right]$$

A rather similar expression can be written for the more indirect Shubnikov-de Haas effect (oscillatory magnetoresistance), derived from the rather elaborate theory of Adams and Holstein. This requires a knowledge of relaxation processes in magnetic

fields [5]. The expression for the oscillatory magnetoresistance is $\tilde{\rho}(B,T) \propto R_T R_D R_S \tilde{D}$, although one must remember that the oscillatory magnetoresistance will be scaled by the classical, temperature dependent, background magnetoresistance.

As already pointed out, the measured oscillation frequency B_F is directly related to an extremal area of Fermi surface (this is usually obtained using a Fourier transform of the oscillatory phenomenon), thus making it possible to extract information about the shape of the Fermi surface from measurements of B_F as a function of the crystallographic orientation. The carrier effective mass may be obtained by a direct fit of the temperature dependence of the oscillation amplitude (at a constant field) to the Lifshitz-Kosevich formula (2.21). The scattering rate of the carriers may also be determined by fitting the field dependence of the oscillation amplitude (at a constant temperature) to (2.21).

Other phenomena complicate the observation and interpretation of the de Haas-van Alphen and Shubnikov-de Haas effects. One is as magnetic breakdown (see this work chapter 3); in sufficiently strong magnetic fields carriers can *tunnel* from an orbit on one part of the Fermi surface to another part, if these are separated by a small enough energy barrier [2,3]. Another complication is the Shoenberg magnetic interaction [2] which was proposed to explain the abnormally rich harmonic content in certain samples; this results from the fact that the actual magnetic flux density that affects the carriers is $\mathbf{B} = \mu_0(\mathbf{H} + \mathbf{M})$, where $\mathbf{H}$ is the applied magnetic field and $\mathbf{M}$ is the magnetisation which also contains the oscillatory de Haas-van Alphen components, causing feedback [6].

2.4 Quantum oscillations in ET salts

The layered arrangement of molecules in ET charge transfer salts leads to a simple Fermi surface topology, making the salts ideal for the study of band formation.

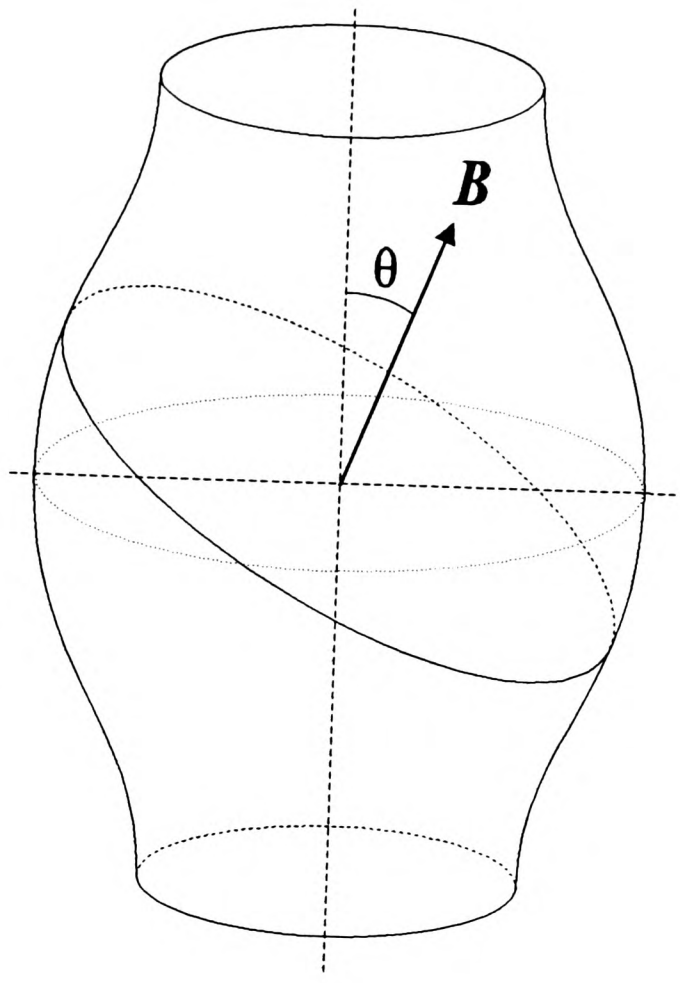

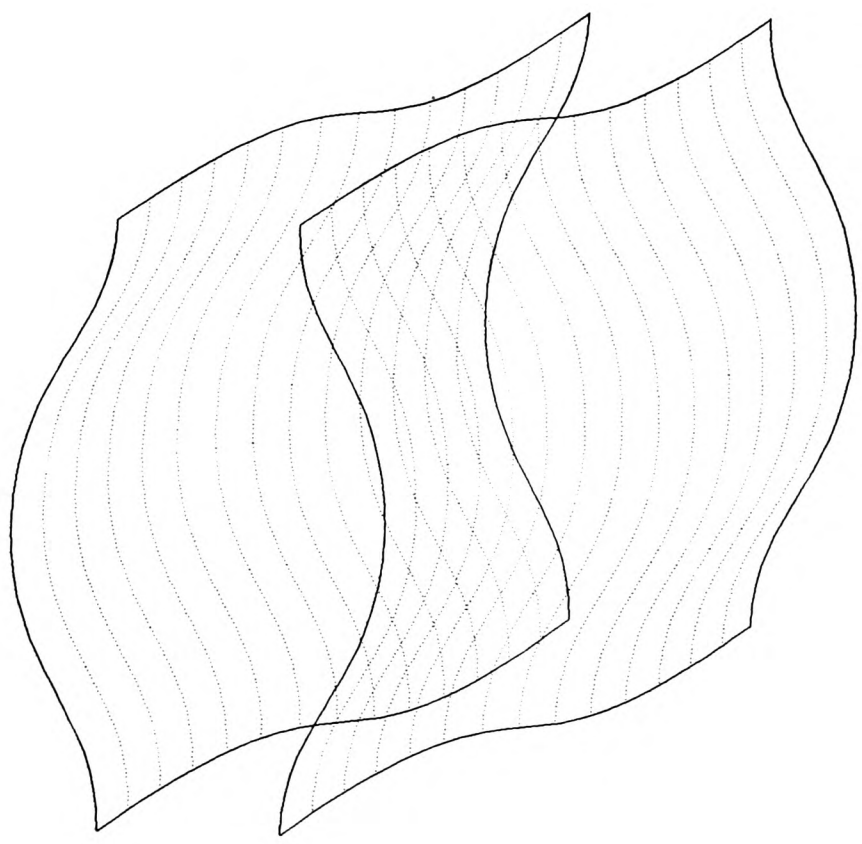

Figure 2 Schematic representation of a (a) Warped cylindrical (quasi-two-dimensional) Fermi surface showing the extremal orbit area in a tilted field; (b) Warped quasi-one-dimensional Fermi surface. The warping in this figure is greatly exaggerated.

Typically the bandstructure computed from the measured crystal parameters possesses a Fermi surface consisting of quasi-two-dimensional and quasi-one-dimensional sections.

In the interlayer (z) direction there is a small but significant orbital overlap (*e.g.* $t_{(x,y)} \approx 100-150\,\text{meV}, t_z \approx 0.5\,\text{meV}$) which leads to *warping* or corrugation of the tubular Fermi surface and Fermi sheets. Figure 2 shows a schematic representation of the warped quasi two-dimensional and quasi one-dimensional Fermi surface sections. In practice the warping in ET salts is so small that the fundamental field (*i.e.* extremal orbit area) measured in the Shubnikov-de Haas oscillations obeys the two-dimensional relationship

$$B_F(\theta) = \frac{B_F(0)}{\cos(\theta)} \tag{2.22}$$

as does the carrier effective mass [7]. In only one case in which the insulating anion layer is rather thin (β-ET_2I_3 [8]) does the warping of the cylindrical Fermi surface lead to two slightly different extremal Fermi surface areas yielding a distinctive beating pattern in the Shubnikov-de Haas oscillations. Fermi surface warping is also essential for both one (Osada effect [9]) and two (Yamaji-Kartsovnik effect [10,11]) dimensional angle dependent galvanomagnetic oscillations; these issues are discussed at length in chapter 5.

References

[1] *Solid State Physics*, N.W. Ashcroft and N.D. Mermin, HRW International editions (1976).

[2] *Magnetic Oscillations in Metals*, D. Shoenberg, (Cambridge University Press, 1984).

[3] *Electrons at the Fermi surface*, edited by M. Springford, Cambridge University press.

[4] R.B. Dingle, *Proc. Roy. Soc. Lond.*, **A211** 517 (1952).

[5] E.N. Adams and T.D. Holstein, *J. Phys. Chem. Solids*, **10** 254 (1959).

[6] Dr. M. Doporto, D. Phil Thesis Chapter 6, Oxford University.

[7] M. Doporto, F.L. Pratt, J. Singleton, M. Kurmoo and W. Hayes, *Phys. Rev. Lett.* **69** 991 (1992).

[8] W. Kang, J.R. Cooper and D. Jerome, *Synth. Metals* **42** 2467 (1991).

[9] T. Osada, R. Yagi, S. Kagoshima, N. Miura, M. Oshima, and G. Saito, *Phys. Rev.* **B 41**, 5428 (1990).

[10] K. Yamaji, *J. Phys. Soc. Jap.* **58**, 1520 (1989).

[11] M. V. Kartsovnik, A. E. Kovalev, V. N. Laukhin, and S. I. Pesotskii, *J. Physique I* **2**, 223 (1992).

Chapter 3

Fermi surface studies of κ-$(ET)_2Cu(NCS)_2$ at high magnetic fields and pressures: The relationship between carrier effective mass and superconductivity

3.1. Introduction

One of the most striking features of superconducting ET charge transfer salts is the rapid decrease of the superconducting critical temperature (T_c) with increasing pressure [1]. This led to the idea of applying 'negative pressure' in order to increase the superconducting T_c in ET salts. Negative pressure can be achieved using chemical synthesis to construct larger anions in order to expand the volume of the unit cell. Using this approach κ-$ET_2Cu(NCS)_2$, a superconductor at 10.4 K, was synthesised in 1988 by Urayama *et al.* [2]. Figure 1 clearly shows the positive, almost linear relationship between T_c and the unit cell volume in ET salts. This approach has continued to be successful not only in the ET salts, but also in the recently discovered alkali-doped C_{60} family of superconductors. Without detailed knowledge of the variation of the bandstructure with pressure it is difficult to envisage the mechanisms behind this relationship.

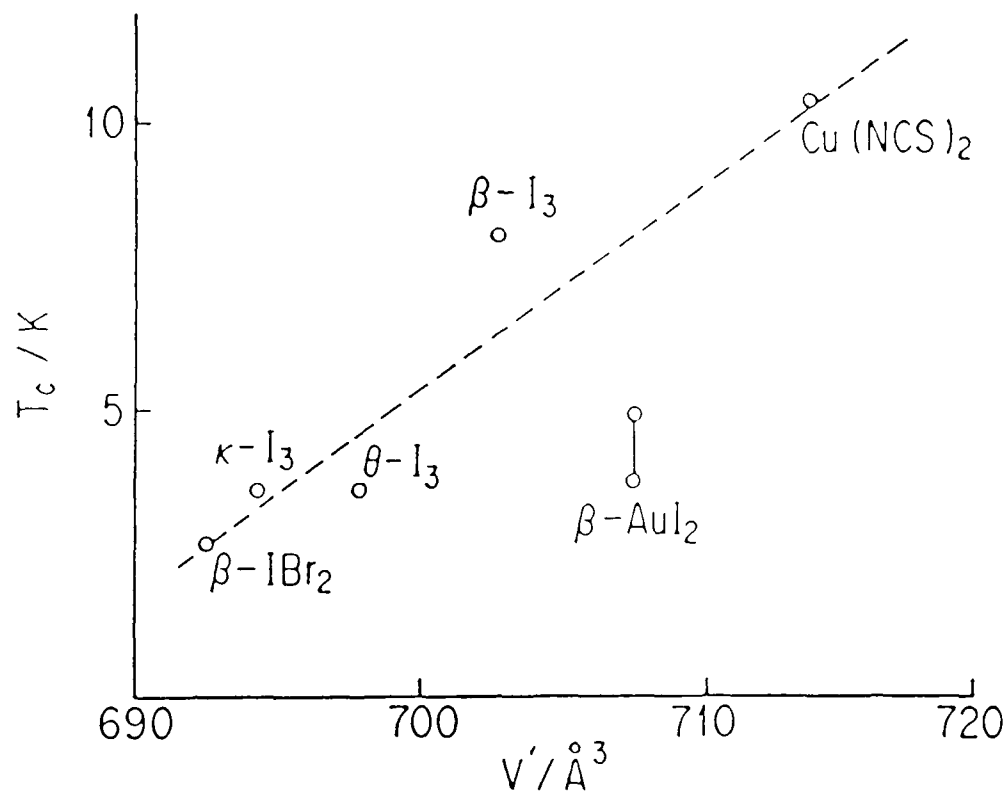

Figure 1 Dependence of the superconducting T_c on the effective volume V_{eff} per ET molecule for several ET_2X compounds [1].

The well separated molecular orbitals and the layered structural arrangements in ET charge transfer salts [3] lead to relatively simple two-dimensional Fermi surface topologies, making the salts ideal for the study of the relationship between bandstructure and electronic properties such as superconductivity. In this context $\kappa-ET_2Cu(NCS)_2$ is an excellent model system. Bandstructure calculations using the room temperature crystal parameters yield a rather simple Fermi surface consisting of a quasi-two dimensional hole pocket plus a quasi-one dimensional electron section [2]. Furthermore, as will be seen below, excellent crystals of the material are available, so that phenomena such as the Shubnikov-de Haas effect may be readily observed, enabling the Fermi surface topology to be measured accurately.

The study in this chapter was motivated by the opportunity to vary the superconducting properties using pressure and to observe simultaneously bandstructure parameters such as the carrier effective mass and Fermi surface pocket area using the Shubnikov-de Haas effect. Thus the bandstructure and quasiparticle properties which determine the superconducting behaviour can be deduced. The carrier effective mass measured by the Shubnikov-de Haas effect is found to fall rapidly with increasing pressure in the region below a critical pressure P_c~5 kbar. Above P_c a much weaker pressure dependence is observed. The superconducting T_c also falls rapidly with pressure, extrapolating to zero around P_c. This strongly suggests that the enhancement of the effective mass and the superconducting transition are directly related in this organic superconductor.

This chapter is organised as follows; the electronic bandstructure, properties and experimental arrangements are described in § 3.2 and § 3.3. The experimental findings at ambient pressure and under hydrostatic pressure are described in § 3.4. To assist in the understanding of the effects of various interactions on the carriers in $\kappa-ET_2Cu(NCS)_2$ a simple model of the bandstructure is used to obtain the variations of the Fermi surface shape and the carrier band mass with pressure in § 3.5-1. The effects of electron-phonon and quasiparticle interactions in renormalising the effective masses are discussed in § 3.5-2. The effects of pressure on the superconducting

properties and the electronic bandstructure is discussed in § 3.5-3: here the experimental data will also be modelled using several current theories of superconductivity. A concluding summary is given in § 3.6.

3.2. Structure, bandstructure and properties of κ-ET$_2$Cu(NCS)$_2$.

In the κ arrangement a two dimensional ET layer is sandwiched in the ***b-c*** plane between Cu(NCS) anion layers (figure 2a) [2]. Two ET molecules form a dimer, and pairs of dimers are arranged almost perpendicularly to one another (figure 2b). The anions form zig-zag polymer-like chains ····SCN-Cu-NCS····along the ***b***-axis (figure 2c). There are two chemical formula units per unit cell. The terminal ethylene end groups of the ET molecule hydrogen bond to the nitrogen and sulphur atoms on the anion polymer. The layered crystal structure has a monoclinic unit cell of the P2$_1$ space group: ***a***=16.242Å, ***b***=8.448Å, ***c***=13.136Å, with an angle between the ***a*** and ***c***-axes of β=110.32° (interlayer separation a_{int}=15.23Å=16.24Å×*sin*(110.3°) along ***a****) and a unit cell volume of V=1690Å^3.

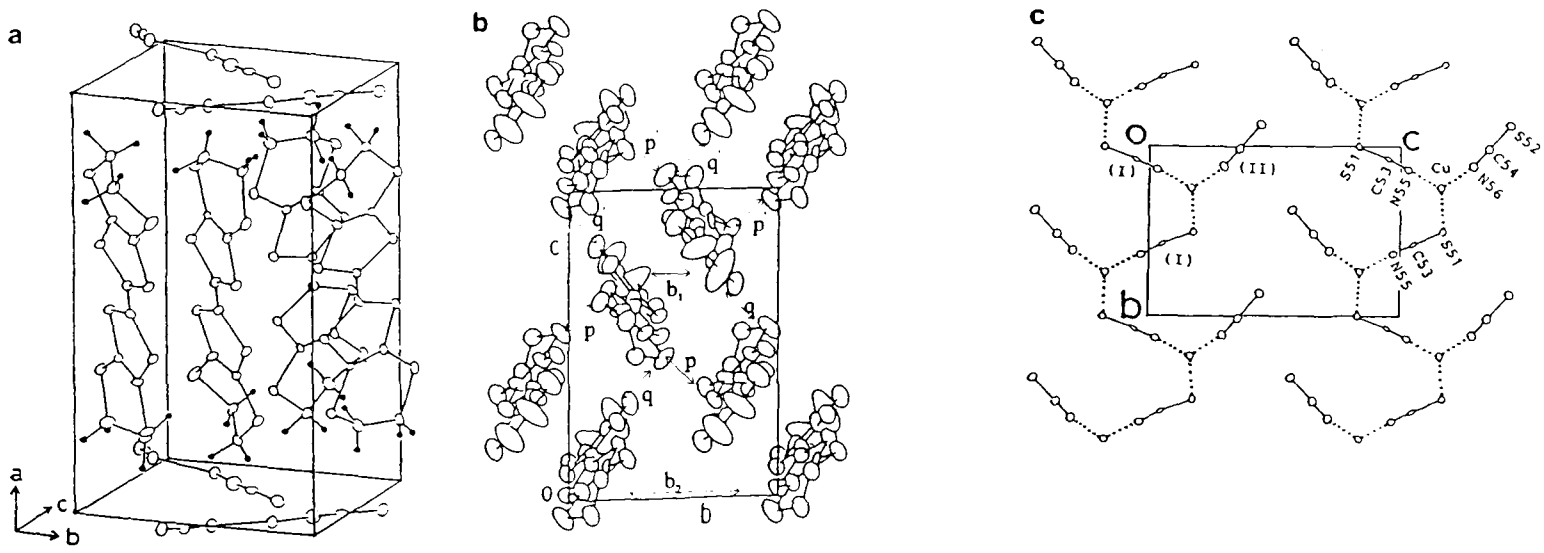

Figure 2 Crystal structure of κ-ET$_2$Cu(NCS)$_2$; (a) unit cell structure, (b) arrangement of ET molecules and (c) anion structure [2].

The result of a two-dimensional tight binding calculation (*i.e.* the dispersion for the direction normal to the two-dimensional ET plane is neglected) using the extended Hückel method is shown in figure 3. As $\kappa-ET_2Cu(NCS)_2$ has four ET molecules per unit cell there are four energy bands produced by the calculation. The intra-dimer overlap of the transfer intergrals is considerably larger than any other overlap; according to the calculation the upper two energy bands and the lower two energy bands are split by the dimerisation gap. There is one hole for every four states. The holes can move via the π-orbitals of the carbon and sulphur atoms. The molecular π-orbitals extend perpendicular to the molecular plane and overlap not only *face-to-face* but also *side-to-side*. The corresponding Fermi surface is shown in figure 4. The whole Fermi surface may be viewed as a cylinder with a slightly elliptical cross section which crosses the Brillouin zone boundary in the ***c*** direction. The band filling in $\kappa-ET_2Cu(NCS)_2$ means that the whole Fermi surface has the same area as the first Brillouin zone. The unit cell contains two dimers; a slight non-symmetrical positioning of the two molecules in each dimer causes the degeneracy along the ZM line (figure 4) to be lifted, splitting the Fermi surface at the ZM zone boundary into a cylindrical closed pocket centred at the Z point (18 % of the Brillouin zone area) and a warped open section running along the k_c direction.

The electrical conductivity in the ***b-c*** plane is rather isotropic, and at 10-50 Scm^{-1} at room temperature some three orders of magnitude lower than that of copper. Perpendicular to the two-dimensional planes the conductivity is about ~600 times lower than that in the ***b-c*** plane. Measurements of the plasma frequency using polarised infrared reflectivity have confirmed the isotropy in the ***b-c*** plane [5]. The temperature dependent electrical resistance has a rather anomalous feature at about 100 K [6]; it shows a broad maximum and then suddenly decreases by two to three orders of magnitude with decreasing temperature; anomalies in the susceptibility, far- and mid-infrared optical conductivity and thermal expansion also occur at this temperature. These anomalies are probably due to a structural transition. X-ray measurements have shown that the interlayer spacing, $\boldsymbol{a}^*$ is a maximum at around

100 K [7] but the reasons for this are not clear at present. The resistance upturn is also suppressed by hydrostatic pressure [8].

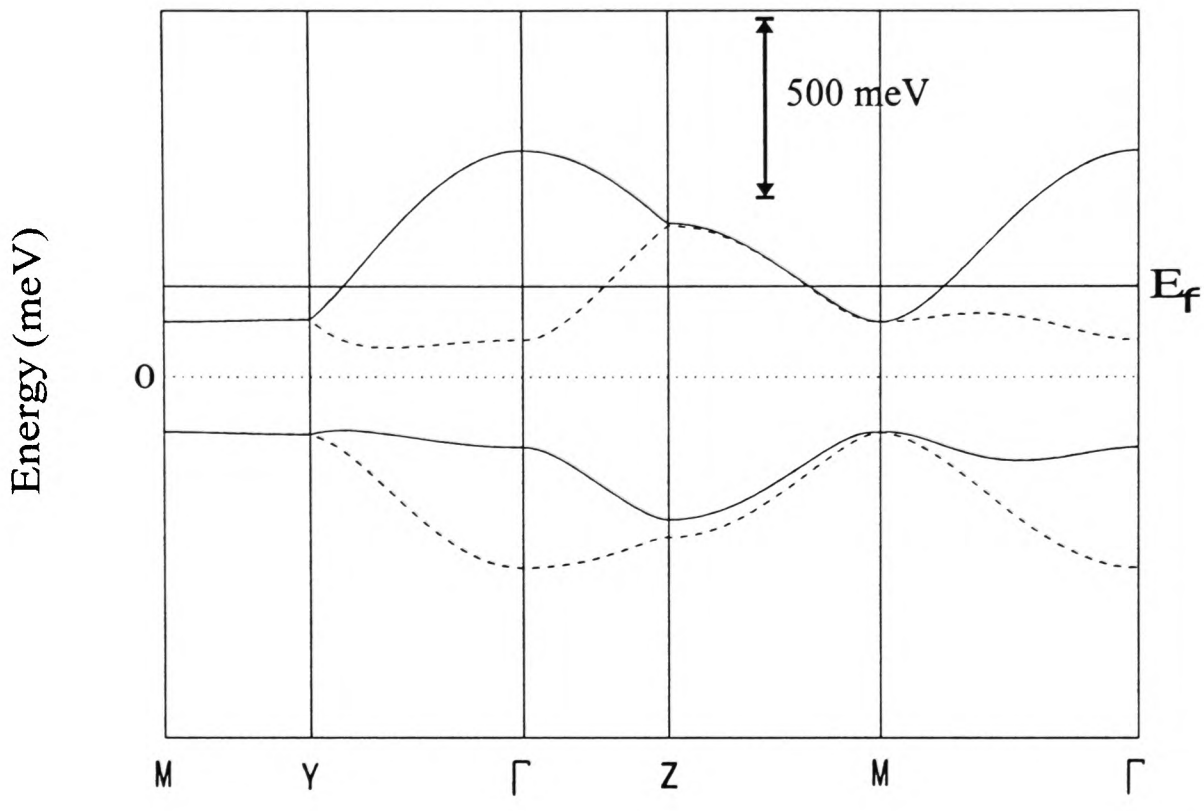

Figure 3 Calculated band structure of κ - $ET_2Cu(NCS)_2$ [4].

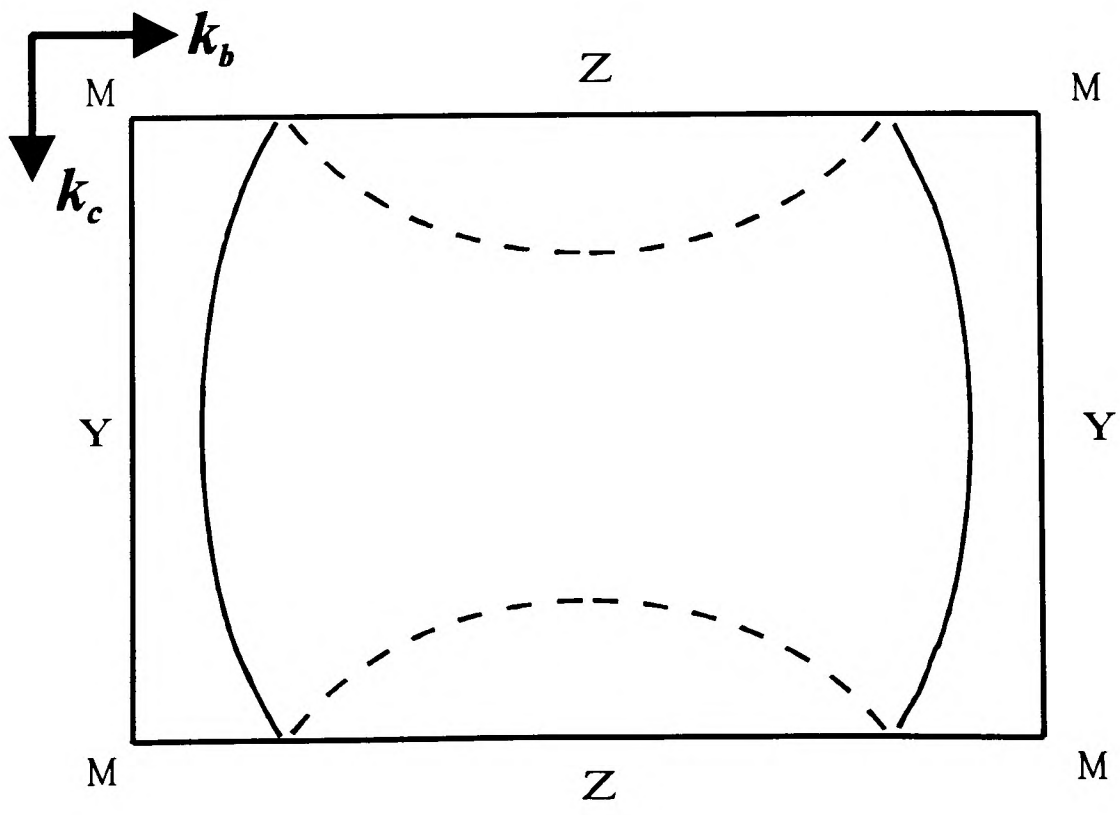

Figure 4 The Brillouin zone and Fermi suface of κ - $ET_2Cu(NCS)_2$ [4].

3.3. Experimental techniques

Single crystals of κ-$ET_2Cu(NCS)_2$ (prepared electrochemically by M. Kurmoo) are generally small (1x1x0.1 mm^3) black hexagonal platelets, with the plane of the plate corresponding to the highly conducting two-dimensional layers. Electrical contacts for ambient pressure measurements were made directly to the sample surface using Platinum paint. For high pressure studies contacts were made with silver epoxy to evaporated gold pads on both platelet faces, resulting in contact resistances of less than 10 Ω. Standard 4-wire AC techniques (5-150 Hz), with the current applied perpendicularly to the sample two-dimensional planes (***a****-direction), were used for all measurements in this chapter. To avoid sample heating, currents were generally 0.2-20 μA. A photograph of the κ-$ET_2Cu(NCS)_2$ crystal used for the ambient pressure magnetoresistance experiments is shown in figure 5.

Magnetoresistance experiments under hydrostatic pressure were carried out using a non-magnetic clamp cell (a schematic of the cell is shown in figure 6) filled with a petroleum spirit medium providing pressures up to 16.5 kbar at helium temperatures. In trial measurements a mixture of equal quantities of n-pentane and iso-pentane was tried as a pressure medium because of its well known properties at high pressures and low temperatures. Unfortunately the pentane mixture evaporated very quickly whilst the sample was being positioned inside the pressure cell, resulting in air bubbles in the sample chamber. Although one measurement was successful using the pentane mixture, in general the pentane mixture was too difficult to use as a pressure medium and therefore all measurements described in this chapter were obtained using petroleum spirit. Pressure was applied at room temperature using a hydraulic press, after which the cell was placed in a specially designed ^{3}He cryostat providing temperatures down to 500 mK in a 17 T superconducting magnet. Cooling from room temperature to 4.2 K was achieved over a period of around 12 hours, to ensure that the pressure was ideally hydrostatic at low temperatures. Indeed, the applied pressures were reasonably hydrostatic as under pressure the observed Shubnikov-de Haas

oscillations were visible down to magnetic fields of ~5 T, implying that phase smearing and hence inhomogeneity were weak.

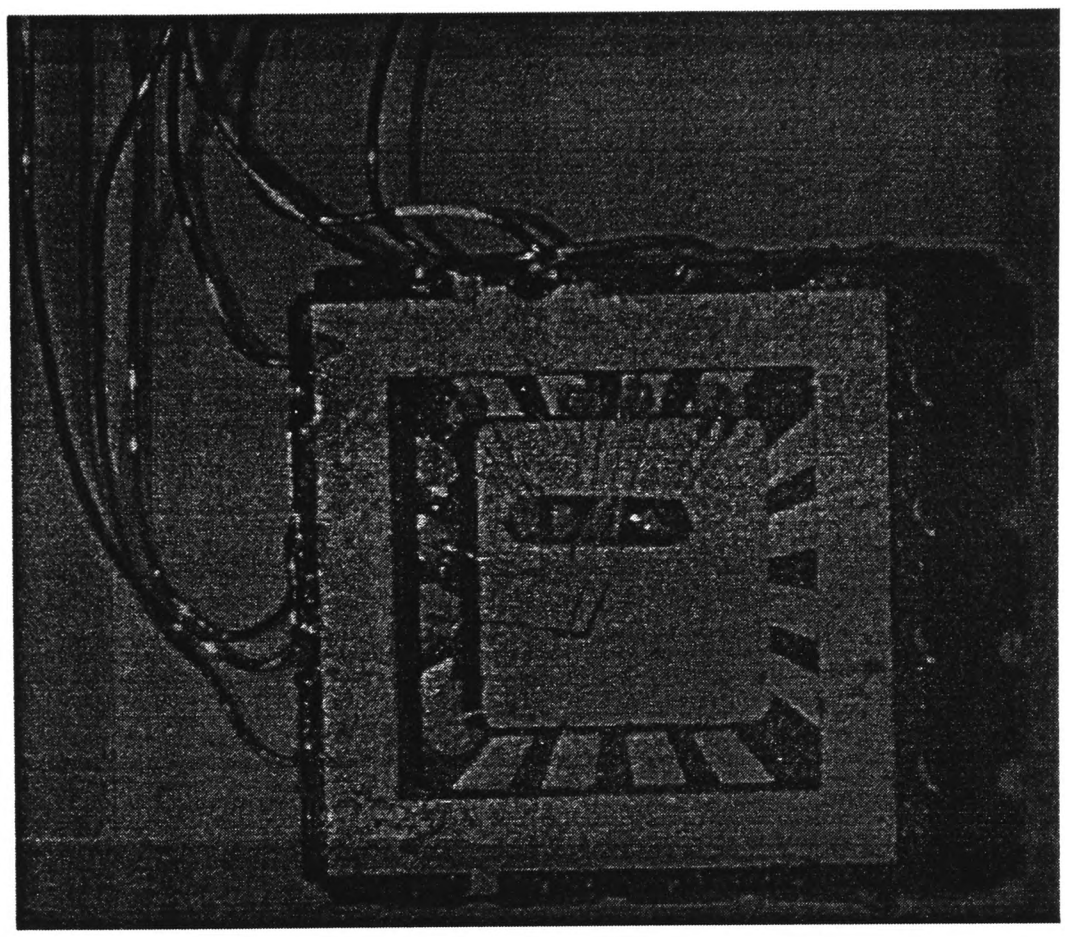

Figure 5 A photograph of the κ-$ET_2Cu(NCS)_2$ crystal used for the ambient pressure magnetoresistance experiments.

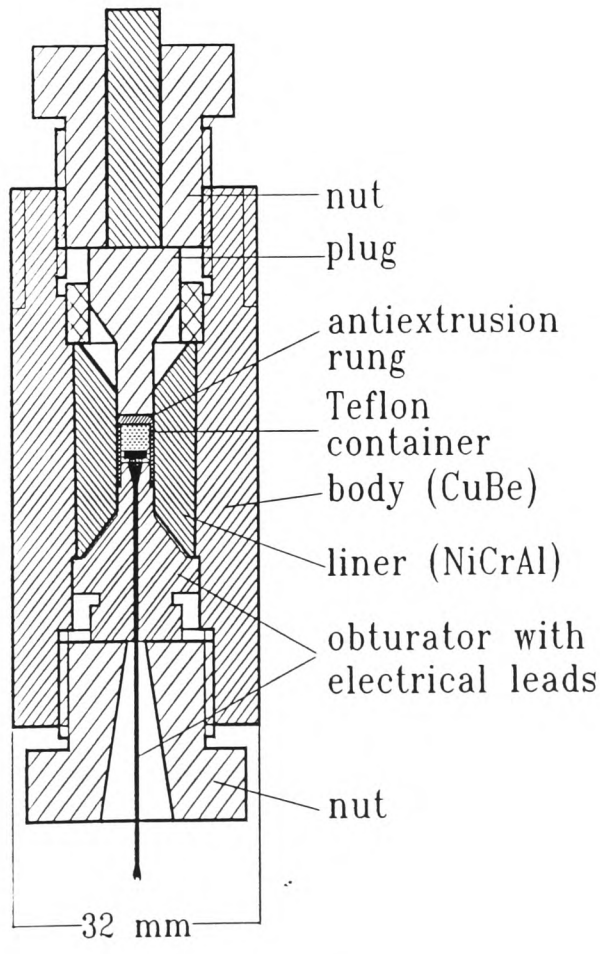

Figure 6 A schematic diagram of the pressure cell used in the experiments.

Furthermore under pressure the transition to superconductivity is found to be sharp, also providing evidence for hydrostatic conditions. The temperature of the sample could be varied between 500 mK and 5 K by a heater and by controlling the vapour pressure of the ^{3}He and ^{4}He. The temperature was measured using a calibrated ruthenium oxide resistor, and the pressure in the cell at all temperatures was monitored using the resistance of Manganin wire with a known pressure and temperature coefficient [9]. Ambient pressure measurements up to 25 T were carried out at Nijmegen in a similar ^{3}He cryostat. In that case, the temperature of the sample could be varied and stabilised between 500 mK and 15 K by use of a heater controlled by a capacitor with a known temperature coefficient in a negative feed-back circuit.

3.4. Experimental results

3.4-1. The Fermi surface at ambient pressure.

Experimental tests of models for superconductivity require a knowledge of the density of states at the Fermi energy, and so a good starting point is a material with a simple Fermi surface. In this context $\kappa-ET_2Cu(NCS)_2$, a superconductor with T_c~10.4 K, is very useful; it has a readily calculated Fermi surface consisting of a quasi-two dimensional closed hole pocket and an open quasi-one dimensional electron section, separated by a small gap (figure 4). Figure 7 shows typical magnetoresistance data for $\kappa-ET_2Cu(NCS)_2$, and illustrates a further attractive feature of this material; the magnetoresistance data exhibit strong Shubnikov-de Haas oscillations. The frequency F_α=600±5T of the Shubnikov-de Haas oscillations enables the area of the closed quasi-two dimensional hole pocket to be deduced (Fermi surface area $S_F = \pi k_F^2 = 5.73 \times 10^{14} cm^{-2}$; as b=8.402 Å and c=12.833 Å then the Brillouin zone area $S_{BZ} = 4\pi^2 / bc = 3.66 \times 10^{15} cm^{-2}$ hence $S_F / S_{BZ} = 15.6\%$ of the Brillouin zone); the value is consistent with calculations in which the area of this pocket is predicted to be 16-20 % of the first Brillouin zone area, S_{BZ} [2]. Furthermore the

temperature dependence of the Shubnikov-de Haas oscillation amplitude may be fitted to the Lifshitz-Kosevich formula to give the hole effective mass [10], $m_\alpha^* = 3.5m_o$.

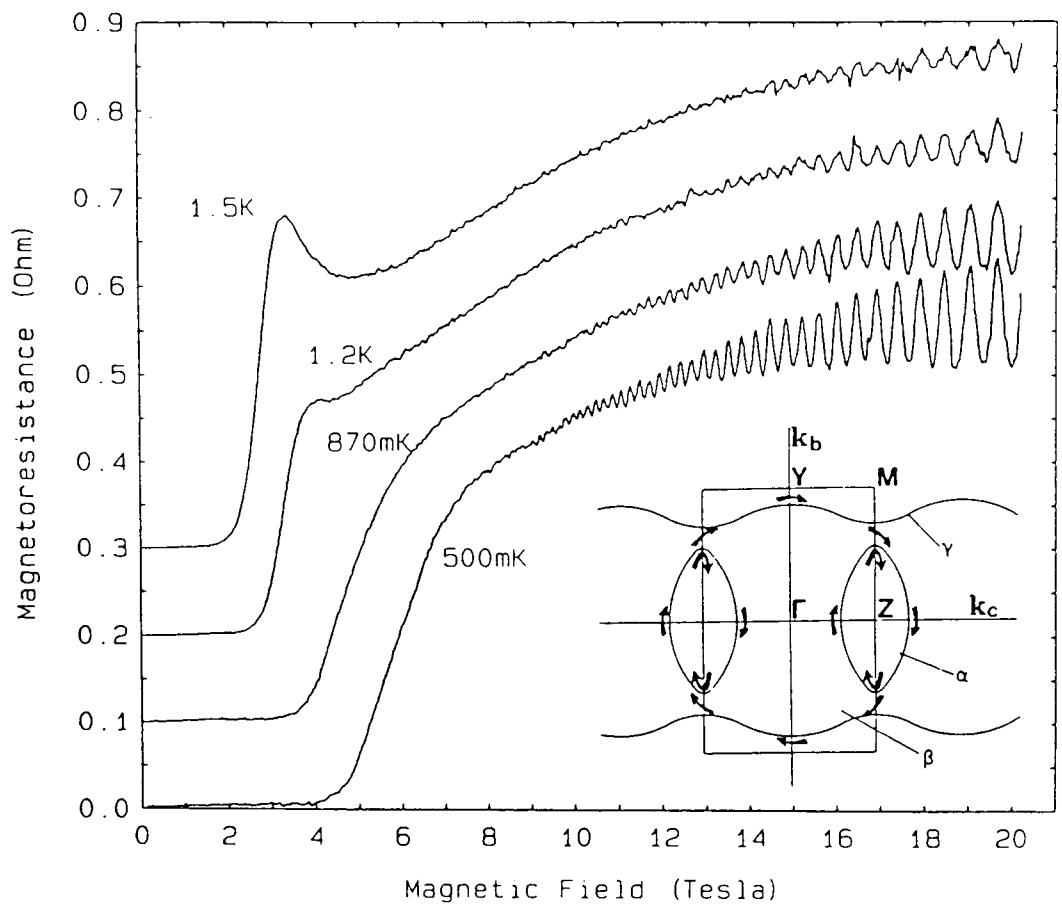

Figure 7 Magnetoresistance of $\kappa-ET_2Cu(NCS)_2$ (magnetic field applied perpendicular to conducting planes) for four different temperatures. The data are offset for clarity. The inset shows calculated Fermi surface of $\kappa-ET_2Cu(NCS)_2$ and the α and β orbits (inset taken from [11]).

In order to understand the complete Fermi surface, however, one also needs to measure the quasi-one dimensional open section of the Fermi surface and the effective mass associated with it. The application of magnetic fields >~14T resolves this problem by permitting the observation of magnetic breakdown [10], visible as a series of Shubnikov-de Haas oscillations of a higher frequency superimposed on the fundamental series (figure 8). Magnetic breakdown is due to electrons tunnelling

between states of equal energy in adjacent sections of Fermi surface when the cyclotron energy is of the order of the splitting between the associated bands, thus describing a larger *k*-space orbit; the inset to figure 7 indicates a breakdown orbit in $\kappa-ET_2Cu(NCS)_2$ around the outer edges of both the quasi-two dimensional and the quasi-one dimensional Fermi surface sections [11-14] (the β-orbit).

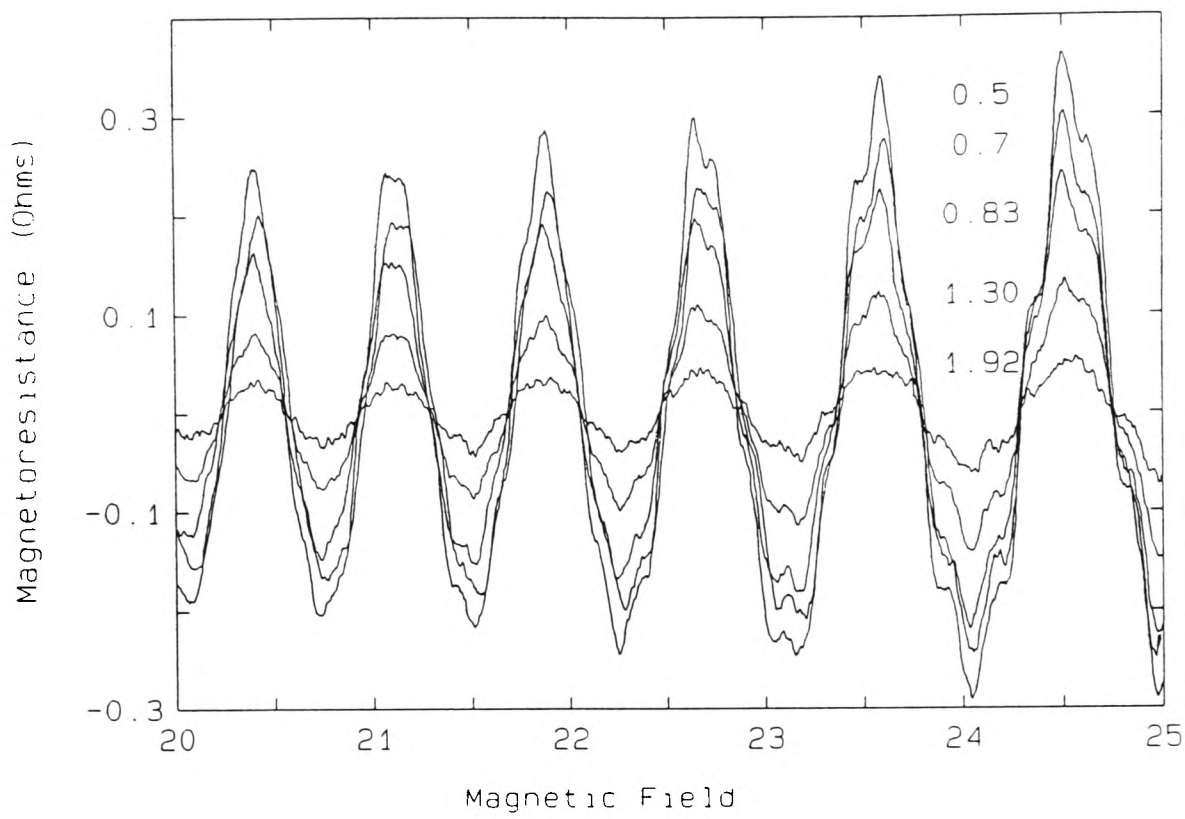

Figure 8 Detail of Shubnikov-de Haas oscillations in $\kappa-ET_2Cu(NCS)_2$, showing structure due to breakdown oscillations. The temperatures for the different data sets are shown (in K) in the figure; the oscillations are attenuated by increasing temperature.

A fast Fourier transform of the data (figure 9) reveals extra Shubnikov-de Haas oscillation frequencies due to the magnetic breakdown. Note that prior to the Fourier transformation the reciprocated data has been numerically differentiated once in order to enhance the higher frequency oscillations with respect to the lower frequency ones. The central peak has a frequency F_β=3919±30 T, and corresponds to the orbit about both the quasi-two dimensional and quasi-one dimensional sections (i.e. the whole Fermi surface) indicated in figure 1; this assignment is possible as the F_β frequency

corresponds to the full area of the Brillouin zone, and this is defined by the band filling in $\kappa-ET_2Cu(NCS)_2$ irrespective of the details of the Fermi surface [2,11-14]. The other two peaks correspond to $F_\beta \pm F_\alpha$; a surprising aspect of the experimental data is that the Shubnikov-de Haas oscillation amplitude of the difference frequency $F_\beta - F_\alpha$ is larger than that of F_β. The higher combination frequency, $F_\beta + F_\alpha$, observed in the fast Fourier transform may be understood by employing a coupled network model [15] in which carriers can make several paths across the Fermi surface sections. However the difference frequency, $F_\beta - F_\alpha$, is not allowed to exist within the framework of the network model [15] as the direction of the electron motion must be abruptly reversed during a cyclotron orbit [15]. We shall explore the origins of this frequency after discussing the temperature dependence of the various Shubnikov-de Haas oscillations.

The temperature dependence of the Shubnikov-de Haas oscillation amplitudes was measured between 0.5-4.2 K in magnetic fields up to 25 T. Effective masses were determined by fitting the Lifshitz-Kosevich formula to the data (see inset Figure 9) to reveal that $m^*_\alpha = (3.5\pm0.1)m_o$, $m^*_{\beta-\alpha} = (4.7\pm0.4)m_o$, $m^*_\beta = (6.5\pm0.1)m_o$ and $m^*_{\beta+\alpha} = (11\pm2)m_o$, values consistent with those of other workers [11,12] (the data reported here cover a larger temperature range, however). With the exception of $m^*_{\beta-\alpha}$, the values obtained may be understood by noting that each mass corresponds to a transit time around a particular section of Fermi surface. For instance, m^*_α and m^*_β are proportional to the times to traverse the quasi-two dimensional hole pocket and the complete Fermi surface respectively. Therefore $m^*_{\beta+\alpha}$, corresponding to two traverses of the quasi-two dimensional hole section and one of the quasi-one dimensional electron sheets, should be given by $m^*_{\beta+\alpha} = m^*_\alpha + m^*_\beta$; within the experimental accuracy this is true.

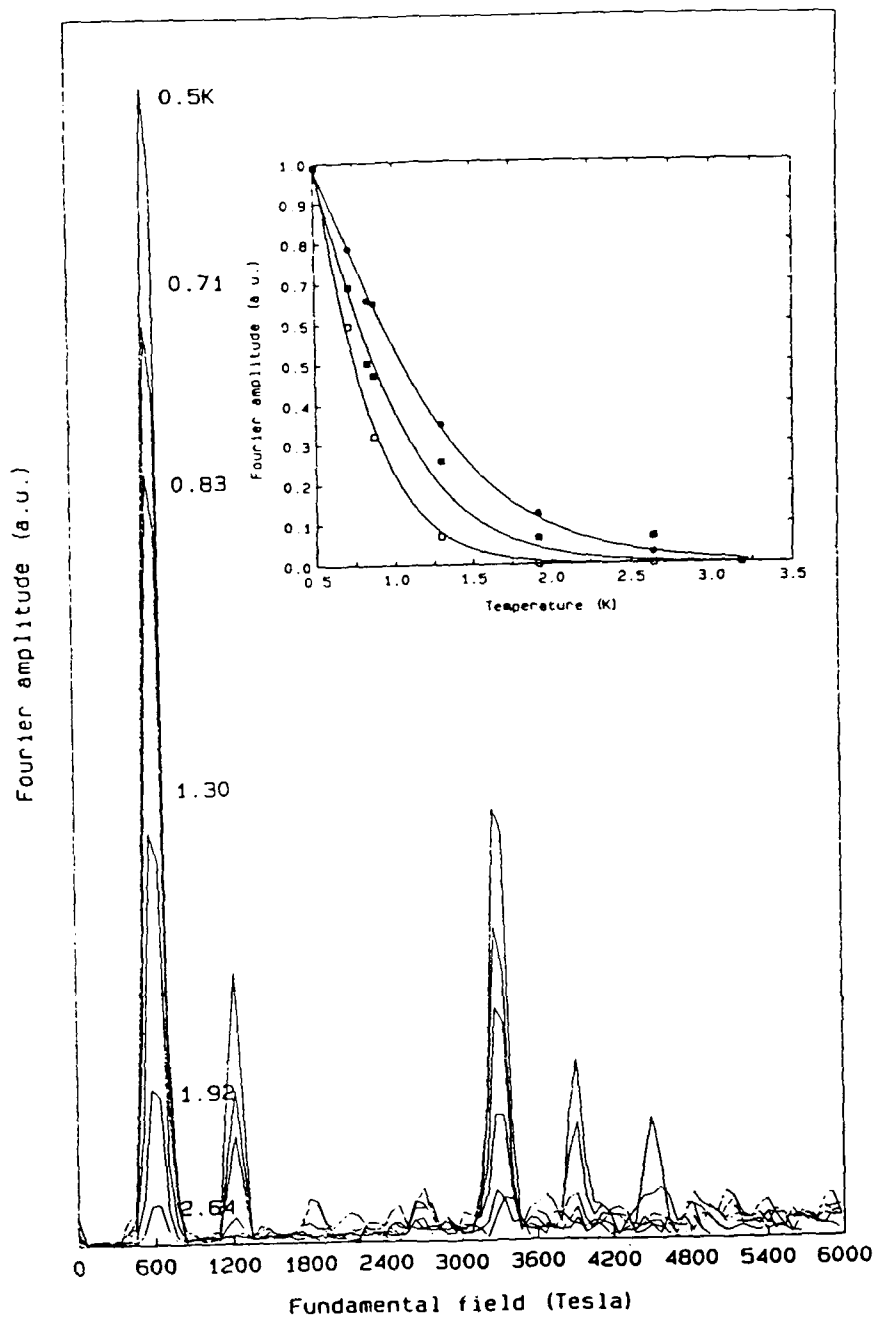

Figure 9 Fourier spectrum of the SdH oscillations. The temperatures for the different data sets are shown (in K) in the figure. The inset shows the temperature dependence of the Shubinikov-de Haas oscillation amplitude. Data for the 610T (dots), 3310T, (filled squares) and 3919T (empty squares) frequencies are shown; the lines are fits to the Lifshitz-Kosevich formula, which yield the effective masses given in the text.

3.4-2. Stark quantum interference in κ-ET$_2$Cu(NCS)$_2$

We now turn to the large amplitude of the difference frequency F_β-F_α in the Shubnikov-de Haas oscillations. This frequency, unlike the sum frequencies F_β+F_α etc., does not correspond to an allowed closed orbit. One mechanism which might lead to the observation of difference frequencies is the Shoenberg magnetic interaction [10],

which has been recently observed in β"ET_2AuBr_2 [16]. This introduces a magnetic feedback term due to the fact that the field experienced by the carriers is $B=\mu_0(H+M)$, where H is the applied field and M is the magnetisation containing the oscillatory de Haas-van Alphen components. The Shoenberg magnetic interaction between the F_β and F_α frequencies could potentially lead to the side-bands found at $F_\beta \pm F_\alpha$ [16]. However, the temperature dependence of the Shubnikov-de Haas oscillations shows the F_β-F_α frequency to be observable at temperatures well above those at which the F β oscillation has disappeared (figure 9), ruling out this possibility.

The most likely mechanism is the transport quantum interference phenomenon described by Shoenberg [10] and Stark and Reifenberger.[17]. In this case the difference frequency F_β-F_α does not arise from orbit quantization but from the electron having two alternative *k*-space paths between two points on the Fermi surface; one path corresponds to a traverse of the two quasi-one dimensional sheets plus one side of the quasi-two dimensional pocket, whilst the other is just the traverse of one side of the quasi-two dimensional pocket. The interference between the two paths causes an alteration in the electron phase (equal to the difference in the phase between the two orbital paths) which appears exactly like a de Haas-van Alphen phase (*i.e.* 'area' in *k* space, although there is no electron which describes this area). Interference of this kind is only observed in transport [10,17]. Only real areas enter into the oscillatory part of the thermodynamical properties; indeed, no evidence of the F_β-F_α frequency was found in de Haas-van Alphen studies [13]. Naively one would expect the temperature and field dependence of the amplitude of the quantum interference oscillations to be related to the average of those orbits involved *i.e.* $m^*_{\beta-\alpha} = (m^*_\beta + m^*_\alpha)/2 = 5.0m_o$ which is approximately equal to the experimentally observed effective mass $m^*_{\beta-\alpha} = (4.7 \pm 0.4)m_o$. One may expect to find a slighty different effective mass, $m^*_{\beta-\alpha}$, to that expected. The two paths around the Fermi surface which make up the difference frequency do involve a different number of magnetic breakdown steps and this is expected to have an effect on their field and

temperature dependences, and hence on the apparent effective mass. Geometrical arguments were applied to the apparent masses of difference frequencies by Heidmann *et al.* [12], who implied that $m^*_{\beta-2\alpha} = 0$ (*i.e.* as $m^*_\beta \sim 7m_o$ and $m^*_\alpha = 3.5m_o$); their arguments are fallacious, as the behaviour of the interference frequencies may only be explained by the application of quantum mechanics. For reference Dingle plots are shown for the α, β and β-α frequencies in figure 10; the α and β orbit Dingle plots reveal similar scattering times. The β-α frequency has a rather short apparent "scattering time". This unusual quantum effect warrants better theoretical understanding and more measurements to fields higher than 25 T.

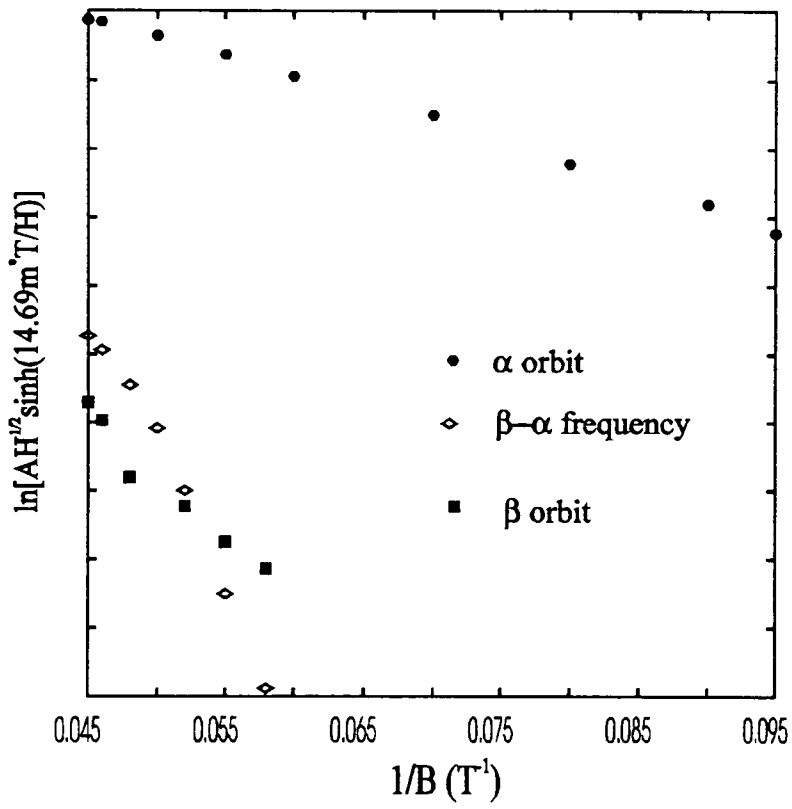

Figure 10 Dingle plot for $\kappa-ET_2Cu(NCS)_2$ at ambient pressure at 0.5 K; data for the α-orbit (filled circles), β-orbit (closed squares) and β-α frequency (open diamonds) are shown.

3.4-3. The Fermi surface under pressure.

One of the most striking features of $\kappa-ET_2Cu(NCS)_2$ is the rapid decrease of its superconducting T_c with increasing hydrostatic pressure (~-3 K/kbar) [18,19], which led to successful proposals for raising the T_c accessible in ET salts using

chemical synthesis [20] (although there was some controversy over the exact pressure dependence of T_c at very low pressures [19]). The following study in this chapter was motivated by the opportunity to vary the superconducting properties using pressure and to observe simultaneously bandstructure parameters such as the carrier effective mass and Fermi surface pocket area using the Shubnikov-de Haas effect. Thus the bandstructure and quasiparticle properties which determine the superconducting behaviour can be deduced.

To test this idea the magnetoresistance experiments in § 3.4-1 were repeated under hydrostatic pressure [22] applied using a clamp cell (figure 6); the cell provides pressures up to 16.5 kbar at temperatures down to 0.5 K in fields up to 18 T.

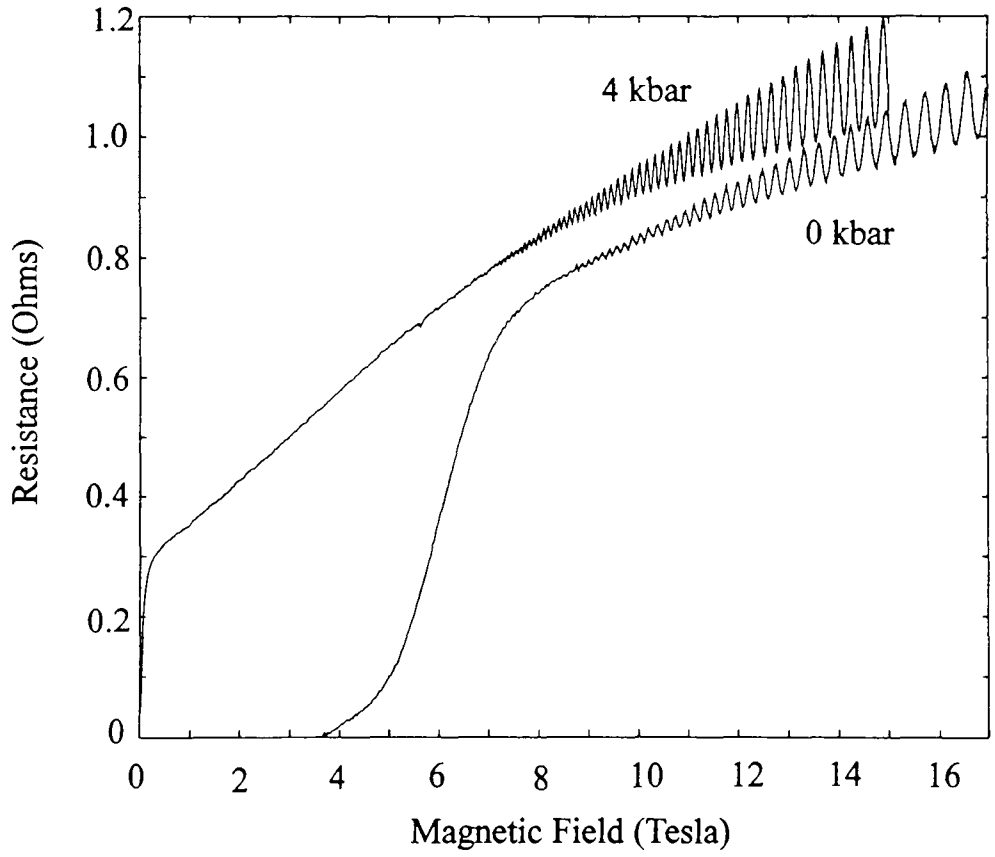

Figure 11 Magnetoresistance of κ-$ET_2Cu(NCS)_2$ at 0.7 K (magnetic field applied perpendicular to the conducting planes) at ambient pressure and at 4 kbar.

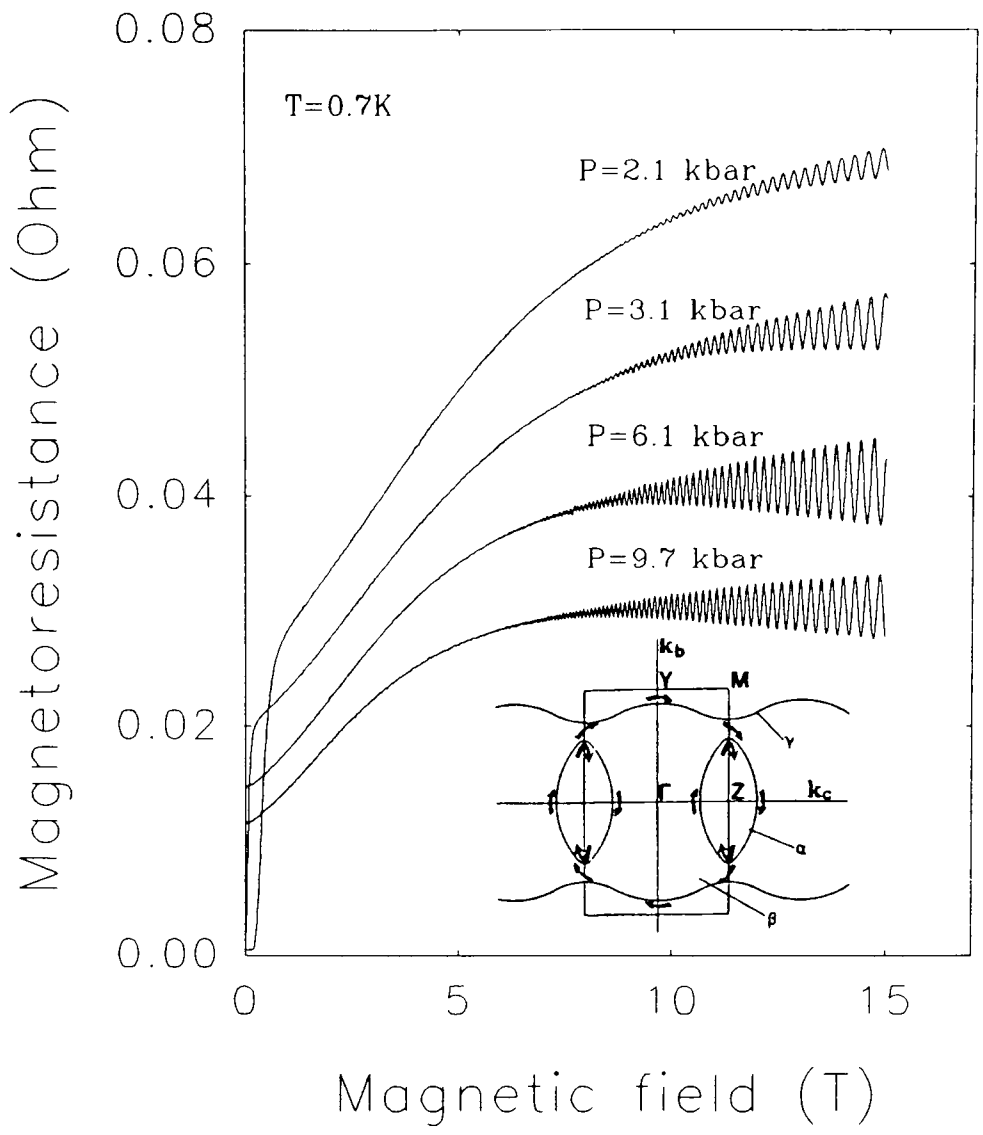

Figure 12 Magnetoresistance of $\kappa-ET_2Cu(NCS)_2$ at 0.7 K (magnetic field applied perpendicular to the conducting planes) for four different pressures. The inset shows the Brillouin zone, Fermi surface and α and β orbits (after Reference [11]).

The magnetoresistance of $\kappa-ET_2Cu(NCS)_2$ at 0.7 K is shown for a number of hydrostatic pressures in figures 11 and 12. The normal state conductivity of the sample increases with pressure and the upper critical field B_{c2}, observed as a steep drop in resistance to zero, decreases sharply. A series of Shubnikov-de Haas oscillations is observed in the magnetoresistance, and both the amplitude and the frequency of the oscillations are visibly affected by pressure. These oscillations correspond to *k*-space orbits around the quasi-two dimensional hole pocket of the Fermi surface (the α orbit, figure 12, inset). As the pressure is raised further (figure 13), a second series of oscillations with a higher frequency is observed in the magnetoresistance, superimposed on the oscillations due to the α-orbit. Similar high frequency oscillations were observed between 20 and 25 T at ambient pressure (see § 3.4-1 figure 8), and are

attributed to magnetic breakdown [11-14]. The inset in figure 12 indicates the primary breakdown orbit (the β orbit) in κ-$ET_2Cu(NCS)_2$ around the outer edges of both the quasi-two dimensional and the quasi-one dimensional Fermi surface sections. With increasing pressure the magnetic breakdown oscillation amplitude increases sharply, indicating that the distance between the open and closed sections of Fermi surface is decreasing (figure 13).

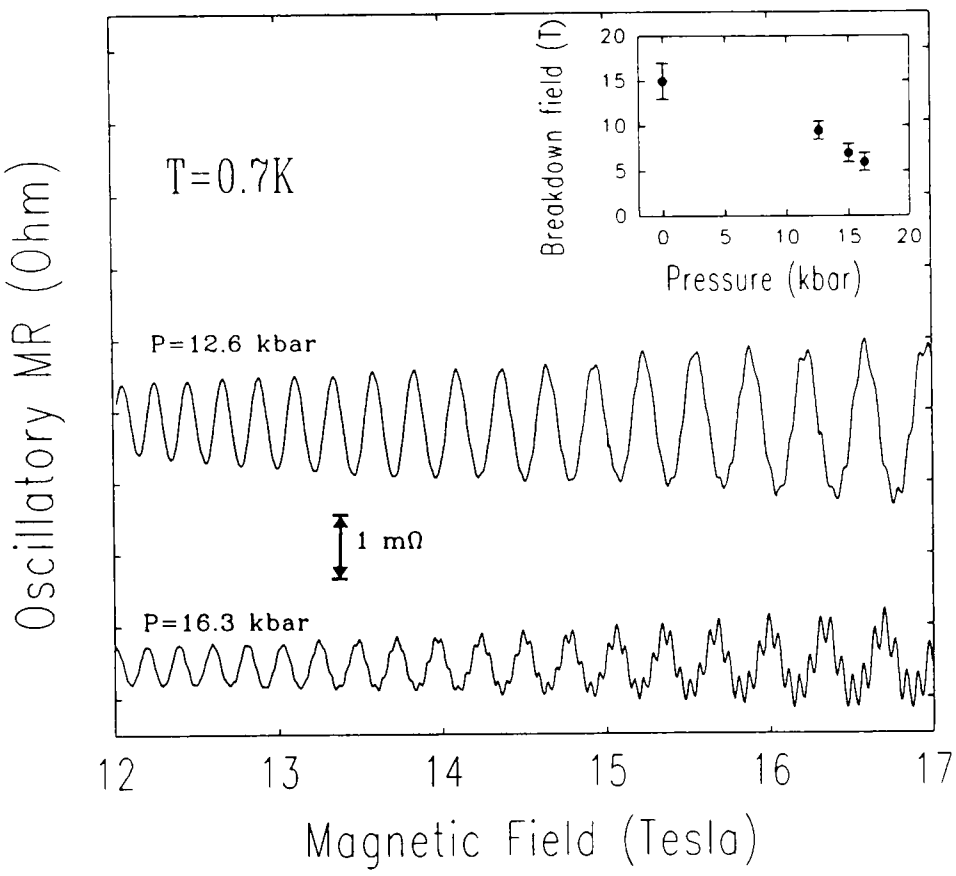

Figure 13 The oscillatory part of the magnetoresistance above 12 T at 0.7 K (magnetic field applied perpendicular to the conducting planes) at two different pressures. The inset shows the characteristic breakdown field B_0 as a function of pressure (see § 3.4-1 for ambient pressure point).

Data similar to those in figures 11 to 13 were Fourier transformed in order to obtain the frequencies of the Shubnikov-de Haas and magnetic breakdown oscillations as a function of pressure; the results of this process are shown in figure 14. The measured α-orbit Shubnikov-de Haas frequency F_α increases rapidly from an ambient pressure value of 600±5 T to 775±5 T at 16.3 kbar. As F_α is directly proportional to

the *k*-space area S_α of the α orbit, this indicates that the quasi-two dimensional section of the Fermi surface has increased in area by around 30%. By contrast, the frequency of the β orbit (3920±10 T at ambient pressure) increases by only 6 % to 4182±10 T over the same pressure range (figure 14, inset). The latter result is not unexpected as the band filling in $\kappa-ET_2Cu(NCS)_2$ means that the β orbit has the same area as the first Brillouin zone so that the slow increase merely reflects the compressibility of the material [21].

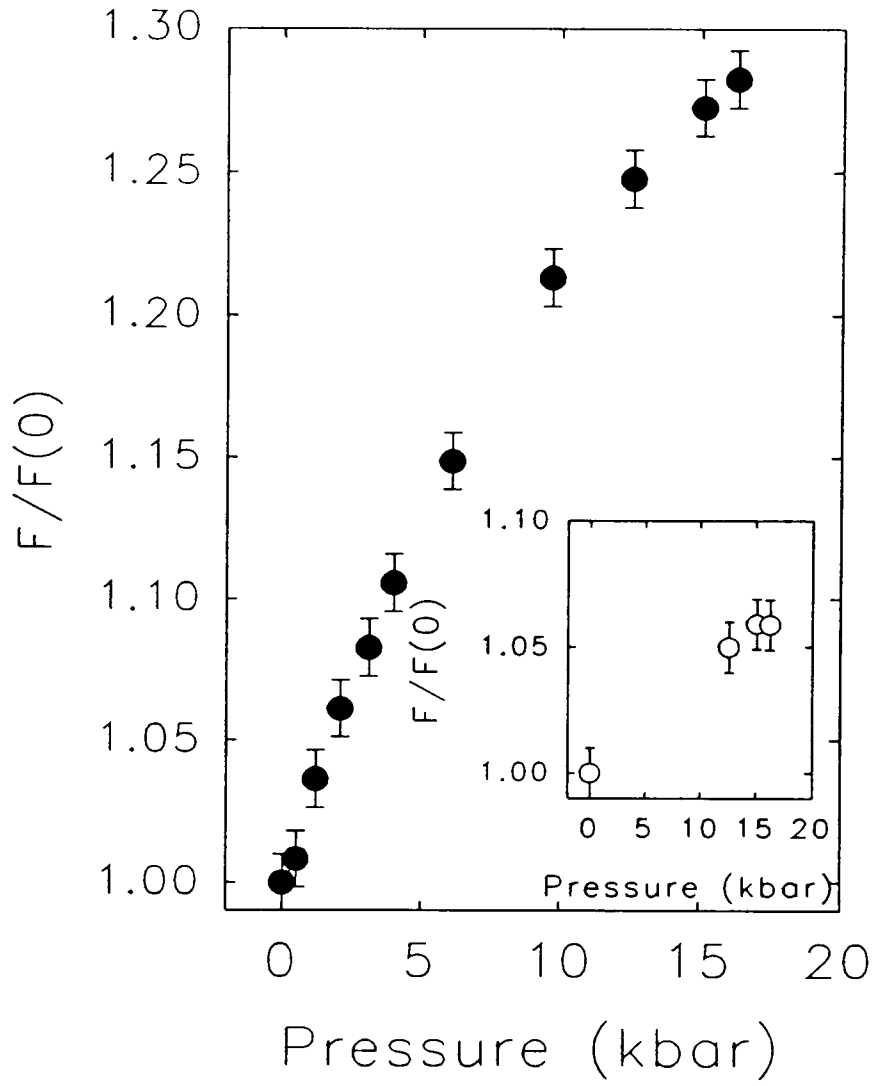

Figure 14 The primary Shubnikov de Haas oscillation frequency F_α normalised to the ambient pressure value as a function of pressure. The inset shows the breakdown frequency F_β normalised to the ambient pressure value versus pressure. The latter frequency corresponds to the full Brillouin zone area.

3.4-4. Carrier effective masses and scattering.

The effective masses associated with the α and β orbits were derived by fitting the temperature dependence of the Shubnikov-de Haas and magnetic breakdown oscillation amplitudes, measured in the temperature range 0.5-5 K at each pressure, to the Lifshitz-Kosevich formula [10]. It should be noted that the interference frequency F β-Fα is only observable just above the noise level at the highest pressures and at the highest magnetic fields attainable. Ignoring the spin-splitting, the field (B) and temperature (T) dependence of the amplitude of the first harmonic of the oscillations is given by [10]:

$$A = \frac{A_o[T\exp(-\lambda\mu T_D / B)\cos(2\pi F / B + \Psi)]}{\sqrt{B}\sinh(\lambda\mu T / B)} \qquad (3.1)$$

where A_o is a constant, $\lambda = 2\pi^2 m_o k_B / eh$, Ψ is an arbitrary phase, T_D is the Dingle temperature and $\mu = m^* / m_o$. As above, F is the frequency of the oscillations. The measured variation of both effective masses with pressure is shown in figure 15. At ambient pressure, m^*_α=3.5±0.1m_o, in good agreement with previous measurements [11-14]. The pressure dependence of m^*_α exhibits two distinct regimes; below a critical pressure P_c , m^*_α decreases approximately linearly with pressure at a rate of $dm^*_\alpha / dP = -0.33m_o$ / kbar, whereas above P_c it decreases at a much lower rate of $\sim -0.04m_o$ / kbar to m^*_α=1.4±0.1m_o at 16.3 kbar. Within the restricted data set available, the effective mass of the magnetic breakdown β orbit, m^*_β, appears to exhibit a similar pressure dependence to m^*_α, initially falling rapidly from an ambient pressure value of m^*_β=6.5±0.1m_o [14] and then decreasing more slowly (m^*_β =3.0±0.1m_o at 12.6 kbar and 2.7±0.1m_o at 16.3 kbar (figure 15). As the background magnetoresistance is almost temperature independent in $\kappa-ET_2Cu(NCS)_2$ the background, or classical, magnetoresistance was simply subtracted from the

experimental data in the analysis of the effective mass (for more discussion on this point see chapter 5).

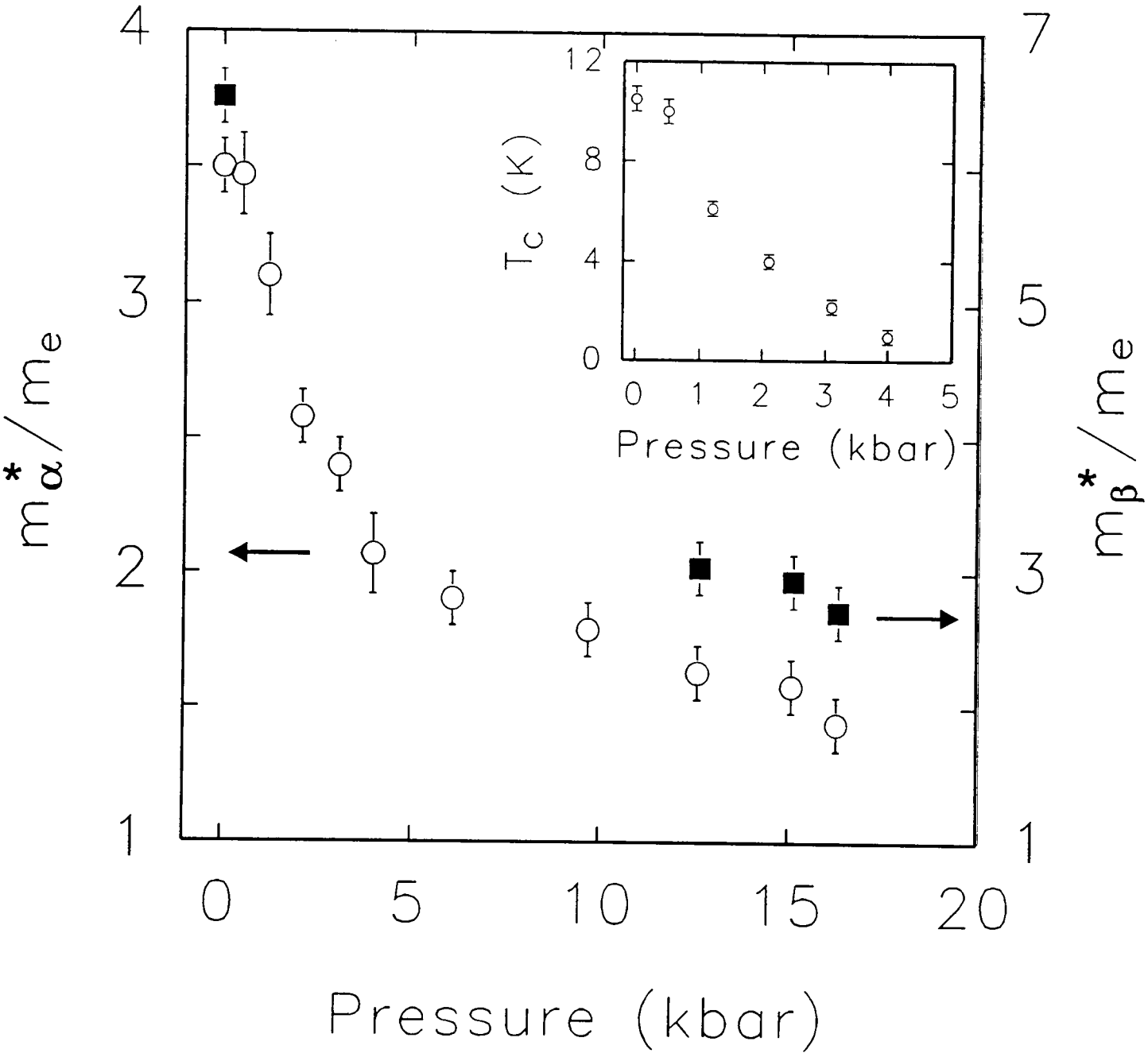

Figure 15 The effective masses of the α-orbit (hollow circles, left hand vertical scale) and β-orbit (filled squares, right hand vertical scale) as a function of pressure. The inset shows the superconducting T_c versus pressure.

For the α-orbit the Dingle temperature T_D is found to be 0.68 K at ambient pressure by a direct fit of the Lifshitz-Kosevich formula (figure 16) to the isothermal field dependent Shubnikov-de Haas data. This implies a scattering time, τ, of 2.1 ps (where $\tau = \hbar / 2\pi k_B T_D$), and a mean free path of ($v_F\tau$)~660 Å. To estimate m^*T_D to a reasonable accuracy the Lifshitz-Kosevich formula must be fitted to the field dependent data over a wide field range, down to magnetic fields where oscillations are just perceivable. As the classical resistance is strongly field dependent, care must be taken in the analysis of the Dingle temperature as the amplitude of the quantum oscillations is scaled by the classical magnetoresistance [23]. The effects of the classical magnetoresistance are removed by dividing the experimental data by the classical magnetoresistance, obtained by a polynomial fit to the data. It should be noted that the value of the Dingle temperature obtained by this analysis is still a slight underestimate of the real Dingle temperature as the warping of the Fermi surface, or curvature factor, is assumed to be zero [10]. The warping leads to a superposition of oscillations in which the frequency, or equivalently the phase, is varied over a small range around the value corresponding to the idealized situation, hence reducing the amplitude of each periodic term. The product m^*T_D is found to be independent of pressure within experimental error (see table 1).

Table 1. The fitted pressure dependence of the product m^*T_D.

Pressure (kbar)	m^*/m_e (α-orbit)	m^*T_D (m_e K)	T_D (K)
0	3.50	2.49	0.68
2.1	2.58	2.64	1.03
4.0	2.07	2.50	1.21
9.7	1.79	2.50	1.40
15.1	1.58	2.48	1.57

Care was taken in the analysis of high pressure data as magnetic breakdown considerably distorts the quantum oscillatory wave form at high magnetic fields.

Therefore only low field data was considered in direct fits to the Lifshitz-Kosevich formula, and the validity of this approach was confirmed by Dingle plot analysis. The strong pressure dependence of the Dingle temperature is further evidence of many body interactions and the renormalisation of m^* and τ will be discussed in § 3.5-2.

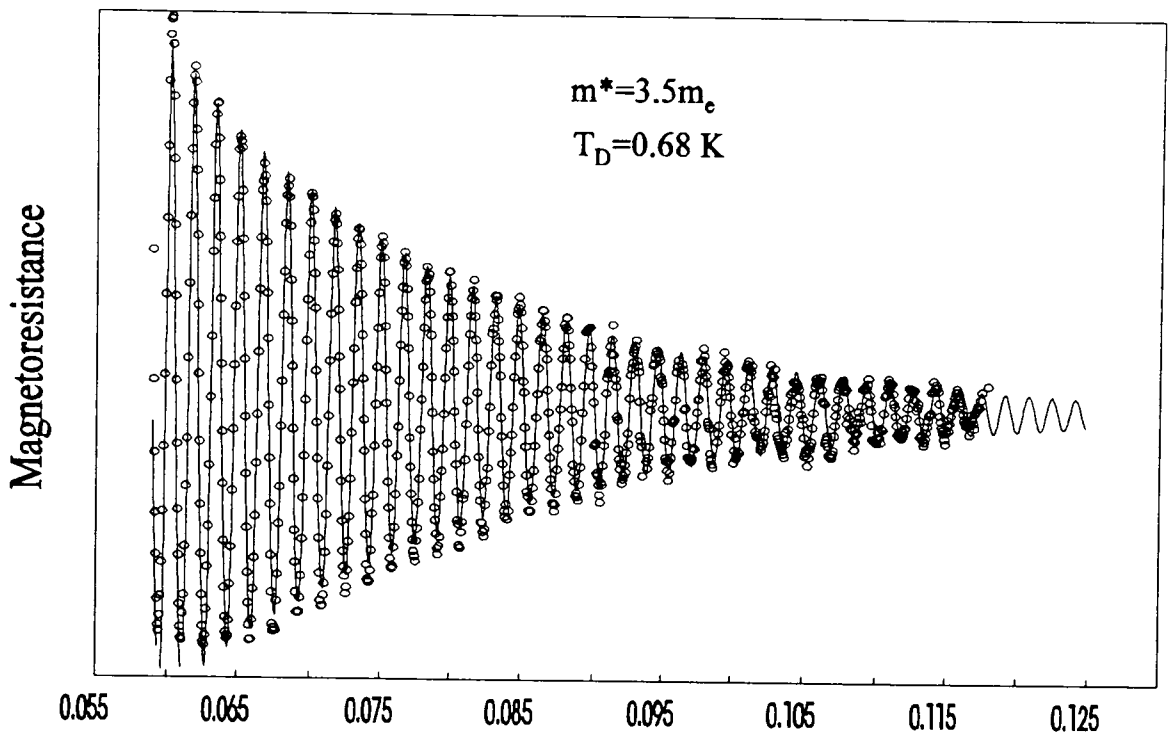

Figure 16 A fit of the Lifshitz-Kosevich formula (§ 2.2-3 [10]) (solid line) to the Shubnikov-de Haas data (dots) of $\kappa-ET_2Cu(NCS)_2$ at 0.7 K at ambient pressure. A value of m^*T_D=2.5m$_o$K is obtained from the fit.

The energy gap E_g between the two bands responsible for the quasi-one dimensional and quasi-two dimensional sections of Fermi surface may be deduced from the field dependence of the oscillatory component of the magnetoresistance using the Lifshitz-Kosevich formula (see equation (3.1)) [10] and the coupled network magnetic breakdown model [15]. This was first applied to $\kappa-ET_2Cu(NCS)_2$ by Sasaki *et al.* [11]. As mentioned above, electron tunnelling can occur at the Brillouin zone boundary between neighbouring sections of the Fermi surface (figure 4) with a probability given by:

$$P = \exp(-\frac{\pi E_g^{\ 2}}{4\hbar\omega_c \sin(2\theta) E_F}) \equiv \exp(-B_o / B) \qquad (3.2)$$

where $\omega_c = eB/m^*$, 2θ is the Bragg reflection angle and $B_o \equiv \pi m^* E_g^{\ 2} / 4e\hbar \sin(2\theta) E_F$. When more than one frequency of Shubnikov-de Haas oscillation is present, the overall oscillatory component of the magnetoresistance is given by a sum of amplitudes from the Lifshitz-Kosevich formulae for each possible closed orbit. The coupled network model [15] shows that the amplitude of every term concerned is weighted by a 'breakdown reduction factor', $R_b = (ip)^{n_1} q^{n_2}$, where breakdown probability $P = |p|^2 = 1 - Q$, and $Q = |q|^2$. The integers n_1 and n_2 are the number of points at which breakdown occurs and the number of Bragg reflection points respectively. In the case of the closed hole pocket (α-orbit) n_1=0 and n_2=2, and for the magnetic breakdown (β orbit)t n_1=4 and n_2=0. Therefore the total amplitude can be described by:

$$A_{TOT} = R_{b,\alpha} A_\alpha + R_{b,\beta} A_\beta \qquad (3.3)$$

where $R_{b,\alpha} = q^2 = 1 - P$ and $R_{b,\beta} = (ip)^4 = P^2$. Using the experimental values of the effective masses, Dingle temperature and Shubnikov-de Haas oscillation frequencies, the field dependence of the oscillatory magnetoresistance has been simulated using equations 3.1-3 with the breakdown field B_0 as the only variable parameter. The breakdown field as a function of pressure is shown in the inset to figure 13. At ambient pressure, the energy gap E_g is estimated to be 55±5 K, in agreement with previous measurements [11]. This is obtained from the fitted value B_0=15±1 T [14] with $2\theta = \pi/2$, E_F=740±100 K [12], m^*_β=6.5±0.1m_0 and $k_F^2\pi$=3.63*10^{15}cm^{-2} (taken from the unit cell parameters); the latter two parameters were measured in magnetic fields of up to 25 T where magnetic breakdown was clearly observed (see § 3.4-1). A linear

extrapolation of the pressure dependence of the breakdown field suggests closure of the gap at around 25 kbar.

3.4-5. Superconducting properties under pressure

The superconducting T_c (midpoint) of κ-$ET_2Cu(NCS)_2$ was also measured at each pressure; the results are shown as an inset to figure 15. The data are consistent with most of the previous reports [18], giving an initial pressure coefficient of ~-3 K/kbar, and there is no evidence for a low pressure plateau extending up to several kbar as reported by some authors [19]. The superconductivity is fully suppressed above 5 kbar. Note that this pressure is the same as P_c, the crossover point in the pressure dependence of the effective mass, to within experimental errors. The relationship between the pressure dependence of the effective mass and T_c will be considered further below.

3.5. Discussion

3.5-1. The Fermi surface: an effective dimer model

The intermolecular overlap integrals and the corresponding tight-binding bandstructure and Fermi surface of κ-$ET_2Cu(NCS)_2$ have been calculated by a number of workers [2,20,21]. The Fermi surface may be viewed as a cylinder with a slightly elliptical cross section (figure 4) which crosses the Brillouin zone boundary in the c^* direction. The unit cell contains two dimers [2]; a slight inequivalence of the two molecules in each dimer causes a small splitting of the bands to be present at the zone boundary, dividing the Fermi surface into open (quasi-one dimensional) and closed (quasi-two dimensional) sections. The calculated bandstructure is therefore in reasonable qualitative agreement with experimental data and the predicted area of the quasi-two dimensional Fermi surface pocket [2] is very close to that given by the α-orbit Shubnikov-de Haas oscillation frequency [11-14,24]. Furthermore, the

observation of magnetic breakdown confirms the existence of the small gap between the two sections of Fermi surface. However, the pressure-dependent measurements reported in this paper potentially allow rather stringent tests of the bandstructure calculations to be carried out. The alterations in the overlap integrals and bandstructure caused by changing the pressure can in principle be predicted from structural data under the same conditions. The crystal structure has been measured at low temperature under ambient pressure and also at room temperature under pressures of up to 7 kbar [21]. The transfer integrals were calculated to increase with pressure [21], as would be expected from the increasing overlap of the molecular orbitals on adjacent molecules. However the gap at the ZM Brillouin zone boundary was calculated to increase with pressure, with a corresponding reduction in the size of the closed orbit. Both of these predictions are contrary to the experimental findings. The Shubnikov-de Haas oscillations described in § 3.4-3 indicate that the quasi-two dimensional section of the Fermi surface increases in area by around 30 % between ambient pressure and 16.3 kbar, whereas the area of the whole Fermi surface, as measured by the frequency of the β orbit, increases by only 6 % over the same pressure range (figure 14). The magnetic breakdown oscillations (figure 13) indicate that the gap decreases with increasing pressure. It must be concluded that whilst present calculations of the bandstructure of $\kappa-ET_2Cu(NCS)_2$ provide a reasonably correct general picture of the Fermi surface, problems arise when the models are applied to the pressure dependence of the band parameters. The difficulty almost certainly results from inconsistencies between the conditions under which the structural data [21] and the results in this work were recorded. It will therefore be necessary to perform X-ray crystallography measurements at both low temperatures and a range of hydrostatic pressures before further quantitative comparisons between detailed bandstructure calculations and these experiments can be made.

Since low temperature structural data under pressure is not available, it is not possible to draw quantitative conclusions from a bandstructure model however sophisticated. Instead, to obtain qualitative understanding of pressure induced Fermi

surface changes, it is sufficient to work with a simplified model which takes into account the highly dimerized nature of the structure [2]. This calculation is referred to as the effective dimer model [25]; a similar approach was used by Tamura and co-workers [26] to analyse the reflectivity of κ-ET_2I_3. The basic unit for the tight binding calculations is taken to be the dimer, which is regarded as a supermolecule (figure 17).

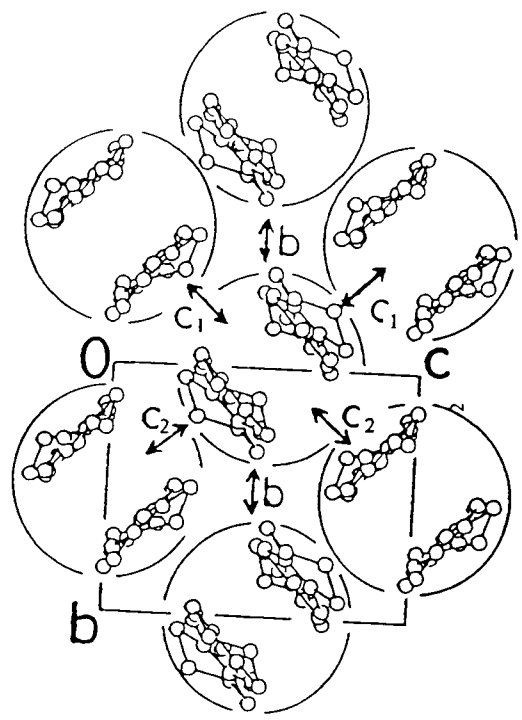

Figure 17 Effective inter-dimer interaction in κ-$ET_2Cu(NCS)_2$. The transfer integrals shown are related to those in figure 2 by $b=b_2$, $c_1=(p-q)/2$ and $c_2=(p'-q')/2$.

There are thus two dimers per unit cell separated by the translational vector $(\boldsymbol{b}+\boldsymbol{c})/2$ and only three (rather than six, see figure 2b) overlap integrals, one, b, corresponding to interdimer overlap in the $\boldsymbol{b}$ direction, and c_1 and c_2 which relate to the overlap in the $\boldsymbol{c}$ direction; these latter two are slightly different due to the non-symmetrical position of the dimer. The energy bands are calculated to be

$$E = 2b\cos k_b \pm \sqrt{2(c_1^2+c_2^2+2c_1c_2\cos k_c)(1+\cos k_b)} \qquad (3.4)$$

where the *k*-vectors are in reduced units (meaning $|k_b|$ and $|k_c| = \pi$ on the respective Brillouin zone boundaries). The two bands described by equation (3.4) are shown in figure 18. Along the ZM zone boundary $\cos k_c = -1$ and furthermore $\cos k_b \sim -0.5$ where the Fermi surface crosses the zone boundary (figure 4). The energy gap at this point thus becomes $\Delta E \approx (c_1 - c_2)$ and this is measured directly from the magnetic breakdown oscillations (References [11,14] and figure 13) to be ~5 meV at ambient pressure, and ~1 meV at 16 kbar [22]. This splitting is small compared to the size of the overlap integrals so that $c_1 \equiv c_2 \equiv c$. Consequently the *shape* of the Fermi surface depends almost entirely on the ratio of the transfer integrals *b* and *c*; figures 19a and 19b show the dependence of various parameters on *b/c*. Using the experimental α-orbit Shubnikov-de Haas oscillation frequencies to give the quasi-two dimensional hole pocket area, *b/c* is deduced to be 0.70 at ambient pressure and 0.88 at 16.3 kbar (figure 19a). Figure 20 shows the consequent calculated shape of the Fermi surface at these two pressures. It is also possible to estimate the ratio of the transfer integrals from polarised infrared reflectance measurements. Care must be taken to separate the intraband from the interband contributions observed in the optical reflectivity data in order to obtain the true intraband plasma frequency. This procedure was carried out at room temperature by Sugano *et al.* [27], giving the values $\omega_p^b = 0.61\,\text{eV}$ and $\omega_p^c = 0.71\,\text{eV}$ for *E//b* and *E//c* respectively, and at 25 K by Ugawa *et al.* [5], who reported values $\omega_p^b = 0.55\,\text{eV}$ and $\omega_p^c = 0.64\,\text{eV}$. Note that the ratio of the plasma frequencies $(\omega_p^b / \omega_p^c) = 0.86$ is the same in both measurements. The ratio of the intraband plasma frequencies calculated using the bandstructure of equation (3.4) is shown as a function of *b/c* in figure b; *b/c*=0.50 is necessary to give the observed plasma frequency ratio. This is significantly lower than the values obtained from the Shubnikov-de Haas oscillations, and figure 20 compares the Fermi surface shapes derived using the effective dimer model from the plasma frequency ratios (*i.e.* optical data) and the magnetotransport data at 0 kbar and 16.3 kbar. The reasons for the

differences between the Fermi surfaces derived from optical and Shubnikov-de Haas data will be discussed in the following section.

So far only the dimensionless ratio *b/c* has been determined from the data. In order to fit the absolute values of the plasma frequencies and the variation of the carrier effective masses with pressure, the sizes of the parameters *b* and *c* must be determined. A relatively straightforward estimation of *b* and *c* may be made by fitting the low temperature optical data of Ugawa *et al.*[5] to the effective dimer model (figure 19c); as the ratio of *b/c* has already been determined from the plasma frequency ratio (figure 19b), it is sufficient to find $(b+c)/2$.

Table 2. Comparison of the parameters of the effective dimer model and the corresponding calculated Fermi surface properties estimated from fitting to optical (Opt.) [5] and magnetotransport data. Characters in bold are measured Fermi surface properties. The resulting Fermi surfaces are shown in figure 20.

	b (eV)	*c* (eV)	*b/c*	E_g (meV)	S_α /S_{BZ} (%)	ω_p^b (eV)	ω_p^c (eV)	ω_p^b/ω_p^c	$m_{b\alpha}$	$m_{b\beta}$
Opt.	0.060	0.12	0.50		**11.4**	**0.55**	**0.64**	**0.86**	0.64	1.27
0 kbar			0.70	**5**	**15.5**			0.96		
16 kbar			0.88	**~1**	**18.7**			1.09		

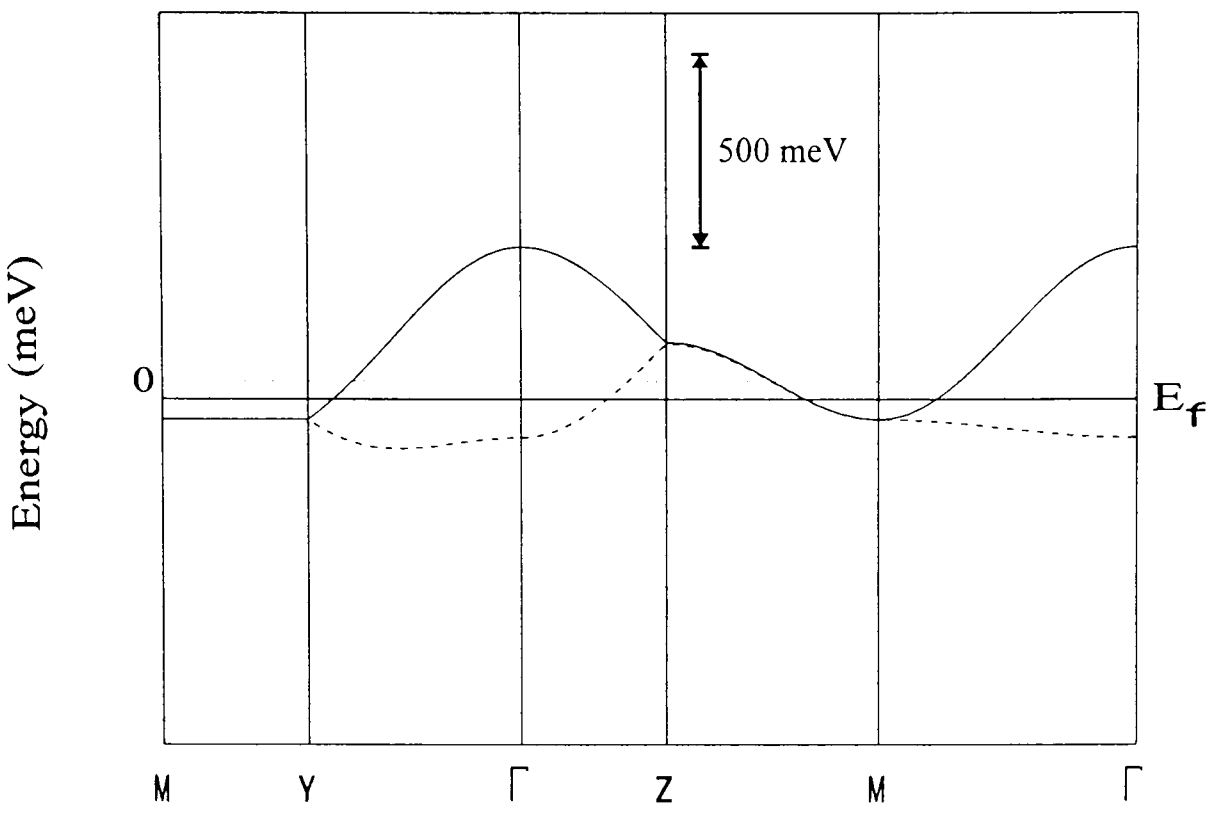

Figure 18 The tight binding bandstructure of κ-$ET_2Cu(NCS)_2$ using the effective dimer model bandstructure fitted to the Fermi surface area determined from magnetotransport data at 0 kbar, and using transfer integrals *b* and *c* determined from optical data (*c.f.* figure 3) [4].

The parameters thus deduced are shown in the first line of table 2 and compared with those derived from the magnetotransport data. Using these parameters, the bare band mass of the quasi-two dimensional hole pocket (corresponding to the α orbit) may be estimated to be $m_{b\alpha} \cong 0.64 m_o$ (figure 19d). A similar procedure gives a bare band mass corresponding to the β orbit to be $m_{b\beta} \cong 1.27 m_o$. These are much smaller than the effective masses observed in the experiments and so before proceeding further, it is necessary to clarify the meaning of the effective mass measured using the Shubnikov-de Haas effect and optical experiments.

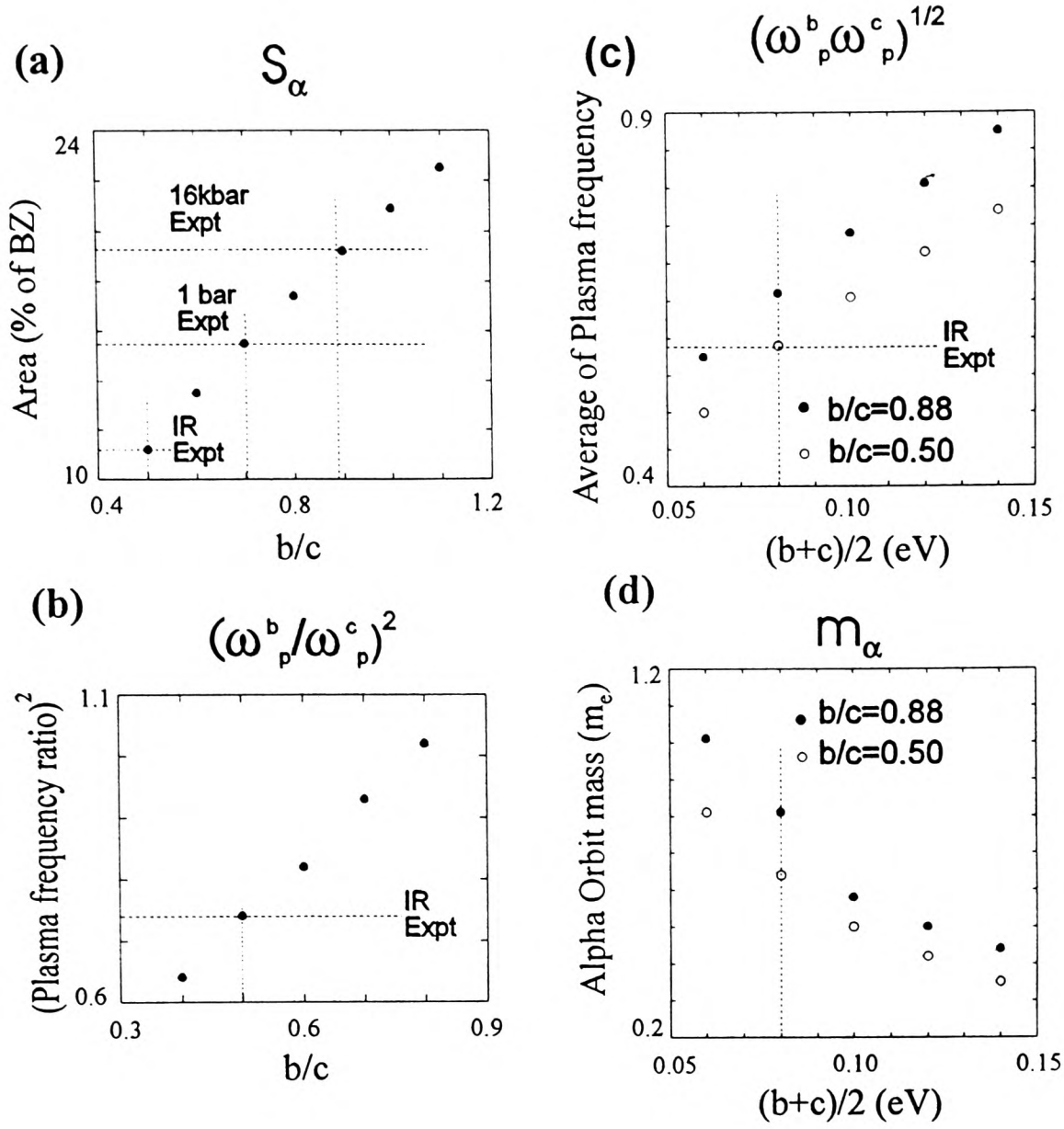

Figure 19 Various Fermi surface properties calculated using the effective dimer model as a function of the transfer integrals *b* and *c;* (a) The two-dimensional hole pocket area (α-orbit); (b) plasma frequency ratio; (c) the average plasma frequency and (d) the α orbit band mass. The dotted lines indicate experimental results taken from magnetotransport data in this paper (1 bar Expt, 16 kbar Expt) and from optical data in Reference [5] (infra-red reflectivity experiment) used to define *b* and *c* (see Section 3.5-1 and Table 2).

3.5-2. Ambient pressure effective masses and the influence of many body effects

It has been clear for some time that the effective masses of carriers in ET charge-transfer salts measured using the Shubnikov-de Haas and de Haas-van Alphen effects are much larger than those predicted by bandstructure calculations [1,24], leading to the suggestion that many body effects are of great importance [28,29].

Within the theory of interacting Fermions a number of quasiparticle 'masses' can be defined, reflecting the differing dynamical behaviour involved in various physical properties [30,31]; the differences between these masses provide important information about the many-body interactions in the system. Perhaps the simplest is the bare band mass m_b, which is derived from single particle bandstructure calculations. This is very close in size to the optical mass m_{opt} which can be experimentally probed by polarised infrared reflectivity measurements of the intra-band plasma frequencies, ω_p, [30,31]; where $m_{opt(j)} = 4\pi ne^2 / (\omega_p)^2_{(j)}$ (j=***b*** and ***c***) and n is the number density of the holes per unit volume.

The bare band masses $m_{b\alpha}$ and $m_{b\beta}$ have already been estimated to be $m_{b\alpha} = 0.64m_o$ and $m_{b\beta} = 1.27m_o$ using the fit of the effective dimer model to optical data (§ 3.5-1). They also can be estimated using the band structure calculated on the basis of the transfer integrals of Mori *et al.* [2], to be $m_{b\alpha}$=(0.9±0.1)m_o and $m_{b\beta}$ =(1.70±0.1)m_o. Using transfer integrals reported by Chasseau *et al.* [21] the band masses are calculated to be $m_{b\alpha}$=(1.6±0.1)m_o and $m_{b\beta}$=(3.3±0.01)m_o using the tight binding approach. Unfortunately, the origin of the difference in the methodology used in the calculation of the transfer integrals, which leads to such different conclusions, is not clear from reference [2] or [21].

Two further quasiparticle masses are important in the context of the experiments reported in this chapter. The effective mass m^* occurs in the thermodynamic density of states; it is renormalised over the band mass (m_b) by both quasiparticle interactions (short range Coulomb electron-electron interactions) and electron-phonon interactions. The enhancement over m_b due to Coulomb interactions may crudely be thought of as arising from a quasiparticle displacing other quasiparticles as it moves through a medium. The back flow of quasiparticles leads to a contribution to the effective mass m^*. The dynamical mass m_λ is the mass which would be observed in the absence of quasiparticle interactions, and the ratio of the two quantities is m^*/m_λ=(1+F^s_1/3), where F^s_1 is the l=1 Fermi liquid parameter [30]. The

dynamical mass therefore represents the band mass renormalised only by electron-phonon interactions. The ratio of the masses m_λ/m_b is the electron-phonon enhancement factor $1+\lambda$. The dynamical mass and effective mass may be measured using low energy experimental probes; the temperature dependence of phenomena such as the Shubnikov-de Haas and de Haas-van Alphen effects determines the effective mass m^* whereas a microwave cyclotron resonance experiment measures m_λ [28,30,31].

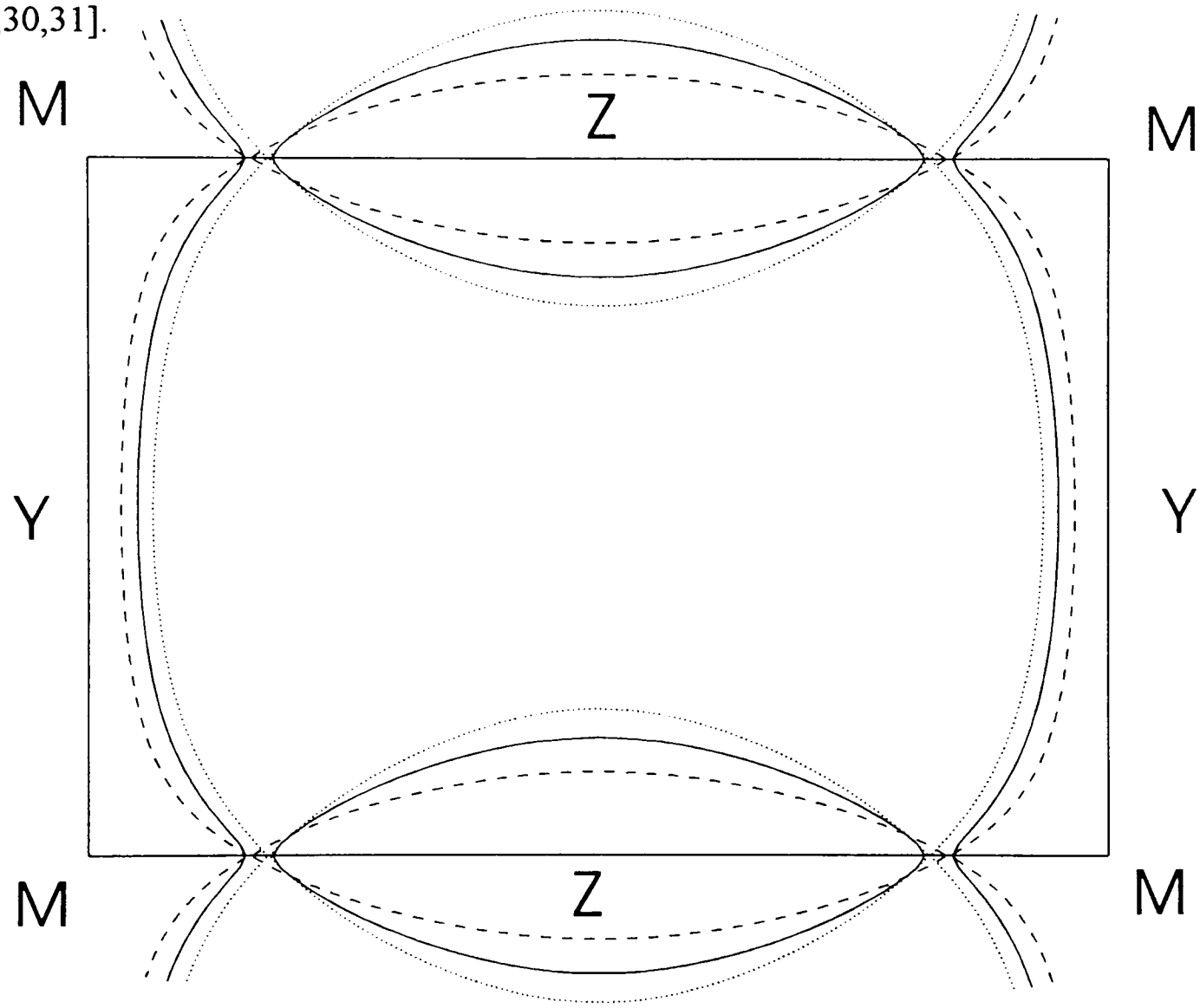

Figure 20 The Fermi surface of κ-$ET_2Cu(NCS)_2$ calculated using the effective dimer model bandstructure fitted to magnetotransport data at 0 kbar (solid line) and 16.3 kbar (dotted line) and to optical data [5] (dashed line). The *k*-vectors are in reduced units and the Brillouin zone has been kept the same size for each Fermi surface for clarity. See table 2 for parameters used.

Although electron-phonon interactions lead to a renormalisation of the band mass to give the dynamical mass, they do not change the shape of the Fermi surface. However, quasiparticle interactions can change the shape of the Fermi surface but

according to Luttinger's theorem [32] the volume of the Fermi surface should remain unchanged. This suggests a possible reason for the difference in Fermi surface shapes deduced from the Shubnikov-de Haas and optical measurements (figure 20); the 'optical Fermi surface' represents the shape in the absence of quasiparticle interactions whereas those determined from the magnetotransport data include the effects of those interactions.

Table 3. Comparison of the various quasiparticle masses in $\kappa-ET_2Cu(NCS)_2$.

Orbit	B_f (T)	Measured		Calculated			Mass enhancement		
		m^*/m_o	$m\lambda/m_o$	m_b/m_o			m^*/m_b		
			[33]	(a)	(b)	(c)	(a)	(b)	(c)
α	610(5)	3.5(1)	1.2	0.64	0.9	1.6	5.5	3.9	2.2
β-α	3310(30)	4.7(4)	-	-	-	-	-	-	-
β	3920(30)	6.5(1)	-	1.27	1.7	3.3	5.1	3.8	2.0
β+α	4530(30)	11(2)	-	1.91	2.7	4.9	5.8	3.9	2.2

(a) Based on the effective dimer model.

(b) Based on Mori transfer integrals [2].

(c) Based on Chasseau transfer integrals [21].

The various quasiparticle masses which can be deduced from theory and from ambient pressure experimental data are shown in table 3. Microwave magneto-optical studies have been performed on $\kappa-ET_2Cu(NCS)_2$ at ambient pressure by Hill *et al.* [33]. The features observed were interpreted as cyclotron resonances due to the quasi-two dimensional hole pocket (*i.e.* α-orbit) and a value of $m_{\lambda\alpha}=1.18m_o$ was obtained [33]. Using $m_{b\alpha}\cong 0.64m_o$, obtained above by fitting the low temperature optical data using the effective dimer model (table 1), the value of $m_{\lambda\alpha}/m_{b\alpha}=1+\lambda$ implies that $\lambda\cong 0.7$-0.8. This is similar in size to, but larger than, estimates of a total intramolecular $\lambda\cong 0.3$-0.5 for various ET salts derived by analysis of the frequencies of the phonons

observed in infrared and Raman spectroscopy [34] and by thermodynamical approaches using the Gruneisen parameters and BCS theory [36]. It is also typical of λ values proposed for other similar organic radical salts [1,20,34]. Note that relatively small shifts in $m_{b\alpha}$ would result in comparitively large changes in λ.

A value of $m^*_\alpha=3.5m_o$ was measured above using the temperature dependence of the Shubnikov-de Haas effect at ambient pressure (figure 9). This represents an enhancement by a factor of ~3 over $m_{\lambda\alpha}$. The quasiparticle interactions therefore represent a rather larger renormalisation of the quasiparticle mass than do the electron-phonon interactions. No cyclotron resonance data corresponding to the β-orbit has yet been observed. However, the ratios $m^*_\alpha/m_{b\alpha}$ and $m^*_\beta/m_{b\beta}$ are similar whichever theory is used (table 3), indicating that the overall renormalisation of the bare band mass is relatively uniform over the whole Fermi surface.

Table 1 indicates that the product m^*T_D is independent of pressure. This effect was predicted by Toyota *et al.* [29] and may be understood in terms of a classical picture: a heavy quasiparticle has a slow Fermi velocity and hence scatters from fixed impurities less frequently than one with a light mass and faster Fermi velocity. This means that the expected single-particle scattering time τ_b will be also enhanced by the factor $Z = m^*/m_b$. Thus the resistivity $\rho=m^*/n_oe^2\tau=Zm_b/n_oe^2Z\tau_b$ and the mean free path are not renormalised. Using the experimental parameters the Fermi velocity in $\kappa-ET_2Cu(NCS)_2$ is estimated to be 0.4×10^7cm^{-1}sec ($\upsilon_F = (2\hbar eB_F)^{1/2}/m^*_\alpha$).

The comparison of the values of $m_{b\alpha}$ and $m_{b\beta}$ deduced from the fit of the optical data to the effective dimer model and the value of m^*_α and m^*_β gives very good quantitative evidence of the renormalisation of the effective mass and hence the thermodynamic density of states due to many body effects. More indirect measurements by several other workers lend good qualitative support to these ideas and will be summarised in the remaining part of this section. A value for the renormalisation factor, $Z = m^*/m_b$, was also obtained by Toyota *et al.* [37] from low temperature spin susceptibility measurements on single crystals of $\kappa-ET_2Cu(NCS)_2$.

The spin susceptibility is $\chi_{spin} = 2\mu_B^2 g^{\chi}(\varepsilon_F)$, where $g^{\chi}(\varepsilon_F)$ is the density of states at the Fermi surface, obtained from the observed χ_{spin}. From the measured χ_{spin}, $g^{\chi}(\varepsilon_F)$ was found to be 4.6×10^{33} erg^{-1}cm^{-3}spin^{-1}. Toyota *et al.* inferred that this was enhanced by a factor of $Z\cong2.6$ over a calculated bare-bandstructure density of states. A similar enhancement factor of $Z\cong2$ was obtained by comparing the density of states obtained from a measurement of electronic specific heat component $(\gamma = \frac{2}{3}\pi^2 k_B^2 g^{\gamma}(\varepsilon_F) = 25\ \mathrm{mJ/(mol\ K^2)})$ *i.e.* $g^{\gamma}(\varepsilon_F)=4.0\times10^{33}$ erg^{-1}cm^{-3}spin^{-1} [38] with a calculation of the bare-bandstructure density of states.

The transfer integrals in $\kappa-ET_2Cu(NCS)_2$ have also been estimated by fitting the temperature dependent thermopower data, measured by Mori *et al.* [39], using a tight binding approach. It was found that the fitted transfer integrals are approximately four times smaller than those predicted using the single particle extended Hückel approach which yields the bare band masses shown in column (b) of table 3. Small fitted transfer integrals suggest a narrow bandwidth and hence a larger than expected effective mass.

The effects of Coulomb interactions have been included in a theoretical calculation of the bandstructure by Pratt *et al.* [24]. From optical reflectance data the interdimer hopping energy, U, was estimated to be between 0.2 and 0.5 eV and the intradimer hopping energy, V, to be 1.3 eV. As the hopping energy U is larger than the single particle bandwidth, t, the doubly occupied band is expected to split by an energy U. The density of states at the Fermi energy calculated from this narrowed band is close to that deduced from the effective masses derived from the Shubnikov-de Haas data.

In summary, the effects of many body interactions appear to be very important in renormalising the bare bandstructure masses and scattering times of the quasiparticles in $\kappa-ET_2Cu(NCS)_2$ at ambient pressure. The single particle tight binding bandstructure calculation, although in good agreement with the measured size and shape of the Fermi surface, overestimates the band width by a factor of 3-4. The

largest many body effect on the bandwidth comes from the quasiparticle interactions, which appear to renormalise the dynamical mass by a factor ~2-3.

3.5-3. The effect of pressure on the effective masses and superconducting behaviour

Figure 15 shows the pressure dependence of the effective mass of the α-orbit, m^*_α. Two distinct regions are observed. Above a pressure P_c the masses lie approximately on a straight line with a low value of dm^*_α/dP which extrapolates back to $m'_{\alpha 0} = 2.1m_e$ at zero pressure, whereas below P_c the data lie on a line with dm^*_α/dP some eight times larger which extrapolates $m^*_{\alpha 0} = 3.5m_e$ at zero pressure. Qualitatively similar changes also occur in the effective mass of the β-orbit. The variation of the superconducting critical temperature with pressure and its disappearance at P_c (figure 15, inset) appears to be connected with the rapid variation of the effective mass in this region.

Pressure dependent transfer integrals have been reported by Chasseau *et al.*[21]; however on the basis of their data we calculate a coefficient of only dm_α/dP~-5.5%/kbar, rather than the -10%/kbar found here. The larger than expected pressure effect may be understood if the effective mass renormalisation due to quasiparticle interactions is strongly affected by the application of pressure (this point is discussed in more detail in § 3.6). Such observations may be relevant to recent FIR absorption experiments by Dressel *et al.*[40], which revealed no correlation between T_c and the lattice softness; these authors implied that the superconducting state is more complicated than that described by BCS theory. However, the dominant influence on T_c in ET salts may well be the many-body renormalisation of the effective mass, which appears to be critically affected by external variables such as pressure.

A model of superconductivity should potentially allow one to relate the critical temperature to the effective mass. In the weak coupling BCS scheme [41] the superconducting transition temperature is given by

$$T_c = 1.13 \cdot \Theta \exp(-1/(\lambda - \mu^*)) \tag{3.5}$$

where λ is the electron-phonon coupling constant and μ^* is the Coulomb pseudopotential, representing the effective repulsion between the electrons in a Cooper pair [5,32]. Θ is typically the Debye temperature and sets the energy scale of the interaction.

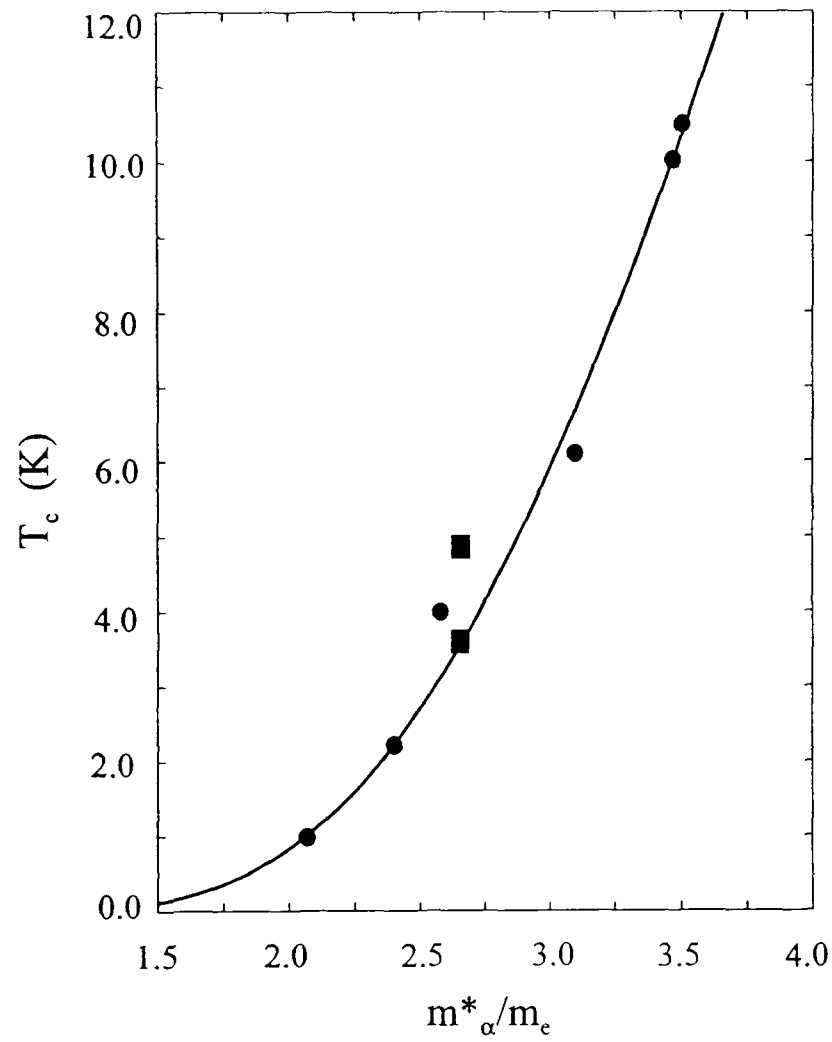

Figure 21 The relationship between the effective mass of the α orbit and the superconducting T_c for κ-$ET_2Cu(NCS)_2$. The filled circles are from the pressure-dependent magnetotransport data in this chapter and the filled squares are data for other superconducting κ-phase salts at ambient pressure (upper point κ-$ET_2Ag(CN)_2$ [43], lower point κ-ET_2I_3 [44]. The solid line is a fitted curve derived using a weak coupling BCS formula (equation (3.5)) and parameters given in § 3.5-3.

The electron-phonon coupling constant is proportional to the density of states at the Fermi surface which is in turn proportional to the effective mass. Figure 15 shows that the effective mass varies rapidly at low pressures, and so the strongest effect influencing T_c is likely to be the variation in the density of states at the Fermi energy.

In figure 21 the $T_c(P)$ data is modelled (solid line) using equation (3.5) with $\lambda(P)= \lambda(0)m^*_\alpha(P)/m^*_\alpha(0)$ and the other parameters held constant [42]; with $\lambda(0)=0.30\pm0.03$, $\mu^*=0$ (*i.e.* $\mu^*<<\lambda$) and $\Theta=265\pm10$ K, a good fit to the transition temperature as a function of the effective mass can be obtained. Ambient pressure data from two other κ-phase ET salts [43,44] are also included in figure 21 and are fitted well by the curve.

Whilst the $T_c(P)$ against $m^*_\alpha(P)$ curve in figure 21 fits the experimental data well, equation (3.5) must be seen as merely a convenient parameterisation of the data rather than a test of the nature of superconductivity in organic metals. Several points suggest that the applicability of weak coupling BCS theory to κ-$ET_2Cu(NCS)_2$ remains an open question; for example the value of $\mu^*=0$ contradicts expectations for a strongly correlated electron system [45], and the Debye temperature of κ-$ET_2Cu(NCS)_2$ obtained from specific heat measurements is around 215 K [38]. It is, however, clear that the variation in T_c corresponds directly to changes in the electronic density of states resulting from changes in the effective mass.

Tunnelling and point contact spectroscopy measurements by Nowack *et al.* [46] on β_L-ET_2I_3 indicate that the universal weak coupling BCS ratio $2\Delta / kT_c=3.53$ is not obeyed, and that the value varies greatly between similar materials. Two values of $2\Delta / kT_c$ are quoted due to possible uncertainties in the actual contact to the superconducting sample. They have further deduced from their data the strength of electron-phonon coupling over a range of frequencies, using the Eliashberg function $\alpha^2(\omega)F(\omega)$ where ω is the phonon frequency, $F(\omega)$ is the phonon density of states and $\alpha(\omega)$ is the Mc Millan coupling constant (note that the dimensionless coupling constant is expressed as an integral over the phonon spectral function

$\lambda \equiv 2\int_0^\infty \alpha^2(\omega)F(\omega)/\omega d\omega)$. The results show a strong peak at low energy ~1 meV corresponding to coupling to the translation or libration modes of the ET molecule, a shoulder around 4 meV and also a peak at a higher energy, ~15 meV, corresponding to the I-I stretching mode of the I_3 anion. The spectrum corresponds well to Raman spectroscopy data [20]. No significant coupling to the low lying internal molecular vibration modes are observed. Unfortunately no such data exists for $\kappa-ET_2Cu(NCS)_2$ due to surface preparation problems.

Recent neutron scattering data by Toyota *et al.* [47], on single crystals of $\kappa-ET_2Cu(NCS)_2$ have revealed that the phonon density of states consists of a broad peak in the low energy regime, 0-25 meV, and two rather sharp peaks centred at 32 meV and 56 meV. The latter peaks, which are also observed in neutral ET crystals, are assigned to librations involving hydrogen. Below T_c three distinct peaks appear centred about 2, 5 and 8 meV. It is noted that the energy range of these low-lying modes is comparable to the superconducting energy gap of 3.5-4.0 meV estimated from the discontinuous change in the specific heat [38]. It is suggested by the authors of reference [47] that the appearance of low-lying new states, might be correlated with the superconducting state.

As the applicability of weak coupling BCS theory to $\kappa-ET_2Cu(NCS)_2$ is an open question, and because of the recent experimental data by Toyota *et al.* [47] and Nowack *et al.* [46], T_c has been calculated by Lee *et al.* [48] using the data presented in this chapter by solving the linearised Eliashberg equations [49], an approach which should be valid for all coupling strengths. T_c may be obtained from the Eliashberg equations by linearising the gap equation (equation 74 in reference [49]), *i.e.* by ignoring Δ^2 (order parameter)) terms, as Δ is small near T_c, and by ignoring all *k*-dependence. In the calculations of Lee an Einstein spectrum is used to simulate the electron-phonon coupling function $\alpha^2(\omega)F(\omega)$; this is not intended to be a rigorous representation of the excitation spectrum, but it is useful in understanding the spectral

dependence of the physical quantities. As in the weak coupling model the pressure dependence of the density of states at the Fermi energy is derived by assuming that it scales with the measured effective mass; the density of states is then used to determine the pressure dependence of μ^* and $\alpha^2F(\omega)$. Fits to the data are accomplished by specifying the Einstein phonon frequency and the ambient pressure values of λ and μ^*.

The data was fitted with various combinations of λ and μ^* for several Einstein phonon energies [48]; fits are shown for Einstein phonon energies 2 meV (figure 22a), 5 meV (figure 22b) and 15 meV (figure 22c). The solid lines represent the numerical solutions of the Eliashberg equations; the fitting parameters are shown in the figure. From the fitting parameters in figure 22 it appears that a phonon energy of 5 meV gives the overall best fit using ambient pressure values of λ=0.4 (*c.f.* 0.3-0.5 in [34]) and μ^*=-0.22. As the data may only be fitted with either a small or in part attractive Coulomb pseudopotential this implies that the superconductivity may involve direct quasiparticle interactions, although there is no evidence of any anomalous magnetic properties in $\kappa-ET_2Cu(NCS)_2$ which might accompany such interactions. However, $\kappa-ET_2Cu[N(CN)_2]Cl$, an ambient pressure insulator which becomes a superconductor at 12.8 K under an applied pressure of 300 bar, exhibits a pronounced magnetic anomaly at T<22 K, reminiscent of weak ferromagnetism [35].

Many other experimental properties of $\kappa-ET_2Cu(NCS)_2$, such as the temperature dependence of the magnetic penetration depth [50] indicate that the superconductivity is BCS-like. Using two different approximations of BCS theory, the T_c versus effective mass data in this chapter have been fitted using reasonable values of λ and phonon frequency or Debye temperature. However, two problems until recently appeared to contradict this hypothesis. Firstly, the large renormalisation of the effective mass due to quasiparticle interactions ($m_\alpha^* / m_{\lambda\alpha} \sim 3$) would appear to contradict the small or negative values of μ^* derived from fits of the T_c versus effective mass data. Secondly, there is no clear evidence for an isotope effect in $\kappa-ET_2Cu(NCS)_2$ [51].

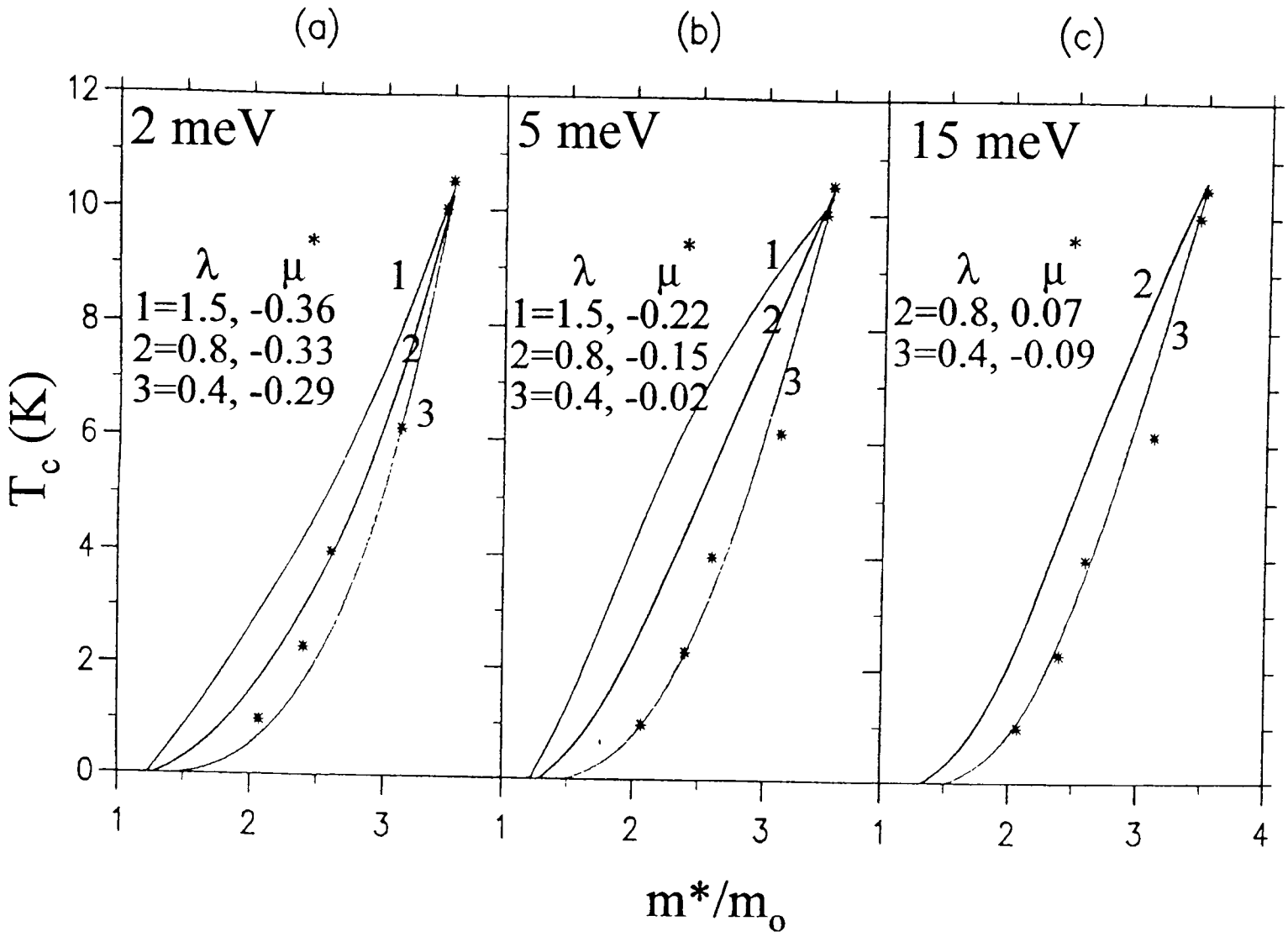

Figure 22 The relationship between the effective mass of the α orbit and the superconducting T_c for $\kappa-ET_2Cu(NCS)_2$. The open circles are from the pressure-dependent magnetotransport data in this chapter. The solid lines are fitted directly using the Eliashberg equation [49] for various values of μ* and λ (shown in the figure) for Einstein phonon frequencies of (a) 2 meV, (b) 5 meV and (c) 15 meV (from [48]).

These apparent contradictions have been resolved in a very recent paper by Weger *et al.* [52], who point out that in a system of interacting quasiparticles (such as the carriers in ET salts), excitations at energies ε well away from the Fermi energy, E_F, have very short lifetimes τ_{e-e}; usually $\tau_{e-e} \propto |\varepsilon - E_F|^{-2}$ or $|\varepsilon - E_F|^{-1}$. Thus energetic excitations will have too short a lifetime to polarise the lattice. Weger *et al.* simulate this effect by solving the Eliashberg equations with an imposed cut-off which excludes high energy (*i.e.* short lived) excitations. For cut-off energies of the order of the

phonon energy, this has the effect of suppressing the effect of μ* almost totally, and removing the isotope effect, in agreement with experimental data.

Phonon based mechanisms are by far the most popular explanations of superconductivity in ET salts, and most theoretical effort is in the development of modifications to the strong and weak BCS theory. However, workers in the field sometimes point out that there are indications that the coupling mechanism in superconducting ET salts may be electron rather than phonon mediated (for example see chapter 8 in reference [1]). The ET family of superconducting salts have many similarities with the 'exotic' heavy Fermion systems and ceramic superconductors (*e.g.* strongly enhanced hole carrier effective masses, small Fermi velocities, low carrier densities, strong electron-electron interactions and competition between antiferromagnetism and superconductivity) [1,53]. The coherence lengths in ET salts are rather short, of the order of a few unit cells, so that more local pairing mechanisms may be important [1]. An attraction between electrons may arise as a result of an electron-electron interaction causing local anti-parallel spin configurations. This situation is thought to occur even in materials which do not show any special magnetic properties, such as the perovskite $BaPbO_3$. To test whether such a novel mechanism is at play, spin-fluctuation theory was consulted (for example see [55]), from which the following relation is obtained [54]

$$T_C \cong \Gamma \exp \frac{-3m^*/m\lambda}{(m^*/m\lambda - 1)} \ldots\ldots \qquad \ldots\ldots(3.7)$$

where Γ is the spin fluctuation rate defined as $\Gamma \approx \gamma\chi^{-1}k_{BZ}$, γ is a constant depending on the Fermi surface topology, k_{BZ} is the characteristic wave vector of the Brillouin zone (measured as a function of pressure via the β-orbit) and χ is the normal state spin susceptibility at low temperatures (which is proportional to the effective mass; χ has been measured at ambient pressure [37]).

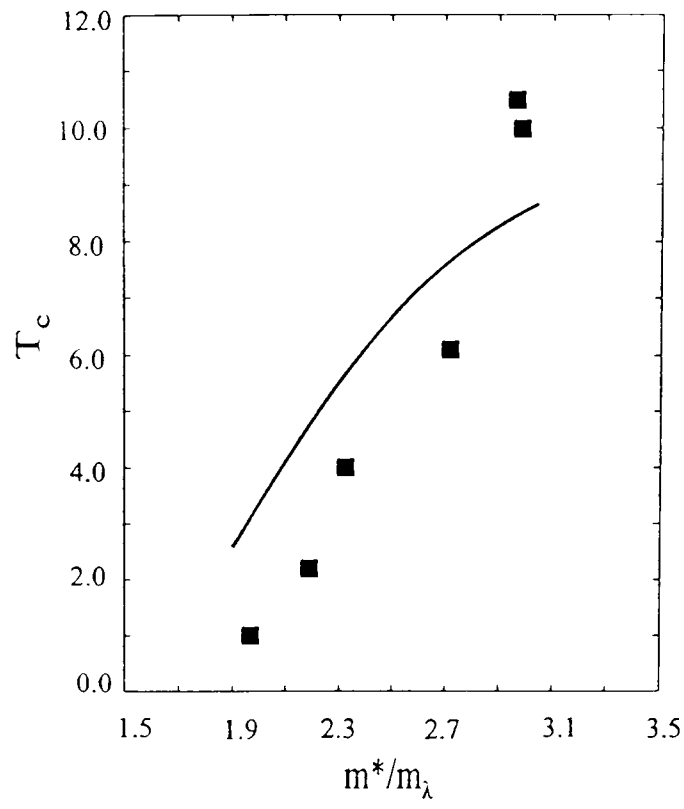

Figure 23 The relationship between the ratio of effective mass to the dynamical mass of the α orbit and the superconducting T_c for $\kappa-ET_2Cu(NCS)_2$. The solid line is a fitted curve derived using a spin fluctuation theory [55] (equation (3.7)) and parameters given in § 3.5-3.

The pressure dependence of ratio of the effective mass to the dynamical mass (m^*/m_λ) is unknown. As no cyclotron resonance under pressure has yet been carried out, it is assumed that the dynamical mass (m_λ=1.18m$_o$ at ambient pressure) has the same relative pressure dependence as dm^*_α/dP above 5 kbar (see § 3.6 for a discussion of this point) so that equation (3.7) may be fitted to the experimental data. The fit to the data is shown as a curve in figure 23, indicating that the above equation is of the wrong functional form. In fact equation (3.7) cannot be forced to fit the data regardless of the choice of $m_\lambda(0)$, for any reasonable choice of the function m_λ(P) (as $m^*/m_\lambda \rightarrow 1$ with pressure). Using the above assumption of the pressure dependence of m_λ the best fit is obtained with $\gamma=5\times10^{14}$ Km^2/emu (at present no information exists on the pressure dependence of such a quantity).

In passing it should be noted that the Mc Millan formula [56], another extreme case derived from BCS theory, valid for the strong electron-phonon coupling scenario,

could not be made to fit the data unless energy scales much larger than the Debye temperature were used.

In summary spin fluctuation theories and strong coupling BCS approximations have the wrong functional form to fit the T_c versus effective mass data. On the other hand, the weak coupling BCS expression and the numerical solutions of the Eliashberg equations fit the data well and indicate that λ~0.3-0.4, in agreement with other estimates [33,34,46,47] and that μ^* is small or even negative. Recent work by Weger *et al.* [52] satisfyingly reconciles the apparent small value of μ^* observed with the large effective mass renormalisation due to the quasiparticle interactions indicated by $m_\alpha^* / m_{\lambda\alpha} \sim 3$.

3.6. Summary

Magnetotransport measurements have been carried out on the organic superconductor $\kappa-ET_2Cu(NCS)_2$ at temperatures down to 500 mK in magnetic fields up to 25 T and also in hydrostatic pressures up to 16.3 kbar. The observation of Shubnikov-de Haas and magnetic breakdown oscillations has allowed the pressure dependences of the area of the closed pocket of the Fermi surface, the carrier effective masses, scattering times and the energy gap between Fermi surface sections to be deduced and compared with simultaneous measurements of the superconducting critical temperature T_c. The effective mass measured by the temperature dependence of the Shubnikov-de Haas oscillations is found to fall rapidly with increasing pressure up to a critical pressure $P_c \cong 5$ kbar. Above P_c a much weaker pressure dependence is observed. T_c also falls rapidly with pressure from 10.4 K at ambient pressure to zero at around P_c. This strongly suggests that the enhanced effective mass and the superconducting transition temperature are directly connected in this organic superconductor.

It therefore seems that large effective masses are a prerequisite for superconductivity in ET salts and, following the discussion in § 3.5-2, that the mechanisms primarily responsible for producing the effective mass enhancement are due to the interactions between quasiparticles, with the electron-phonon interactions playing a smaller role. The quasiparticle interactions are expected to depend critically on the bandwidth or the ratio of the Hubbard onsite Coulomb correlation energy U divided by the bandwidth, (see *e.g.* Reference [57]), being larger in general for narrower bands. An increase in the hydrostatic pressure (or decrease in anion length) will bring the ET molecules closer together and hence broaden the bands. The initial strong decrease in effective mass with pressure could therefore represent the suppression of a component of the quasiparticle interactions which depends strongly on the bandwidth. Indeed Ko *et al.* [58] have recently theoretically reproduced the qualitative effective mass versus pressure observations by applying the Hubbard model to calculate the effective mass as a function of U divided by the bandwidth. Above P_c the more gentle decrease in m^* with pressure may well reflect the increasing bandwidth and the concomitant decrease in the bare band masses.

Spin fluctuation theories and strong coupling BCS approximations have the wrong functional form to fit the T_c versus effective mass data. On the other hand, the weak coupling BCS expression and the numerical solutions of the Eliashberg equations fit the data well and indicate that λ~0.3-0.4, in agreement with other estimates [33,34,46,47] and that μ^* is small or even negative. Recent work by Weger *et al.* [52] satisfyingly reconciles the apparent small value of μ^* observed with the large effective mass renormalisation due to the quasiparticle interactions indicated by $m^*_\alpha / m^*_{\lambda\alpha} \sim 3$. An understanding of the nature of these interactions is an important question for further experimental and theoretical studies.

References

[1] T. Ishiguro and K. Yamaji, *Organic Superconductors*, (Springer-Verlag, Berlin 1990).

[2] H. Urayama, H. Yamochi, G. Saito, K. Nozawa, T. Sugano, M. Kinoshita, S. Sato, K. Oshima, A. Kawamoto and J. Tanaka, *Chem. Lett.* **1988**, 55 (1988); K. Oshima, T. Mori, H. Inokuchi, H. Urayama, H. Yamochi and G. Saito, *Phys. Rev.* **B 38** 938 (1988).

[3] For a recent review see Proc. Int. Conf. on Science and Technology of Synthetic Metals, Göteborg, Sweden, August 1992, *Synth. Met.*, **55-57** (1993) also Proc. Conf. European MRS, Strasbourg, France, 1993, *Synth. Met.* **61**, (1993).

[4] Calculated using a Quick Basic tight binding bandstructure calculation program written by Dr Francis Pratt and Dr Andrew Fisher using molecular overlaps given in [2].

[5] A. Ugawa, G. Oshima, K. Yakushi and H. Kuroda, *Phys. Rev.* **B 38**, 5122 (1988).

[6] K. Oshima, H. Urayama, H. Yamochi and G. Saito, *Physica* **C. 153-155** 1148 (1988).

[7] Y. Watanabe, T. Sasaki, H. Sato, N. Toyota, *J. Phys. Soc. Japan* . **60,** 2118 (1991).

[8] K. Murata, M. Tokumoto, H. Anzai, Y. Honda, N. Kinoshita, T. Ishiguro, N. Toyota, T. Sasaki and Y. Muto, *Synth. Met.*, **27**, A263 (1988).
W. Kang, D. Jerome, C. Lenoir and P. Bateil, *J. Phys. Cond. Matter.* **2** 1665 (1990).

[9] E.S. Itskevich, *Cryogenics*, **1964**, 365 (1964).

[10] *Magnetic Oscillations in Metals*, D. Shoenberg, (Cambridge University Press, 1984).

[11] T. Sasaki, H. Sato and N. Toyota, *Physica* **C**, **185-189,** 2687 (1991); *Solid State Commun.* **76**, 507 (1990).

[12] C.-P. Heidmann, H. Müller, W. Biberacher, K. Neumaier, C. Probst, K. Andres A.G.M. Jansen and W. Joss, *Synth. Met.*, **41-43**, 2029 (1991).

[13] J. Wosnitza, G.W. Crabtree, H.H. Wang, U. Geiser, J.M. Williams and K.D. Carlson, *Phys. Rev.* **B**., **45**, 3018 (1992).

[14] J. Caulfield, J. Singleton, F.L Pratt, M. Doporto, W. Lubczynski, W. Hayes, M. Kurmoo, P. Day, P.T.J. Hendriks and J.A.A.J. Perenboom, *Synth. Met.* **61**, 63 (1993).

[15] A. B. Pippard, *Proc. Roy Soc.* **A287**, 165 (1965).

[16] M. Doporto, J. Singleton, F.L Pratt, J. Caulfield, W. Hayes, J.A.A.J. Perenboom, I. Deckers, G. Pitsi, M. Kurmoo and P. Day, *Phys. Rev.* **B, 49** 3934 (1994).

[17] R.W. Stark and R. Reifenberger, *J. Low Temp. Phys.* **26**, 763 (1977).

[18] J.E. Schirber, E.L. Venturini, A.M. Kini, H.H. Wang, J.R. Whitworth and J.M. Williams, *Physica* **C 152** (1988), 157-158; K. Oshima, T. Mori, H. Inokuchi, H. Urayama, H. Yamochi and G. Saito, *Synth. Met.* **27** A165 (1988); W. Kang, D. Jerome, C. Lenoir and P. Batail, *J. Phys. Cond. Matter* **2**, 1665 (1990).

[19] I.D. Parker, R.H. Friend, M. Kurmoo, P. Day, C. Lenoir and P. Batail, *J. Phys. Cond. Matter* **1** (1989) 4479-4484; H. Fujii, K. Kajita, K. Kawada, Y. Nishio, H.Kobayashi, A. Kobayashi and R. Kato, *Synth. Met.* **55-57,** 2939 (1993).

[20] See various contributions by J.M. Williams *et al.* in *Organic Superconductivity,* eds. V.Z. Kresin and W.A. Little (Plenum Press, New York, 1990).

[21] D. Chasseau, J. Gaultier, M. Rahal, L. Ducasse, M. Kurmoo and P. Day, *Synth. Metals.*, **41-43** (1991) 2039. M. Rahal, D. Chasseau, J. Gaultier, L. Ducasse, M. Kurmoo and P. Day, *Acta Cryst. B,* to be published (1994).

[22] J. Caulfield, W. Lubczynski, F.L. Pratt, J. Singleton, D.Y.K. Ko, W. Hayes, M. Kurmoo and P. Day, *J. Phys. Cond. Matter.* **6** 2911 (1994).

[23] E.N. Adams and T.D. Holstein, *J. Phys. Chem. Solids*, **10** 254 (1959).

[24] F.L. Pratt, J. Singleton, M. Kurmoo, S.J.R.M. Spermon W. Hayes and P. Day, in The Physics and Chemistry of Organic Superconductors, eds. G. Saito and S. Kagoshima, *Springer Proceedings in Physics* **51**, 200 (1990).

[25] The effective dimer model was calculated by Dr F.L. Pratt, using the expressions given in [26].

[26] M. Tamura, H. Tajima, K. Yakushi, H. Kuroda, A. Kobayashi, R. Kato and H. Kobayashi, *J. Phys. Soc. Japan* . **60,** 3861 (1991).

[27] S. Sugano, H. Mori, H. Yamochi and G. Saito, *Phys. Rev.* **B 47**, 14374 (1993).

[28] J. Singleton, F.L. Pratt, M. Doporto, W. Hayes, T.J.B.M. Janssen, J.A.A.J. Perenboom, M. Kurmoo and P. Day, *Phys. Rev. Lett.* **68**, 2500 (1992).

[29] N. Toyota, E.W. Fenton, T. Sasaki, and M. Tachiki, *Solid State Commun.*, **72,** 859 (1989).

[30] K.F. Quader, K.S. Bedell and G.E. Brown, *Phys. Rev.* **B 36**, 156 (1987).

[31] *Many Particle Physics,* G.D. Mahan, (2nd edition, Plenum Press, New York, 1990); A.J. Leggett, *Annals of Physics.* **46**, 76 (1968).

[32] J.M. Luttinger, *Phys. Rev.* **121**, 1251 (1961).

[33] S. Hill, J. Singleton, F.L. Pratt, M. Doporto, W. Hayes, T.J.B.M. Janssen, J.A.A.J. Perenboom, M. Kurmoo and P. Day, *Synth. Metals.* **55-57**, 2566 (1993).

[34] J.C.R. Faulhaber, D.Y.K. Ko and P.R. Briddon, *Synth. Met.* **60**, 227 (1993); R.M. Vlasova, S. Ya. Priev, V.N. Semkin, R.N. Lyubovskaya, E.I. Zhilyaeva, E.B. Yagubskii and V.M. Yartsev, *Synth. Met.* **48**, 129 (1992); D.Y.K. Ko, P.R. Briddon and J.C.R. Faulhaber, *private communication.*

[35] Y.V. Sushko, H. Ito, T. Ishiguro, S. Horiuchi and G. Saito, *Solid State Commun.* **87** 997 (1993) and references therein.

[36] N. Toyota, Y. Watanabe and T. Sasaki, *Synth. Met.* **55-57**, 2536 (1993)

[37] N. Toyota, T. Sasaki, H. Sato and Y. Watanabe, *Physica* **C, 178** 339 (1991).

[38] B. Andraka, J.S. Kim, G.R. Stewart, K.D. Carlson, H.H. Wang and J.M. Williams, *Phys. Rev.* **B 40**, 11345 (1989).

J.E. Graebner, R.C. Haddon, S.V. Chichester, S.H. Glarun, *Phys. Rev.* **B 41**, 4808 (1990).

[39] T. Mori and H. Inokuchi, *J. Phys. Soc. Japan* **57** 3674 (1988).

[40] M. Dressel, J.E. Eldridge, J.M. Williams and H.H. Wang, *Physica* **C**, **203** 247 (1992).

[41] J. Bardeen, L.N. Cooper and J.R. Schrieffer, *Phys. Rev.* **108**, 1175 (1957).

[42] Strictly $m^*_\beta(P)$, which represents the effective mass of the whole Fermi surface, should be used to scale λ. However, the pressure dependences of m^*_α and m^*_β are very similar when conditions permit m^*_β to be measured (figure 15), and the ratios $m^*_\alpha/m_{b\alpha}$ and $m^*_\beta/m_{b\beta}$ are almost the same (table 3), indicating that the overall renormalisation of the bare band mass is relatively uniform over the whole Fermi surface. The pressure dependences of $m^*_\alpha(P)/m^*_\alpha(0)$ and $m^*_\beta(P)/m^*_\beta(0)$ are therefore taken to be identical.

[43] K. Oshima, K. Araki, H. Yamazaki, K. Kato, Y. Maruyama, K. Yakushi, T. Mori, H. Inokuchi, H. Mori and S. Tanaka, *Physica* **C 185-9**, 2689 (1991).

[44] K. Oshima, H. Yamazaki, K. Kato, Y. Maruyama, R. Kato, and H. Kobayashi, *Synth. Met.* **55-7**, 2334 (1993).

[45] Professor Maki, University of Southern California, has suggested that μ* would be zero for the case of d-wave pairing, *private communication.*

[46] A. Nowack, M. Weger, D. Schweizer and H.J. Keller, *Solid State Commun.*, **60** 199 (1986).

A. Nowack, U. Poppe, M. Weger, D. Schweitzer and H. Schwenk, *Z. Phys.* **B-***Cond. Matt.*, **68** 41 (1987).

For a review of point contact spectroscopy see: A.G.M. Jansen, A.P. van Gelder and P. Wyder, *J. Phys C: Solid St. Phys.* **13** 6073 (1980).

[47] N. Toyota, T. Kajitani, T. Shimazu, K. Shibata, T. Sasaki, M. Lang and S. Ikeda, *Proc. 5th Int. Symp. on Advanced Nuclear Energy Research,* p 479 (in press).

[48] Dr Wonmin Lee (Lancaster University), *submitted to.Phys. Rev.* **B**.

[49] The Eliashberg equations are given in equations (74) and (75) page 500 in *Superconductivty Volume 1*, ed. Park (Marcel Dekker inc, New York 1969).

[50] M. Lang, N. Toyota, T. Sasaki and H. Sato, *Phys. Rev.* **B 46** 5822 (1992).

[51] U. Geiser, A. Kini, H. Wang, J. Schlueter, K. Carlson and J.M. Williams, *submitted to Synth. Met.*

[52] M. Weger, B. Barbiellini and M. Peter, *Z. Phys.* **B 94** 387 (1994).

[53] Y.J. Uemua, L.P. Le, G.M. Luke, B.J. Sternlieb, W.D. Wu, J.H. Brewer, T.M. Riseman, C.L. Seaman, M.B. Maple, M. Ishikawa, D.G. Hinks, J.D. Jorgensen, G. Saito and H. Yamochi, *Phys. Rev. Lett.*, **66** 2665 (1991).

[54] Professor G.G. Lonzarich, (Cambridge University), *private communication.*

[55] G.G. Lonzarich, N.R. Bernhoeft, D.McK. Paul, *Physica* **B, 156** 699 (1989).

[56] W.L. Mc Millan, *Phys. Rev.* **B 12**, 905 (1975).

[57] W.F. Brinkman and T.M. Rice, *Phys. Rev.* **B 2**, 4302 (1970).

[58] Dr D.Y.K. Ko (Oxford University), *private communication.*

Chapter 4

κ-$(ET)_2Cu(NCS)_2$ in the vortex state.

4.1 Introduction

Many of the features of ET superconductors resemble those of the layered oxide-based high T_c superconductors [1]. In fact, apart from the order of magnitude difference in their transition temperature, these systems share a layered structure with a large effective mass anisotropy [2], a short coherence length [3,4] (between 70and 100 Å in $\kappa-ET_2Cu(NCS)_2$) and a large Ginzburg-Landau parameter κ (~70) [4]. The phenomenon of high temperature superconductivity remains without a satisfactory explanation. The normal state properties of ET salts are also unusual. For both families of materials experiments that explore the character of the electronic excitations, in both the normal and superconducting state, are of considerable interest. The de Haas-van Alphen effect provides a powerful tool for studying the quasiparticle excitations in such metals.

It is nearly twenty years since the first observation by Graebner and Robbins [5] of de Haas-van Alphen and magnetothermal oscillations in the layered superconductor $2H-NbSe_2$ at magnetic fields *below* B_{c2}. Since then there have been clear demonstrations of de Haas-van Alphen oscillations in the vortex state of $2H-NbSe_2$ [6], V_3Si [7] and Nb_3Sn [8]. The observation of quantum oscillations in the vortex state of strongly type II superconductors has also motivated great theoretical interest recently [9-14].

In this chapter previous studies of the de Haas-van Alphen effect in the strongly type II superconductor $\kappa-ET_2Cu(NCS)_2$ [2] (λ=5350 Å [4], ξ=70-100 Å [3], κ=76) are extended to lower magnetic fields in an attempt to observe quantum oscillations in the vortex state. Successful measurements of this type potentially allow one to probe both the magnitude and symmetry of the order parameter (Δ) directly. The chapter is organised as follows: § 4.2 provides a brief overview of the theoretical background behind quantum oscillatory phenomena in the vortex state; remarks are also made on the practical possibilities of its experimental observation. The experimental arrangements and

the principles of the techniques used are described in § 4.3, and the observations are presented in § 4.4. The results are summarised and discussed in § 4.5.

4.2 The vortex state

In any BCS superconductor Cooper pairs are formed due to a phonon mediated attractive potential between electrons at the Fermi surface. An energy gap of 2Δ opens up, centred on the Fermi energy (E_F) thus removing the density of states at the Fermi energy. It is not obvious how the de Haas-van Alphen effect, which depend on a modulation of the density of states at E_F, might then occur. The problem is not an issue in type I superconductors, where the Meissner effect prevents flux penetration anyway. In type II superconductors, magnetic flux can penetrate in the form of vortices where the material is normal. One might think that because the density of states at E_F is finite in these regions, de Haas-van Alphen oscillations might be observable;. however, the size of the cyclotron orbit in real space (at 4 T the characteristic cyclotron radius in real space is $r_c = \sqrt{(2\pi^2\hbar F / eB_z^2)} \approx 700$ nm in $\kappa\text{-ET}_2\text{Cu(NCS)}_2$) is significantly greater than the distance between vortices (flux separation [21] $a = \sqrt{(4\phi_0 / \sqrt{3}B)} \approx 35$ nm). Therefore quantum oscillations observed in the vortex state cannot just be due to Landau quantisation inside vortex cores.

There have been several theoretical treatments of de Haas-van Alphen oscillations in type II superconductors to date [10-12] put forward in an attempt to understand the origin of the oscillations observed by Graebner and Robbins [5]. All of the proposed models focus on different treatments of vortex cores; the main theoretical results are briefly discussed below.

In a paper by Brandt *et al* [9] in 1967, the theory of the density of states of pure type II superconductors was dealt with using a Green's function approach. Brandt derived an approximate expression for the Green's function of electrons in the superconducting mixed state close to B_{c2}, making use of the fact that the function has the periodicity of the flux lattice. In comparison to the normal state the Green's function

is altered by a correction term which is proportional to the square of the order parameter. This term is strongly dependent on the direction of the electron momentum with respect to the applied magnetic field. If the electron wave vector is parallel to the magnetic field then one finds the Green's function of the BCS state (*i.e.* an energy gap 2Δ at the Fermi energy); the density of states is thus identical to that of the BCS state. The modification of the Green's function with respect to the BCS state is strongest for wave vectors directed perpendicular to the magnetic field; for wave vectors perpendicular to the magnetic field the density of states is that of the normal state, and the quasiparticle excitation spectrum is essentially gapless. These electrons, with wave vectors perpendicular to the magnetic field, are exactly those probed by the de Haas-van Alphen effect.

The electron self energy (crudely speaking, the change in the single particle energy due to interactions) can be altered by quasiparticle interactions, which results in scattering among the excitations-*i.e.* the quasiparticle states will have a finite lifetime; they will decay. Consequently the actual self energy is a *complex* parameter. Brandt's calculations show that only the imaginary part of the self energy (*i.e.* the quasiparticle scattering rate) is affected upon entering the vortex state.

The observation of de Haas-van Alphen oscillations in the mixed state of $2H-\mathrm{NbSe}_2$ [5] prompted Maki [11] to investigate Landau quantization in the vortex state of type II superconductors theoretically. Maki began his treatment with the "Brandt" Green's function for electrons in the superconducting mixed state, close to B_{c2}, and derived an expression for the de Haas-van Alphen effect. He found that the main effect of superconductivity was to introduce an extra effective scattering rate, proportional to the square of the order parameter. Close to B_{c2}, where the Ginzburg-Landau parameter $\kappa>>1$ (*i.e.* the magnetic penetration depth is large in comparison with the coherence length), most of the material is composed of normal electrons and the magnetic field is virtually constant throughout the sample. In Maki's analysis the gap function (Δ) is considered as an extra scattering parameter likened to that of an impurity or inhomogeneity which is then shown to add to the Dingle temperature. The field and

temperature dependence of Δ are also inserted into the amplitude reduction factor formula by a suitable choice of the $\Delta(B,T)$ function. The term Γ is defined as the width of the broadened (Lorentzian shaped) Landau level caused by the combined effects of impurity scattering and the gap parameter Δ which becomes:

$$\Gamma = \frac{\hbar}{\tau} + \frac{2\sqrt{\pi}\Delta^2}{\alpha} \tag{4.1}$$

where $\alpha = v_F\left(2e\hbar B\cos[\theta]\right)^{1/2}$ is used as a scaling parameter (~10^3 K) within the self energy, and θ is the angle between the applied magnetic field and the crystal ***ac***-plane. Perpendicular to the magnetic field the superconductor in the mixed state is essentially gapless, so the *cos(θ)* in the self energy term becomes unity. The self energy derived by Maki [11], is proportional to Δ^2, giving rise to the the square dependence in the scattering term. From [11] the Dingle temperature is now given as:

$$T_D' = \frac{\Gamma}{2\pi k_B}\left[1+2\left(\frac{\Delta}{\alpha}\right)^2\right]^{-1} \tag{4.2}$$

(*c.f.* $T_D = \hbar / 2\pi k_B \tau$).

$$T_D' = T_D + \frac{\Delta(B,T)^2}{v_F\sqrt{2\pi eB}} \tag{4.3}$$

This model has recently been supported by Wasserman and Springford [12] using a more general approach. They derive the thermodynamic potential of electrons in the mixed state in terms of the calculated electron self energy. They find that averaged over a cyclotron orbit the extra contribution from the environment of the mixed state to the real part of the electron self energy is zero, but the orbitally averaged imaginary part of the electron self energy is proportional to $\Delta^2(B,T)$. Hence on entering the vortex state from the normal state the de Haas-van Alphen frequency is unchanged, but the oscillation amplitude is reduced by an additional effective quasiparticle scattering rate proportional to $\Delta^2(B,T)$. Thus the magnitude of magnetic quantum oscillations in the vortex state is

determined by the total size of a Dingle temperature including this term. Mikaye [13] has also pointed out that one may use this technique of quantum oscillations in the mixed state to determine whether there are nodes in the order parameter occurring at particular points on the Fermi surface, as along these orbits the scattering rate will be considerably reduced.

When considering the amplitude of quantum oscillations in the vortex state the extent to which the inhomogeneous field, induced by the spatially varying order parameter, produces broadening of the Landau levels must be taken into account. Under the experimental conditions at, for example, B=4 T in κ-$ET_2Cu(NCS)_2$, the extremal orbit area in k-space corresponds to a real-space orbit of radius ~700 nm and the separation of the flux lines is ~35 nm (about half the Ginzburg-Landau coherence length ξ in the ***bc***-plane). This implies that at 4 T the cyclotron orbit in real space encloses ~1600 vortices. An estimate of the Landau level broadening [7] is $\tau^{-1} \approx v_F \delta k_F$, where δk_F is the variation in radius of orbits cutting the same flux and v_F is the average Fermi velocity. An upper bound to the variation in area δA of orbits cutting the same flux is $B\delta A = B2\pi r_c \delta r_c \approx \delta B 2 r_c a$, where δB is the variation of the local magnetic field $\boldsymbol{B}$(r) along the cyclotron orbit due to the flux lattice [7]. Thus $\delta k_F = \delta r_c (eB/\hbar) \approx ae\delta B / \pi\hbar$. Using the estimate [17] $\delta B \sim (B_{c2} - B)/\kappa$ and the measured average Fermi velocity $v_F = (2\hbar e B_F)^{1/2} / m^* = 0.4\times10^7$ cm/s, (B_F is the de Haas-van Alphen frequency in Tesla) the estimated Landau level broadening due to the inhomogeneous magnetic field at B=4 T is $\tau^{-1}=0.7\times10^8$ s^{-1} *i.e.* an effective Dingle temperature of ~8 mK. The Landau level broadening due to impurity scattering in ET salts is typically of the order 10^{12} s^{-1} (corresponding to a Dingle temperature of ~0.5 K). Hence the damping arising from the inhomogeneous magnetic field **B** is unimportant compared with damping effects arising from impurities and the superconductivity.

A rough estimate can be made as to whether the observation of de Haas-van Alphen oscillations in the vortex state of κ-$ET_2Cu(NCS)_2$ is viable. In de Haas-van

Alphen measurements by Wosnitza *et al.* on κ-$ET_2Cu(NCS)_2$ at 0.5 K [2] using the field modulation technique, oscillations were observed down to 6.5 T; far from B_{c2} (B_{c2} is ~4.5 T, estimated from magnetoresistance results presented in chapter 3). Hence by calculating the amplitude reduction factors due to thermal and impurity broadening at 6.5 T, 0.5 K and with a Dingle temperature of 0.5 K, the limit to the reduction factor can be estimated. Using the system at Bristol, temperatures down to 0.02 K can achieved. If 0.02 K was attainable in a system similar to Wosnitza's one would expect to just be able to perceive oscillations down to 4.3 T in the absence of the damping experienced upon entering the vortex state. The observation of quantum oscillations in the vortex state of κ-$ET_2Cu(NCS)_2$ is difficult due to the small B_{c2} and the damping effects due to impurity scattering experienced at such low magnetic fields, therefore great care was taken to reduce electrical and vibrational noise to an absolute minimum in order to achieve a better signal-to-noise ratio than that of Wosnitza's system.

4.3 Experimental techniques

The de Haas-van Alphen effect is notoriously more difficult to observe than the Shubnikov-de Haas effect in ET salts as Shubnikov-de Haas signals are typically of the order of a few milli-volts whereas de Haas-van Alphen signals are less than one micro-volt, due to the small crystal volume, low carrier density and therefore tiny magnetic moment. In a situation where the oscillatory magnetisation signal is expected to be small, phase sensitive detection techniques are a requirement.

4.3-1 Field modulation technique

The most thoroughly developed method used to study the de Haas-van Alphen effect is the inductive field modulation method [18,19]. It is based on superimposing a small periodic magnetic field $b_0 \cos(\omega t)$ on a background magnetic field B. In this way the magnetisation is made to vary periodically with time. The sample is placed inside a

pair of balanced pick-up coils. The induced electromotive force can be examined by means of a phase sensitive detector at the angular frequency ω or at higher harmonics $k\omega$. Assuming that $b_0 << B$ then the fundamental de Haas-van Alphen term in the Lifshitz-Kosevich formula [18] can be written as

$$M(t) = A\sin\left[\frac{2\pi B_F}{B + b_0\cos\omega t} + \phi\right] \approx A\sin\left[\frac{2\pi B_F}{B} - \frac{2\pi B_F b_0\cos(\omega t)}{B^2} + \phi\right] \qquad (4.4)$$

$$= A\{\sin\left[\frac{2\pi B_F}{B} + \phi\right]\cos(\lambda\cos(\omega t)) - \cos\left[\frac{2\pi B_F}{B} + \phi\right]\sin(\lambda\cos(\omega t)\} \qquad (4.5)$$

where $\lambda = \dfrac{2\pi B_F b_0}{B^2}$

The functions $cos(\lambda cos(\omega t))$ and $sin(\lambda cos(\omega t))$ can be expressed as the sum of the time dependent harmonics $cos(k\omega t)$ with coefficients proportional to Bessel functions of the first kind $J_k(\lambda)$:

$$\cos(\lambda\cos(\omega t)) = J_0(\lambda) + 2\sum_{k=1}^{\infty}(-1)^k J_{2k}(\lambda)\cos(2k\omega t) \qquad (4.6)$$

$$\sin(\lambda\cos(\omega t)) = 2\sum_{k=1}^{\infty}(-1)^k J_{2k+1}(\lambda)\cos((2k+1)\omega t) \qquad (4.7)$$

Now equation (4.4) can be written as

$$M(t) = A\{J_0(\lambda)\sin\left[\frac{2\pi B_F}{B} + \phi\right] + 2\sum_{k=1}^{\infty} J_k(\lambda)\cos(k\omega t)\sin\left[\frac{2\pi B_F}{B} + \phi - \frac{k\pi}{2}\right] \qquad (4.8)$$

The induced e.m.f. in the pick-up coils is

$$V_{pu} = c\frac{dM}{dt} = \sum_{k=1}^{\infty} v_k \sin(k\omega t) \qquad (4.9)$$

$$v_k = -2cA\,\omega k J_k(\lambda)\sin\left[\frac{2\pi B_F}{B} + \phi - \frac{k\pi}{2}\right] \qquad (4.10)$$

where c is a factor representing the coupling of the sample to the pick-up coil. Every time harmonic of V_{pu} is weighted by a coefficient $J_k(\lambda)$. Figure 1 (taken from [18] figure 3.7, page 105) shows the behaviour of $J_k(\lambda)$ for a few values of k. The figure

shows that by suitable choice of modulation amplitude (*i.e.* of λ) the amplitude of any particular harmonic of ν can be considerably enhanced.

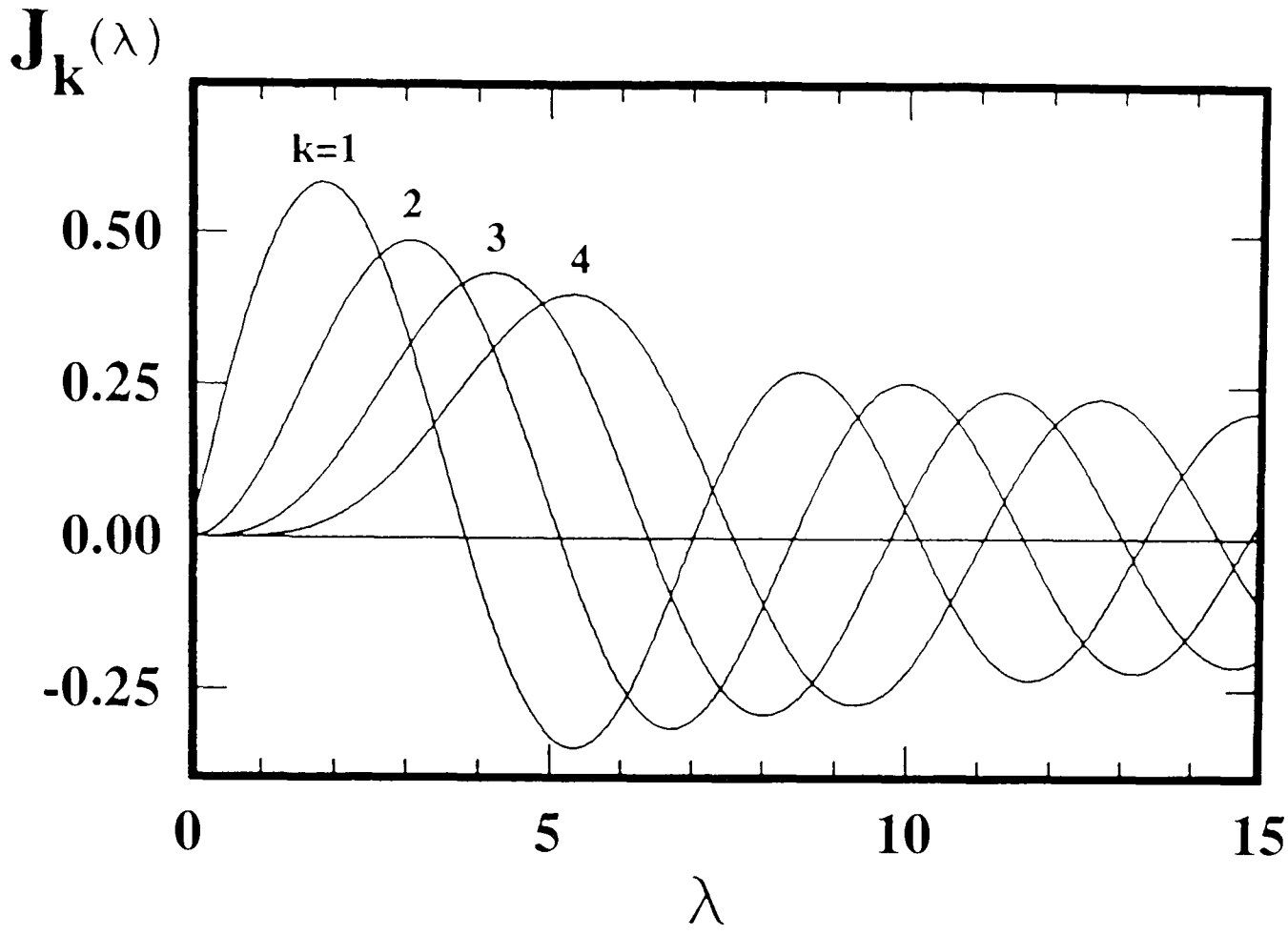

Figure 1 Bessel functions $J_k(\lambda)$ of the first kind for k=1,2,3 and 4 [18].

4.3-2 Detection method

The pick-up coil surrounding the sample measures the time derivative of the total flux through the coil when a uniform magnetic field $(\boldsymbol{B} + \boldsymbol{b}_0 \cos(\omega t))$ is applied, with $\boldsymbol{b}_0 // \boldsymbol{B}$. It detects not only the small magnetic moment of the sample but also the $\boldsymbol{b}_0 \cos(\omega t)$ signal from the modulation field. To compensate for this another coil is added to the circuit in opposition to the coil containing the sample. This coil has a much weaker inductive coupling to the sample but picks up the modulation field. Thus the net induced voltage will be entirely due to the magnetic moment of the sample itself.

Due to the presence of the $J_k(r\lambda)$ terms, the observed voltage v_k as a function of $1/B$ will in general not resemble the behaviour of $M(1/B)$. Only in the case of very weak modulation, are the Bessel functions proportional to p^k (where p^k is a de Haas-van Alphen harmonic). The observed waveform for v_k is then proportional to

$d^k M / dB^k$. The data presented in this chapter was mathematically transformed using a Lab View computer program to remove the effects of the Bessel functions.

For several reasons it proves to be advantageous to monitor the behaviour of the pick-up voltage at a *harmonic* rather than at the fundamental modulation frequency. First of all, if the pick-up coils are not quite balanced, the net voltage fed into the phase sensitive detector contains a considerable $\sin(\omega t)$ component which is not associated with the magnetisation of the sample but stems directly from the modulation field itself. If this component is too large, it influences the detection resolution. Another reason for avoiding detection at the fundamental frequency is that, even at low ω, the balance of the pick-up coils is upset by eddy currents induced in the sample. The effect is field dependent because of sample magnetoresistance, *i.e.*, the (un)balance is field dependent, causing a sloping baseline on top of which the oscillations appear. Again, detection at 2ω or higher harmonics almost completely eliminates this complication. Finally, the current in the modulation coils causes eddy currents to flow in metal parts of the cryostat, which results in a vibration noise component at ω, yet another reason to detect at higher harmonics.

4.3-3 Experimental set up

A schematic diagram of the modulation and detection circuit is shown in figure 2. A top loading dilution refrigerator was used for the measurements reported in this chapter, capable of temperatures down to 0.02 K. The temperature was measured using a calibrated germanium sensor.

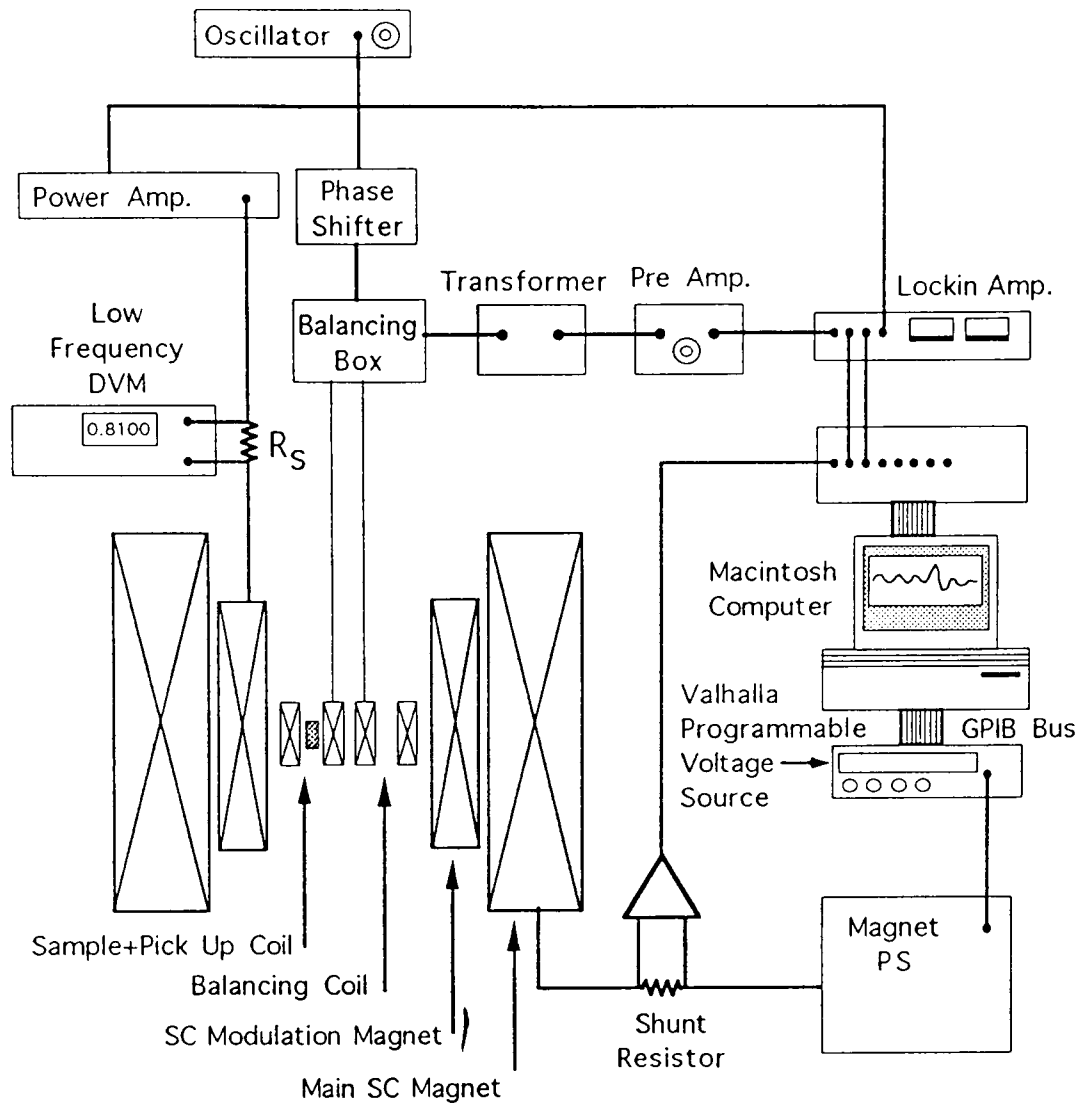

(a)

Schematic drawing of the modulation and detection circuit.

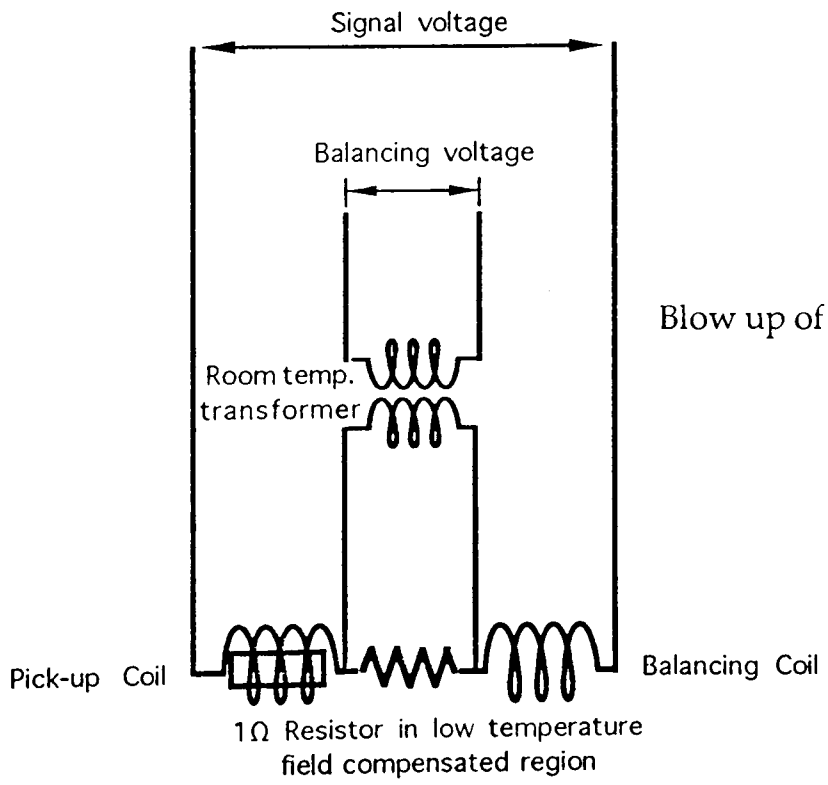

(b)

Blow up of coil detection circuit.

Figure 2 (a) Schematic drawing of the modulation and detection circuit, (b) Blow up of the coil detection circuit.

The cryogenics and thermometry are described in detail elsewhere [20]. The superconducting magnet, indicated in figure 2, can achieve magnetic fields up to 14.5 T. Typically the modulation field (b_o) is set to obtain a particular Bessel function, and hence a signal maximum for the de Haas-van Alphen frequency ($B_F \sim 600$ T in this case) and field range (around the upper critical field B_{c2} in this case) of interest. At fixed magnetic fields noise spectra were taken in order to select a modulation frequency distant from noisy regions of the frequency spectrum. Low modulation amplitudes (up to 200 gauss) and frequencies (~18 Hz) were selected in order to avoid eddy current heating in the sample. The single crystal of κ-$ET_2Cu(NCS)_2$ was placed inside one of a pair of balanced rectangular pick-up coils of dimensions (1.1×1.6) mm² of length 4 mm, each coil consisting of 1100 turns of 50 μm copper wire. The largest single crystals of κ-$ET_2Cu(NCS)_2$ (prepared electrochemically by M. Kurmoo) available were used for the measurements to maximise the filling fraction of the coil. Nevertheless it is clear that the coil used for these measurements was not ideal as the filling fraction of the coil volume was never better than ~10 %. The sample and coils could be rotated with respect to the applied magnetic field using a worm drive axial rotation system. The magnetic field, B, was typically swept at a rate of ~0.01 T/min.

4.4 Experimental results.

4.4-1 De Haas-van Alphen oscillations in the vortex state

A typical example of the de Haas-van Alphen signal is shown in figure 3 at a temperature of 20 mK, with the magnetic field applied at an angle of $\theta = 29°$ to the ***a***-axis. The inset shows the de Haas-van Alphen data at the lowest magnetic fields with the smooth background magnetisation subtracted, as the sample enters the vortex state. As in the low field Shubnikov-de Haas experiments (see chapter 3) one series of oscillations is observed. A Fourier transform (figure 4) reveals a single frequency $B_F = 597 \pm 5$ T (corresponding to a Fermi surface area of 15.6 % of the room temperature Brillouin zone, as predicted by the bandstructure calculation [22]) at $\theta = 0°$ with an associated

effective mass of $m^* = 3.5 \pm 0.1\, m_e$, derived from the temperature dependence of the oscillation amplitude. The oscillation frequency and carrier effective mass were found to be independent of the applied magnetic field, within experimental error.

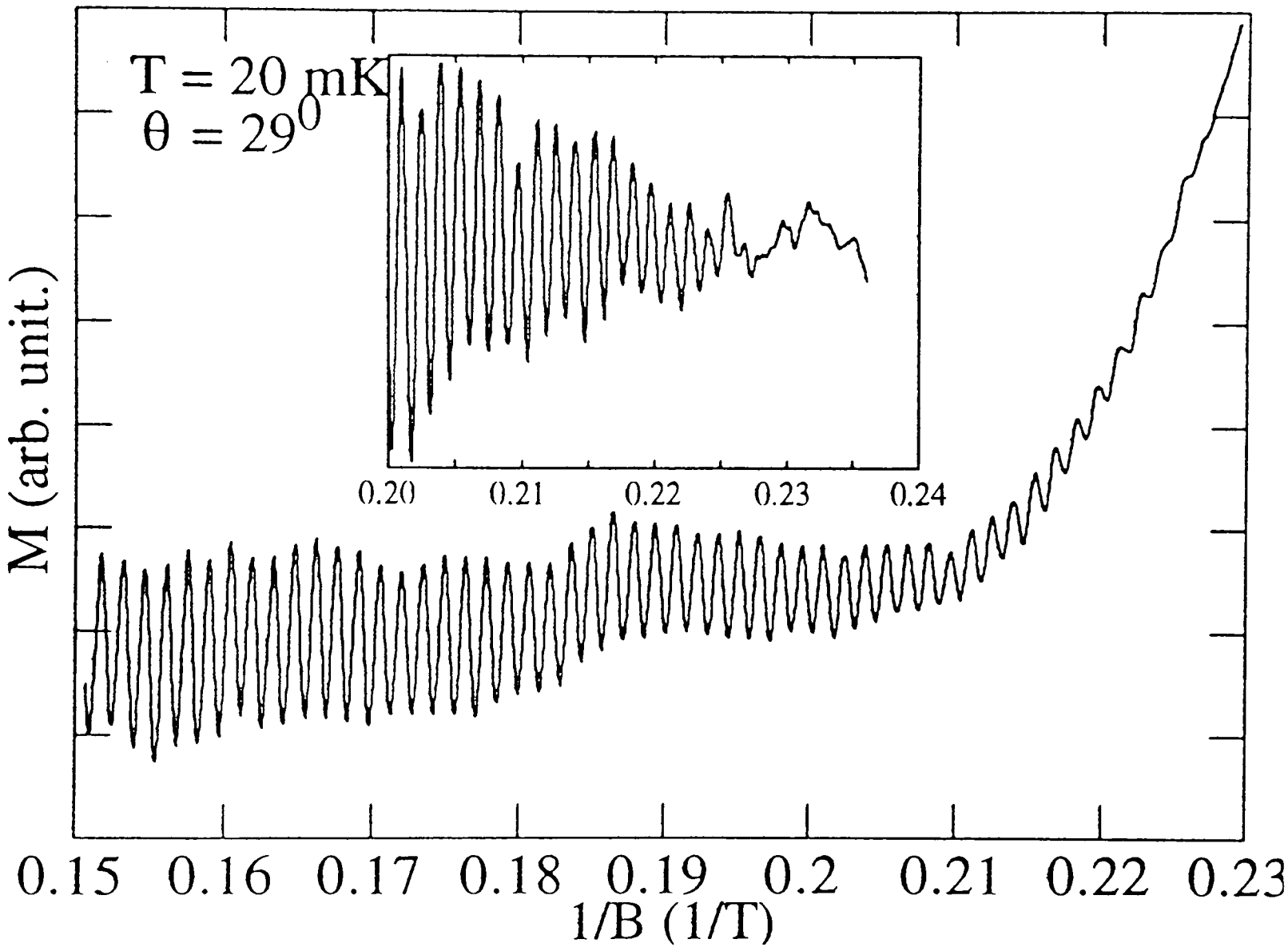

Figure 3 De Haas van-Alphen signal in $\kappa - ET_2Cu(NCS)_2$ at 20 mK with the ***a***-axis 29° from the field direction. The inset shows data at the lowest fields with a smooth background subtracted.

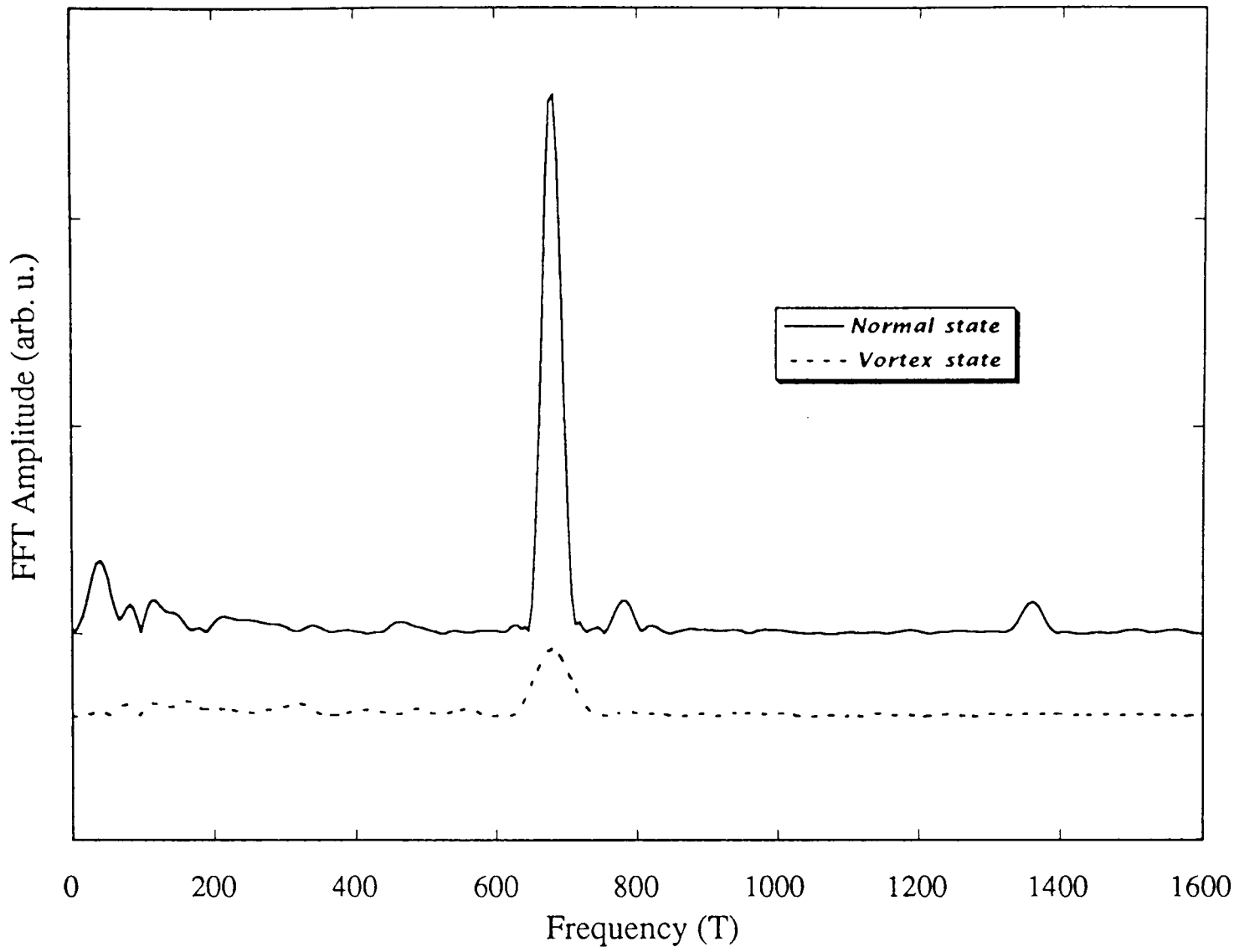

Figure 4 Fourier spectra of the de Haas-van Alphen oscillations observed in κ-$ET_2Cu(NCS)_2$ (shown in figure 3), transformed above and below 5 T.

Figure 5 shows the signal predicted by the Lifshitz-Kosevich formula [18] using the parameters measured in the normal state. Above B_{c2} the Lifshitz-Kosevich formula fits the data well but below B_{c2} the experimental de Haas-van Alphen oscillations are attenuated more quickly than is predicted by the Lifshitz-Kosevich formula.

From the field dependence of the oscillation amplitude one can estimate the broadening of the Landau levels due, for example, to scattering by impurities. The "Dingle plot" shown in figure 6 demonstrates that for magnetic fields $B > B_{c2}$ the Dingle temperature is 0.49 K and field independent, *i.e.* a scattering rate or broadening of $\tau_0^{-1} = 0.4 \times 10^{12}$ s^{-1} (a mean free path of $l = v_F\tau \approx 1000$ Å). The Dingle plot shows the onset of the additional attenuation on passing from the normal to the superconducting state. Figure 7 shows the field dependent scattering rate, determined from figure 6.

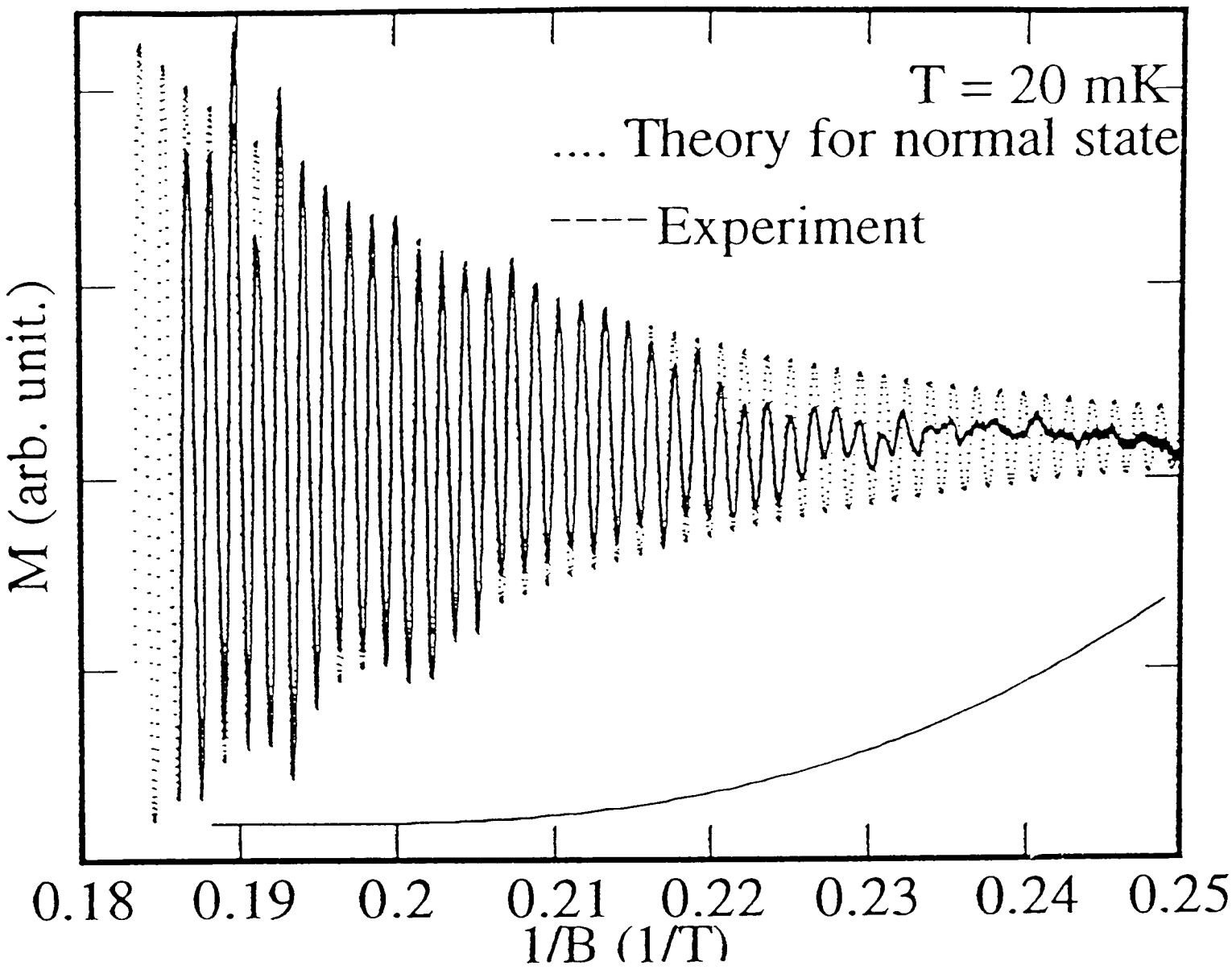

Figure 5 The solid line shows the de Haas-van Alphen signal at 20 mK with the slowly varying background subtracted. The dotted line is the signal predicted by the Lifshitz-Kosevich formula using fitting parameters derived from data taken well above B_{c2}. Above the Lifshitz-Kosevich formula fits the data well but below the experimental de Haas-van Alphen oscillations are attenuated more quickly than is predicted by the Lifshitz-Kosevich formula.

On approaching the vortex state the scattering rate starts to increase from the constant value τ_0^{-1} which is due to impurity scattering. Similar increases have been observed in other superconductors and the interpretation of this phenomenon is discussed below.

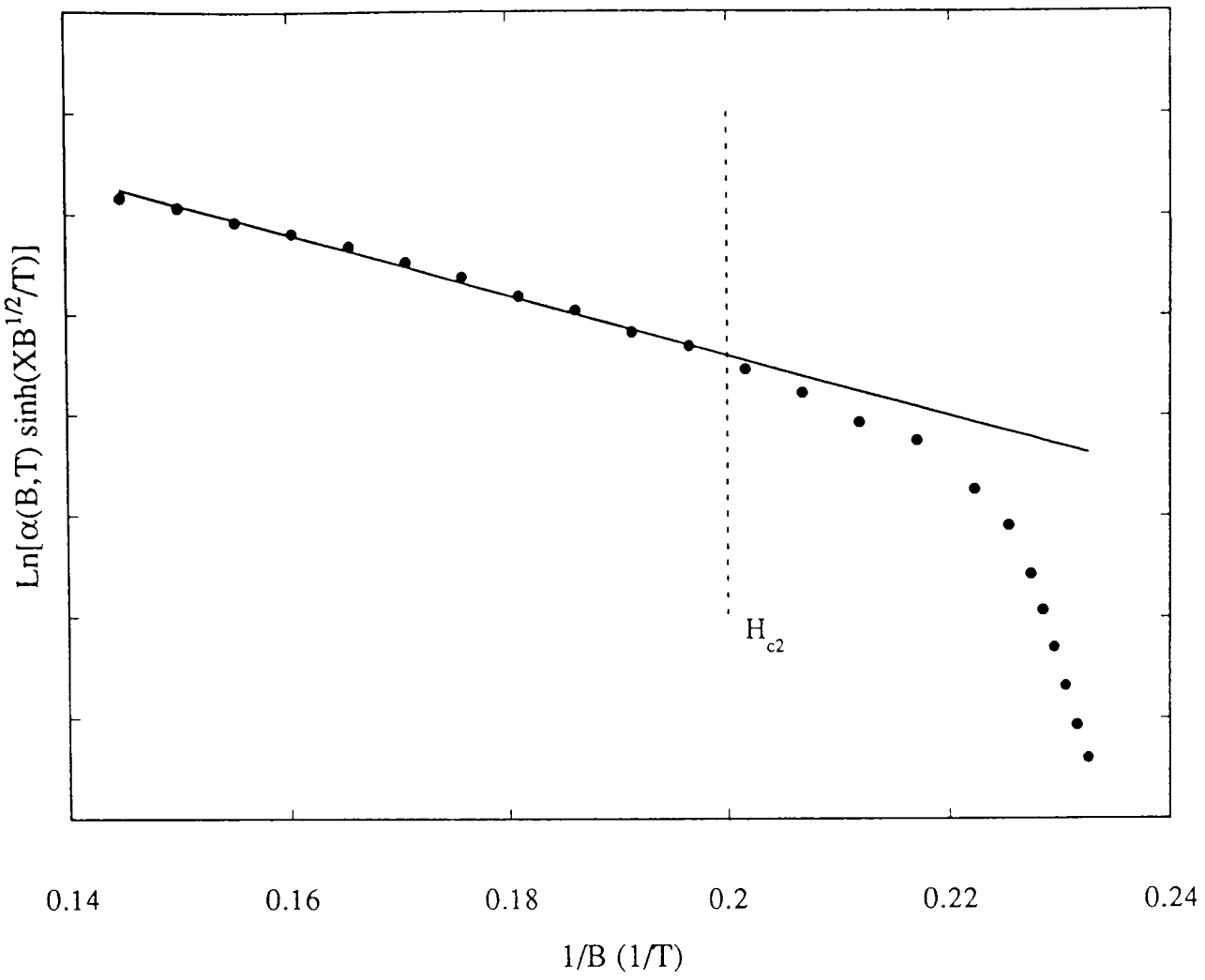

Figure 6 A Dingle plot showing the onset of the additional attenuation on passing from the normal to the superconducting state. The Dingle temperature in the normal state is 0.49 K.

As mentioned earlier studies in a number of type II superconductors [5,6,7,8] have shown that quantum oscillations (*e.g.* de Haas-van Alphen oscillations) persist below B_{c2}, into the vortex state. Although oscillations are still present, there is a suppression of their amplitude which can be interpreted as an additional energy broadening of the Landau levels or scattering of the quasiparticles. Theoretical models (this work § 4.2, [11,12]) strictly valid only near B_{c2}, suggest that the effect of the vortex state can be incorporated into an additional field dependent scattering rate $\tau^{-1} = \tau_0^{-1} + \tau_s^{-1}(B_0)$ where $\tau_s^{-1}(B_0) \propto \Delta^2$ [11] (Δ is the superconducting gap). Such a model has been used to successfully account for observations in $NbSe_2$ [6] and the A15 superconductor V_3Si [7] where oscillations are observed down to $B_0 \sim 0.5B_{c2}$.

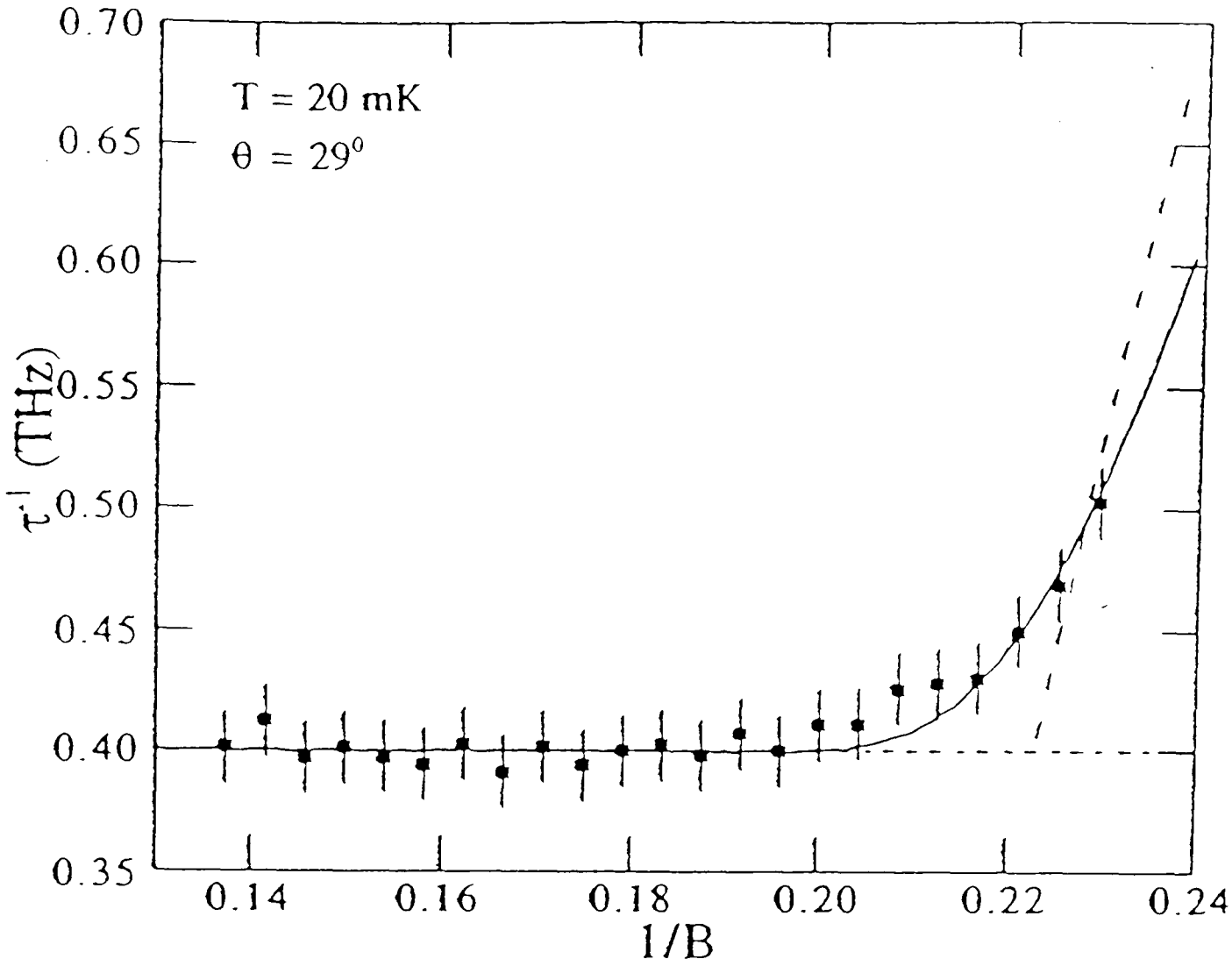

Figure 7 Field dependent quasiparticle scattering rate determined from the Lifshitz-Kosevich formula. The dashed line is a fit to the Maki model [11]. The solid line is a fit to the Maki model including a spread of B_{c2} (half width at half maximum) of 4.8 % in the model.

The persistence of quantum oscillations into the mixed state of κ-$ET_2Cu(NCS)_2$ could, in principle, be due to a small portion of the sample remaining normal. However, the superconducting anomaly observed in the specific heat capacity of similar samples indicate that κ-$ET_2Cu(NCS)_2$ is a bulk superconductor [16]. In most superconductors there is a sudden disturbed region of magnetisation at B_{c2} followed by a steep rate of change of magnetisation; this is thought to be due to the creation or destruction of the flux lattice. In κ-$ET_2Cu(NCS)_2$ there is no sudden redistribution of the flux at B_{c2}, probably due to the broadened nature of the superconducting transition. The short superconducting coherence length of κ-$ET_2Cu(NCS)_2$ means that the superconducting properties are probably very sensitive to spatial inhomogeneities in the system [15]. Such inhomogeneities may be responsible for the broadened superconducting anomaly in the heat capacity observed in other samples of this material

[16]. It is postulated that due to inhomogeneities a typical $\kappa-ET_2Cu(NCS)_2$ sample will contain a spread of B_{c2} values (it has already been demonstrated in the previous chapter how sensitive the superconducting properties are to pressure). Indeed it has been shown that the broadness of the superconducting transition is directly related to the to the purity of the starting anion [23]. Even in the purest crystals of $\kappa-ET_2Cu(NCS)_2$ the broadness of the transition is typically ~2 K (from the onset to zero resistance) [23]. In a magnetic field the transition from the superconducting to the normal state resistance occurs over a region of ~2 T (*e.g.* figure 7 in chapter 3). Hence B_{c2} is impossible to determine precisely.

In the present case a detailed comparison with theory is precluded because it is not possible to get a precise estimate of $<B_{c2}>$ from other experimental data, due to the broadened nature of the superconducting transition. The dashed line in figure 7 is a fit of the Maki model [11] assuming a BCS value for Δ of 1.6 meV (and assuming Δ evolves according to the expression [11] $\Delta^2 = \Delta^2(0)(1-B/B_{c2}))$ which gives B_{c2}~4.5 T. It can be seen that the model does not account for the "smooth" variation of τ^{-1} on entering the superconducting state. The solid line in figure shows the effect of including a Gaussian spread of B_{c2} (half width at half maximum) of 4.8 % in the model (due to sample inhomogeneities. In this case the fit is considerably improved and an estimate of $B_{c2}\cong$4.6 T is obtained using $\Delta(0)$=1.6 meV. However, without a reliable measurement of B_{c2} a precise estimate of $\Delta(0)$ cannot be made.

By repeating the above measurements with the sample at different tilt angles with respect to the magnetic field, one can in principle determine the symmetry of the superconducting order parameter. As the sample is tilted in the magnetic field B_{c2} increases approximately as $1/\cos(\theta)$, as one would expect for a two dimensional system. The field dependence of the scattering rate was measured with the magnetic field applied at several angles to the ***a***-axis (figure 8). At these angles the noise level was quite large and the points shown are averaged values from several traces. It appears from the data that the rate of increase of the scattering rate on entering the vortex state is not very

angle dependent; the points at which the scattering rate starts to increase moves to higher fields with increasing tilt angle, as it follows the same angle dependence as B_{c2}. From the data it appears that the order parameter is fairly isotropic, although many more measurements at different tilt angles with better signal-to-noise ratios are required to prove this conclusively.

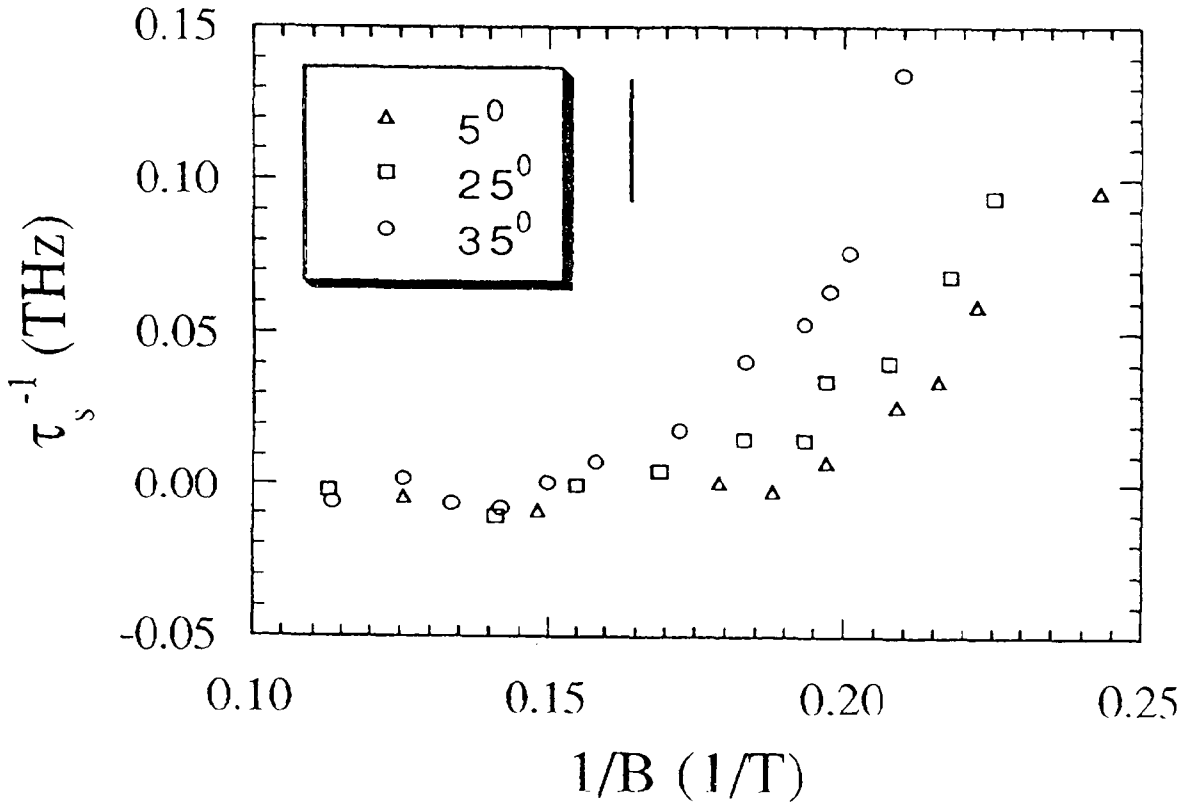

Figure 8 A plot of the field dependent quasiparticle scattering rate (relative to that in the normal state) with the magnetic field applied at several angles to the ***a***-axis. The bar denotes the error (which is large). The points are averaged over several traces.

4.5 Summary

In summary, de Haas-van Alphen oscillations have been observed for applied magnetic fields as low as 4.3 T in $\kappa-ET_2Cu(NCS)_2$. At the lowest fields, the quantum oscillatory magnetisation exhibits a decrease in amplitude greater than that predicted by the standard Lifshitz-Kosevich theory. Maki's theory of the de Haas-van Alphen effect in the superconducting mixed state was applied to the experimental data in order to estimate the superconducting gap parameter $\Delta(0)$. The Maki model [11] does not

account for the "smooth" variation of τ^{-1} on entering the superconducting state. It was postulated that the onset to superconductivity in $\kappa-ET_2Cu(NCS)_2$ is very broad due to sample inhomogeneities. By including a broadening in B_{c2} of 4.8 % into the Maki model a good fit to the experimental data was obtained using a BCS superconducting gap of $\Delta(0) = 1.6$ meV and a B_{c2} of 4.3 T. However, without a reliable measurement of B_{c2}, a precise estimate of $\Delta(0)$ cannot be made. The suppression of the de Haas-van Alphen amplitude signals the presence of the vortex state and may provide a novel method of determining an estimate of the bulk average of B_{c2} in this material. Further studies are in progress using a coil custom built for these samples which will improve the signal-to-noise ration by approximately an order of magnitude .

References

[1] *Organic Superconductors,* T. Ishiguro and K Yamaji (Springer, Berlin,1990).

[2] J. Wosnitza, G.W. Crabtree, H.H. Wang, U. Geiser, J.M. Williams and K.D. Carlson, *Phys. Rev.* **B 45** 3018 (1992).

[3] M. Dressel, O. Klein, G. Grümer, K.D. Karlson, H.H. Wang and J.M. Williams, *Phys. Rev.* **B** *in press.*

[4] M. Lang, N. Toyota, T. Sasaki and H. Sato, *Phys. Rev.* **B 46** 5822 (1992).

[5] J.E. Graebner and M. Robbins, *Phys.Rev.Lett.* **36** 433 (1976).

[6] R. Corcoran, P. Meeson, Y. Onuki, P-A. Probst, M. Springford and T. Takita, *Physica* **B 194-196** 1573 (1994).

[7] R.Corcoran, N.Harrison, S.M.Hayden, P.Meeson M.Springford and P.J. van der Wel, *Phys.Rev.Lett.* **72** 701 (1994).

[8] N. Harrison, S.M. Hayden, P. Meeson, M. Springford P.J. van der Wel and A.A. Menovsky, to be published, *Phys.Rev.***B**.

[9] U. Brandt, W. Pesch and L. Tewordt, *Z. Phys.* **201** 209 (1967).

[10] M.J. Stephen, *Phys. Rev.* **B 43**, 1212 (1991).

[11] K. Maki, *Phys. Rev.* **B 44**, 2861 (1991).

[12] A. Wasserman and M. Springford, *Physica* **B 194-196** 1801 (1994).

[13] K. Miyake, *Physica* **B 186-188** 115 (1993).

[14] K. Maki, *Physica* **B 186-188** 847 (1993).

[15] For example F.Hellman and T. H. Geballe, *Phys. Rev.* **B 36**, 107 (1987).

[16] J.E.Graebner, R.C. Haddon, S.V.Chichester and S.H.Clarum, *Phys.Rev.***B. 41** 4808 (1990).

[17] E.H. Brandt, *Phys. Rev.* **B 18**, 6022 (1978).

[18] *Magnetic Oscillations in Metals*, D. Shoenberg, (Cambridge University Press, 1984).

[19] D. Shoenberg and P.J. Stiles, *Proc. Roy. Soc.* (London) **A281**, 62 (1964).

[20] P.H.P. Reinders, M. Springford, P. Hilton, N. Kerley and N. Killoran, *Cryogenics* **27** 689 (1987).

[21] M. Tinkham, "*Introduction to Superconductivity*"; Robert E. Krieger Publishing Co.: Huntingdon, New York, 1980.

[22] H. Urayama, H. Yamochi, G. Saito, K. Nozawa, T. Sugano, M. Kinoshita, S. Sato, K. Oshima, A. Kawamoto and J. Tanaka, *Chem. Lett.* **1988**, 55 (1988).

[23] H. Mori, S. Tanaka, H. Yamochi, G. Saito and K. Oshima, *Springer Proceedings in Physics*, **51** 150 (1990).

Chapter 5

High field magnetoresistance oscillations in α-$ET_2KHg(SCN)_4$: the effects of magnetic breakdown, exchange interactions and Fermi surface re-ordering.

5.1. Introduction

Charge-transfer salts of the form ET_2X (where X is a monovalent anion) have been the subject of intense experimental study since high quality single crystals became available [1,2]. The ET molecules are linked to each other by overlap of their molecular π-orbitals and stack along side one another, separated by sheets of the anion X, to form a two-dimensional conductive network. Within this family of materials $\alpha-ET_2MHg(SCN)_4$, (M=K [3], Tl [4], Rb [5] or NH_4 [6]) were synthesised as modifications of $\kappa-ET_2Cu(NCS)_2$ in an attempt to obtain a higher superconducting transition temperature (T_c). The salts are isostructural (the so-called α-phase) and as a consequence have almost identical predicted Fermi surfaces consisting of a two-dimensional closed hole pocket and a pair of one-dimensional planar Fermi surface sheets [6] (figure 1(a)).

The salt $\alpha-ET_2NH_4Hg(SCN)_4$ is a superconductor, with T_c~1 K. In contrast, the salts $\alpha-ET_2MHg(SCN)_4$ (where M=K, Tl and Rb) remain metallic down to ~<100 mK [7] and all show the onset of antiferromagnetic order at temperatures $T_N \sim 8-10$ K with the easy axis in the highly conducting ***ac***-plane [8,9]. Electron spin resonance [10] and nuclear magnetic resonance [11] measurements also show anomalous changes below T_N in the intensity of the electron spin resonance signal and in the proton-relaxation time respectively. Hall resistance measurements [12] have demonstrated that the carrier density steeply decreases below T_N. These phenomena have been linked to the possible presence of a spin density wave ground state as evidenced by a recent muon spin rotation study of the M=K salt [13]. No such behaviour has been observed in $\alpha-ET_2NH_4Hg(SCN)_4$.

Another transition has been discovered in the low temperature resistance of the salts with M=K, Tl and Rb [14], but this time as a function of *field* (see figure 2). This so called `kink transition' [15] is not observed in $\alpha-ET_2NH_4Hg(SCN)_4$ (Figure 2(b)) below 50 T; instead, a series of Shubnikov-de Haas oscillations of the conventional form are observed with a periodicity within a few percent of that expected from the predicted

two-dimensional hole pocket and superimposed upon a monotonically increasing magnetoresistance. However, in $\alpha-ET_2KHg(SCN)_4$ the magnetoresistance rapidly increases up to ~10 T (at 0.5 K), but above this field, the magnetoresistance decreases until at ~23 T a 'kink' in the magnetoresistance appears, above which the magnetoresistance increases with increasing field (figure 2(a)). Below the kink and above ~7 T the magnetoresistance exhibits significant hysteresis [8,9,16,17], particularly when the ***ac***-plane of the sample is tilted with respect to the magnetic field [18]. It has been suggested that this kink transition is the point at which the external field destroys the low temperature antiferromagnetic state [16], but the low temperature bandstructure and the field-induced changes giving rise to the kink have remained the subjects of speculation.

Recently, a spin density wave ground state with a nesting vector $\mathbf{Q}=\zeta\mathbf{A}/6+\mathbf{C}/6+(2\eta-1)\mathbf{B}$ has been proposed for $\alpha-ET_2TlHg(SCN)_4$ [9,19] (where **A**,**B** and **C** are reciprocal lattice vectors of the room temperature crystal structure and η and ζ ±1 [9,19]). The proposed spin density wave occurs in the open sections of the Fermi surface opening up a gap at the Fermi level and consequently removing of the open Fermi surface completely. The new periodicity imposed by the spin density wave results in a new Brillouin zone and hence a reorganisation of the two dimensional Fermi surface. The action of the proposed spin density wave state on the calculated band structure results in a warped quasi-one-dimensional Fermi surface tilted by ~26° with respect to the ***b*c*** plane, plus small two-dimensional pockets (figure 1(b)). It is believed that a similar effect takes place in $\alpha-ET_2KHg(SCN)_4$.

In this chapter, the results of a detailed study of the magnetoresistance as a function of magnetic field and angle in single crystal samples of $\alpha-ET_2KHg(SCN)_4$ are presented. The character of the Shubnikov-de Haas oscillations for a range of samples, temperatures, and field regimes are examined. This reveals the extent to which exchange-enhanced spin-splitting and magnetic breakdown involving the various sections of the reorganised Fermi surface are important in determining the harmonic structure of the observed Shubnikov-de Haas oscillations. Angle-dependent magnetoresistance oscillations in magnetic fields up to 30 T in $\alpha-ET_2KHg(SCN)_4$ have been used to

investigate the Fermi surface topology both below and above the kink transition. Below the kink, it is shown that the low magnetic field bandstructure is dominated by a one-dimensional open section of Fermi surface inclined at ~21° to the crystallographic ***b*c*** plane, agreeing well with the model discussed in Ref. [9]; magnetic breakdown between the small two-dimensional pockets and the one-dimensional sheets (figure 1(b)) explains the various Shubnikov-de Haas oscillations frequencies and their anomalous field dependences. Above the kink, the magnetoresistance change in character, indicating that the Fermi surface now posseses a two-dimensional closed section in the form of a distorted cylinder. The data therefore give definitive proof that the kink is the signature of a magnetic-field-induced change in the Fermi surface.

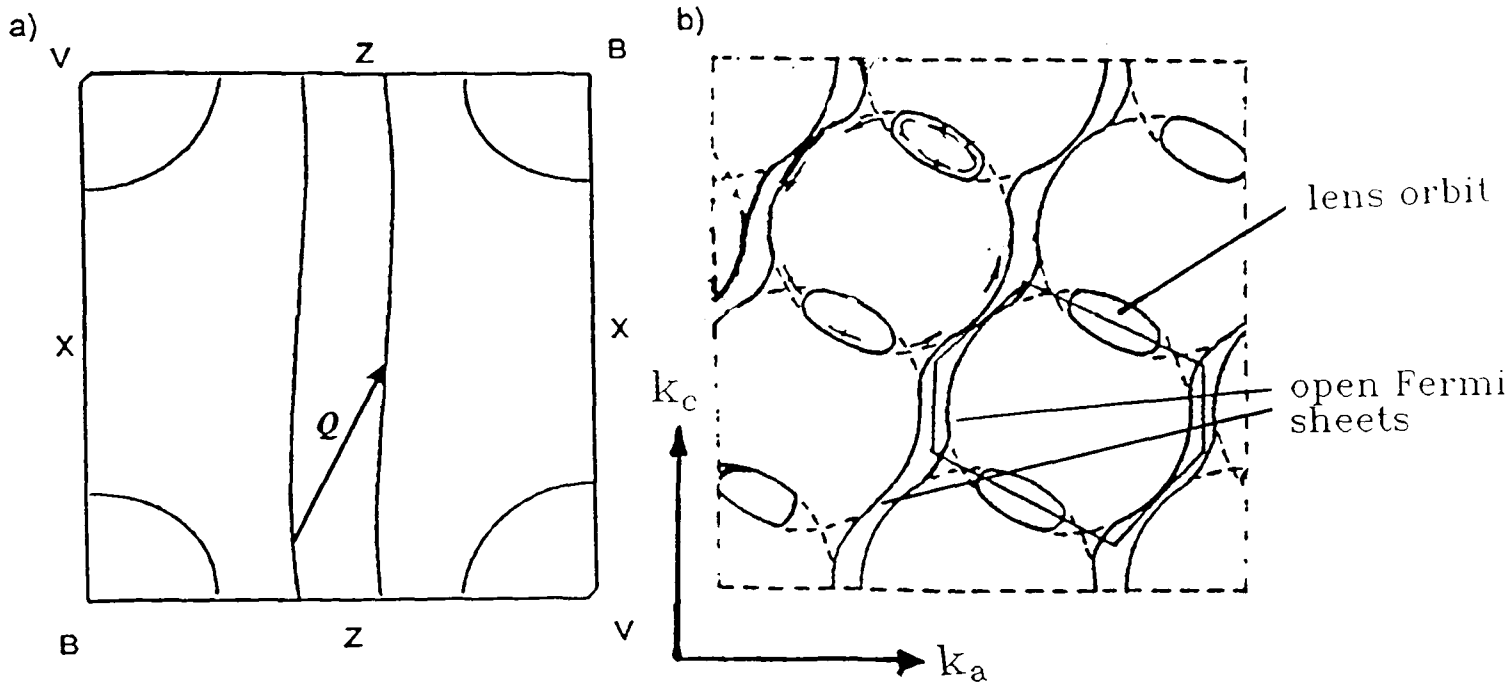

Figure 1 (a) Calculated Fermi surface for $\alpha - ET_2KHg(SCN)_4$ (after [3]). (b) Below T_N, the Fermi surface is modified to form new open sheets and small cylinders: thus a magnetic breakdown network arises (after [9]).

This chapter is organised as follows: In § 5.2, the structure and bandstructure of properties of $\alpha-ET_2KHg(SCN)_4$ are described. The experimental techniques are described in § 5.3. In § 5.4 the measured field dependent resistance of $\alpha-ET_2KHg(SCN)_4$ are presented along with a discussion of the importance of spin-splitting and magnetic breakdown. § 5.5 contains a full description of a series of angle dependent magnetoresistance measurements below and above the kink transition. The main results of these experiments are discussed in § 5.6 and the conclusions are summarised in § 5.7.

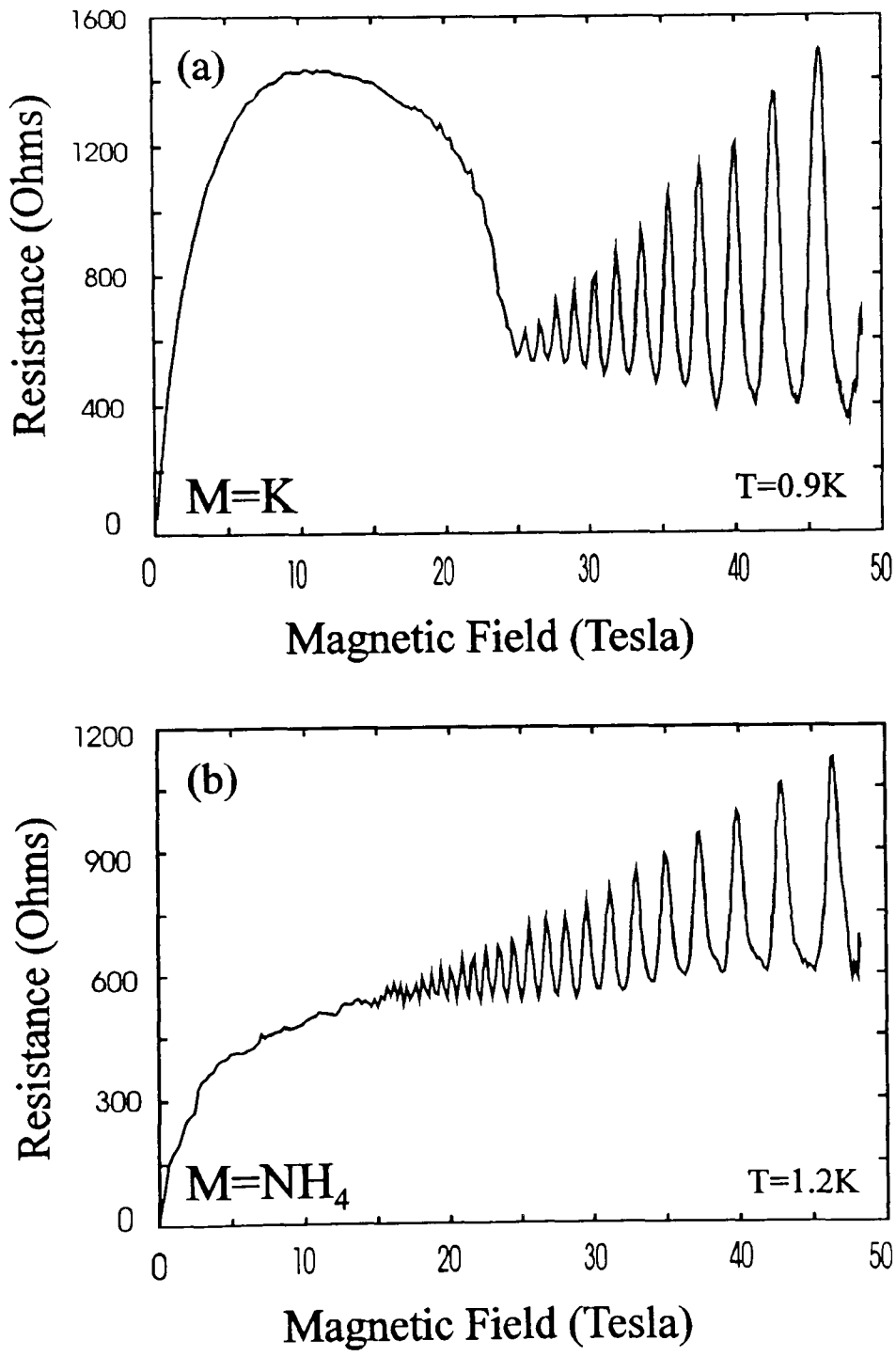

Figure 2 Magnetoresistance measured in a pulsed magnetic field for with $\alpha-ET_2MHg(SCN)_4$ (a) M=K and (b) $M=NH_4$. The magnetic field is applied along the b^* direction. After Ref [30].

5.2. Structure and bandstructure of α-$ET_2KHg(SCN)_4$

In an attempt to obtain new superconducting charge transfer salts with higher superconducting transition temperatures than in $\kappa-ET_2Cu(NCS)_2$, larger anion structures were created in order to increase the size of the unit cell (see figure 1, chapter 3). Chemists attempted to do this by substituting Hg for Cu in the starting materials of $\kappa-ET_2Cu(NCS)_2$. Instead the $ET_2MHg(SCN)_4$, (M=K [3], Tl [4], Rb [5] or NH_4 [6]) family of charge transfer salts were synthesised, with the ET molecules arranged in an α rather than κ motif (figure 3). In the α-phase the ET molecules stack in the ***ac***-plane in two separate columns along the ***a***-axis. This phase appears less favourable for superconductivity as only $\alpha-ET_2NH_4Hg(SCN)_4$ is a superconductor, with T_c~1 K. The crystal structure is triclinic with space group $P\bar{1}$. The lattice parameters of the $\alpha-ET_2KHg(SCN)_4$ salt are: ***a***=10.082 Å, ***b***=20.565 Å, ***c***=9.933 Å, α=103.70 °, β =90.91 °, γ=93.06 ° at 298 K [5]. The bandstructure of $\alpha-ET_2KHg(SCN)_4$ [5] is shown in figure 4.

The anion layer is rather thick, consequently the transfer integrals in the inter-plane direction are weak, making these materials highly two-dimensional. The triple layer insulating anion sheets consists of a sheet containing Hg^{2+} and M^+ sandwiched between two sheets of linear SCN groups. Hence a thick two-dimensional network of -M-NCS-Hg-SCN- spreads over the ***ac***-plane.

By substituting different cations, M^+, only slight structural differences are made [5]. Nevertheless there are vast differences in their groundstate properties; understanding the reasons behind these differences has been the major motivation of this chapter.

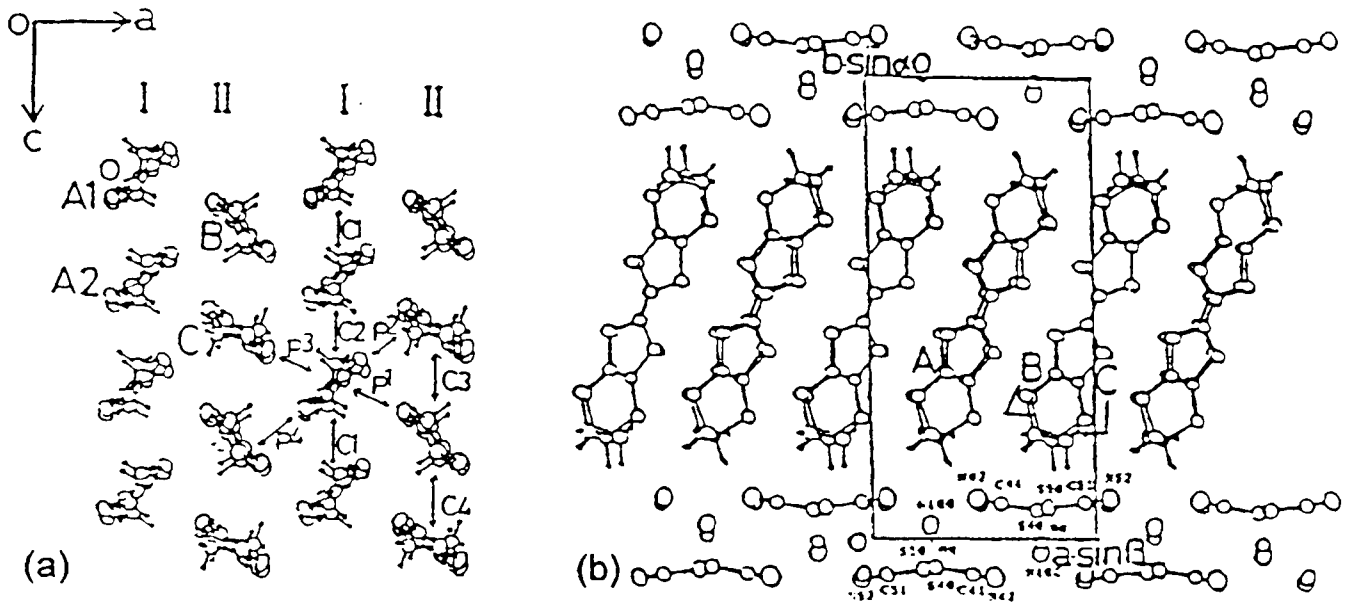

Figure 3 (a) Herring bone arrangement of the ET molecules in the ***ac***-plane (b) The crystal structure of α-$ET_2KHg(SCN)_4$; the triple layered polymetric anions separate the ET layers.

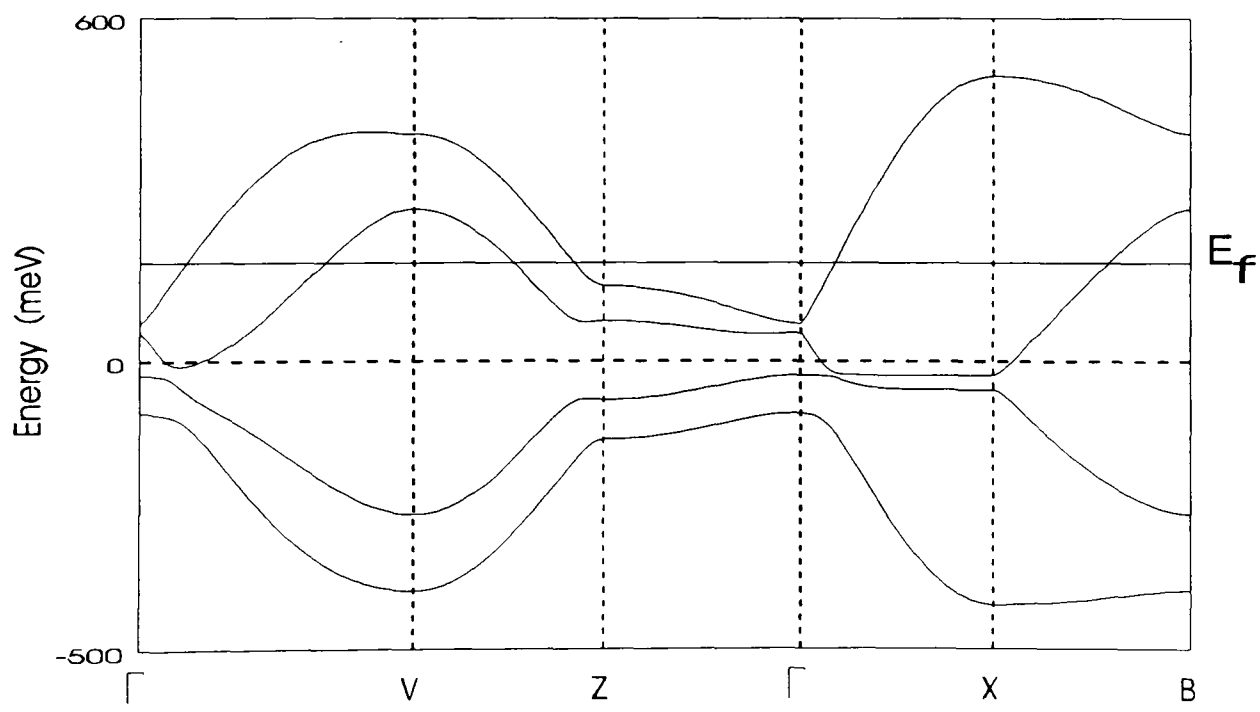

Figure 4 The tight binding bandstructure of α-$ET_2KHg(SCN)_4$ [5], based on the room temperature unit cell.

5.3. Experimental techniques

High purity single crystals of $\alpha-ET_2KHg(SCN)_4$ were prepared electrochemically by M. Kurmoo using the method of Larsen and Lenoir [21]. Typical dimensions for the resulting black distorted-diamond-shaped platelets are 1×0.5× 0.05 mm^3, with the plane of the plate corresponding to the highly conducting two-dimensional layers. Gold wires were attached to both ***ac*** platelet faces using platinum paint (figure 5), resulting in contact resistance values of less than 60 Ω at 300 K.

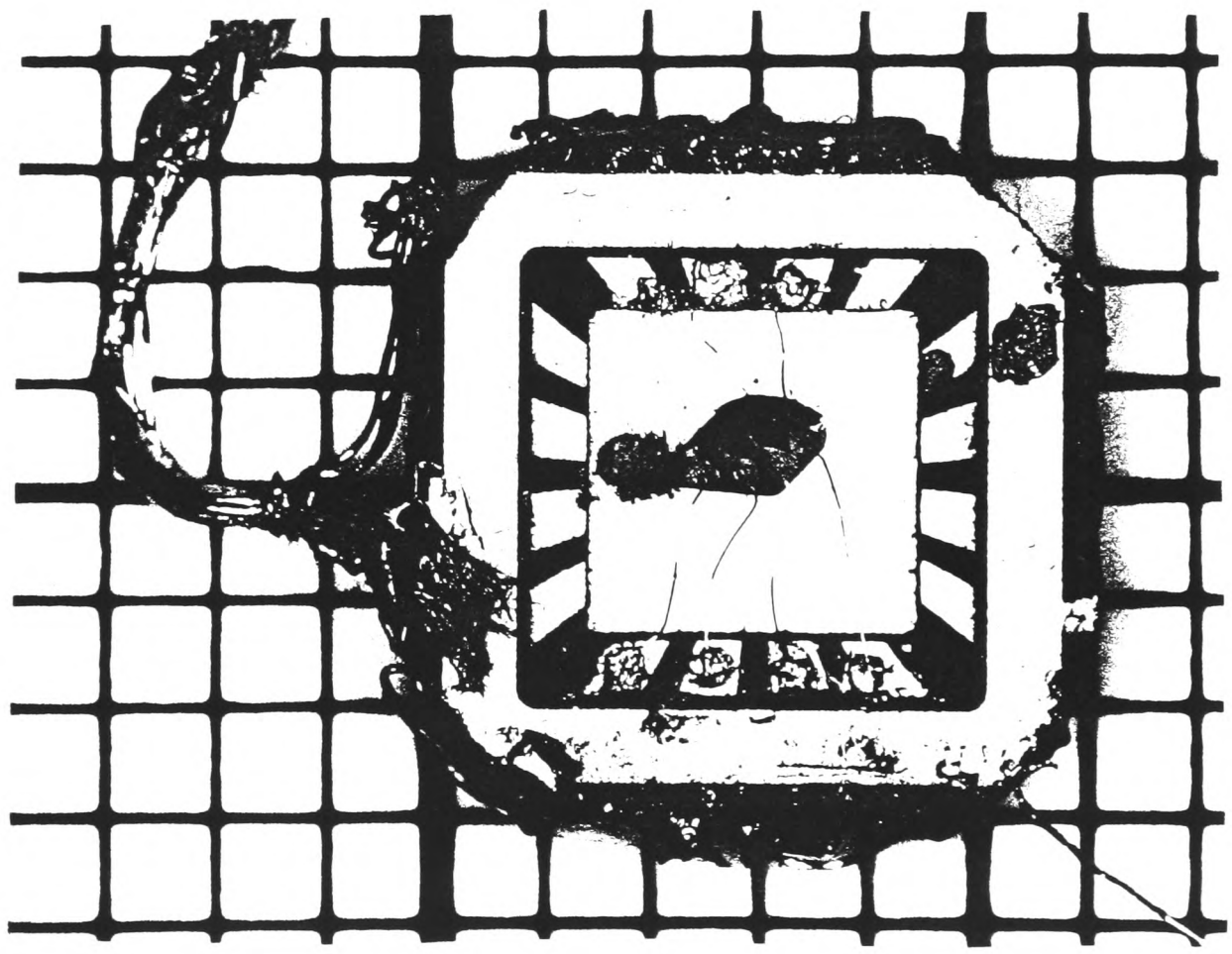

Figure 5 A photograph of a $\alpha-ET_2KHg(SCN)_4$ after several angular magnetoresistance experiments.

5.3-1. Pulsed field techniques

The pulsed fields, used in figure 2, were generated by the electrical discharge of a 500 MJ (5 kV, 40 mF) capacitor bank into a reinforced copper coil cooled by liquid nitrogen at Leuven. The pulse length is ~10-20 ms, with maximum fields up to 69 T. The Leuven pulsed field system is described in detail elsewhere [22]. During the pulse a voltage is generated by a calibrated pick-up coil and the integrated signal is recorded for the field measurement. The magnetoresistance contains large induced pick-up voltages from the sample and its wiring. This can be subtracted from the voltage derived from two compensation coils placed close to the sample. The data in figure 2 were recorded in a ^{3}He bath cryostat. The tail of the ^{3}He cryostat is constructed from glass to avoid eddy current heating. The sample is mounted at the end of a Hysol probe (figure 6) which is immersed directly into the ^{3}He; the probe was designed to hold up to four samples simultaneously.

Standard 4-wire D.C. techniques were used and to avoid sample heating currents were generally 10-200 μA applied in the ***b**** direction. On the sample probe, in figure 6, it was found that a strip of strictly parallel current and voltage wires (50 μm copper wire) was preferable to the usual twisted pair arrangement, which behaves as a series of small pick-up loops. To eliminate the pick-up voltages that were not completely removed by the compensation circuits several averaging techniques were attempted, using different combinations of magnetic field and sample current directions. The most satisfactory technique was to subtract two measurements with the same magnetic field direction but with opposite current directions. Analysis was principally carried out on the down sweep signals, since vibrational noise and heat input to the sample are generally much less significant on the down sweep of the pulse. Inductive heating in ET salts does not appear to be a problem, as reliable measurements of the effective masses (when compared to steady field measurements) of the $\alpha-ET_2KHg(SCN)_4$ and $\alpha-ET_2NH_4Hg(SCN)_4$ have been made in pulsed fields using temperatures down to 300 mK [23].

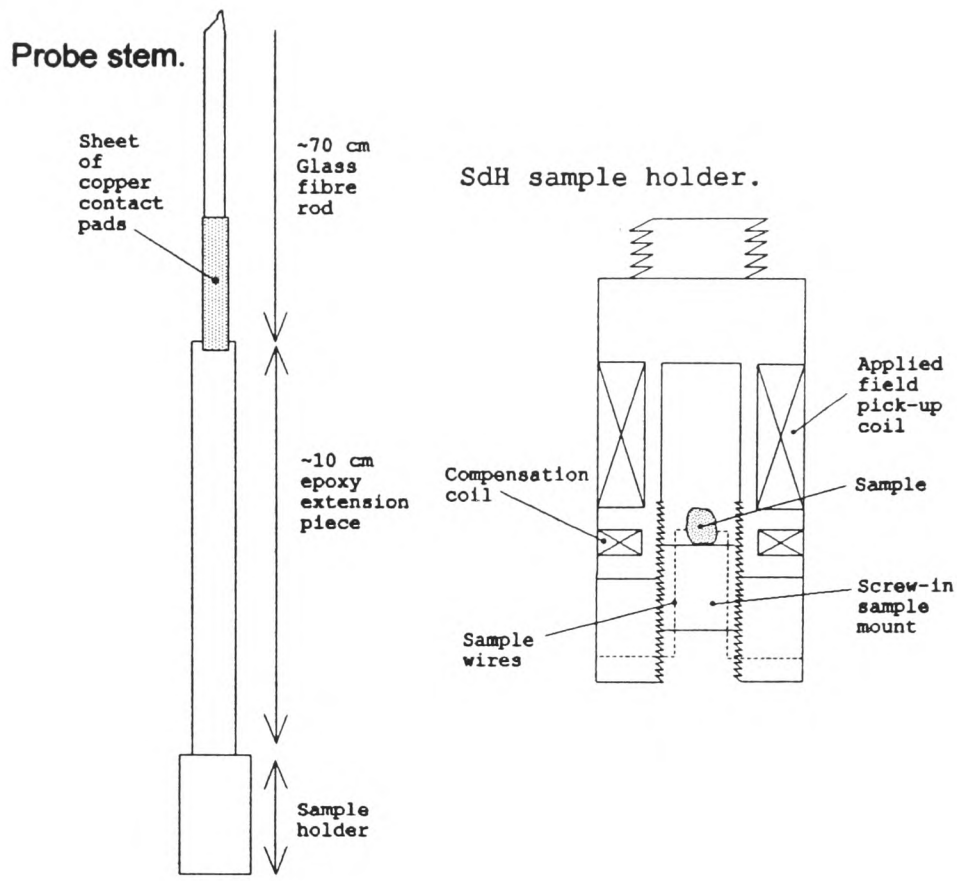

Figure 6 The Hysol sample holder, designed to hold four ET samples simultaneously during pulsed field measurements.

5.3-2. Angle dependent magnetoresistance techniques

Magnetoresistance measurements were carried out over a wide range of orientations of the crystals in the field using ^{3}He and ^{4}He cryostats which allowed the sample to be rotated about two perpendicular axes *in situ* with a precision of ±1°. The insert used for the angle dependent measurements is shown in figure 7. The sample orientation was determined to ±1° by X-ray techniques [24] and by measuring the polarised infrared reflectivity at room temperature [25,26]. Magnetic fields up to 20 T were provided by the Nijmegen Bitter magnets, and the Nijmegen Hybrid II magnet was used to study the magnetoresistance of $\alpha - ET_2KHg(SCN)_4$ up to 30.4 T [27].

Standard 4-wire a.c. techniques (5-150 Hz) were used for all measurements (except those done in pulsed magnetic fields); the current was directed in the inter-plane ***b**** direction. Great care was taken to avoid sample heating: the currents used depended on the geometry of the sample and were generally in the range 0.2-20 μA.

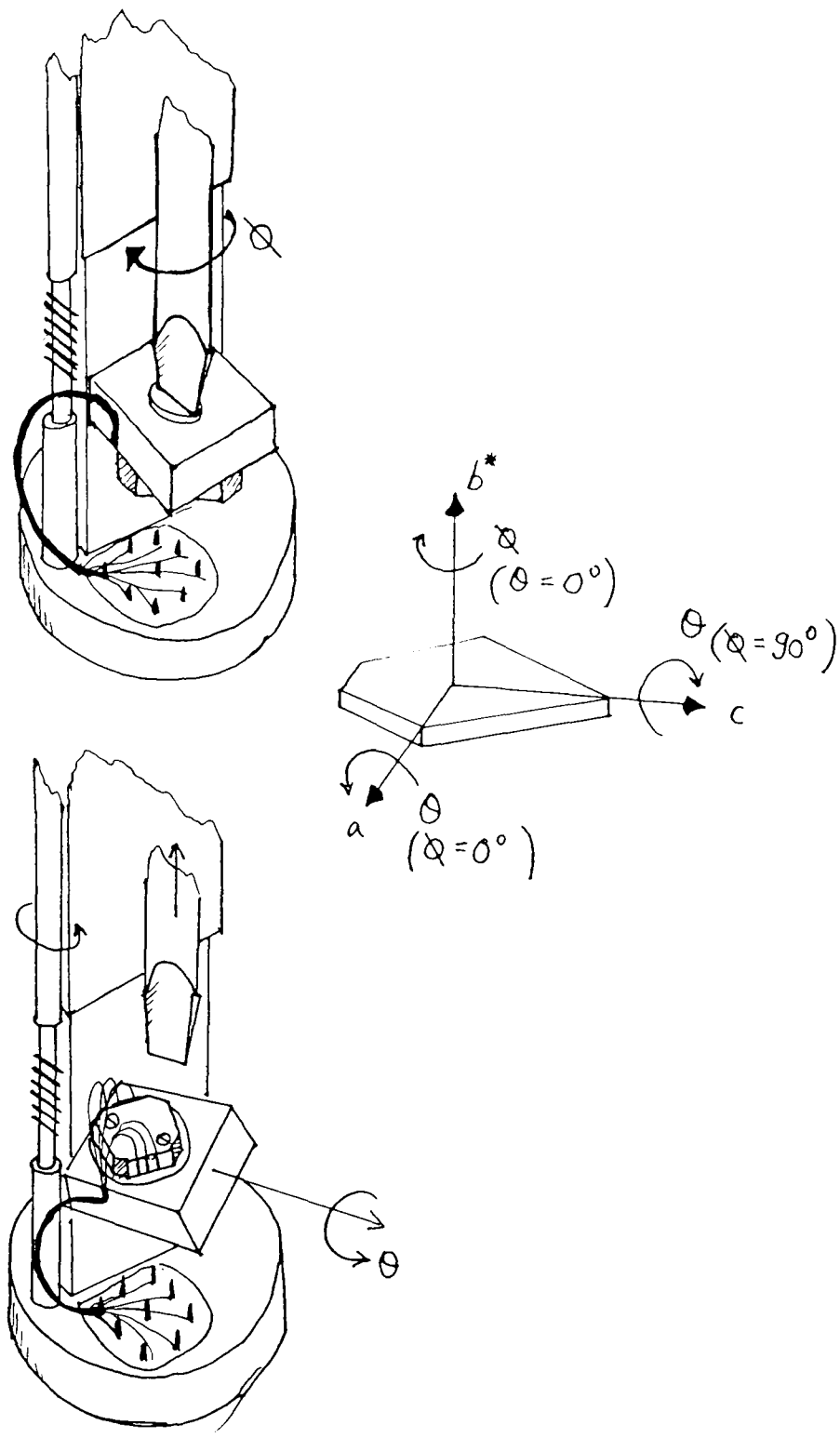

Figure 7 The insert used for the angle dependent magnetoresistance measurements, which allows the sample to be rotated about two perpendicular axes *in-situ*. The sample (figure 5) is mounted on the underside of a turn-table A long shaft ending in a screw driver blade is manually positioned into a slot in the turn-table to adjust the desired angle ϕ. The shaft and screw driver blade is then pulled clear. A worm drive axial rotation system, powered by a D.C. motor (connected to the worm drive via a gearing system, constructed from *Meccano*) whose speed is controlled by the operator, is used to sweep the angle θ.

5.4. Magnetoresistance

5.4-1. General features

The magnetoresistance of $\alpha-ET_2KHg(SCN)_4$ shows a number of striking features which may be summarised as follows:

1. There is a region of strong negative magnetoresistance (the kink) around 22 T when the field is parallel to $\boldsymbol{b}^*$ [8,9,15-17,28,29] (figure 2(a)).
2. At magnetic fields around and below the kink, there is strong hysteresis in the magnetoresistance [8,9,16,17].
3. Above the kink, there is one series of conventional Shubnikov-de Haas oscillations of frequency $B_F = 656 \pm 10\,\mathrm{T}$ which are similar in character to those observed in $\alpha-ET_2NH_4Hg(SCN)_4$. Below the kink, the oscillations are of a similar frequency $B_{F1} = 670 \pm 5\,\mathrm{T}$ but more complex, exhibiting a strong second harmonic component at certain angles [8,9,15-17,20,29]. The frequency of the oscillations is within a few per cent of that expected from band structure calculations. In addition, depending on sample quality (Dingle temperature), a second series of Shubnikov-de Haas oscillations can be clearly observed below the kink transition in $\alpha-ET_2KHg(SCN)_4$ and $\alpha-ET_2TlHg(SCN)_4$ [17,30].
4. The background magnetoresistance oscillates in size as the sample is tilted in the field [9,16].

Observations 1 and 3 will be examined in the context of the proposed Fermi surface (figure 1(b)) in detail in this section; the fourth, concerning the angular dependence of the magnetoresistance, is reserved for the following section.

5.4-2. Effective mass and scattering

The temperature dependence of the magnetoresistance in $\alpha-ET_2KHg(SCN)_4$ is shown in figure 8. Shubnikov-de Haas oscillations ('quantum' magnetoresistance) are seen as superimposed upon a ('classical' magnetoresistance) background; both effects are strongly temperature dependent. Since the amplitude of the quantum oscillations are scaled by the classical magnetoresistance (a sample with larger resistance has larger-amplitude quantum oscillations) [31], great care must be taken when analysing the temperature dependence of the oscillations in order to find the effective mass. A simple 'background subtraction' is insufficient in this case since the background is strongly field and temperature dependent [32], and so the measured data were *divided* by a fitted field and temperature dependent background. An effective mass of $(1.9\pm0.1)m_o$ is obtained by a direct fit to the Lifshitz-Kosevich formula and is field independent, as is the Dingle temperature. This is in disagreement with previous reports which estimate a somewhat lower value of $1.4m_o$ [17,20]; this may be due to an incorrect analysis by simple background subtraction rather than background division or to an insufficient temperature range used in the analysis. The measured effective masses of the higher harmonics up to third order behave as predicted by the semiclassical theory [33], indicating the validity of the approach. Above the kink transition, the effective mass is measured to be $(2.1\pm0.2)m_o$ which is of the same value as below the kink transition within experimental error.

Dingle plots are shown in figure 9 for applied fields below and above the kink. At the kink transition, a discontinuous change in slope (parameterised by the Dingle temperature T_D), and hence scattering time τ_D (since the effective mass is the same below and above the kink) is observed, corresponding to a change in Dingle temperature which is typically in the range 1.5-2.3 K ($\tau_D \sim 0.5-0.8$ ps) below the kink to ~6.5 K ($\tau_D \sim 0.2$ ps) above the kink. This observation is in good qualitative agreement with an unpublished de Haas-van Alphen study [34].

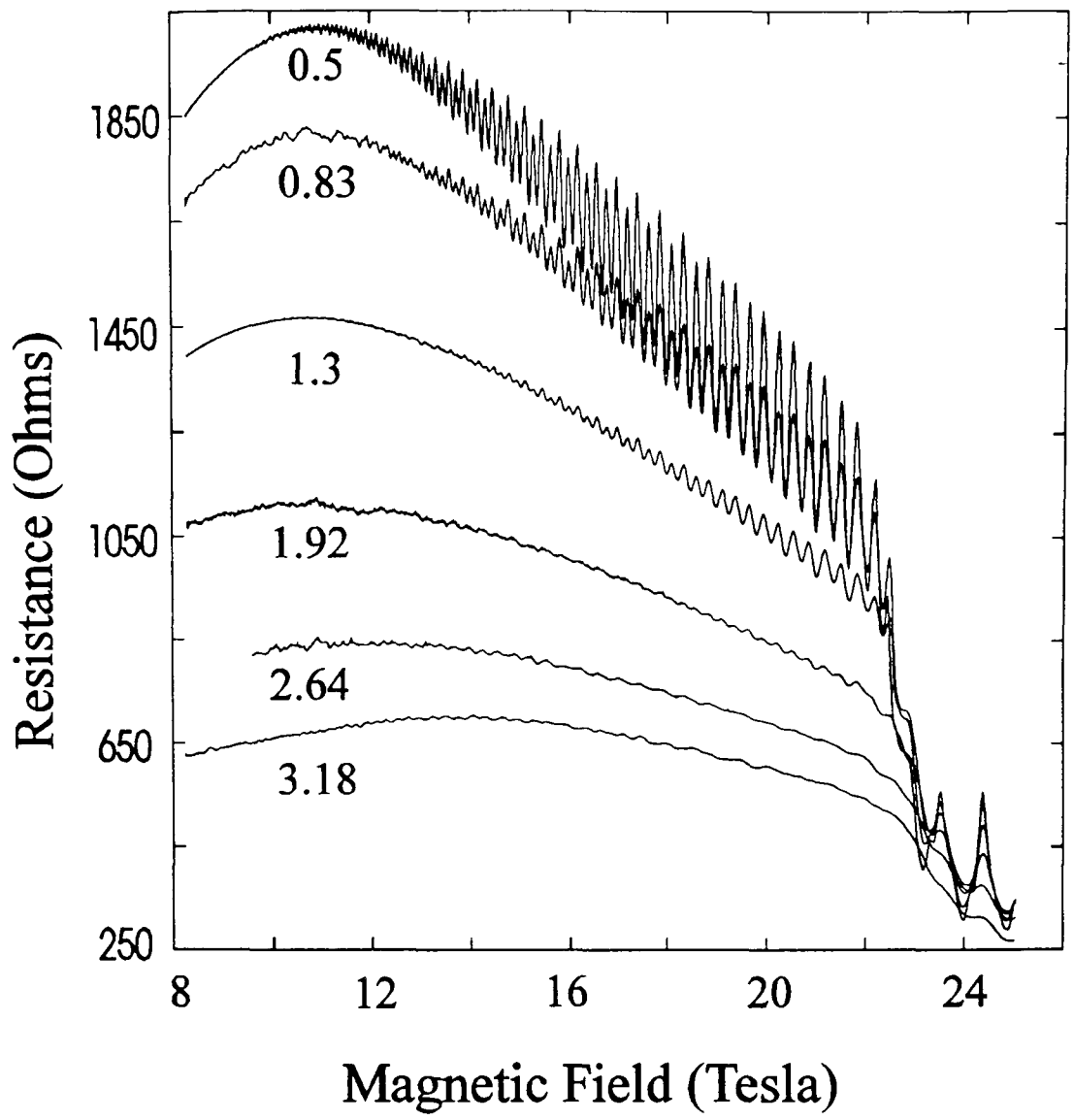

Figure 8 Magnetoresistance of a single crystal of $\alpha-ET_2KHg(SCN)_4$ at several temperatures. The temperature in degrees Kelvin is marked by each trace. Shubnikov-de Haas oscillations and the field-induced resistive kink at ~22 T can be clearly seen.

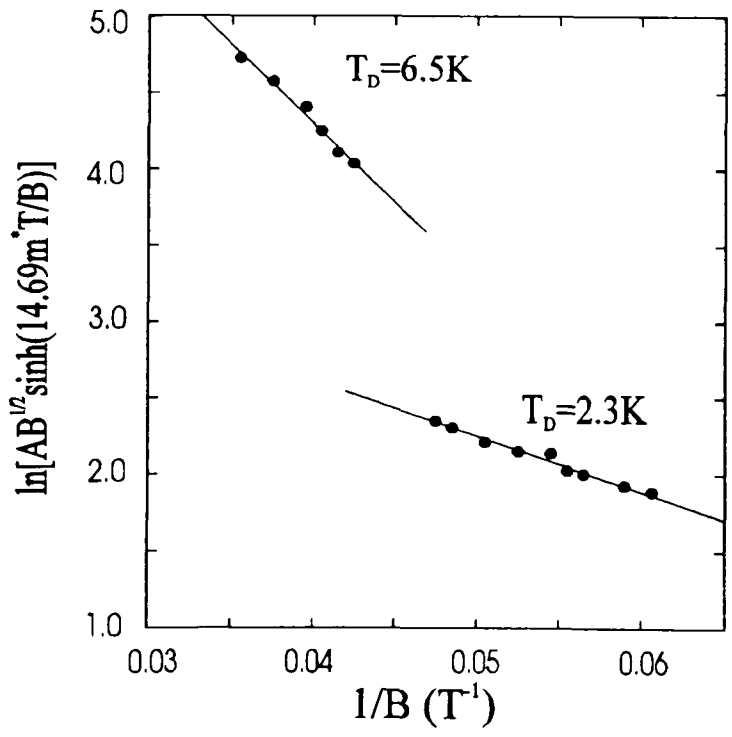

Figure 9 Dingle plot for oscillations below and above the kink transition. The measured Dingle temperatures are shown in the figure.

5.4-3. Spin splitting

In a magnetic field, the Landau levels (themselves separated in energy by $\hbar\omega_c$) can be further split into a set of spin-up and spin-down levels (Zeeman levels), each separated by $g\mu_B B$. Each set of splittings lead to quantum oscillations of the same frequency [33] but a phase difference equal to the field independent ratio $g\mu_B B/\hbar\omega_c$.

The g-factor for $\alpha-ET_2KHg(SCN)_4$ has been estimated by the Harmonic ratio method [16] which utilises the fact that the Zeeman splitting is angle independent whereas the cyclotron splitting depends on the perpendicular component of the magnetic field. Spin-splitting gives rise to a $\cos(pg\pi m^*(\theta)/2m_o)$ reduction factor in the Lifshitz-Kosevich formula [33] (where p is the harmonic number). Tilt angle experiments [16] yielded $gm^*(0)/m_o \sim 3.1$ (in the range 16-19 T) so that together with the value $m^*(0) \sim 1.9m_o$ a a g-factor of 1.6 was deduced [35].

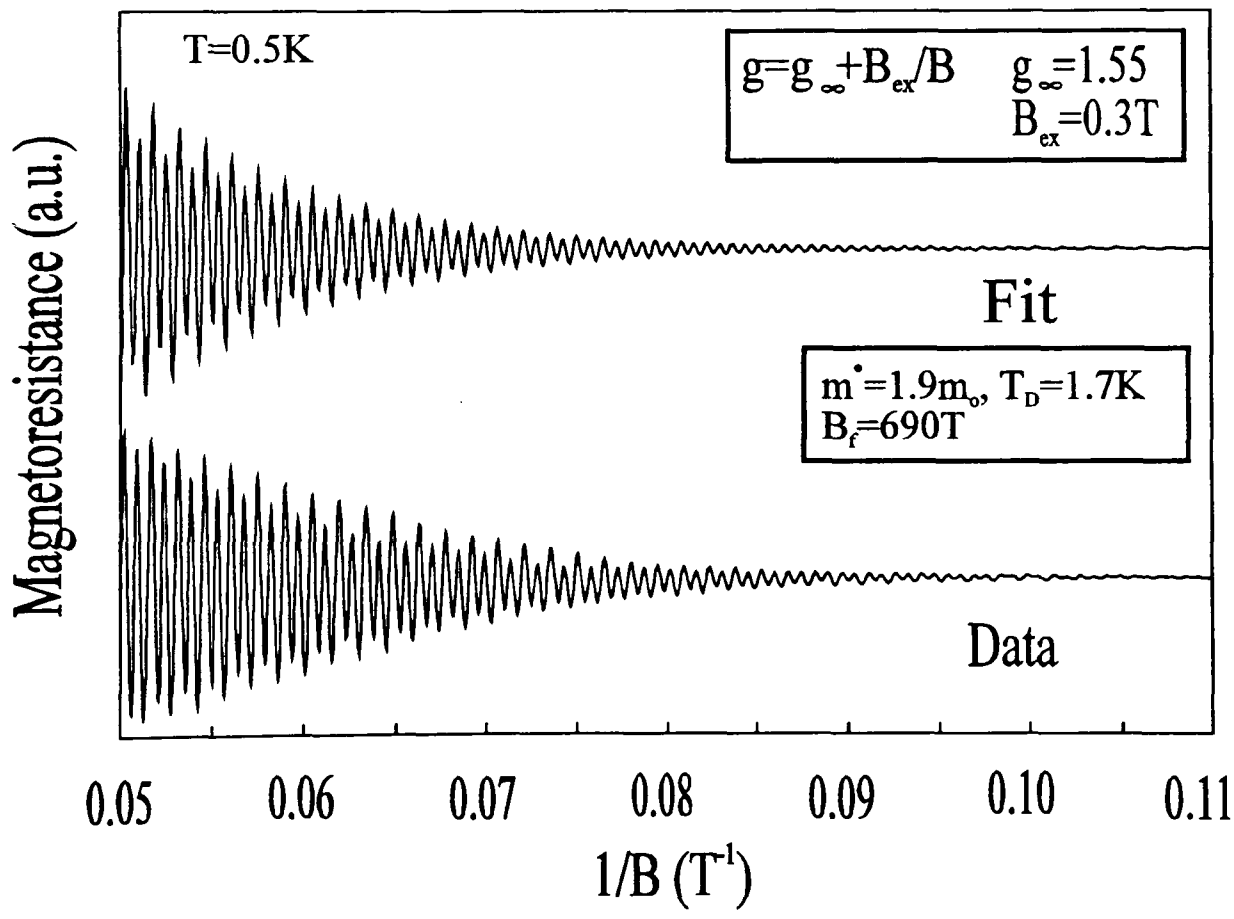

Figure 10 The data shown in figure 8 at 0.5 K is shown with the background divided out, together with a fit to the Lifshitz-Kosevich formula with the field-dependent g-factor $g = 1.55 + 0.3/B$.

In the lower half of figure 10, the oscillatory component of the lowest temperature magnetoresistance data is shown, obtained by dividing by the classical background magnetoresistance from the data shown in figure 8. The Fourier transform of these data (figure 11(a), showing data for temperatures between 0.5 K and 1.92 K) shows very high harmonic content: the effective mass of the peak of the second harmonic is twice as large as that of the fundamental, in accordance with the Lifshitz-Kosevich formula [33]. Strong spin-splitting at such low magnetic fields is not inconceivable if the Zeeman splitting were to be strongly enhanced by a magnetic exchange interaction.

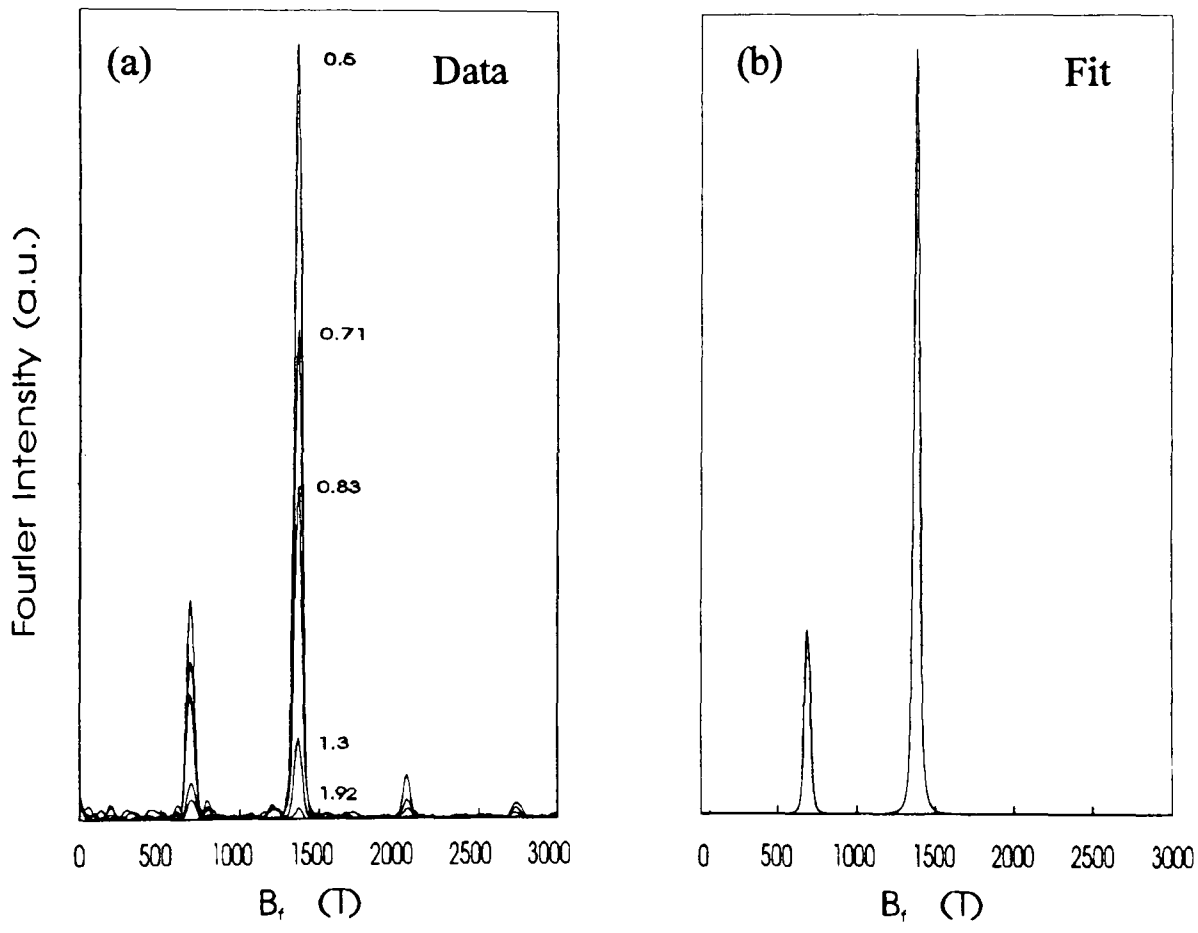

Figure 11 (a) The Fourier transform of the data in figure 8, the transform being performed after division by the background magnetoresistance. The temperature is as indicated in degrees Kelvin. The two most significant peaks are the fundamental (B_{F1}) and its second harmonic ($2B_{F1}$) which is much larger. (b) The Fourier transform of the fit in figure 10 for data at 0.5 K.

The best fit to the Lifshitz-Kosevich formula (summed up to the p=2 term) was obtained by using a magnetic field dependent g-factor [20] $g = g_\infty + B_{ex}/B$ using the experimentally determined Fermi surface parameters, where the exchange field is defined by $B_{ex} \equiv \Delta E / \mu_B$. A good fit is obtained using $g = 1.55 + 0.3/B$ (figures 10 (upper half) and 11(b)). These results are in agreement with those of Sasaki and Toyota [20] except that their value of B_{ex} is substantially larger. The g-factor agrees well with the above mentioned results of the Harmonic ratio method carried out in the same field range.

5.4-4. Magnetic breakdown

In addition to the fundamental frequency ($B_{F1} = 670$ T) and its second harmonic (both discussed above), other frequency components are observed which are denoted as $B_{F1} + B_{F2} = 820 - 870$ T, whose amplitudes and frequencies are slightly sample or cooling method dependent. The ranges quoted for these additional oscillations reflect the variation in B_{F2} from sample to sample. One can relate these additional frequencies to the model of the proposed low-field Fermi surface discussed in the introduction: B_{F2} corresponds to the small two-dimensional pocket (lens orbit) in figure 1(b); B_{F1} corresponds to the larger orbit produced by breakdown and includes the one-dimensional Fermi sheets. All of the frequencies observed have a magnetic field dependence characteristic of a magnetic breakdown network [36]. The amplitude of the small Fermi surface pocket frequency B_{F2} is large at low magnetic fields; its amplitude decreases steadily above 12 T, whilst in the same region the amplitudes of B_{F1} and $B_{F1} + B_{F2}$ steadily increase.

In some samples, the amplitudes of the frequencies B_{F2} and $B_{F1} + B_{F2}$ are small relative to that of B_{F1} (*e.g.* see figure 11). In other samples, the amplitudes of all three frequencies are comparable, and strong beating is found in the oscillatory part of the magnetoresistance (figure 12); in these samples, the magnetic field dependence of the amplitude of B_{F1} differs from that predicted by the standard Lifshitz-Kosevich formula.

The difference between these samples could be related to the degree of Landau level broadening induced by sample quality and/or electron heating. This is demonstrated by considering in detail the data presented in figure 12 which are shown for the same sample but under different experimental conditions. When the applied current is 4 μA, the electron heating is small and the Landau level broadening is low. Consequently, the magnetoresistance is dominated by spin-splitting effects and can be fitted using the same parameters and analysis as that presented above (figure 12(a)). With a larger current of 10 μA, the spin-splitting features are suppressed, but a strong beating pattern is evident.

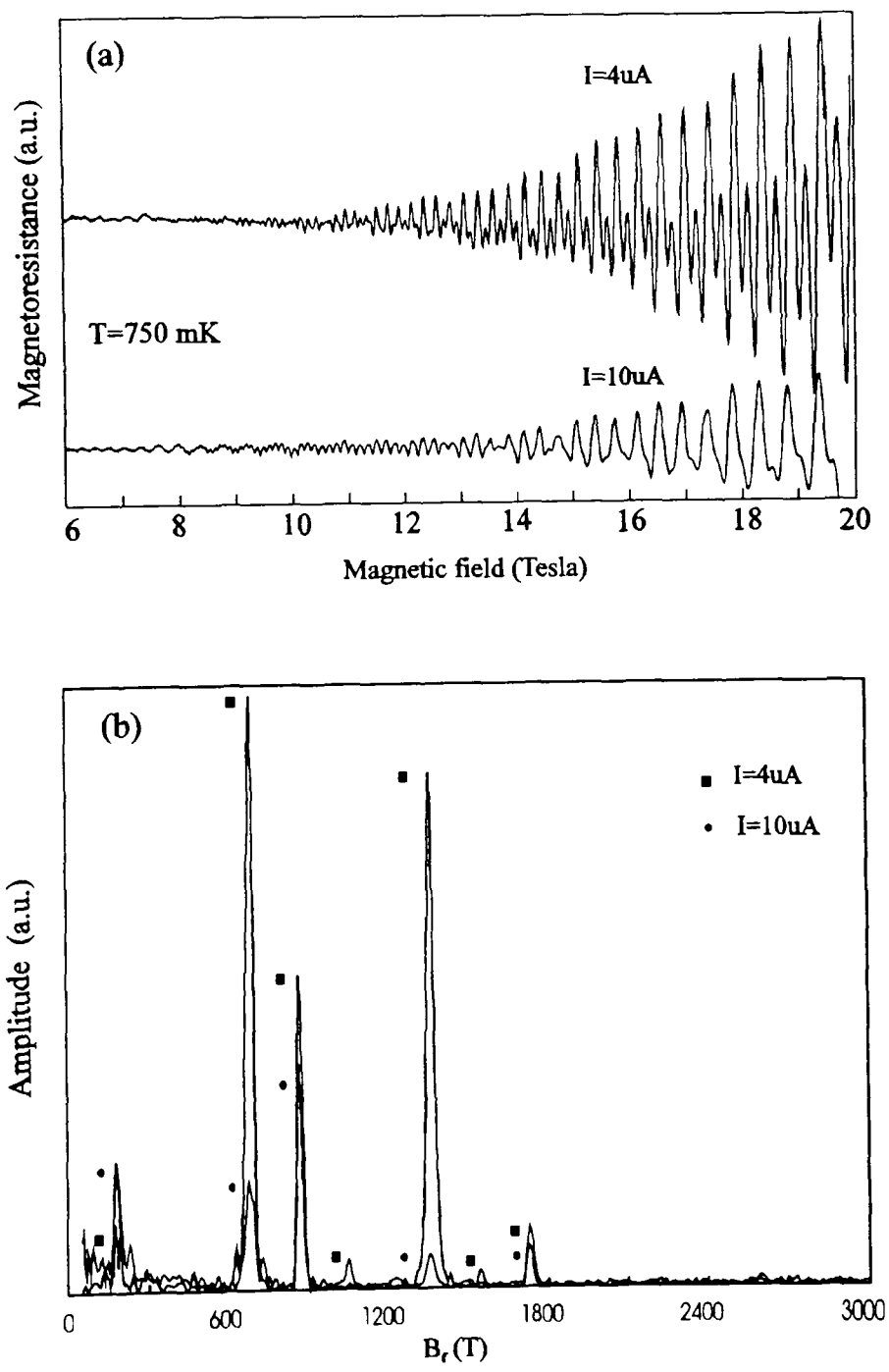

Figure 12 (a) The oscillatory component of the magnetoresistance at 0.75 K is shown for sample currents of 4 μA and 10 μA. (b) The Fourier transform of the data in (a) [37].

The Fourier transforms of the two cases are shown in figure 12(b) and illustrate that the effect of the electron heating is to suppress the first breakdown orbit (B_{F1}) and especially its harmonics (reflecting their relatively large effective mass) while only mildly reducing the amplitude of orbits involving one or more circuits of the small pocket, thereby increasing their relative importance.

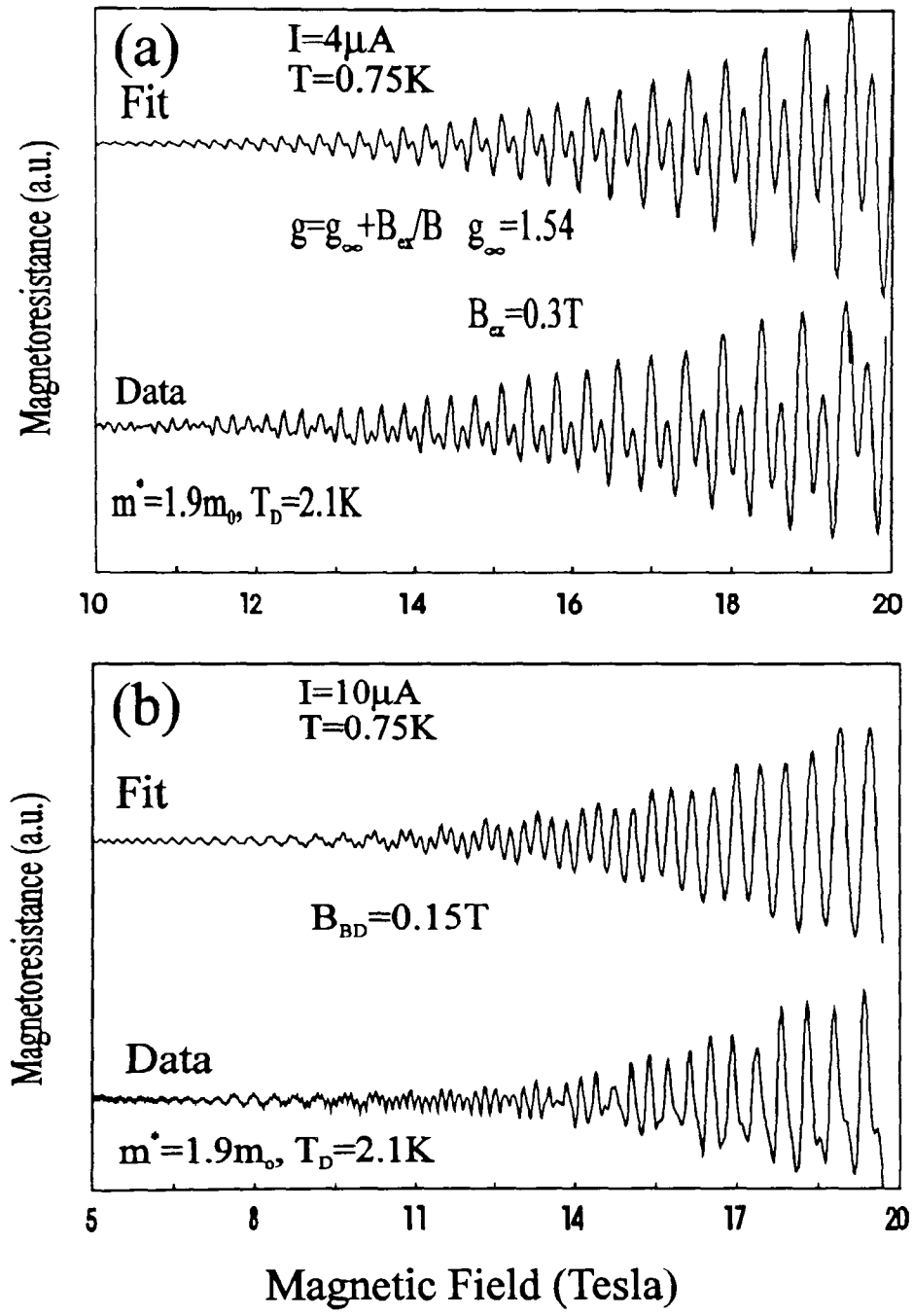

Figure 13 (a) The 4 μA data in figure 12(a) is plotted against B and can be compared with a fit using a field-dependent g-factor using the same parameters used to fit another sample in figure 10.(b) The 10 μA data in figure 12(a) is plotted against B and is shown with a fit to a coupled network model using measured band parameters and a breakdown field of 0.15 T [37].

The magnetic breakdown orbits which dominate the 10 μA oscillations can be fitted using a coupled network breakdown model [38]. The proposed Fermi surface has a small quasi-two dimensional section ($B_{F2} = 150 - 200\,\mathrm{T}$) which is separated by a very small gap from a quasi-one dimensional section. As the magnetic field is increased, electrons may tunnel between adjacent sections of Fermi surface, thus describing a larger *k*-space orbit which is observable as a higher frequency series of oscillations ($B_{F1} = 670\,\mathrm{T}$). Other closed semiclassical orbit combinations are observable such as $2B_{F1} - B_{F2} = 1140 - 1190\,\mathrm{T}$ and $B_{F1} + B_{F2} = 820 - 870\,\mathrm{T}$. A reasonable fit to the experimental data (figure 13(b)) can be thus obtained using the experimentally measured Fermi surface parameters and a magnetic breakdown field of $B_o = 0.15\,\mathrm{T}$. The effective mass of the B_{F2} orbit could not be measured as its Shubnikov-de Haas oscillations amplitude is so low.

As a first approximation, the effective mass of an orbit is assumed to scale with its area (so that $m_2^* = 0.6m_o$). The data imply that the small Fermi surface pocket corresponding to B_{F2} is separated by a small energy gap of 9 K from the quasi-one-dimensional sections. The tunnelling of electrons across this gap allows the observation of the oscillations of frequency B_{F1}. The gap is so small that breakdown occurs at very low fields, but, as discussed above, is most clearly observable when the Landau level broadening induced by high electron heating or large Dingle temperatures reduces the usually dominant effect of the spin-splitting. The observed variation from sample to sample in the area B_{F2} of the small two-dimensional pocket may be due to the formation of slightly different spin density wave ground states, each with a different nesting vector, thus giving rise to a slightly different low temperature Fermi surface, depending on the precise cooling method and/or sample quality.

5.4-5. Summary

Below the kink, the Shubnikov-de Haas oscillations are of a similar frequency ($B_{F1} = 670\,\mathrm{T}$) to those observed in $\alpha-\mathrm{ET_2NH_4Hg(SCN)_4}$ but are more complex, exhibiting a prominent second harmonic at low tilt angles which is attributed to spin splitting. In agreement with Sasaki *et al* [20], a field-dependent exchange enhancement of the spin splitting is found due to antiferromagnetic order which can explain the observed change in oscillation phase with magnetic field. The *g*-factor deduced is in excellent agreement with harmonic ratio data. Depending on sample quality and the value of the current used, other Shubnikov-de Haas oscillations frequencies are present which have a magnetic field dependence reminiscent of strong magnetic breakdown [36]. This is in qualitative agreement with the model of the low field Fermi surface.

Above the kink, a single series of oscillations ($B_F = 656 \pm 10\,\mathrm{T}$) grow strongly in amplitude; at very high field (~40 T), the data for $\alpha-\mathrm{ET_2KHg(SCN)_4}$ and $\alpha-\mathrm{ET_2NH_4Hg(SCN)_4}$ become very similar. The difference in the behaviour between the two nominally identical materials at fields below the kink can be attributed to the onset of a spin-density wave at temperature below T_N, associated with a pair of one-dimensional sheets nesting together in $\alpha-\mathrm{ET_2KHg(SCN)_4}$ (figure 1(b)). The high field data is in qualitative agreement with the Fermi surface in figure 1(a), with the magnetoresistance primarily resulting from the two-dimensional sections of the Fermi surface. The kink represents the field induced transition between the two regimes.

The presence of a spin density wave which alters the Fermi surface at the kink can be most firmly established by angle-dependent measurements; these provide proof of the geometry of the model for the low field band structure and allow a qualitative test of the proposed changes in the Fermi surface at the kink transition; such measurements are the subject of the following section.

5.5. Angular-Dependent Magnetoresistance oscillations

5.5-1. Introduction

Magnetoresistance data have been recorded whilst single crystals of $\alpha-ET_2KHg(SCN)_4$ were rotated in different magnetic fields up to 30 T (see figure 7). In figures 14-17 the horizontal axis represents the angle θ between the magnetic field and the $\boldsymbol{b}^*$ axis. Each trace can be labelled with an azimuthal angle ϕ describing the plane of rotation; $\phi = 0°$ represents rotation about the ***a***-axis and increasing values of ϕ represent angular displacement of the rotation axis in the ***ac***-plane towards the ***c***-axis; rotation about the ***c***-axis corresponds to ϕ~90°. The experiment was performed by first setting ϕ at a particular magnetic field; the sample was then rotated through the angle θ in that magnetic field.

There exist two types of angle-dependent magnetoresistance oscillations depending on whether the Fermi surface is quasi-one-dimensional or quasi-two-dimensional:

5.5-2. 1D oscillations

Recently, Osada *et al.* [39] have proposed a model to explain the dips observed in the resistivity of the organic conductors $(TMTSF)_2X$ (X = ClO_4, PF_6) as a function of the direction of the applied magnetic field. They have calculated the conductivity for a band structure consisting of weakly corrugated quasi-one-dimensional sheets across which electrons travel in open-orbits. They find that at particular directions of the applied magnetic field there are large resonances in the conductivity when the condition for the existence of periodic orbits of sufficiently small period is satisfied.

This model has recently been applied to $\alpha-ET_2KHg(SCN)_4$ [40]. If the one-dimensional sections of the Fermi surface are inclined at an angle ϕ_0 to the $\boldsymbol{b}^*\boldsymbol{c}$ plane, then resonances are expected to be observed when [15]

$$\tan\theta\cos(\phi-\phi_0)=\frac{m}{n}\times\frac{b}{c} \tag{5.1}$$

where m and n are integers. This theory predicts that resistivity dips at fractional values of m/n should be observed, as well as at integer values (n=1), that there should be a missing dip at m=0 and that the oscillations should be symmetric in $\tan\theta$. As shown below, it is found experimentally that this is not the case: fractional effects are only weakly observed under certain conditions (if at all), there is no missing dip at m=0 and the symmetry in $\tan\theta$ is broken by an offset. These points are inadequately treated in Ref. [40].

To accurately model the data, it is necessary to include the fact that the Fourier components of the corrugations in the one-dimensional Fermi sheets (which correspond to transfer integrals along particular lattice vectors) should be properly defined on an *oblique* (rather than rectangular) lattice since $\alpha-ET_2KHg(SCN)_4$ is triclinic, and as will be shown below, the quasi-one-dimensional planes cut the Brillouin zone at an angle. The obliquity of this two-dimensional lattice on which the transfer integrals are defined will be parameterised by the quantity d. Consider a weakly corrugated quasi-one-dimensional Fermi surface with dispersion relation given by

$$E(k)=\hbar v_F(|k_x|-k_F)-\sum_{m,n}t_{mn}\cos((mb+nd)k_y+nck_z) \tag{5.2}$$

which consists of a pair of sheets at $k_x=\pm k_F$ (for simplicity of description, the axes have been chosen so that ϕ_0=0° when the one-dimensional planes are perpendicular to the x-axis). The t_{mn} are the Fourier components of the sheet corrugation associated with the lattice vector $\mathbf{R}_{mn}=(0,mb+nd,nc)$ and b and c are the size of the unit-cell (assumed orthorhombic). We are free to set $t_{00}=0$ since this term only produces a shift in the Fermi energy. The velocity $\boldsymbol{v}$ of each electron as a function of momentum $\boldsymbol{k}$ can then be calculated using $\boldsymbol{v}(\boldsymbol{k})=\hbar^{-1}(dE(\boldsymbol{k})/d\boldsymbol{k})$. This quantity will be time-dependent since the electron's momentum $\boldsymbol{k}$ varies with time according to the equation of motion $\hbar\dot{\boldsymbol{k}}=-e\boldsymbol{v}\times\mathbf{B}$ with the magnetic field $\mathbf{B}$ given by $\mathbf{B}=(0,B\sin\theta,B\cos\theta)$. In this chapter, only the effects of the magnetic field in the quasi-one dimensional plane ϕ=0 will be

considered. If there is an out of plane component, then one can approximately treat the problem as if the effective (in-plane) magnetic field is $B\cos\phi$. This ignores the fact that the electron motion in the Fermi sheets is no longer along straight lines (this feature will be treated elsewhere [41]).

The conductivity can be calculated with the Boltzmann transport equation and it is found that

$$\sigma_{xx} = e^2 g(E_F) v_F^2 \tau \tag{5.3}$$

and $\sigma_{xy} = \sigma_{yx} = \sigma_{xz} = \sigma_{zx} = 0$ but

$$\begin{pmatrix} \sigma_{yy} & \sigma_{yz} \\ \sigma_{yz} & \sigma_{zz} \end{pmatrix} = \frac{g(E_F)e^2}{\hbar^2} \sum_{m,n} \begin{pmatrix} (mb+nd)^2 & (mb+nd)nc \\ (mb+nd)nc & (nc)^2 \end{pmatrix} t_{mn}^2 \frac{\tau}{1+(G_{mn}\tau v_F)^2} \tag{5.4}$$

where $G_{mn} = \frac{eB}{\hbar}((mb+nd)\cos\theta - nc\sin\theta)$. A resonance in the conductivity occurs when $G_{mn} = 0$ *i.e.* when

$$\tan\theta = \frac{mb}{nc} + \frac{d}{c} \tag{5.5}$$

When the magnetic field is applied in an arbitary direction the electron's velocity will not be strongly correlated with itself (the v_b and v_c components will be strong) as the electron moves over the undulations in the Fermi surface. This weak correlation results in incoherent motion and hence to a weak current. When the magnetic field is applied along one of the real space lattice vectors $\mathbf{R}_{mn}$ such that equation (5.5) is satisfied, $G_{mn} = 0$ for that particular Fourier component. This leads to a reduction in the v_b and v_c components of the electron velocity, and hence to more coherent motion, giving a larger conductivity.

5.5-3. 2D oscillations

Peaks in the angle dependent magnetoresistance oscillations of quasi-two-dimensional materials have been treated elsewhere [42,43] and are connected with the vanishing of the electronic group velocity perpendicular to the two-dimensional layers.

The angles θ_i at which the maxima occur are given by $b'k_{\|}\tan(\theta_i) = \pi(i \pm 1/4) + A(\phi)$, where the signs - and + correspond to positive and negative θ_i respectively, b' is the effective interplane spacing, $k_{\|}$ is the maximum Fermi wave vector projection on the plane of rotation of the field, and i=±1, ±2, ... [42]. Here positive i correspond to $\theta_i > 0$ and negative i to $\theta_i < 0$ [42]. The gradient of a plot of $\tan\theta_i$ against i may thus be used to find one of the dimensions of the Fermi surface and, if the process is repeated for several planes of rotation of the field, the complete Fermi surface may be mapped out. $A(\phi)$ is determined by the inclination of the plane of warping; hence this may also be found [42].

5.5-4. Experimental data

In figure 14, data is presented from a low-field experiment on $\alpha - ET_2KHg(SCN)_4$ at 1.5 K. Strong angle dependent magnetoresistance oscillation dips are seen which become more pronounced as the field increases. Although the dips become sharper and the peaks flatter with increasing field, the positions of the dips do not change. Figure 15 shows data from an experiment on a different sample in fields up to 19 T as θ is varied in the full range between -90° and 90°. Notice that the traces are asymmetric in θ; there is no perfect mirror reflection symmetry about θ=0 as one might expect from a straightforward application of the theory in [39]; as described above, the asymmetry in the angle magnetoresistance oscillation traces is due to the obliquity of the two-dimensional lattice whose points correspond to Fourier components of the corrugation of the Fermi sheets.

In figure 16(a), angle dependent magnetoresistance oscillation data at 15 T are shown as θ is varied for a range of values of ϕ. Notice that when $\theta = 0°$, the magnetic field is parallel to $\boldsymbol{b}^*$ independently of the value of ϕ, so that these points show identical resistance; each trace has been offset for clarity. $\phi = 0°$ corresponds to rotation in the $\boldsymbol{b}^*\boldsymbol{c}$ plane; $\phi = 90°$ corresponds to rotation in the $\boldsymbol{b}^*\boldsymbol{a}$ plane. The minima in the

magnetoresistance are very sharp and are periodic in $\tan\theta$ at each azimuthal angle ϕ, although the period is a function of ϕ.

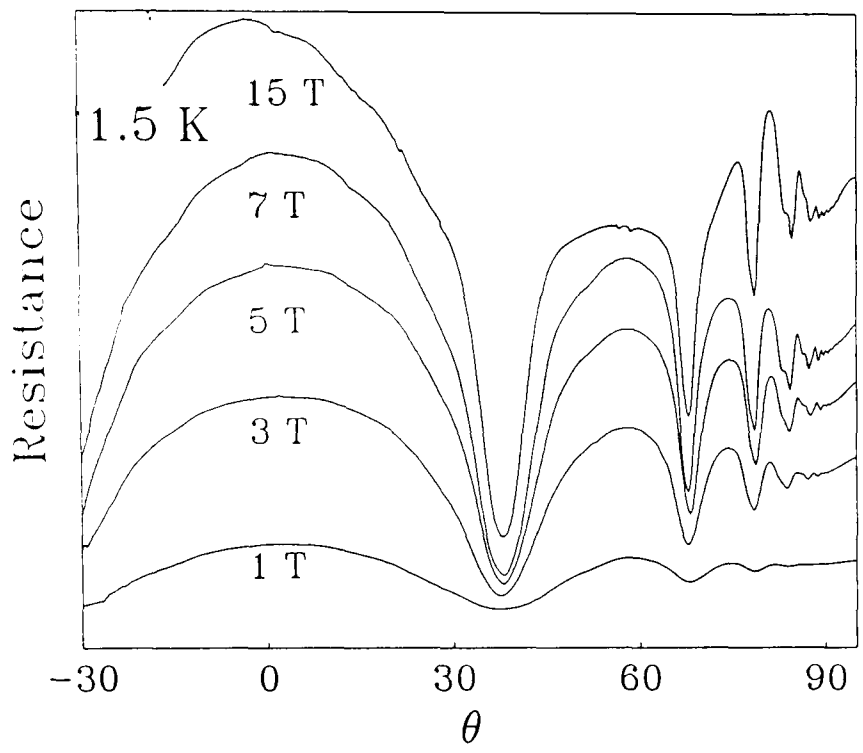

Figure 14 Angle-dependent magnetoresistance in $\alpha-ET_2KHg(SCN)_4$ at 1.5 K for magnetic fields in the range 1-15 T. The azimuthal angle ϕ is set to 0°.

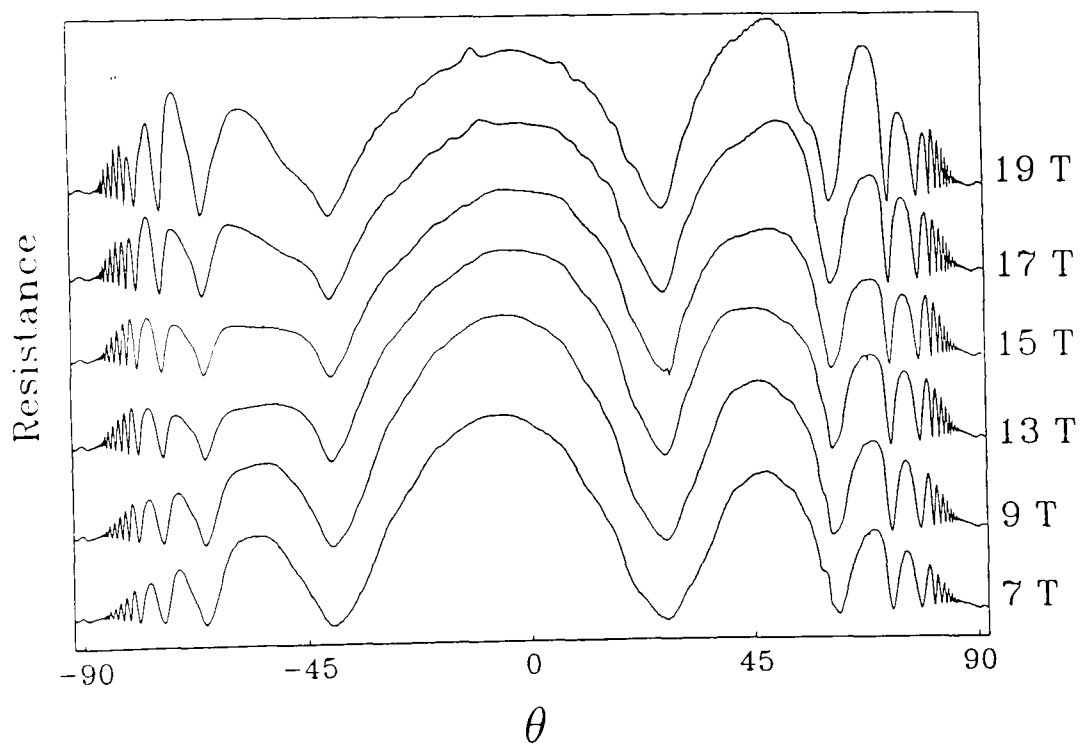

Figure 15 Angle-dependent magnetoresistance in $\alpha-ET_2KHg(SCN)_4$ at 1.5 K for magnetic fields in the range 7-19 T for θ in the full range $-90 < \theta < 90$. The azimuthal angle ϕ is set to 0°. Note the asymmetry in the traces.

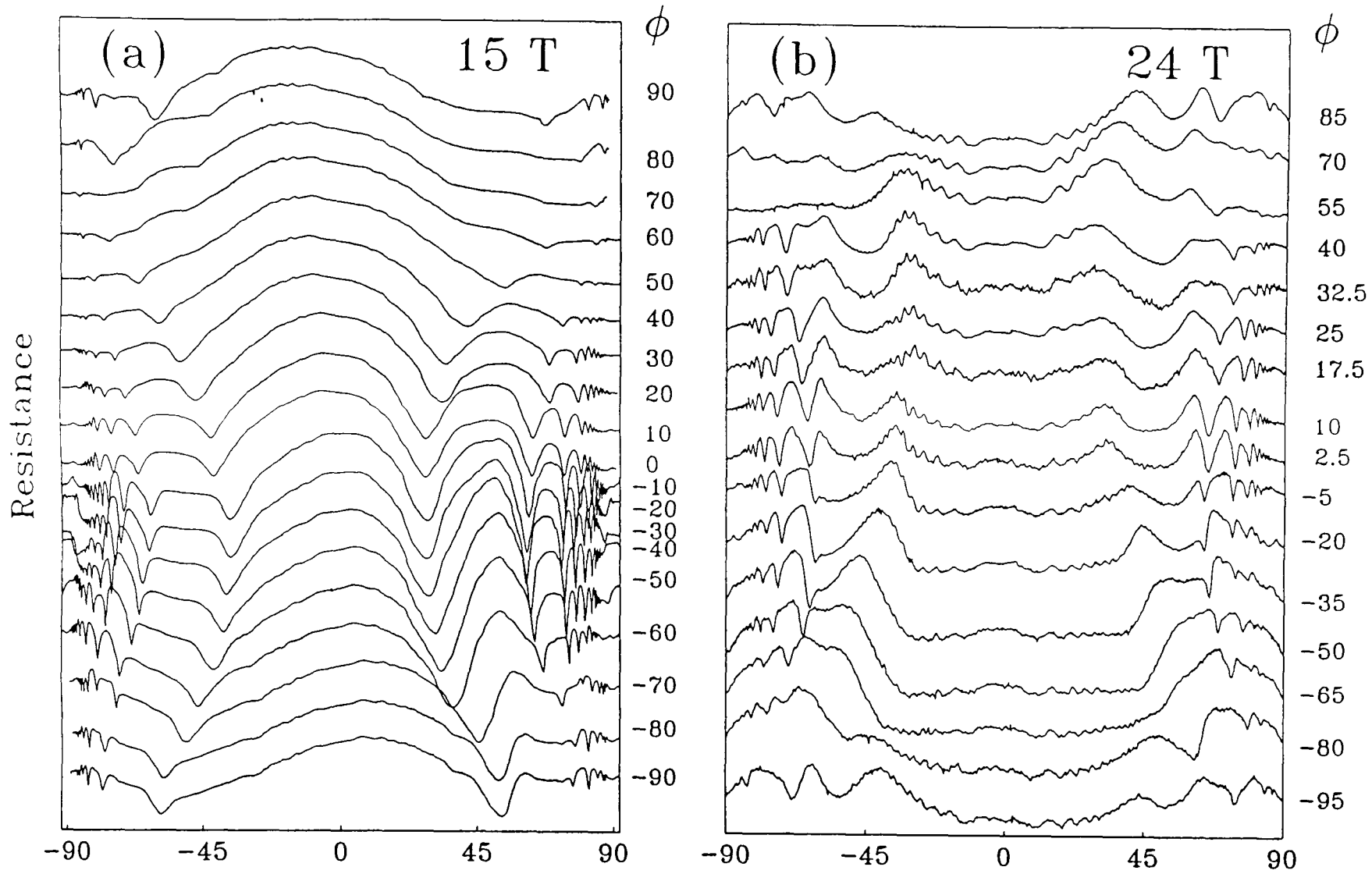

Figure 16 Angle dependent magnetoresistance oscillations in $\alpha-ET_2KHg(SCN)_4$ at 1.5 K for several values of the angle ϕ at an applied field of (a) 15 T and (b) 24 T.

The periodicity of the minima (deduced from a plot of minimum index versus $\tan\theta$) can be plotted against the azimuthal angle ϕ (figure 17(a)) and is seen to vary as $(1.25\pm0.05)/\cos(\phi-\phi_0)$, where $\phi_0=-21\pm3°$. Thus the maximum amplitude and minimum periodicity in $\tan\theta$ occur when the field rotation plane forms an angle $21\pm3°$ with the ***b*c*** plane. A polar plot of the positions of the resistance minima shows a characteristic family of lines inclined at this angle to the vertical (figure 17(a) inset).

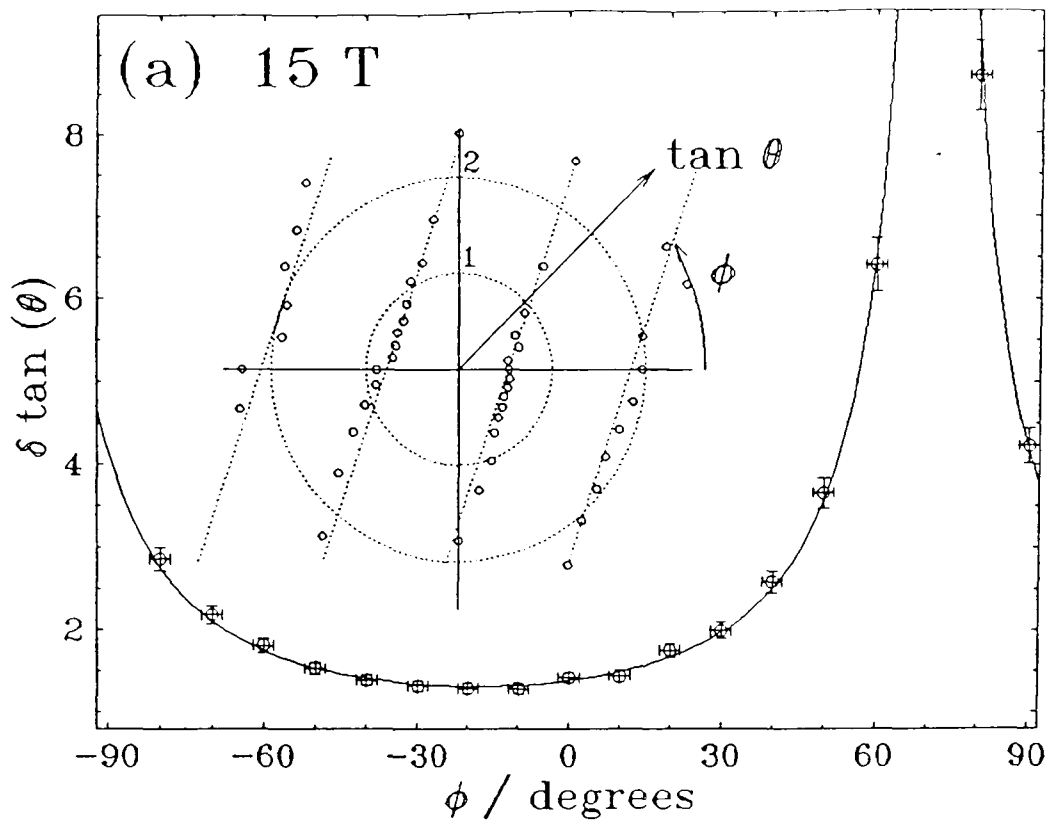

Figure 17 Analysis of the ϕ and θ dependence of the angle dependent magnetoresistance oscillations (a) minima at 15 T and (b) maxima at 24 T. The inset in (a) shows a polar plot of the θ and ϕ values of the resistance minima. The main figure shows a fit of $1.25/\cos(\phi-\phi_0)$ to the observed ϕ dependence of the period in $\tan\theta$ of the minima. This fit was used to determine the dotted straight lines in the inset and corresponds to a one-dimensional Fermi sheet inclined at ~21° to the ***b*c*** plane. A similar result can be obtained for the one-dimensional minima in the 24 T data but, in the range $-60° \le \theta \le 60°$, the one-dimensional minima vanish and two-dimensional maxima appear. For each ϕ, the positions of the minima can be fitted to $b' k_{\|} \tan(\theta_i) = \pi(i \pm 1/4) + A(\phi)$ (an example fit at ϕ= -95° is shown on the left side of (b)) so that the shape of the two-dimensional Fermi surface can be mapped out ((b), right).

This corresponds to a one-dimensional sheet tilted with respect to the ***b**c*** plane by this angle, in reasonable qualitative agreement with the model for the low temperature band structure discussed in the Introduction, which predicts a one dimensional plane tilted by 26° [9]. Similar behaviour is observed in all of the samples studied in this work and in a majority of samples examined by other workers [44]. Before turning to higher field data, two further points should be noted. In this field region, below the kink, the only effect of increasing the magnetic field is to make the angle dependent magnetoresistance oscillation dips more pronounced (figures 14 and 15); there is no evidence for a Fermi surface transition resulting from a phase boundary in the low field region (below 10 T) of the type recently suggested by some authors [45]. Furthermore, hysteresis is observed in both swept field and swept angle (angle dependent magnetoresistance oscillations) experiments below the kink, but appears to vanish at angle dependent magnetoresistance oscillation minima. This interesting effect will be the subject of a future paper [41].

As the magnetic field rises through the kink, a dramatic change in the angle dependent magnetoresistance oscillations are observed. This can be seen (for a fixed value of ϕ) for magnetic fields in the range 17-30 T in figure 19 [46,47]. The angle dependent magnetoresistance oscillations change from a series of sharp dips to a series of sharp peaks. A measurement of the ϕ dependence of these peaks at 24 T (figure 16(b)) shows that they are observable with similar amplitudes at all azimuthal angles and their position in θ shows much weaker dependence on ϕ than the dips observed below the kink [18], strongly suggesting that the mechanism responsible for the peaks is quasi-two-dimensional in nature. Note that the quasi two-dimensional peaks are only observed for $|\theta| \leq 60°$ at 24 T; the oscillations for $60° < \theta < 120°$ are rather similar to those obseved at 15 T (sharp minima rather than peaks) and may be fitted by a minimum period in $\tan(\theta)$ of 1.25 ± 0.05 (as at 15 T) and an offset angle of $\phi_o = -14 \pm 4°$. The reason for this apparently complex behaviour may be seen in figure 18; it is due to the angle dependence of the kink transition. It has been argued that the kink represents a phase boundary between two different states of the $\alpha - ET_2MHg(SCN)_4$ salts, and that the true position of the boundary is marked by the field at which the hysteresis disappears, denoting the

destruction of the domain structure due to internal fields [8,17]. Applying this criterion to the data of figure 18, it will be seen that the end of the hysteretic behaviour occurs just below 24 T for angles up to $\theta \cong 57°$ and then moves to higher fields.

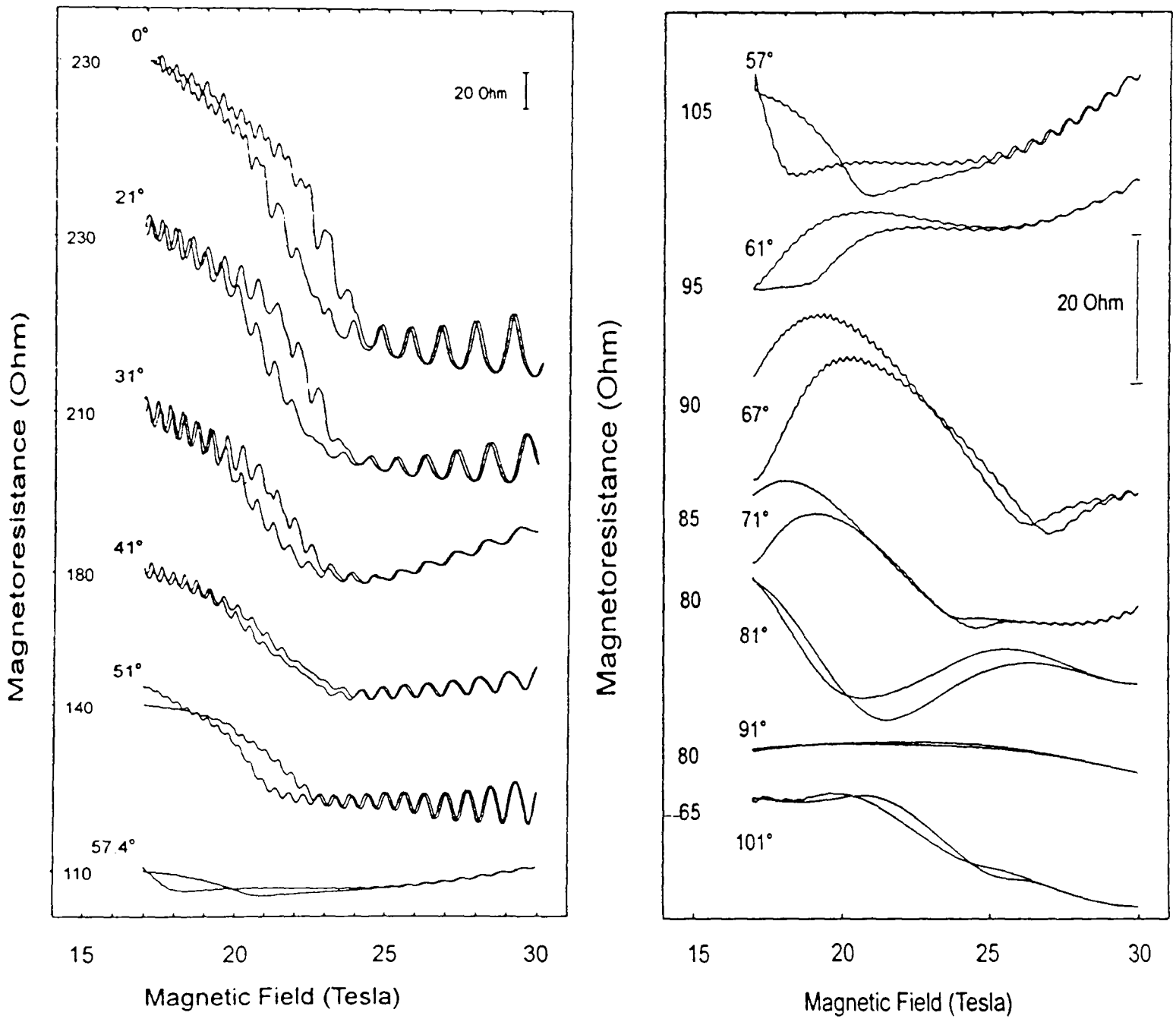

Figure 18 Magnetoresistance of an $\alpha - ET_2KHg(SCN)_4$ at 500 mK; data for both up- and down-sweeps of the field are shown (some of this data was previously presented in [16]). The field is applied in the b^*c plane; labels denote the angle between the field and the b^* axis. Data are offset for clarity; the resistance at the origin of each trace is marked on the left axes [37].

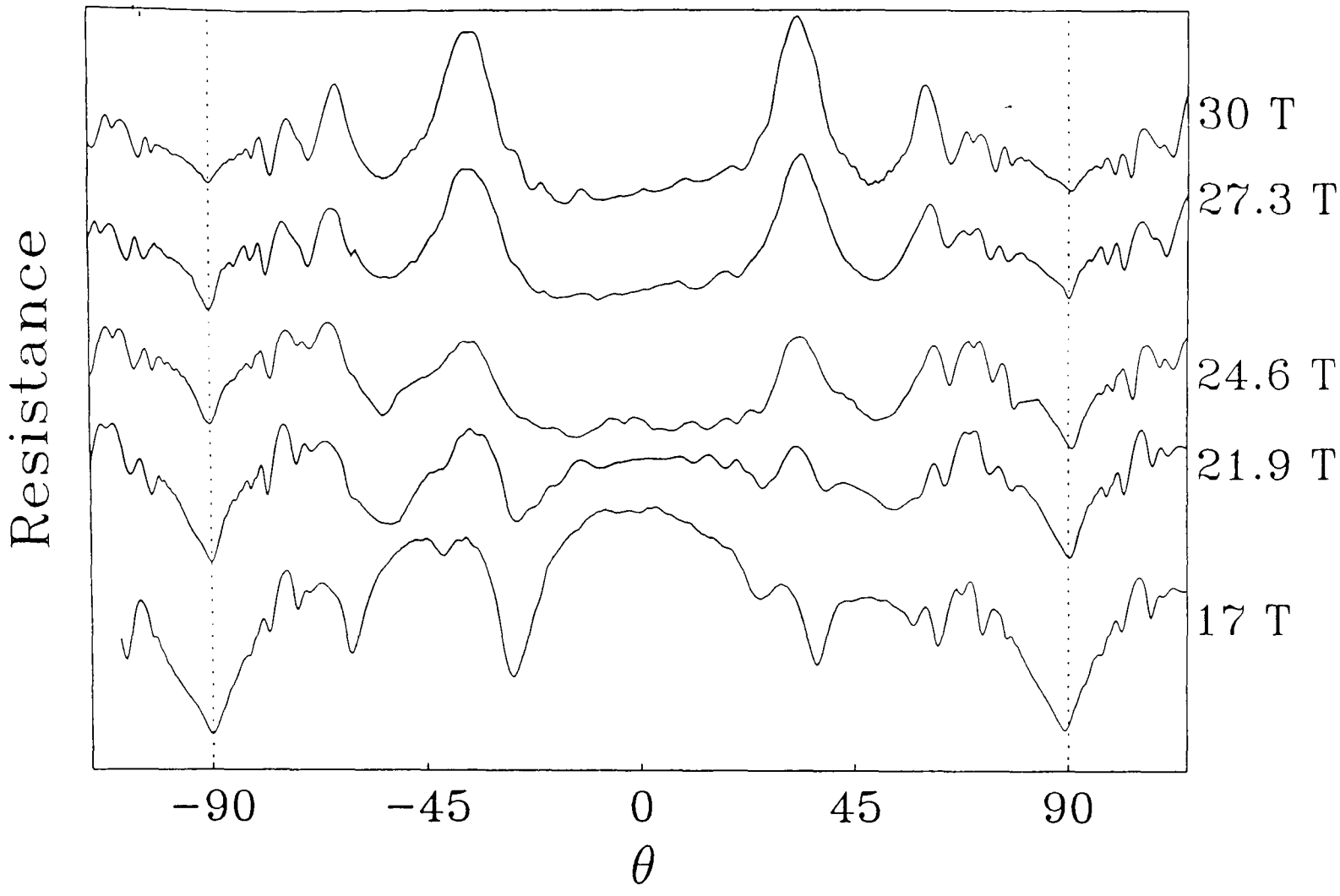

Figure 19 Evolution of the peaks in the angle-dependent magnetoresistance of $\alpha-ET_2KHg(SCN)_4$ at 1.5 K with increasing magnetic field in the range 17-30 T. The sharp magnetoresistance minima characteristic of quasi-one-dimensional angle dependent magnetoresistance oscillations give way to pronounced maxima characteristic of quasi-two-dimensional angle dependent magnetoresistance oscillations. This reflects the proposed magnetic field-induced change in the Fermi surface.

It may therefore be said that the peaks in the magnetoresistance at 24 T observed in the range $|\theta| \leq 60°$ (figure 16b) represent phenomena characteristic of the high field phase of $\alpha-ET_2KHg(SCN)_4$ whilst the sharp dips in the magnetoresistance remaining outside this angular range (*i.e.* $|\theta| > 60°$) are characteristic of the low-field 'below the kink' phase. As the field increases further, the peaks associated with the high-field phase persist to higher θ. This is seen in the data of figure 18, where the magnetoresistance peaks at $\theta = 33 \pm 1°, 59 \pm 1°$ and $70 \pm 1°$ [16]

The two-dimensional peaks in the angle dependent magnetoresistance oscillation data at 24 T can be used to determine the two-dimensional Fermi surface at high fields: the gradient of a plot of $\tan\theta_i$ against i can be used to find the dimension of the Fermi surface in one direction; if the process is repeated for several planes of rotation, the complete Fermi surface shape may be mapped out. For the 24 T raw data, a Fermi surface shape (figure 17(b)) is derived which is of roughly the correct area to account for the frequency of the Shubnikov-de Haas oscillations above the kink. A two-dimensional hole pocket of approximately this size is also predicted by band-structure calculations [6], although the derived Fermi surface is more elongated.

5.6. Discussion

The sharp change in the angle dependent magnetoresistance oscillation behaviour near the kink can be attributed to the transition between a Fermi surface dominated by quasi-one-dimensional sections to one dominantly quasi-two-dimensional. Thus a direct one-dimensional $\rightarrow$ two-dimensional transition in the Fermi surface has been observed which is induced by a magnetic field. The same transition in Fermi surface occurs with heating through T_N: a recent experiment on $\alpha-ET_2KHg(SCN)_4$ at 14 T showed that as the temperature was raised through 8 K the angle dependent magnetoresistance oscillations changed in character, indicating that the Fermi surface has changed from predominantly one-dimensional to predominantly two-dimensional in form [48]. The preliminary measurements of angle dependent magnetoresistance oscillations on $\alpha-ET_2KHg(SCN)_4$ as a function of temperature support this observation [49].

The angle dependent magnetoresistance oscillations and Shubnikov-de Haas oscillations results leads to the conclusion that for magnetic fields above the kink, or for temperatures $T>T_N$, the Fermi surface is similar to that in figure 1(a), and by implication similar to that in $\alpha-ET_2NH_4Hg(SCN)_4$, whereas the rearranged low temperature Fermi surface below the kink is in qualitative agreement with that in figure 1(b), consisting of a tilted one-dimensional section and a small closed pocket (corresponding

to the Shubnikov-de Haas oscillations frequency B_{F2}. However, it should be noted that the angle dependent magnetoresistance oscillation data for $\alpha-ET_2KHg(SCN)_4$ at fields below the kink imply a one-dimensional Fermi surface sheet tilted by 21° with respect to the ***b*c*** plane, whereas the model shown in figure 1(b), derived for $\alpha-ET_2TlHg(SCN)_4$, predicts a one dimensional plane tilted by 26° [44]. This suggests that the spin density wave nesting vectors in $\alpha-ET_2KHg(SCN)_4$ and $\alpha-ET_2TlHg(SCN)_4$ are different. It has been pointed out that the operation of the spin density wave nesting vector implied by the 21° Fermi surface sheet angle in $\alpha-ET_2KHg(SCN)_4$ on the calculated bandstructure would not result in any small pockets such as those in figure 1(b) [50-52]. However, the presence or absence of small pockets in the rearranged bandstructure depends on the exact shape of the two dimensional section in the original Fermi surface; as observed in the experiments reported here and in other works [20,48], this seems more elongated than the almost circular cross-sections suggested by the bandstructure calculations (figure 1(a)).

It is interesting that only dips at occur integer values of tanθ in the angle dependent magnetoresistance of $\alpha-ET_2KHg(SCN)_4$ due to the one-dimensional Fermi surface sheets. This may be explained by the fact that in the ***b**** direction not only is the warping extremely weak, due to the thick anion layer, but the warping (according to the bandstructure calculations) is also cosinusoidal and in reality probably has a very low harmonic content; the consequence of this is to suppress the fractional peaks. Whereas in the ***ac***-plane of the reorganised Fermi surface the warping of the open sections (figure 1(b)) and its harmonic content are expected to be high; as the two dimensional Fermi surface has been simply "folded up" by the action of the spin density wave. The measured ratio *b/c* (from the minimum period in $\tan\theta = 1.25 \pm 0.05$ (figure 17(a)) is approximately that expected in the reorganised Brillouin zone, as predicted by the model of Kartsovnik *et al.* [9]. The angular magnetoresistance traces were also found to be slightly asymmetric (shown directly in the polar plot of figure 17(a)), this is explained by the fact that $\alpha-ET_2KHg(SCN)_4$ is triclinic; the amount of asymmetry is a measure of the lattice obliquity (*d/c*). This has been estimated from the room temperature crystal structure

along the direction of the reconstructed Fermi surface (*i.e.* 21° to the original *c*-axis) to be close to the measured *d*/*c* ratio [53].

Because the nesting vectors in $\alpha-ET_2KHg(SCN)_4$ and $\alpha-ET_2TlHg(SCN)_4$ are almost incommensurate, the spin density wave may possibly be poorly locked in to a particular orientation, so that slight changes in cooling, or differences in sample quality might slightly alter the angle of the one-dimensional Fermi surface observed by angle dependent magnetoresistance oscillations or give rise to the variation in the area of the closed pocket and hence the observed spread in the values of B_{F2}.

Additional low frequency Shubnikov-de Haas oscillations have been observed in experiments carried out at very low temperatures [45]; these oscillations were attributed to a further rearrangement of the Fermi surface at low fields [45]. As discussed above, the field independence of the positions of the angle dependent magnetoresistance oscillation minima at fields below the kink does not support this conclusion. The low frequency Shubnikov-de Haas oscillations observed are instead likely to be due to vestigial imperfectly nested parts of the one-dimensional Fermi surface [54]. An analogous situation is known to occur in $\beta''-ET_2AuBr_2$, where Shubnikov-de Haas oscillations frequencies due to small pockets left by imperfect nesting of a spin density wave are clearly seen [55]. The Fermi surface in figure 1(b) is made up of a rearrangement of the two-dimensional pocket in figure 1(a) only (the one-dimensional section is assumed to nest), as evidenced by the B_{F2} mass being the same on either side of the kink transition; imperfect nesting would lead to additional very small Fermi surface pockets.

Recent experiments have used a field modulation technique to give enhanced detection of high frequency Shubnikov-de Haas oscillations in $\alpha-ET_2KHg(SCN)_4$; a frequency was observed which appeared to correspond to a breakdown orbit with the same area as the whole, unrearranged, Brillouin zone (*i.e.* figure 1(a) of [56]). Uji *et al.* [56] took this to imply that the Fermi surface in their samples was not rearranged, but identical to that at high temperatures (figure 1(a)); a breakdown orbit involving

tunnelling between the two and one dimensional sections would have the same area as the Brillouin zone.

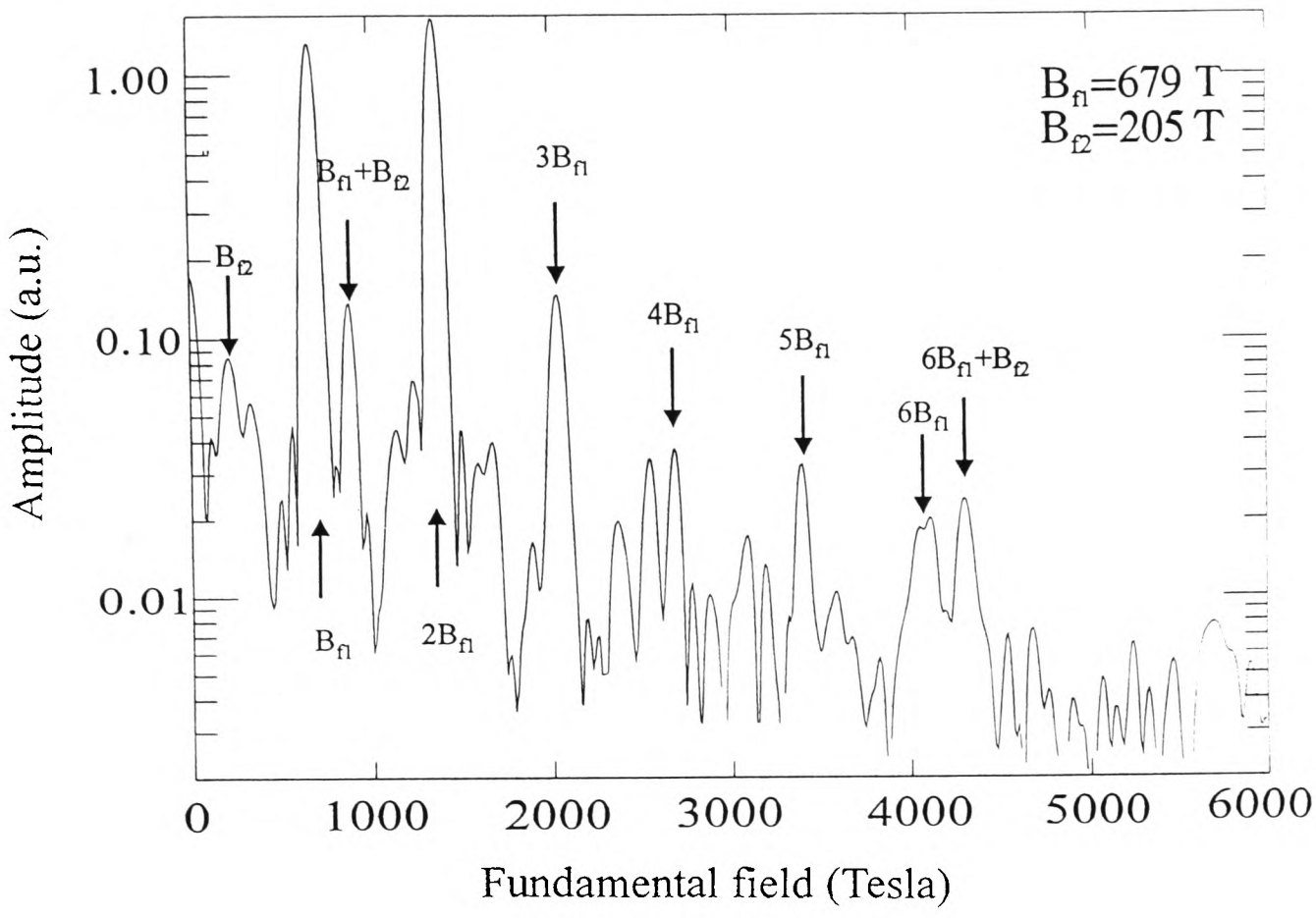

Figure 20 The Fourier transform of the magnetoresistance of $\alpha-ET_2KHg(SCN)_4$ below the kink plotted on a logarithmic scale to show high order harmonics.

A similar frequency (at about 4300 T) is observed in Fourier spectra of the magnetoresistance of samples studied in this work (see figure 20); as the other data discussed above seem to unambiguously indicate that the low temperature Fermi surface is radically rearranged from its high temperature form, two possible reasons for the presence of the "whole Brillouin zone" frequency are suggested:

1. It is likely that the peak in the Fourier spectrum corresponds to a mixed harmonic of the other Shubnikov-de Haas oscillations frequencies ($6B_{F1}+B_{F2}$); several other mixed harmonics of this kind are present in figure 20 and in the data of Uji *et al* [56]. Recent work on $\beta''-ET_2AuBr_2$, which also possesses a spin density

wave groundstate at low temperatures, has shown that such mixed harmonics are enhanced by the Shoenberg magnetic interaction [55].

2. The low temperature groundstates of $\alpha-ET_2MHg(SCN)_4$ (M=K, Rb) are very sensitive to hydrostatic pressure or uniaxial stress [14,52]. It has therefore been suggested that small strained regions of samples (due to contacts, adhesive *etc.* could retain a Fermi surface characteristic of the high temperature phase [50]; these small regions could be responsible for the "whole Brillouin zone" frequency.

It has also been suggested [56] that magnetic breakdown is responsible for the whole form of the magnetoresistance. However, magnetic breakdown is a very tiny effect in the classical magnetoresistance, and the enormous magnetoresistance effects such as angle dependent magnetoresistance oscillations that are observed in $\alpha-ET_2KHg(SCN)_4$ must be due to the gross features of the Fermi surface, like the presence of the one-dimensional sheets. In the model described above the Fermi surface rearrangement at the kink transition adequately accounts for the observed properties without having to invoke further exotic effects or appeal to sample inhomogeneities.

5.7. Summary

Magnetoresistance measurements have been performed as a function of temperature, field strength, and field direction on single crystal specimens of the charge transfer salt $\alpha-ET_2KHg(SCN)_4$. Below the kink transition in field, the Shubnikov-de Haas oscillations are of a similar frequency to those observed in $\alpha-ET_2NH_4Hg(SCN)_4$ but are more complex, exhibiting a prominent second harmonic at low tilt angles due to spin splitting. Evidence of a field-dependent exchange enhancement of the Landau level splitting due to the antiferromagnetic order has been found which can explain the change in oscillation phase with magnetic field. Depending on sample quality and the value of the

current used, other Shubnikov-de Haas oscillations frequencies are present which have a magnetic field dependence which can be fitted using a coupled network model to describe magnetic breakdown. The angle dependent magnetoresistance oscillations are one-dimensional in character and indicate the presence of a quasi-one-dimensional section of Fermi surface inclined at an angle of $21\pm3°$ to the ***b*c*** plane. Above the kink, a single series of oscillations grow strongly in amplitude and at high field (~40 T) are very similar to those observed in $\alpha-ET_2NH_4Hg(SCN)_4$; the angle dependent magnetoresistance oscillation dips observed below the kink give way to sharp peaks which are fairly independent of azimuthal angle and indicate a Fermi surface with predominantly quasi-two-dimensional character.

The difference in the behaviour between the two very similar materials at low fields can be attributed to the onset of a spin density wave in $\alpha-ET_2KHg(SCN)_4$ at temperatures below T_N; associated with the nesting of a pair of one-dimensional sheets. This difference in behaviour is perhaps related to the volume of the unit cell, and hence to the warping of the one-dimensional sheets. The size of the unit cell is related to that of the Brillouin zone and hence the two-dimensional hole pocket area, which is ~14 % of the Brillouin zone when M=NH_4 [57,58] and 16 % for M=K [15,16,17]. This trend continues for M=Rb which has a slightly larger two-dimensional hole pocket than the K salt, a transition to antiferromagnetic order at ~10 K and a kink at ~35 T [59]; in other words the spin density wave groundstate appears to be more stable. This can be related to the increasing flatness of the one-dimensional sheets which accompanies the increase in the size of the hole-pocket; this favours nesting and hence the spin density wave ground state.

It is proposed that angular magnetoresistance oscillations due to open sections of Fermi surface do not occur in $\alpha-ET_2NH_4Hg(SCN)_4$ and $\alpha-ET_2KHg(SCN)_4$ at fields above the kink transition because these open sheets are rather flat and have low harmonic content. In $\alpha-ET_2KHg(SCN)_4$ at temperatures below T_N and at magnetic field below the kink, due to the folding of the two dimensional pocket (caused by the action of the spin density wave) the resulting one dimensional sheets are very warped

with high harmonic content; points necessary for the detection of angle dependent magnetoresistance oscillations [53].

References

[1] *Organic Superconductors*, by T. Ishiguro and K. Yamaji, (Springer-Velag, Berlin 1990).

[2] *Organic Superconductivity*, eds V.Z. Kresin and W.A. Little, (Plenum Press, New York 1990).

[3] M. Oshima, H. Mori, G. Saito and K. Oshima, *Chem. Lett.* **1989**, 1159 (1989).

[4] N.D. Kushch, L.I. Buravov, M.V. Kartsovnik, V.N. Laukhin, S.I. Pesotskii, R.P. Shibaeva, L.P. Rozenberg, E.B. Yagbuskii and A.V. Zvarikina, *Synth. Met.* **46**, 271 (1993).

[5] H. Mori, S.Tanaka, K. Oshima, M. Oshima, G. Saito, *Solid State Commun.* **74**, 1261 (1990).

[6] H. Mori, S.Tanaka, M. Oshima, G. Saito, T. Mori, Y. Maruyama and H. Inkuchi, *Bull. Chem. Soc. Jpn.* **63**, 2183 (1990).

[7] Recently, the salts with M=K, Rb, and Tl have been shown to develop a resistance decrease at 0.3 K, 0.5 K, and 0.1 K, respectively and this has been interpreted as a weak onset of superconductivity, although zero resistance is not achieved. The decreases are suppressed by a magnetic field less than 0.2 T. See H. Ito *et al,* to be published; see also H. Ito, H. Kaneko, T. Ishiguro, H. Ishimoto, K. Kono, S. Horiuchi, T. Komatsu and G. Saito, *Solid State Commun.* **85**, 1005 (1993);

[8] T. Sasaki, N. Toyota, M. Tokumoto, N. Kinoshita, and H. Anzai, *Solid State Commun.* **75**, 93 (1990); T. Sasaki and N. Toyota, *Solid State Commun.* **82**, 447 (1992);T. Sasaki, H. Sato and N. Toyota, *Synth. Met.* **42**, 2211 (1991).

[9] M. V. Kartsovnik, A. E. Kovalev and N. D. Kushch, *J. Phys. I France* **3**, 1187 (1993).

[10] N. Kinoshita, M. Tokomoto and H. Anzai, *J. Phys. Soc. Jpn.* **59**, 3410 (1990).

[11] T. Takahashi, R. Tsuchiya, K. Kanoda, M. Watabe, T. Sasaki and N. Toyota, *Synth. Met.* **55-57**, 2513 (1993).

[12] T. Sasaki, S. Endo and N. Toyota, *Phys. Rev.* **B 48**, 1928 (1993).

[13] F. L. Pratt, T. Sasaki, N. Toyota, and K. Nagamine, submitted to *Phys. Rev. Lett.*

[14] S. J. Klepper, J. S. Brooks, G. J. Athas, X. Chen, M. Tokumoto, N. Kinoshita, and Y. Tanaka, *Surf. Sci* **305**, 181 (1994).

[15] T. Osada, R. Yagi, A. Kawasumi, S. Kagoshima, N. Miura, M. Oshima, T. Nakamura and G. Saito, *Synth. Met.* **42**, 2171 (1991); T. Osada, R. Yagi, S. Kagoshima, N. Miura, M. Oshima, and G. Saito, *Phys. Rev.* **B 41**, 5428 (1990).

[16] F. L. Pratt, J. Singleton, M. Doporto, A. J. Fisher, T. J. B. M. Janssen, J. A. A. J. Perenboom, M. Kurmoo and P. Day, *Phys. Rev.* **B 45**, 13904 (1992).

[17] J. S. Brooks, C. C. Agosta, S. J. Klepper, M. Tokomoto, N. Kinoshita, H. Anzai, S. Uji, H. Aoki, A. S. Perel, G. J. Athas and D. A. Howe, *Phys. Rev. Lett.* **69**, 156 (1992).

[18] J. Caulfield, J. Singleton, P.T.J. Hendriks, J.A.A.J. Perenboom, F.L. Pratt, M. Doporto, W. Hayes, M. Kurmoo and P. Day, *J. Phys. Condens. Matter* **6**, L155 (1994).

[19] M. V. Kartsovnik, A. E. Kovalev, V. N. Laukhin, and S. I. Pesotskii, *J. Physique I* **2**, 223 (1992).

[20] T. Sasaki and N. Toyota, *Phys. Rev.* **B** 48, 11457 (1993).

[21] J. Larsen and C. Lenoir, *Synthesis* **2** 134 1988).

[22] F. Herlach, M. van der Burgt, I. Deckers, G. Heremans, G. Pitsi and L. van Bockstal, *Physica* **B 63** 177 (1992).

[23] John Singleton, Jason M. Caulfield, S.O. Hill, P.T.J. Hendriks, F.L. Pratt, M. Doporto, I. Deckers, G. Pitsi, F. Herlach, W. Hayes, T.J.B.M. Janssen, J.A.A.J. Perenboom, M. Kurmoo and P. Day, *Conf. Physique en Champs Magnetiques Tres Intenses et Technologies Associees*, Toulouse, 8-9 April 1993

[24] The orientation of the sample was determined after the magnetoresistance measurements were completed by using x-ray techniques by Miss D. Corker, Oxford University.

[25] The orientation of the sample was determined before the magnetoresistance measurements began by using room temperature infra-red reflectivity by Dr F.L. Pratt, Oxford University.

[26] F. L. Pratt, W. Hayes, A. J. Fisher, J. Singleton, S. J. R. M. Spermon, M. Kurmoo, and P. Day, *Synth. Met.* **29**, F667 (1989); H. Kuroda, K. Yakushi, H. Tajima, A. Ugawa, M. Tamura, Y. Okawa, A. Kobyashi, R. Kato, H. Kobyashi, and G. Saito, *Synth. Met.* **27**, A491 (1988).

[27] J. A. A. J. Perenboom and K. van Hulst, *Physica* **B 155**, 74 (1989).

[28] J. Singleton, F. L. Pratt, M. Doporto, J. Caulfield, W. Hayes, I. Deckers, G. Pitsi, F. Herlach, T. J. B. M. Janssen, J. A. A. J. Perenboom, M. Kurmoo and P. Day, *Synth. Met.* **55-57**, 2198 (1993).

[29] M. Tokumoto, A. G. Swanson, J. S. Brooks, C. C. Agosta, S. T. Hannahs, N. Kinoshita, H. Anzai, and J. R. Anderson, *J. Phys. Soc. Jap* **59**, 2334 (1990);

[30] J. Singleton, F. L. Pratt, M. Doporto, J. M. Caulfield, S. O. Hill, T. J. B. M. Janssen, I. Deckers, G. Pitsi, F. Herlach, W. Hayes, J. A. A. J. Perenboom, M. Kurmoo and P. Day, *Physica* **B 184**, 470 (1993).

[31] E. N. Adams and T. D. Holstein, J. *Phys. Chem. Solids* **10**, 254 (1994).

[32] The use of background subtraction leads to data which can only be fitted to the Lifshitz-Kosevich formula by assuming a field-dependent effective mass and Dingle temperature; this assumption is unlikely to be correct.

[33] *Magnetic oscillations in metals*, D. Shoenberg (Cambridge University Press, 1984).

[34] T. Sasaki, Ph. D thesis, Tohoku University, Sendai (1992).

[35] It is not surprising that the measured g is not equal to 2 (the value observed in ESR experiments). For a discussion of this point, see Ref. [16].

[36] J. Caulfield, W. Lubczynski, F.L Pratt, J. Singleton, D.Y.K. Ko, W. Hayes, M. Kurmoo and P. Day, J. Phys. *Condens. Matter* **6**, 2911 (1994).

[37] This data was collected by Dr M. Doporto and analysed by the author.

[38] A. B. Pippard, *Proc. Roy. Soc.* **A 287**, 165 (1965).

[39] T. Osada, S. Kagoshima, and N. Miura, *Phys. Rev.* **B** 46, 1812 (1992).

[40] Y. Iye, R. Yagi, N. Hanasaki, S. Kagoshima, H. Mori, H. Fujimoto and G. Saito, *J. Phys. Soc. Jap.* **63** 674 (1994).

[41] S. J. Blundell *et al*, in preparation.

[42] M. V. Kartsovnik, V. N. Laukhin, S. I. Pesotskii, I. F. Schegolev and V. M. Yakovenko, *J. Physique I* **2**, 89 (1993).

[43] K. Yamaji, *J. Phys. Soc. Jap.* **58**, 1520 (1989).

[44] M. V. Kartsovnik, H. Ito, T. Ishiguro, H. Mori, T. Mori, G. Saito and S. Tanaka, *J. Phys. Condens. Matter.* **6**, L479 (1994)

[45] S. Uji, H. Aoki, M. Tokumoto, T. Kinoshita, N. Kinoshita, Y. Tanaka and H. Anzai, *Phys. Rev.* **B 49**, 732 (1994).

[46] Similar behaviour has been measured in the region 17-25 T for a different value of ϕ; see figure 4 of Ref. [18].

[47] In the 17 T data in figure 12 some small features are observed in addition to the one-dimensional resistivity dips corresponding to $\tan\theta = (mb+d)/c$ (*c.f.* equation (5.5)). These are observed under certain conditions and can be ascribed to `fractional angle dependent magnetoresistance oscillations' in which $n>1$ equation (5.5). Their comparitive weakness reflects the small interplane overlap and consequent low value of the Fourier components of the sheet corrugation in the $\boldsymbol{b}^*$ direction.

[48] A. E. Kovalev, M. V. Kartsovnik, R. P. Shibaeva, L. P. Rozenberg, I. F. Schegolev, and N. D. Kushch, *Solid. State Commun.* **89** 575 (1994).

[49] A. House, M. S. L. du Croo de Jongh, S. J. Blundell and J. Singleton, *unpublished results.*

[50] Prof. J.S. Brooks, Massachusetts Institute of technology, *private communication.*

[51] Dr. M.V. Kartsovnik, Institute of Chemical Physics, Chernoglovka, *private communication.*

[52] J.S. Brooks, X. Chen, S.J. Klepper, S. Valfels, Y. Tanaka, T. Kinoshita, N. Kinoshita, M. Tokumoto, H. Anzai and S.W. Tozer, Synth. Met, *in press.*

[53] Dr. S.J. Blundell, Oxford University, *private communication.*

[54] Dr. M. J. Naughton, State University of New York, Buffalo, *private communication.*

[55] M. Doporto, J. Singleton, F. L. Pratt, J. Caulfield, W. Hayes, J. A. A. J. Perenboom, I. Deckers, G. Pitsi, M. Kurmoo and P. Day, *Phys. Rev.* **B** 49, 3934 (1994).

[56] S. Uji, H. Aoki, J. S. Brooks, A. S. Perel, G. J. Athas, S. J. Klepper, C. C. Agosta, D. A. Howe, M. Tokumoto, N. Kinoshita, Y. Tanaka, and H. Anzai, *Solid State Commun.* **88**, 683 (1993).

[57] J. Wosnitza, G. W. Crabtree, H. H. Wang, K. D. Carlson, M. D. Vashon and J. M. Williams, *Phys. Rev. Lett.* **67**, 263 (1991).

[58] M. Doporto, F. L. Pratt, J. Singleton, M. Kurmoo and W. Hayes, *Phys. Rev. Lett.* **69**, 991 (1992).

[59] J. S. Brooks, S. J. Klepper, C. C. Agosta, M. Tokomoto, N. Kinoshita, Y. Tanaka, S. Uji, H. Aoki, A. S. Perel, G. J. Athas, X. Chen, D. A. Howe and H. Anzai, *Physica* **B**, *in press.*

Chapter 6

Fermi surface studies of the pressure induced organic superconductor $ET_3Cl_2 2H_2O$

6.1. Introduction

$ET_3Cl_22H_2O$ is the only superconducting ET charge transfer salt where the ET ions each have +2/3e charge. The calculated Fermi surface consists of two parallel one dimensional sections and an elongated closed electron pocket [1]. The Fermi surface thus slightly resembles those of the TMTSF salts, except that the latter have only one band crossing the Fermi energy. $ET_3Cl_22H_2O$ is a semimetal under ambient pressure according to thermopower and conductivity measurements [2], but undergoes a (semi)metal-semiconductor transition at ~160 K [2-4]. Recent DC van der Pauw resistivity results [5] under ambient pressure indicate that the 160 K transition may be due to charge or spin density wave formation caused by nesting of the open sections of the Fermi surface. The application of pressure gradually reduces the onset temperature of the charge or spin density wave state and eventually stabilises a superconducting state between 10.2 kbar and 13.5 kbar. Using high magnetic fields and low temperatures the bandstructure of $ET_3Cl_22H_2O$ has been investigated whilst using hydrostatic pressure simultaneously to pass through the superconducting part of the phase diagram.

This chapter is organised as follows. § 6.2 provides an introduction to the crystal structure, bandstructure and properties of $ET_3Cl_22H_2O$. In § 6.3 the experimental arrangements are described. The significant experimental findings are described in § 6.4, and discussed in § 6.5.

6.2 Structure, band structure and properties of $ET_3Cl_22H_2O$

$ET_3Cl_22H_2O$ crystallises in the triclinic space group $P\bar{1}$ with a=11.314Å, b=13.894Å, c=15.924Å, α=94.74°, β=109.27°, γ=97.03° and a unit cell volume of V=2304Å^3 [3]. The structure consists of sheets of ET molecules separated by layers of the anions as shown in figure 1. The unit cell contains slipped stacks of three crystallographically independent ET molecules, and there are two formula units per unit cell. All ET molecules are oriented approximately parallel to one another (the c axis

roughly parallel to the long ET molecular axis). On lowering the temperature the lattice contracts anisotropically; the ***a*** axis reduces smoothly until ~75 K and then remains constant and the ***b*** axis reduces continuously down to 12 K, while the ***c*** axis remains constant in the temperature range 12-300 K [6].

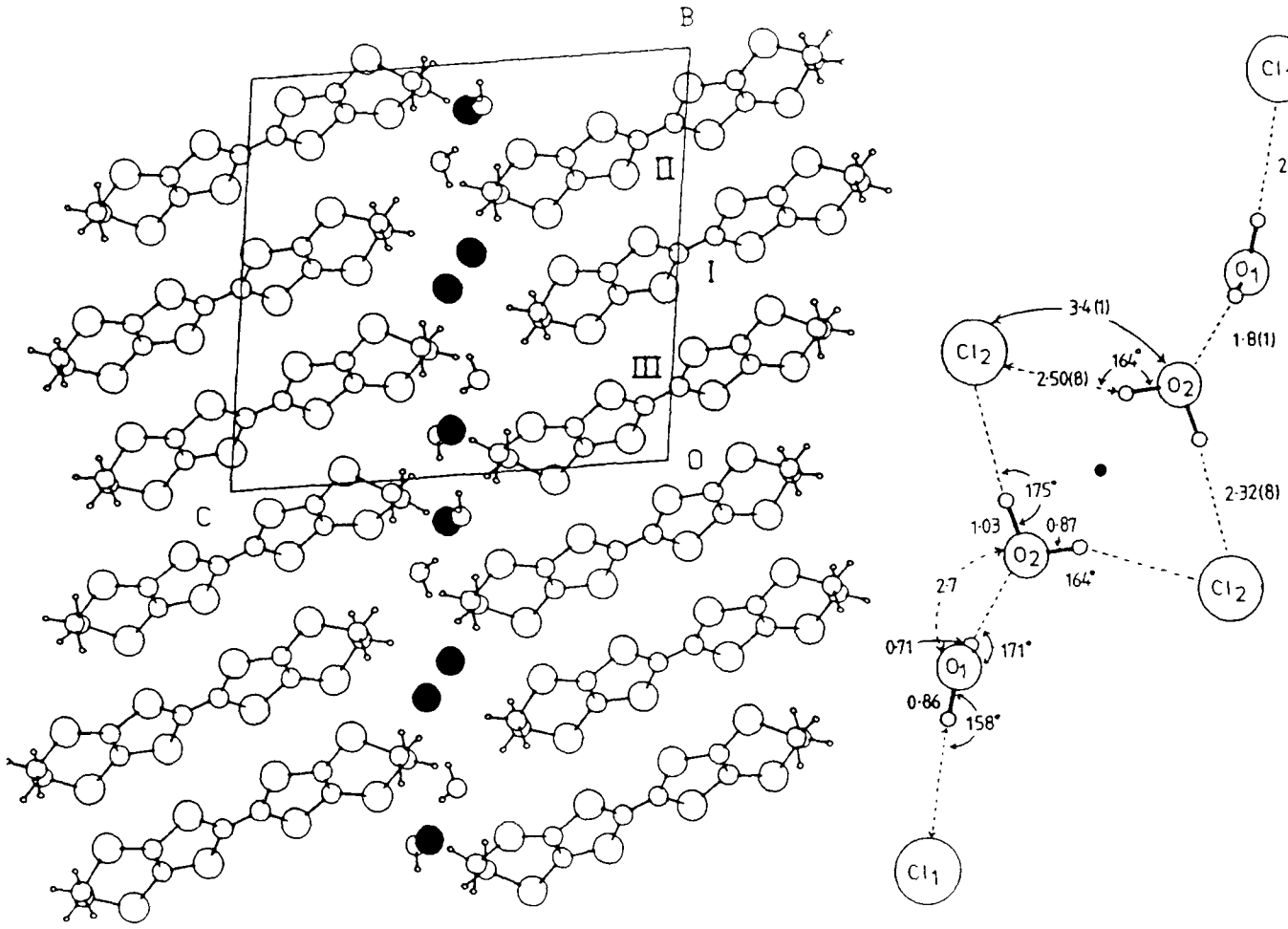

Figure 1 Crystal structure of $ET_3Cl_2 2H_2O$; (a) the view along ***a****, (b) anion structure [3].

The electronic band structure has been calculated by Whangbo *et al* [1] using the extended Hückel model. The transfer integrals were calculated using a double zeta-basis set of Slater type orbitals derived from the ambient pressure atomic co-ordinates [3]. The six ET molecules in the unit cell donate four electrons to the counterions so that the resulting band structure (figure 2) is two thirds filled by electrons. According to Whangbo *et al* [1] the Fermi level crosses the three upper bands (labelled *A*, *B* and *C* in figure 2) which results in the predicted Fermi surface shown in figure 3. Band *A* leads to an elongated closed electron pocket (figure 3a) centred at point M on the Brillouin zone. Band *B* leads to an open electron Fermi surface (figure 3b), and band *C* an open hole Fermi surface (figure 3c) both along the Γ⇒Y direction.

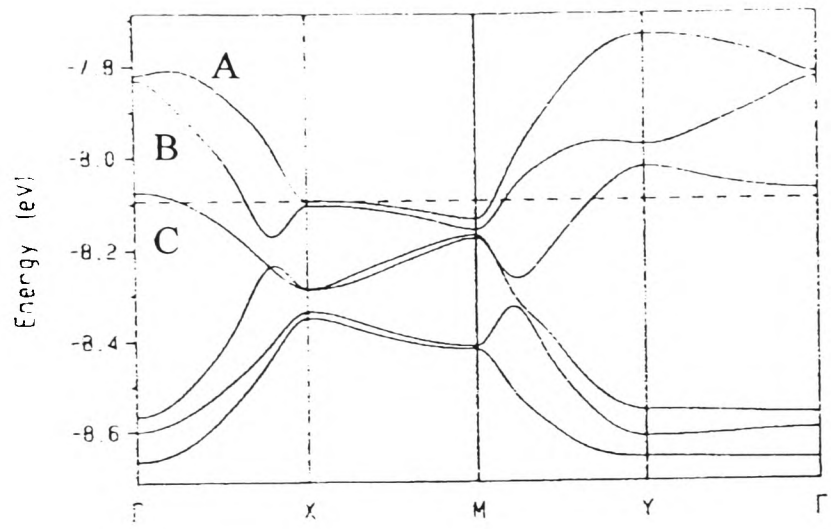

Figure 2 Dispersion relations of the six highest occupied bands calculated for $ET_3Cl_2.2H_2O$. The dashed line corresponds to the Fermi level. Γ=(0,0), Y=(0,b^*/2) and M=(a^*/2, b^*/2) [1].

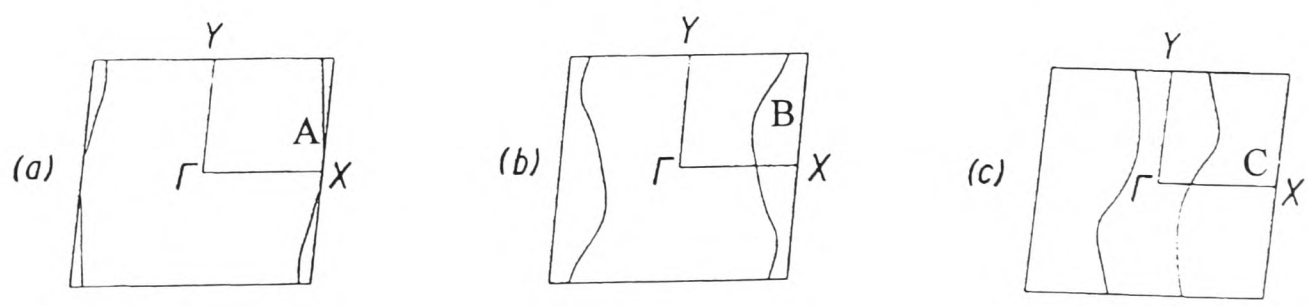

Figure 3 Fermi surfaces associated with the (a) upper (A), (b) middle (B), and (c) lower (C) of the three partially filled bands in figure 2 [1].

Mori and Inokuchi [2] were the first to calculate the dispersion relationship in $ET_3Cl_22H_2O$. Their results predict that $ET_3Cl_22H_2O$ is a semimetal, and that its Fermi surfaces consist of closed electron and hole pockets. The latter implies that $ET_3Cl_22H_2O$ would have a nearly isotropic electrical conductivity within the plane of the ET layers. The differing theoretical results are due to the fact that Mori and Inokuchi use a single zeta-basis set, a lower order approximation than the double zeta-basis set used by Whangbo *et al*, to calculate the transfer integrals. The practical difference between the two methods is that in the single zeta-basis set model the calculated molecular wave functions do not protrude as far in real space; this can be critical in some cases [7], especially when the Fermi energy is small.

The existence of both hole and electron carriers has been confirmed by thermopower measurements [2,8]. Hall effect data [9] indicate that the mobility difference between the electrons and holes is small. Determination of the anisotropy of the optical conductivity from measurements of the infra-red reflectivity [8] are in good agreement with the anisotropic Fermi surface predicted by reference [1] but inconsistent with the Mori two dimensional Fermi surface in reference [2]. Under ambient conditions the measured conductivity, using a standard four-probe method, is large and highly anisotropic [2,4]; along the ***b*** direction (the direction of strong sulphur-sulphur contact) the room temperature value is 700 Scm^{-1}. This is in contrast to many ET salts which often exhibit comparatively low room temperature conductivity *e.g.* in κ-$ET_2Cu(NCS)_2$, $\sigma \approx 50$ Scm^{-1}. The electrical resistivities along the intrastack, the interstack and interlayer directions (*i.e.* ***b***, ***a***, and ***c****-axis directions, respectively) have the ratios 7:1:1000 at 4 K [4]. The conductivity results [2,4] and the possible observation of a charge density wave are thus in broad agreement with the bandstructure calculations of Whangbo *et al* [1], rather than those of Mori and Inokuchi [2].

Four circle X-ray diffractometry measurements on a single crystal of $ET_3Cl_22H_2O$ have been carried out down to 12 K at ambient pressure by Chasseau *et al* [6]: the data do not indicate significant changes in the overall crystal structure at low temperature. Unfortunately from the data one cannot conclude whether or not a charge

density wave occurs as the extra Bragg reflections or diffuse scattering that may occur in the presence of a Peierls transition were not measured. A better method would be to take a long exposure X-ray photograph at each temperature [10].

The temperature dependence of the resistivity of a single crystal of $ET_3Cl_2 2H_2O$ at 1 bar is shown in figure 4 [11]. In the temperature range 160 K to 300 K the resistivity is linear with temperature. A (semi)metal-semiconductor transition occurs at about 160 K (the resistance minimum). Below 160 K, the resistivity does not show simple Arrhenius behaviour, but instead exhibits small peaks and dips superimposed on a monotonic increase with decreasing temperature. The features may indicate further slight changes in the Fermi surface. The mean slope of a log (resistivity) versus 1/(temperature) plot in this region indicates an activation energy of around 0.04 eV. Similar activated behaviour is also found in the spin susceptibility [8]), indicating a sharp decrease in the density of states at the Fermi energy below 160 K. Thermopower measurements [2] also indicate a similar steep fall in the density of states at the Fermi energy, to a small but finite value at low temperatures. The Hall coefficient is small and positive at temperatures above the transition and large and negative below [9].

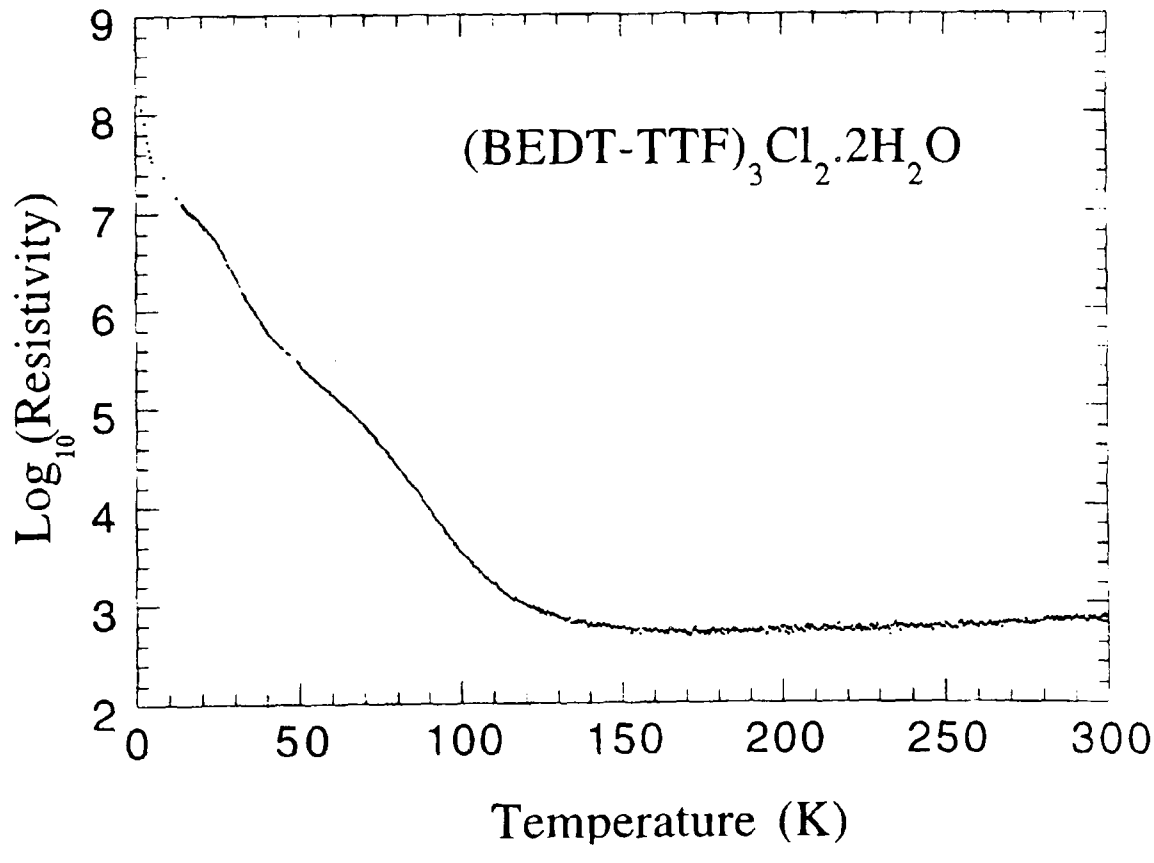

Figure 4 Log resistance against temperature for a single crystal of $ET_3Cl_2 2H_2O$ [11]. The data presented here were obtained using the same batch of crystals as the one used for measurements reported in this chapter [11].

Previous measurements have shown that the application of pressure gradually lowers the (semi)metal-semiconductor transition [12,13]. At ~12 kbar superconductivity has been reported in $ET_3Cl_2 2H_2O$ with a critical onset temperature of ~4 K. The onset temperature was found to gradually decrease with further increases in pressure. Figure 6 shows the measured resistance against temperature for two crystals of $ET_3Cl_2 2H_2O$ between 10 kbar and 15 kbar [13].

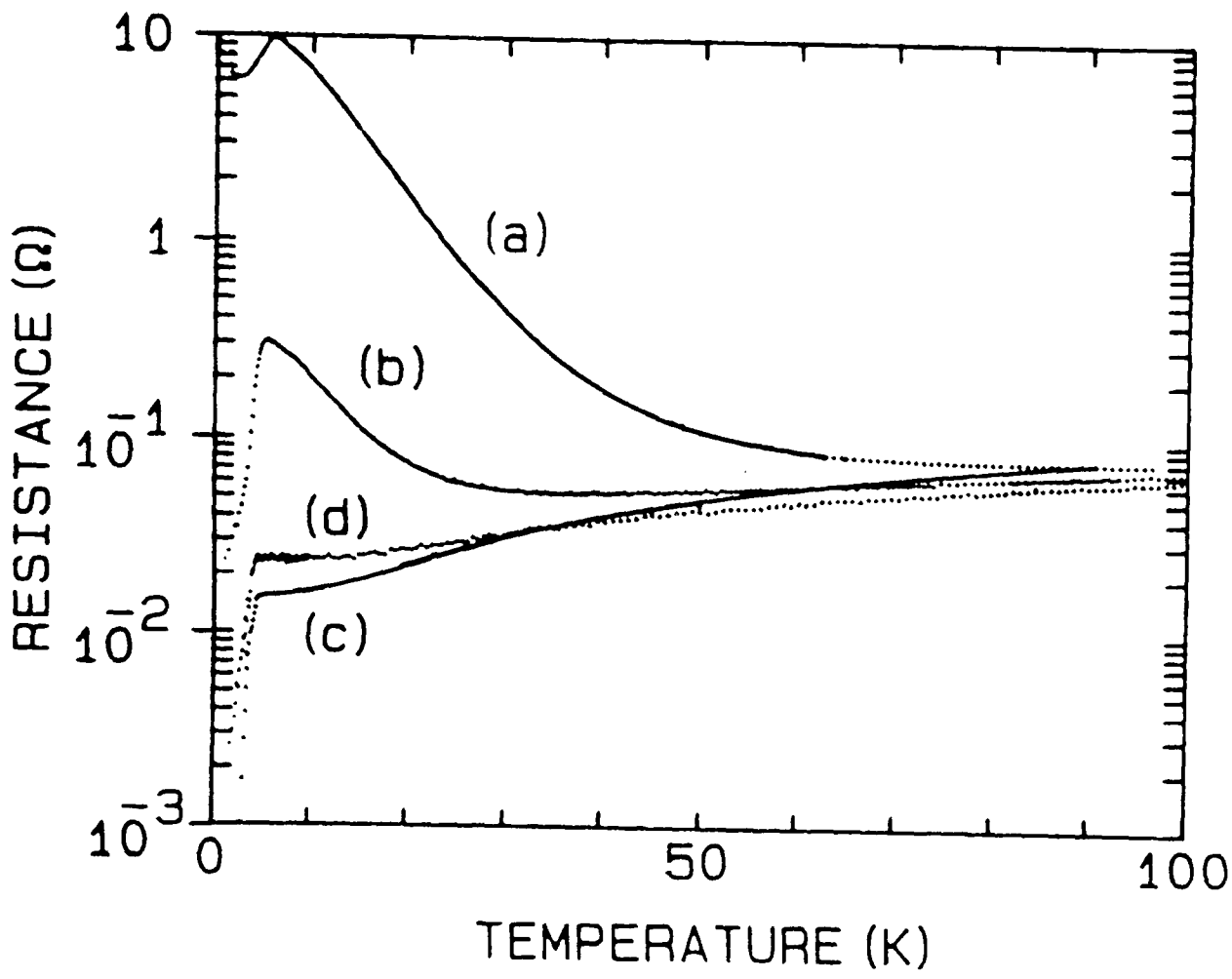

Figure 5 Temperature dependence of the resistivity of $ET_3Cl_2 2H_2O$ at several pressures (taken from reference [13]).

In this chapter a detailed examination of the changes in the bandstructure of $ET_3Cl_2 2H_2O$ are made (at low temperatures, down to 700 mK and high magnetic fields, up to 17 T) whilst using hydrostatic pressure simultaneously to pass through the superconducting part of the phase diagram.

6.3 Experimental techniques

High purity single crystals of $ET_3Cl_2 2H_2O$ were prepared electrochemically by M. Kurmoo [3]. The crystals are generally small (~2x2x0.05 mm^3) black distorted hexagonal platelets with a metallic lustre, with the plane of the plate corresponding to the highly conducting layers. Gold wires were attached with silver epoxy to previously evaporated ~500 nm thick gold pads on the platelet face. The resulting two terminal contact resistances were less than 10 Ω per pair at 300 K. Magnetoresistance measurements were made using standard 4-wire AC techniques (5-150 Hz) with the current applied in the ***ab***-plane of the crystal plate (generally 20-100 μA). The magnetic field was applied in the c^* direction.

Magnetoresistance experiments under hydrostatic pressure were carried out using a non-magnetic clamp cell (a schematic of the cell is shown in figure 6 of chapter 3) filled with a petroleum spirit medium. The cell provides pressures up to 16.5 kbar at helium temperatures. For pressures between 16.5 kbar and 20 kbar the sample was transferred to a larger clamp cell. Pressure was applied at room temperature using a hydraulic press after which the cell was placed in a specially designed ^3He cryostat providing temperatures down to 500 mK in a 17 T superconducting magnet. The measurements above 16.5 kbar were limited to pumped ^4He temperatures due to the larger size of the pressure cell. All pressures quoted in this chapter are those at 4 K and all data shown were taken on one crystal of $ET_3Cl_2 2H_2O$. The same experimental precautions and techniques were followed as outlined in § 3.3.

6.4 Experimental Results

6.4-1 Pressure induced superconductivity

DC van der Pauw measurements on these samples indicate that the resistivity of $ET_3Cl_2 2H_2O$, at ambient pressure and at temperatures below the (semi)metal-

semiconducting transition, is electric field dependent and chaotic in nature. The non-Ohmic behaviour has been interpreted as a charge density wave sliding between pinning sites in the applied electric field [5]. Charge density waves also tend to settle into configurations in which a small disturbance will cause a violent change (*i.e.* they organise themselves into a critical state), which may account for the chaotic appearance of the temperature dependent resistivity. The results are not affected by the application of a magnetic field (up to 15 T), so it is tentatively proposed that the low temperature behaviour is due to charge (not spin) density wave formation [5].

The lowering of the temperature of the (semi)metal to semiconductor transition with increasing pressure has been mentioned above. In the present experiments it was found that at 11.3 kbar, for example, the resistivity has a minimum around 50 K (*c.f.* 160 K at ambient pressure) , followed by a thirty-fold increase to a maximum at 3.5 K and then another rapid decrease. In this chapter we focus on the low temperature behaviour. The temperature dependence of the resistance of a single crystal of $ET_3Cl_22H_2O$ at five different hydrostatic pressures in the low temperature regime is shown in detail in figure 6. Between 10.2 kbar and 12.5 kbar the resistivity at 3 K drops by almost three orders of magnitude.

At the four lowest pressures shown in figure 6, there is a marked drop in the resistivity at the very lowest temperatures which is suppressed by the application of a magnetic field (figure 7). For the 11.3 kbar and 12.5 kbar data this behaviour is very obviously characteristic of superconductivity. However, at 10.2 kbar there is only a tendency to superconductivity (at ~3 K), which starts to 'short out' the semiconductor state. At this pressure zero resistance is not actually attained down to 0.7 K, although the onset is still suppressed by the application of magnetic fields. Similar behaviour (*i.e.* non-zero resistance in a superconducting state) has been observed in other ET salts [14] and high T_C superconductors, and has been attributed to a 'Bose glass state' [15]. The onset of superconductivity at ~10 kbar is perhaps surprising as the material possesses a rather small density of states for the formation of Cooper pairs.

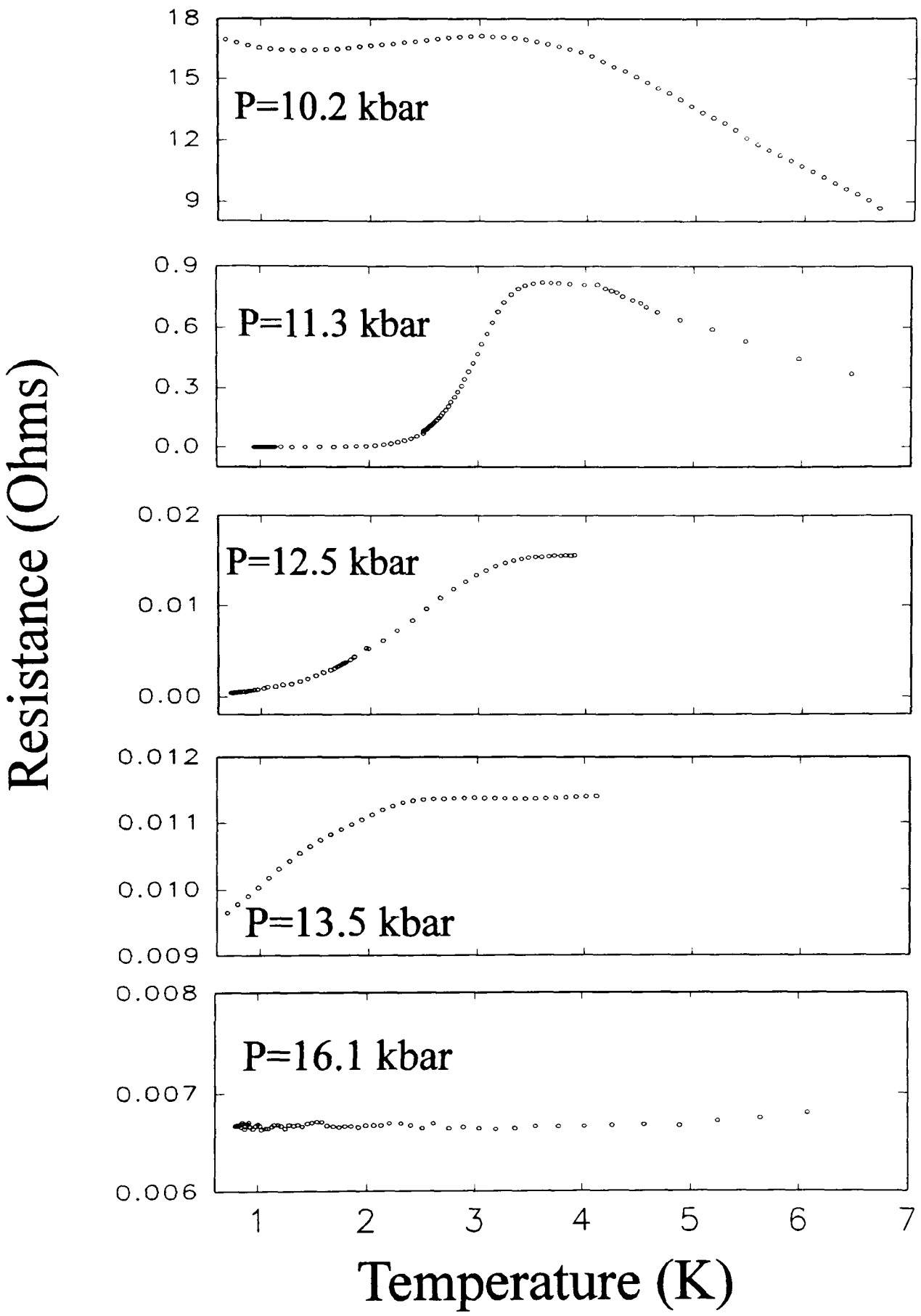

Figure 6 The measured resistance versus temperature (0.7-7 K) for a single crystal of $ET_3Cl_2 2H_2O$ at five different hydrostatic pressures.

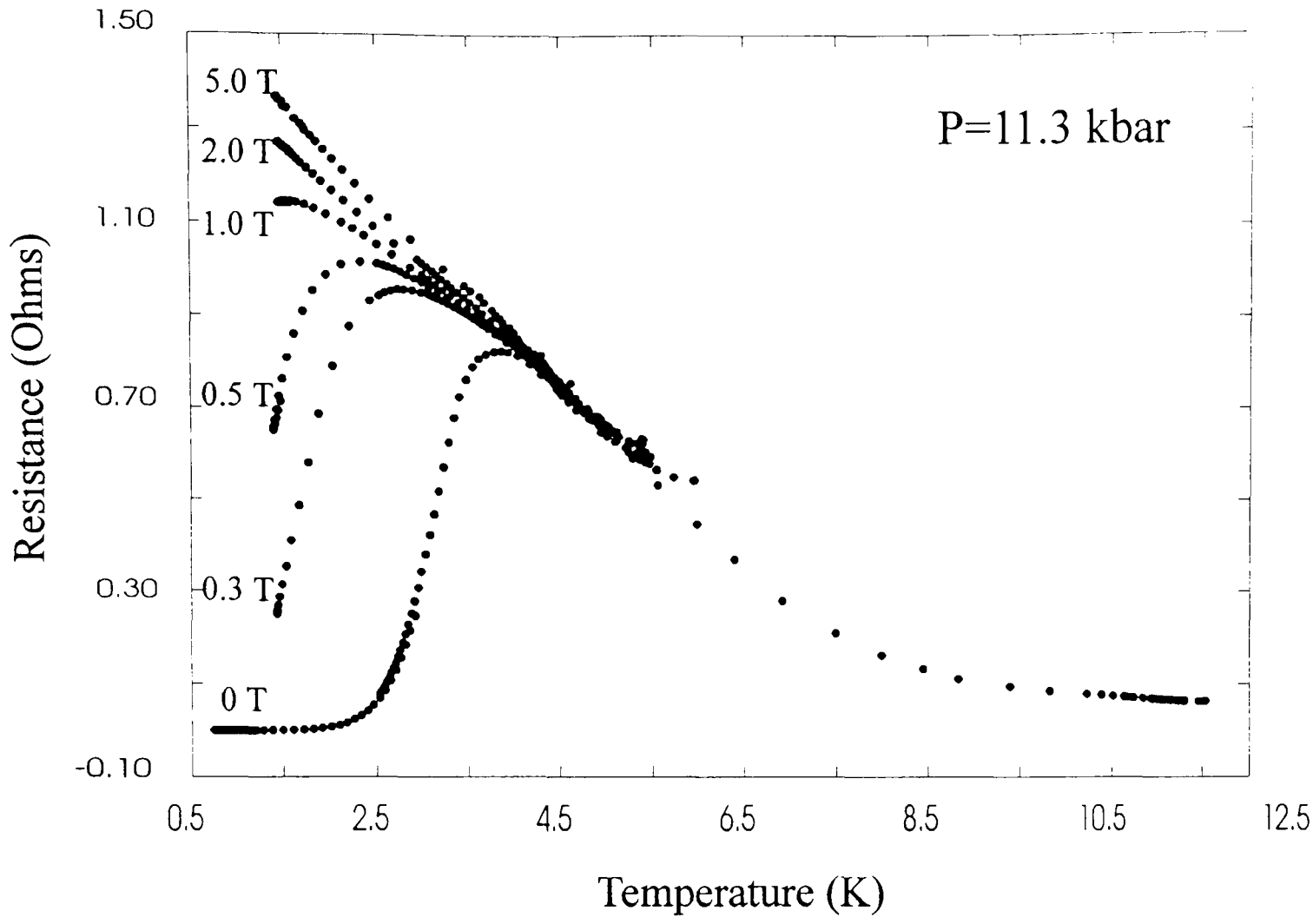

Figure 7 The suppression of superconductivity in $ET_3Cl_22H_2O$ at 11.3 kbar using magnetic field.

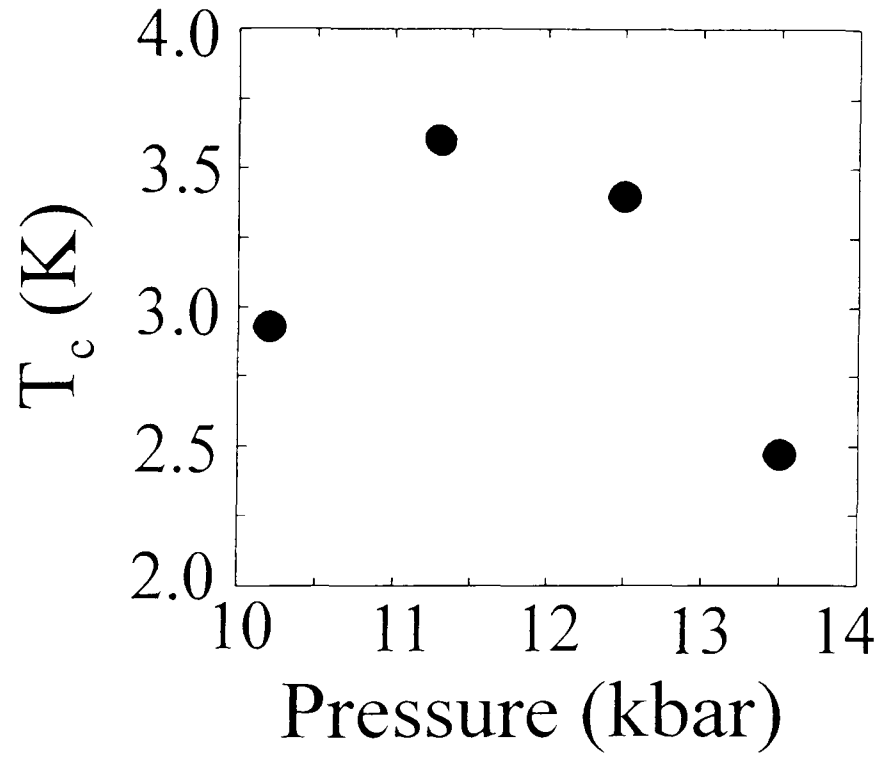

Figure 8 The pressure dependence of the superconducting transition temperature (T_C), derived from the measured resistive onset (95 % normal resistance point) to superconductivity.

The superconducting transition temperature, T_c, (measured at 95 % of the extrapolated normal resistance) increases with pressure, peaking at ~3.6 K (figure 8) at a pressure of 11.3 kbar. With further increases in pressure T_c decreases, until at ~14.5 kbar the onset of superconductivity is not observable at temperatures above 0.7 K, in agreement with references [12] and [13]. At 13.5 kbar the semiconducting behaviour is completely suppressed, and the material behaves as a normal (semi)metal.

6.4-2 Magnetoresistance

The magnetoresistance of a single crystal of $ET_3Cl_2 2H_2O$ is shown in figure 9 measured at seven different hydrostatic pressures between 10.2 kbar and 16.1 kbar at 0.7 K and at 20 kbar at 1.2 K. At 10.2 kbar and 11.3 kbar the magnetoresistance saturates quickly, whereas above 11.3 kbar the magnetoresistance changes form and grows without limit. One can account for the rather dramatic change in the form the of magnetoresistance between 11 kbar and 12.5 kbar (figure 9) by consulting the theory of magnetoresistance [16].

In a *closed* Fermi surface orbit, if $\omega_c\tau >> 1$, the electron makes many circuits before it is scattered. Thus one can see that the component of average velocity normal to $\boldsymbol{B}$ will tend to zero as B increases. If we measure the conductivity in the x-direction, and the magnetic field is applied along the z-axis, then we expect the conductivity to tend to zero as B increases to infinity (see figure 10). One can show for a closed orbit that as

$$\sigma_{xx} \to A / B^2 \text{ as } B \to \infty \qquad (6.1)$$

where A is a constant that depends on the nature of the scattering processes, the geometry of the Fermi surface, etc.

For *open* orbits normal to the magnetic field there is no symmetry to ensure that the average component of the electron velocity should vanish (see figure 10b). If the x-axis is the direction along which the orbit stretches to infinity, we certainly expect v_y to remain finite even in the strongest magnetic fields. The corresponding component of conductivity would then tend to a constant:

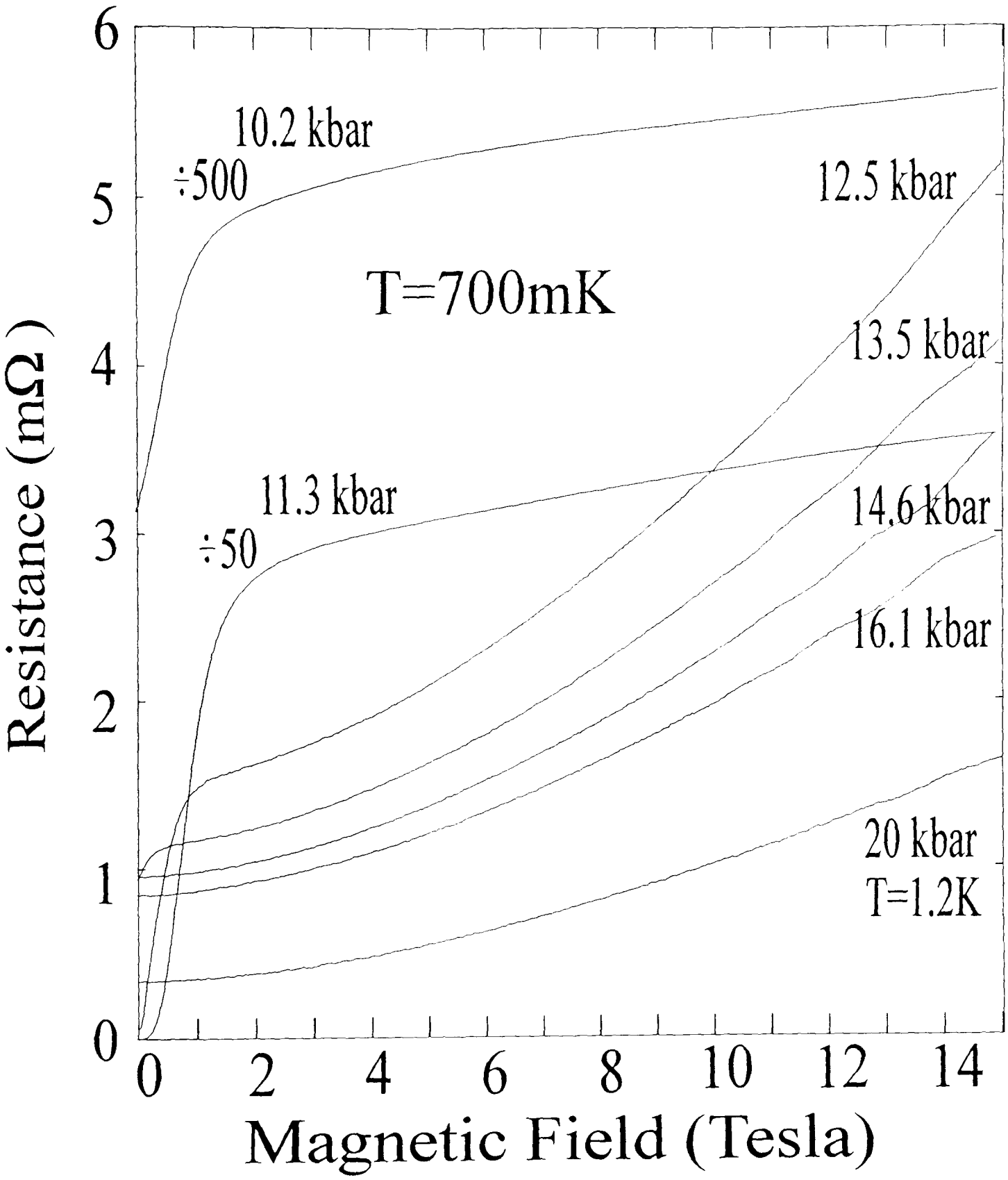

Figure 9 The magnetoresistance of $ET_3Cl_22H_2O$ up to 15 T for seven different hydrostatic pressures between 11.3 kbar and 16.1 kbar, at 700 mK, and 20 kbar at 1.2 K.

$$\sigma_{yy} \to C \text{ as } B \to \infty \tag{6.2}$$

Looking at these two formulae, one might suppose the resistance of a metal transverse to a magnetic field would tend to infinity if all the orbits were closed, but would tend to a finite limit if there were some open orbits in the appropriate directions. Unfortunately the converse is true.

To get the correct result, we write down the tensor relations between current and field (*i.e.* we also consider the Hall effect). In the *xy*-plane we have the following equations.

$$J_x = \sigma_{xx} E_x + (1/RB) E_y \tag{6.3}$$

$$J_y = (-1/RB) E_x + \sigma_{yy} E_y \tag{6.4}$$

The off-diagonal terms express the Hall effect, through the Hall coefficient R. The electric field produced is at right angles to the electric current, and approximately proportional to B.

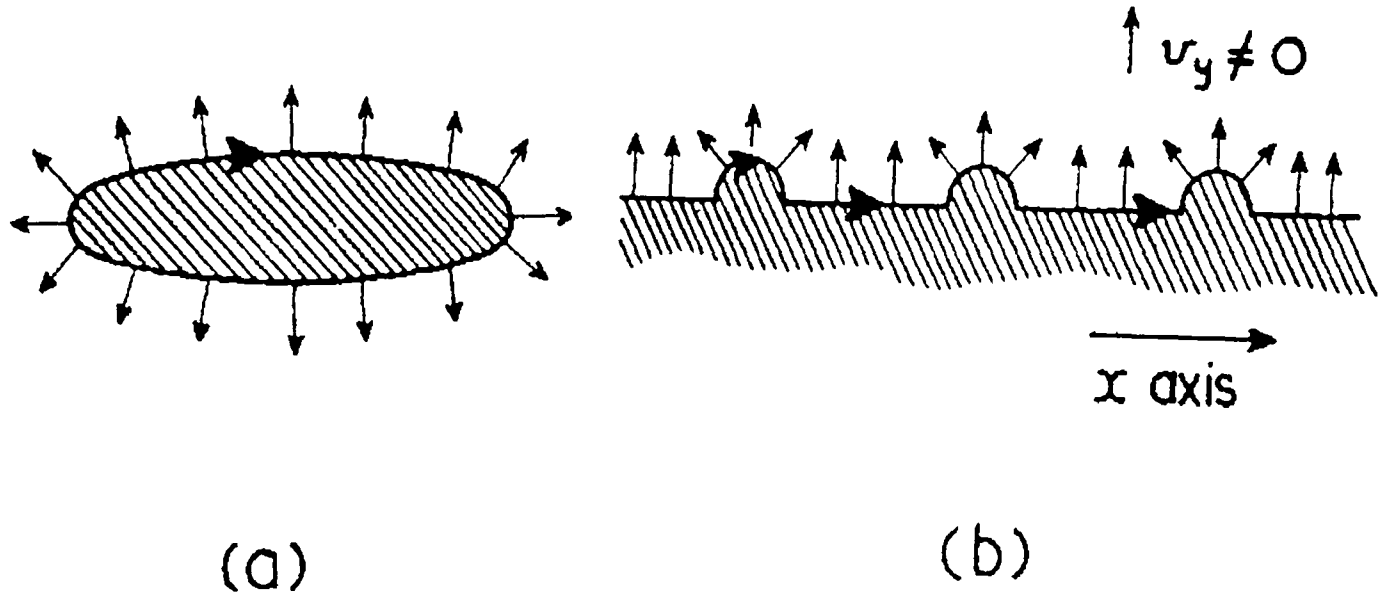

Figure 10 (a) On a closed orbit the average velocity in the plane perpendicular to the magnetic field is zero. (b) On an open orbit, some components of velocity need not vanish.

To discuss the resistivity we must solve equations (6.3) and (6.4) for E_x and E_y as functions of currents J_x and J_y: *e.g.*

$$E_x = \frac{1}{\sigma_{xx} + 1/(R^2 B^2 \sigma_{yy})} J_x + \frac{RB}{1 + R^2 B^2 \sigma_{xx} \sigma_{yy}} J_y \qquad (6.5)$$

The coefficient Jy gives us the Hall effect, which we need not discuss here. But the coefficient of J_x we should interpret as a resistance, ρ_{xx}. It is the electric field in the x-direction, created by unit current flowing in that direction. This is of course, *transverse* to the magnetic field.

Now for closed orbits both σ_{xx} and σ_{yy} behave as A/B^2. The term σ_{xx} in the denominator can be neglected, and

$$\rho_{xx} \sim AR^2 \qquad (6.6)$$

Thus the transverse magnetoresistance saturates in large fields.

But if there is an open orbit along the x-direction, σ_{yy} will tend to a constant, C, and both terms in the denominator will decrease as $1/B^2$.

$$\rho_{xx} = \frac{1}{A/H^2 + 1/(R^2 H^2 C)} \sim \frac{B^2}{A + 1/R^2 C} \qquad (6.7)$$

In this case the magnetoresistance increases without limit, proportionately to B^2.

Applying the above ideas and considering solely the magnetoresistance data (figure 9), it would appear that between 10.2 kbar and 11.3 kbar the saturating magnetoresistance implies a predominantly two dimensional Fermi surface. Above 11.3 kbar the magnetoresistance data indicate that the Fermi surface has become predominantly one dimensional.

6.4-3 The Fermi surface

Evidence of the two dimensionality remains above 12.5 kbar as a single series of low frequency oscillations are superimposed on the magnetoresistance (see figure 11), periodic in reciprocal field (figure 11 inset). The Shubnikov-de Haas frequency increases from 45 T (~1.7 % of the room temperature Brillouin zone area) at 12.5 kbar and then asymptotically approaches 100 T (~3.8 % of the Brillouin zone) at 20 kbar (figure 12).

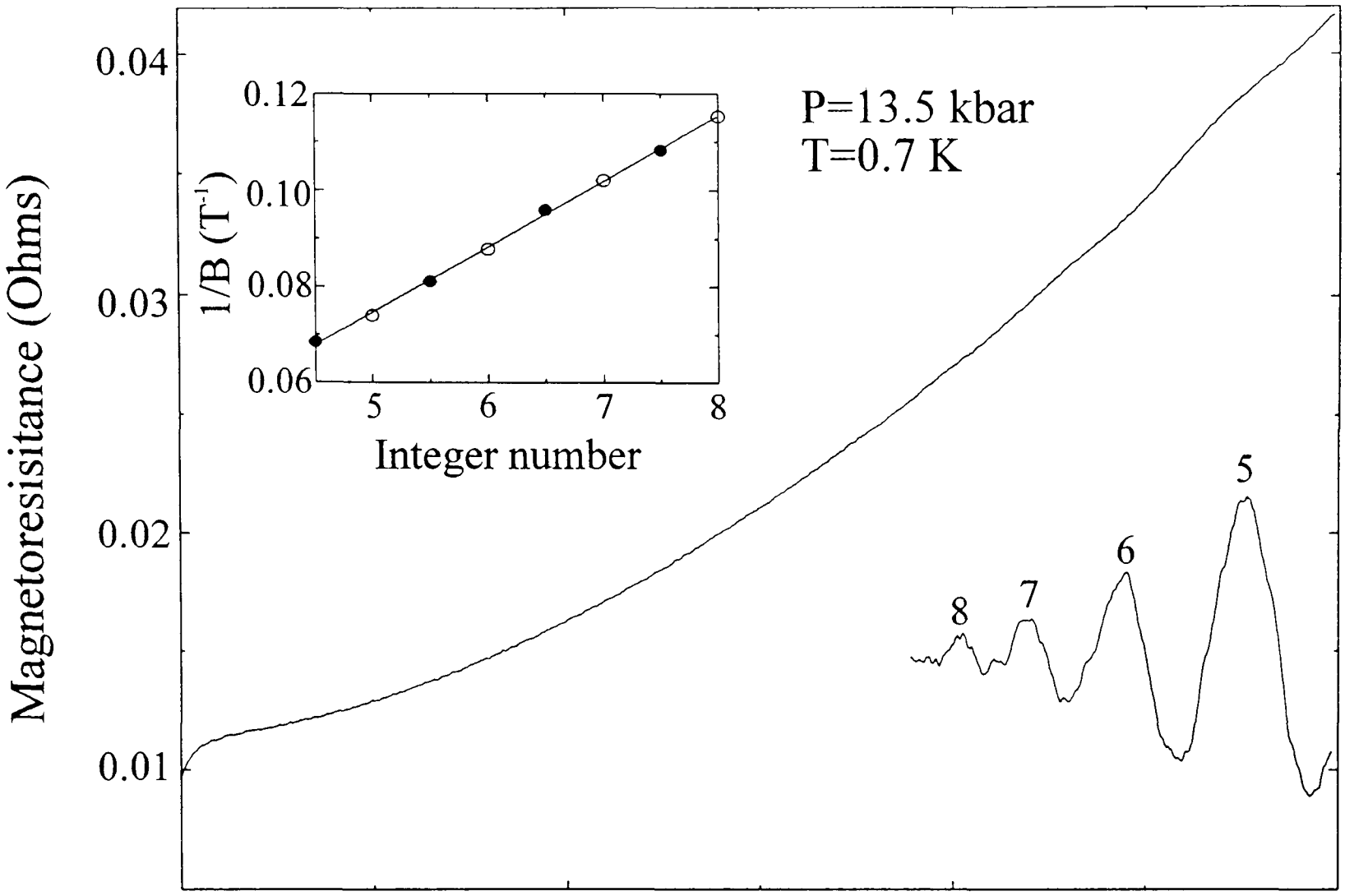

Figure 11 The magnetoresistance of $ET_3Cl_2 2H_2O$ at 700 mK for a hydrostatic pressure if 13.5 kbar is shown upto 15 T. The oscillatory component of the magnetoresistance is also shown after the removal over the slowly varying classical magnetoresistance. In the inset a plot of the inverse field of the oscillatory magnetoresistance peaks (solid points) and dips (hollow points) versus Landau level index is shown. The solid line has a gradient of 74 T.

By fitting the temperature dependence of the Fourier amplitude between 12 T and 17 T to the Lifshitz-Kosevich formula [17] an effective mass of $0.80\pm0.1\ m_e$ was obtained at 13.5 kbar. At 16.1 kbar the effective mass has dropped to $0.75\pm0.1\ m_e$. Unfortunately the Dingle temperature [17] is difficult to measure as there are so few oscillations in the

magnetic fields available, although the rate of increase in amplitude with field does not vary appreciably with pressure. The data imply that the effective mass and mobility are not very pressure dependent within the errors.

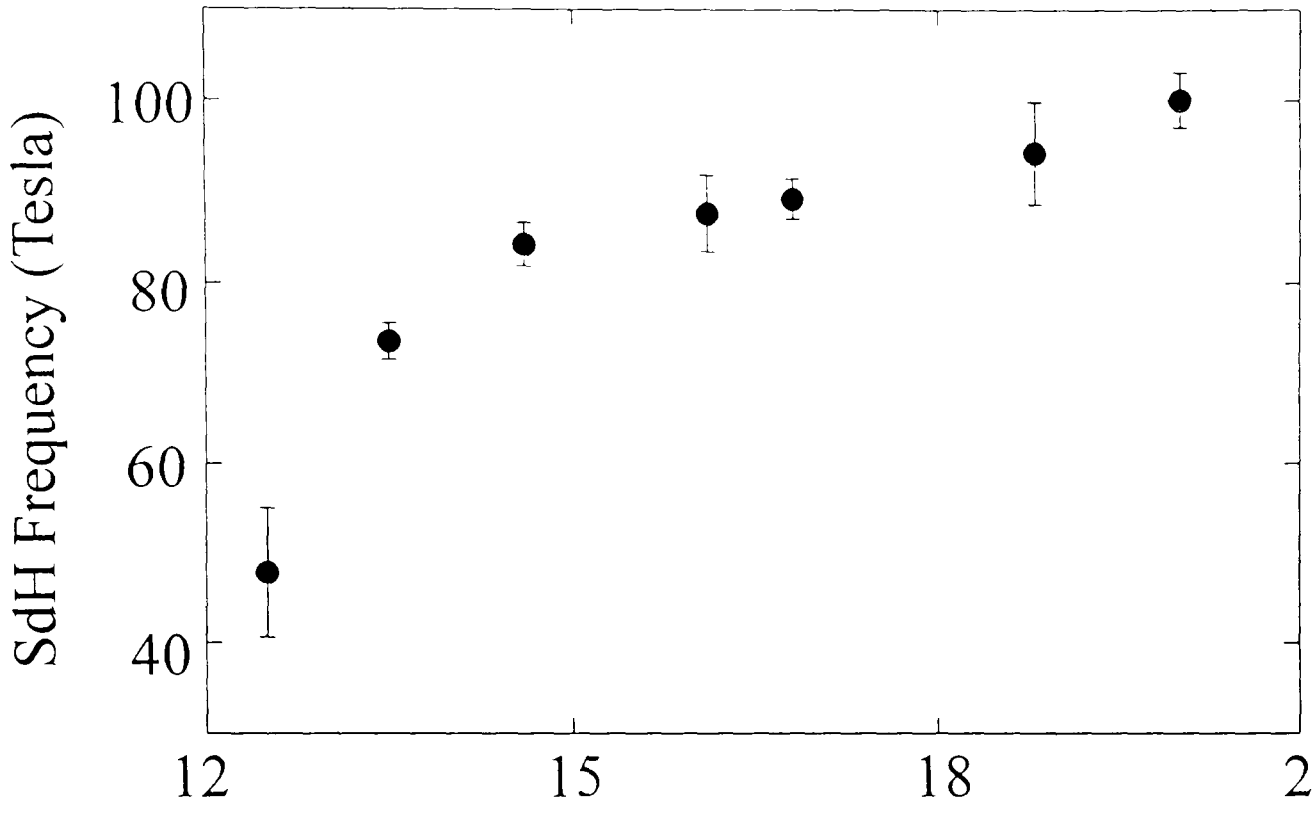

Figure 12 The measured Shubnikov-de Haas frequency plotted as a function of pressure.

From the magnetoresistance data the superconducting critical magnetic field (B_{c2}) may be estimated. Since the measured temperature range is rather limited B_{c2} is defined as the 95 % recovery of the extrapolated normal-state resistance. From the temperature dependence of the magnetoresistance, the temperature dependence of B_{c2} could be measured (figure 13). The magnetic field is applied perpendicular to the conducting ET sheets in the c^* direction, the direction of smallest B_{c2}. At T_c $dB_{c2}/dT \sim -0.40\,\mathrm{T/K}$ at the pressure 11.3 kbar and $\sim -0.33\,\mathrm{T/K}$ at 12.5 kbar The superconducting critical temperatures at these pressures are shown in figure 8. B_{c2} for the temperature T=0 K is derived from Ginzburg-Landau analysis to be [19]:

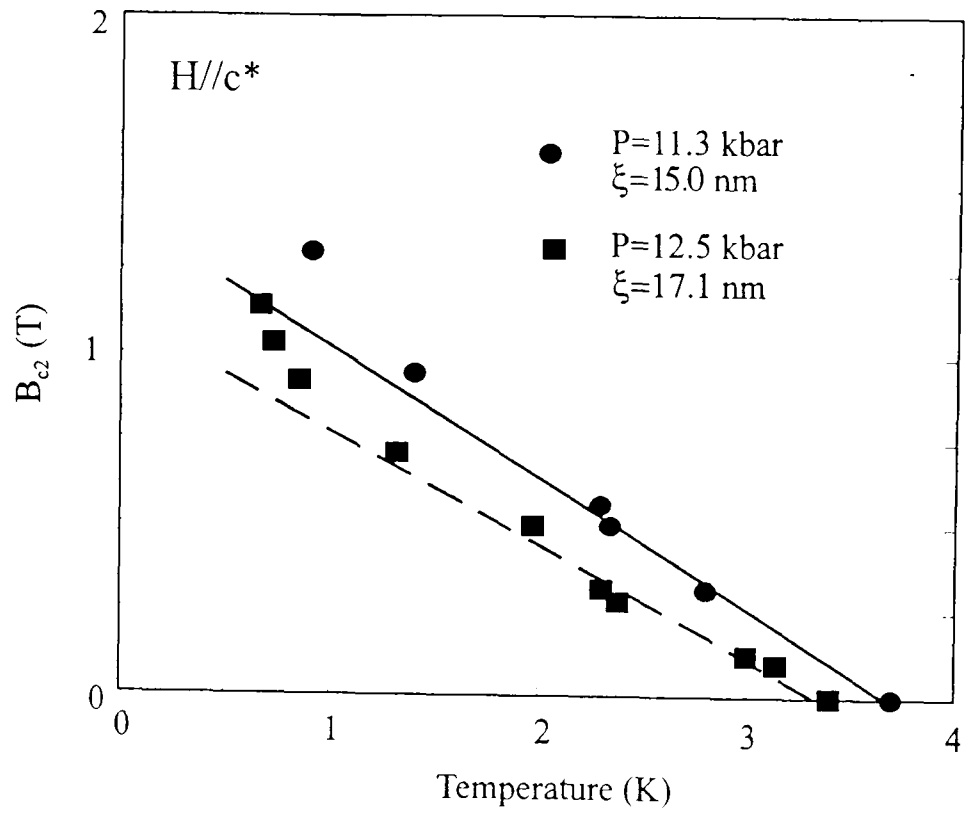

Figure 13 Temperature dependence of the upper critical field (B_{c2}) in the ***ab***-plane (95 % recovery of the extrapolated normal-state resistance) at 11.3 kbar (filled circle) and 12.5 kbar (filled square).

$$B_{c2}(0) = -T_c \left.\frac{dB_{c2}}{dT}\right|_{T_c} \tag{6.8}$$

This prescription of $B_{c2}(0)$ is useful because relationships have been established [20] between the normal state properties (such as resistivity, specific heat and Fermi surface area) and the slope of $B_{c2}(\mathrm{T})$ $\mathrm{d}B_{c2}/\mathrm{d}T$ evaluated at T_c. The coherence length (ξ) can be derived from the expression:

$$B_{c2}(0) = \frac{\phi_0}{2\pi\xi^2} \tag{6.9}$$

where ϕ_0 ($=h/2e$) is the flux quantum ($\phi_0=2.07\times10^{-15}\mathrm{Tm}^2$). Hence the coherence length at 11.3 kbar is ξ~150 Å and at 12.5 kbar ξ~171 Å (in the plane (***ab***) of the ET molecules). Although the choice of definition of T_c is rather arbitrary, the relative change in ξ with pressure is interesting. One can estimate the coherence length theoretically using measured Fermi surface parameters by consulting Pippard's theory [21]

$$\xi = \frac{0.18\hbar v_F}{k_B T_c} \tag{6.10}$$

where v_F is the average Fermi velocity. From the measured Shubnikov-de Haas frequency (B_f) and the carrier effective mass (m*), the average Fermi velocity ($v_F = \sqrt{(2\hbar e B_F)}/m^*$ assuming a circular orbit) around the closed pocket at 12.5 kbar is ~0.37×10^7cm/sec (*c.f.* 0.7×10^7cm/sec in $\kappa-ET_2Cu(NCS)_2$, as shown in chapter 3). Using the measured Fermi surface parameters the coherence length at 12.5 kbar is calculated to be ~150 Å, in reasonable agreement with the experimentally determined value (this of course assumes that the two dimensional carriers mediate the superconductivity). At 11.3 kbar no Shubnikov-de Haas oscillations were observed, so we can make use of the measured coherence length and T_c to estimate the average Fermi velocity of the two dimensional carriers from equation (6.10). If we assume that the effective mass is approximately independent of pressure, the data imply that the Fermi surface at 11.3 kbar is ~14 % smaller than at 12.5 kbar *i.e.* the fundamental field at 11.3 kbar is estimated to be 38.5 T. (~1.5 % of the Brillouin zone area)

Previous work has shown that the critical field exhibits considerable anisotropy; dB_{c2}/dT measured for B//***b*** and B//***c**** is ~8:1 according to Mori and Inokuchi [12]. The anisotropy ratio is rather small compared to other typical ET salt superconductors, and is consistent with a slightly smaller than average separation between the conducting layers, due to the small counterion. The ratio of $B_{c2\parallel}(0)/B_{c2\perp}(0)$ is identical to the ratio of the coherence lengths, $\xi_\parallel / \xi_\perp$ ($\perp$ means perpendicular to the highly conducting ***ab***-planes). So this implies a coherence length along ***c**** of ~20 Å, which is of the order of the separation of the conducting ET layers (***c****~15 Å). This suggests that Josephson coupling or proximity effects may be important in connecting segregated superconducting ET layers.

A pressure-temperature phase diagram for $ET_3Cl_2 2H_2O$, using the data presented in this chapter (shown as dots) and references [12] (shown as diamonds) and [13] (shown as squares) is shown in figure 14. The data points mark the boundaries

(dashed lines) to clear superconducting, metallic or semiconducting behaviour. The vertical thick dashed line represents the point at which experimental evidence of open sections of Fermi surface was observed.

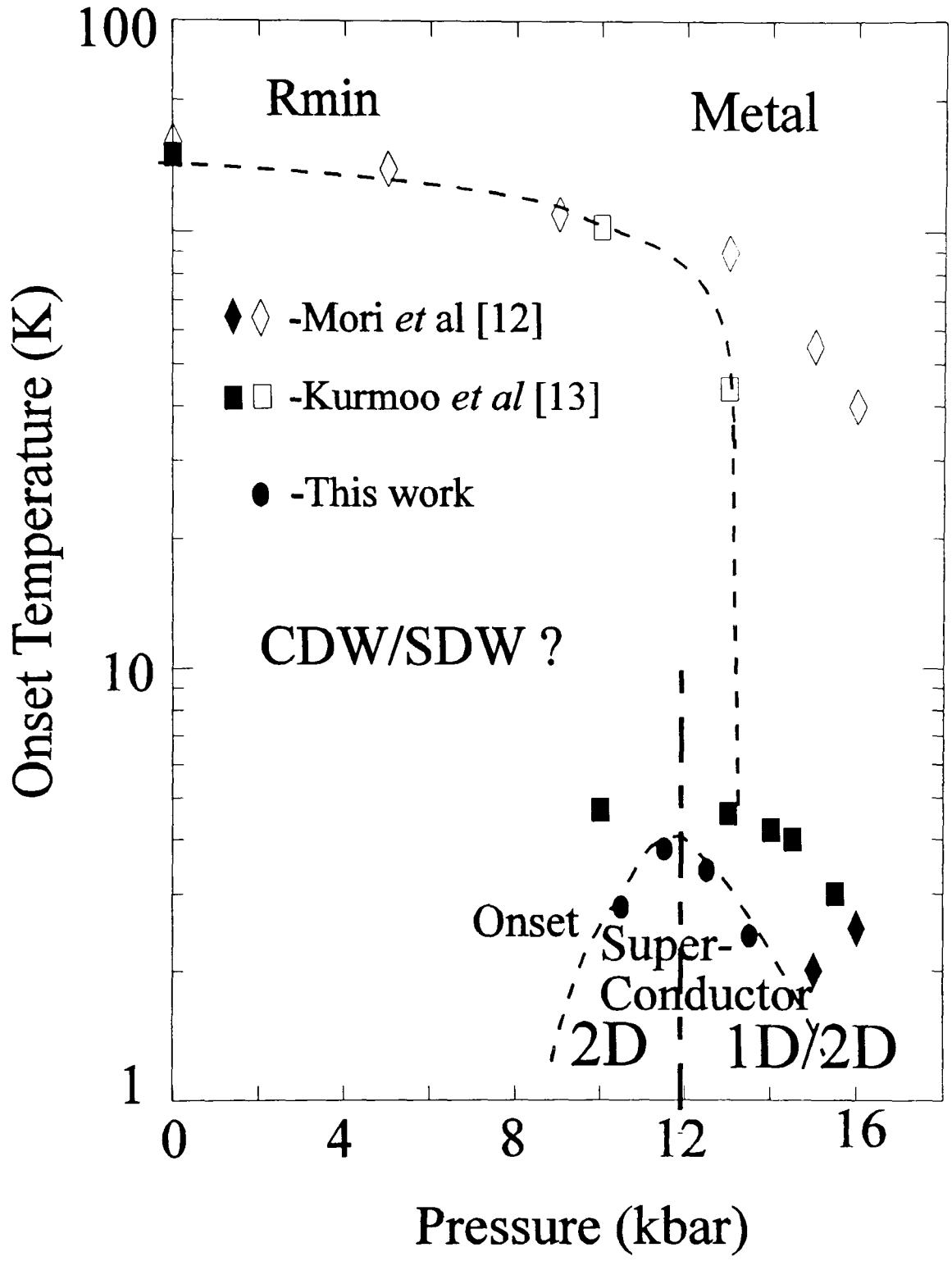

Figure 14 Temperature-pressure phase diagram: diamonds, squares and circles, taken from [12], [13] and this chapter respectively. The open symbols mark the points of the temperature of the minimum in resistivity indicating the (semi)metal to semiconductor transition and the filled symbols represent the onset of superconductivity. The dased line shows the separate phase regions. The thick dashed line shows the pressure at which non-saturating magnetoresistance is observed.

The data from this chapter and reference [13] are in reasonably good agreement; the slight differences may be due to differing techniques in the application of pressure. The data points from reference [12] appear offset by ~3 kbar; the quoted pressure readings may be room temperature values and therefore not adjusted for the loss in pressure experienced as the pressure cell is cooled. This point is not clear from the text of reference [12].

6.5 Summary

From the experimental evidence it is proposed that pressure has the effect of gradually reducing the ordering temperature of the charge or spin density wave. Pressure also has the effect of forming a closed section of Fermi surface, responsible for the Shubnikov-de Haas oscillations and the two dimensional nature of the magnetoresistance. The two dimensional Fermi surface appears 'suitable' for superconductivity. Further increases in pressure make the formation of a charge density wave unfavourable, closing the band gap in the one dimensional sections of the Fermi surface and decreasing the resistivity by a factor of ~1000 (the change in the sample resistivity cannot be explained by the change in mobility of the two dimensional carriers). The predominantly one dimensional Fermi surface appears to be unfavourable to superconductivity, perhaps because of screening of the pairing interaction. Alternatively, the structural changes brought about by the application of pressure may lead to changes in the phonon spectrum which affect the formation of the superconducting state.

References

[1] M.H. Whangbo, J. Ren, D.B. Kang and J.M. Williams, *Mol. Cryst. Liq. Cryst.*, **181** 17 (1990).

[2] T. Mori and H. Inokuchi, *Chem. Lett.*, **1987** 1675 (1987).

[3] M.J. Rosseinsky, M. Kurmoo, D.R. Talham, P. Day, D. Chasseau and D. Watkin, *J. Chem. Soc., Chem. Commun.*, **1988** 88 (1988).

[4] R.P. Shibaeva, R.M. Lobkovskaya, L.P. Rozenberg, L.I. Buravov, A.A. Ignatiev, N.D. Kushch, E.E. Laukina, M.K. Makova, E.B. Yagubskii and A.V. Zvarykina, *Synth. Met.*, **27**, A189 (1988).

[5] S. Demishev, L. Ducroo de Jongh, J. Singleton, M. Kurmoo, *et al*, *unpublished results.*

[6] G. Bravic, D. Chasseau, J. Gaultier, M.J. Rosseinsky, M. Kurmoo, P. Day and A. Filhol, *Synth. Met.*,**41** 2035 (1991).
D. Chasseau (x-ray measurements down to 12 K), *unpublished results.*

[7] L. Ducasse and A. Frisch, *Solid State Commun.*, **91** 201 (1994).

[8] S.D. Obertelli, I.R. Marsden, R.H. Friend, M. Kurmoo, M.J. Rosseinsky, P. Day, F.L. Pratt and W. Hayes, Springer Proceedings in Physics **51**, 181 (1990).

[9] Dr F.L. Pratt (Oxford University), *unpublished results.*

[10] Dr M. Kurmoo (Royal Institution, London), *private communication.*

[11] Dr M. Kurmoo (Royal Institution, London), *unpublished results.*

[12] T. Mori and H. Inokuchi, *Solid State Commun.* **64**, 335 (1987).

[13] M. Kurmoo, M.J. Rosseinsky, P. Day, P. Auban, W. Kang, D. Jerome and P. Batail, *Synth. Met.*,**27** A425 (1989).

[14] H. Ito, T. Ishiguro, H. Ishimoto, K. Kono, M.V. Kartsovnik, H. Mori, S. Tanaka, G. Saito and N.D. Kushch, *to be published.*

[15] M.P.A. Fisher, *Phys. Rev. Lett.*, **65** 923 (1990).

[16] *Magnetoresistance in Metals*, A.B. Pippard (Cambridge University Press, 1989).

[17] *Magnetic Oscillations in Metals*, D. Shoenberg, (Cambridge University Press, 1984).

[18] W. Lubczynski, J. Caulfield, J. Singleton, W. Hayes, M. Kurmoo and P. Day, *Synth. Met., in press* (1994).

[19] M. Tinkham, "*Introduction to Superconductivity*"; Robert E. Krieger Publishing Co.: Huntingdon, New York, 1980; Chap. 4, p. 104.

[20] M. Decroux, Ø. Fisher, "*Superconductivity in Ternary Compounds II*", M.B. Maple, Ø. Fisher.; eds.; Springer-Verlag: Berlin, 1982; Chap. 3, p. 57 and references cited therein.

[21] D.R. Tilley and J. Tilley, "*Superfluidity and Superconductivity*", I.O.P publishing Ltd, London, 1994; Chap. 5, p. 152.

List of Publications

1. *Magneto-optical and Magneto-transport studies of electron-electron interactions in Organic Conductors using Fields up to 50T;*
   J. Singleton, F.L. Pratt, M. Doporto, J.M. Caulfield, S.O. Hill, T.J.B.M. Janssen, I. Deckers, G. Pitsi, F. Herlach, W. Hayes, J.A.A.J. Perenboom, M. Kurmoo and P. Day, *Physica* **B**, **184** 470 (1993).

2. *High-field magnetotransport studies of β''-(BEDT-TTF)$_2$AuBr$_2$* ;
   M. Doporto J. Caulfield, F.L. Pratt, J. Singleton, S. Hill, W. Hayes, J.A.A.J. Perenboom, M. Kurmoo, and P. Day, *Synth. Metals*, **56/1** 2572 (1993).

3. *High-field magnetotransport studies of α-(ET)$_2$MHg(SCN)$_4$ salts (M=K, NH$_4$)*;
   J. Singleton, F.L. Pratt, M. Doporto, J. Caulfield, W. Hayes, I. Deckers, G. Pitsi, F. Herlach, T.J.B.M. Janssen, J.A.A.J. Perenboom, M. Kurmoo and P. Day, *Synth. Metals* **56/1** 2198 (1993)

4. *Anomalous negative magnetoresistance in κ-(BEDT-TTF)$_2$Cu(NCS)$_2$*;
   F.L. Pratt, J. Caulfield, L. Cowey, J. Singleton, M. Doporto, W. Hayes, J.A.A.J. Perenboom, M. Kurmoo and P. Day, *Synth. Metals*, **56/1** 2289 (1993)

5. *Electron-electron interactions in the 2D electron gas in Silicon*;
   S.V. Kravchenko, J.M. Caulfield, J. Singleton, Hans Nielsen and V.M. Pudalov, *Phys. Rev. B*, **47**, 12961 (1993)."

6. *The influence of magnetic order in quasi-2D organic conductors*;
   M. Doporto, J. Caulfield, S. Hill, J. Singleton, F.L. Pratt, M. Kurmoo, P.T.J. Hendriks, J.A.A.J. Perenboom, W. Hayes and P. Day, *Surface Science* **305** 187 (1993).

7. *The effects of open sections of the Fermi surface on the physical properties of 2D organic molecular metals*;

J. Caulfield, J. Singleton, F.L. Pratt, M. Doporto, M. Kurmoo, P.T.J. Hendriks, J.A.A.J. Perenboom, W. Hayes and P. Day, *Synth. Metals*, **61/1-2**, 63 (1993).

8. *Organic ferromagnetism in the nitronyl nitroxides p-NPNN and 3-QNNN: MUSR, EPR and AC susceptibility*;

F.L. Pratt, R. Valladares, J. Caulfield, J. Singleton, I. Deckers, M. Kurmoo, T. Sugano, W. Hayes and P. Day, *Synth. Metals*, **61/1-2**, 171 (1993).

9. *High magnetic field studies of two dimensional organic molecular metals based on ET*;

John Singleton, Jason Caulfield, S.O. Hill, P.T.J. Hendriks, F.L. Pratt, M. Doporto, I. Deckers, G. Pitsi, F. Herlach, W. Hayes, T.J.B.M. Janssen, J.A.A.J Perenboom, M. Kurmoo, and P. Day, *Conf. Physique en Champs Magnetiques Très Intenses et Technologies Associées*, Toulouse, 8-9 April 1993

10. *Magnetotransport and Fermi surface topology of β"-(BEDT-TTF)$_2$AuBr$_2$-The effects of spin-density-wave formation*;

M. Doporto, J. Singleton, F.L. Pratt, J. Caulfield, W. Hayes, J.A.A.J. Perenboom, I. Deckers, G. Pitsi, M. Kurmoo, and P. Day, *Phys Rev* **B 45** *3934* (1994).

11. "High-field magnetotransport of the Organic Superconductor κ-(BEDT-TTF)$_2$Cu(NCS)$_2$ under pressure", W. Lubczynski, J. Caulfield, F.L. Pratt, J. Singleton, W. Hayes, M. Kurmoo and P. Day. *Physica B* (in press).

12. *Large magnetic-field-induced Fermi surface changes in α-$(ET)_2KHg(SCN)_4$;*
J. Caulfield, J. Singleton, P.T.J. Hendriks, J.A.A.J. Perenboom, F.L. Pratt, M. Doporto, W. Hayes, M. Kurmoo and P. Day, *J. Phys: Cond. Matter* **6** 155 (1994).

13. *Magnetotransport studies of the organic superconductor κ-$(BEDT\text{-}TTF)_2Cu(NCS)_2$ under pressure: The relationship betwwen carrier effective mass and critical temperature*;
J. Caulfield, W. Lubczynski, F.L Pratt, J. Singleton, D.Y.K Ko W. Hayes, M. Kurmoo and P. Day, *J. Phys. Cond. Matter.*. **6** 2911 (1994).

14. *De Haas-van Alphen effect in the vortex state of the organic superconductor κ -$(BEDT\text{-}TTF)_2Cu(NCS)_2$;*
P.J. van der Wel, J. Caulfield, M. Springford, J. Singleton, M. Kurmoo and P. Day, *Physica.* **C** (in press).

15. *The relationship between carrier effective mass and critical temperature in superconducting BEDT-TTF charge-transfer salts,*
W. Lubczynski, J. Caulfield, S. Hill, A. House, J. Singleton, W. Hayes, M. Kurmoo and P. Day, *Physica.* **C** (to be published).

16. *Angle dependent magnetoresistance oscillations and Fermi surface reordering at high magnetic fields in α-$(ET)_2KHg(SCN)_4$;*
J. Caulfield, S.J. Blundell, J. Singleton, A. House, M.S.L. du Croo de Jongh, P.T.J. Hendriks, J.A.A.J. Perenboom, F.L. Pratt, M. Doporto, W. Hayes, M. Kurmoo and P. Day, *Synth. Metals*, (to be published).

17. *High pressure studies of the relationship between carrier effective mass and superconducting critical temperature in κ-(BEDT-TTF)$_2$Cu(NCS)$_2$;*
J. Caulfield, W. Lubczynski, W. Lee, J. Singleton, F.L Pratt, W. Hayes, M. Kurmoo and P. Day, *Synth. Metals*, (to be published).

18. *De Haas-van Alphen effect in the vortex state of the organic superconductor κ-(BEDT-TTF)$_2$Cu(NCS)$_2$;*
P.J. van der Wel, J. Caulfield, J. Singleton, S.M. Hayden, M. Springford, R. Corcoran, M. Kurmoo and P. Day, *Synth. Metals*, (to be published).

19. *Fermi surface studies of the pressure-induced organic superconductor (BEDT-TTF)$_3$Cl$_2$2H$_2$O;*
J. Caulfield, W. Lubczynski, J. Singleton, W. Hayes, M. Kurmoo and P. Day, *Synth. Metals*, (to be published).

20. *Insulator-metal-quantum-Hall-effect transition induced by temperature*;
S.V. Kravchenko, W. Mason, J.E. Furneaux, J.M. Caulfield, J. Singleton and V.M. Pudalov, *Physica* **C** (to be published).

21. *Fermi surface studies of low-dimensional organic conductors based on BEDT-TTF;*
John Singleton, Jason Caulfield, Stephen Hill, Wieslaw Lubczynski, Andrew House, William Hayes, Jos Perenboom, Mohammedally Kurmoo and Peter Day, *Physica* **C** (to be published).

22. *High field magnetoresistance oscillations in α-(bis-(ethylene-dithio)tetrathiafulvalene)$_2$KHg(SCN)$_4$;*

J. Caulfield, S.J. Blundell, M.S.L. du Croo de Jongh, P.T.J. Hendriks, J. Singleton, M. Doporto, F.L. Pratt, A. House, J.A.A.J. Perenboom, F.L. Pratt, M. Doporto, W. Hayes, M. Kurmoo and P. Day, *Phys. Rev.* **B** (submitted)